EPFL

Controlling the Microstructure and Composition of 3D Printed Soft Load-Bearing Hydrogels

Matteo HIRSCH

École
polytechnique
fédérale
de Lausanne

2023

"The more I learn,
the more I realize how much I don't know."

Albert Einstein

Acknowledgments

First and foremost, I would like to thank my advisor Prof. Esther Amstad. Words cannot express my gratitude for her invaluable mentoring and guidance during my doctorate. I keep great memories of our first online meeting, when Covid-19 and Zoom calls were not a thing yet. I was and still am amazed of how fast she answers back to emails and how brave she was in considering the application of a student she knew nothing about. From the very beginning, she gave me the freedom to explore, test, and even make mistakes on my own to become a better scientist. Even when research did not go as planned, she was always positive and could see the glass half-full. I learned a lot from her in these past four years and I am extremely grateful for her unwavering support throughout this journey. I feel extremely humbled by her continuous endorsement and cannot wait to see what the future holds for her and the Soft Materials Laboratory.

I would also like to acknowledge Prof. Josie Hughes, Prof. Marcy Zenobi-Wong, and Prof. Daeyeon Lee for agreeing to be part of my thesis committee, as well as Prof. Andreas Mortensen for chairing the examination session.

My warmest thank you goes to our secretary Mercedes Quintas. I enjoyed every single minute we spent chatting together in Frespañol. She has always been there whether for administrative support or simply to exchange perspectives. I am looking forward to many more coffee breaks together in the future.

I want to acknowledge all the current and former members of the Soft Materials Laboratory. The journey would have not been the same without you by my side. First, I would like to thank Alvaro Charlet for being my "partner in crime". I really enjoyed sharing ideas, running experiments, and spending quality time together; you certainly made these past four years pass faster. Then, I would like to express my gratitude to Huachuan Du and Mathias Steinacher. Words cannot express how important you have been in setting an example with your undivided love for science and high quality research standards. I

am extremely proud to call two you my friends. Furthermore, I want to acknowledge the restless moral - and nutritional - support from Gaia De Angelis, Francesca Bono, and Lorenzo Lucherini. My mind and belly are full of dAlicious Italian food and laughter. You definitely made the time spent in the lab an absolute blast. I would also like to thank my office colleague, Ran Zhao. I had a lot of fun sharing the office with her and entertaining scientific discussions. A special thank goes to my former Master's student, Eva Baur, who decided to continue her career in science, despite the time spent under my supervision. I wish you all the best in your future academic endeavors. A special thought goes to all the other members of the Soft Materials Laboratory: Michael Kessler, Aysu Okur, Irvine Ong, Chuen-Ru Li, Alexandra Thoma, Pauline Pradal, and Rocio Garcia Montero. Each of you contributed in their own way to maintaining a great atmosphere in the lab.

Then, I would like to thank all the students I supervised during my PhD. This includes Eva Baur, Léa Buswell, Molly Sun, Alexandre Pittet, Clément Viers, Nicola Stiavelli, Sanjay Schreiber, Beatrice Bigoni, Soukaina Ait Said, and Livia D'Onofrio. I really enjoyed working with you. Your success is my success.

Out of the many people I met at EPFL, I would like to thank Alexandra Clarà Saracho, with whom I had the pleasure to collaborate and become good friends. Your positive thinking and insightful perspectives made our scientific collaboration a great success. I am very much looking forward to continue our exchanges in the future.

Then, I would like to acknowledge the scientists and technical collaborators at EPFL that allowed my research to progress smoothly. This includes, Grégoire Baroz, Dr. Pierre Rossi, Jaques Morisod, Yann Lavanchy, and Xavier Dutoit.

Outside of lab, I had the pleasure to meet many fantastic people. First and foremost, I would like to express my deepest gratitude to Gloria Porro and Siria Cristofori for their constant moral support and unwavering happiness. You kept my morale up, even in the toughest times. Then, I would like to thank the nanotech crew for their constant moral support and extravagant friendship. I did not get to choose them but I am happy I met them. I would also like to thank my friends Jamie Pearson and Gianni Presti for being the best game and movie buddies I could ask for. To many more Marvel movies together. I would like to thank my volleyball team, Micmac, for giving me a reason to survive Monday blues. You all really made Lausanne feel like home. Last but not least, I would like to express my gratitude to all my friends from Florence, including Lorenzo Poggi, Tommaso Sferruzza, and Arturo Cianchi, for reminding me that friendship lasts forever.

Lastly, I would be remiss in not mentioning my family. First, I would like to thank my parents, Marta and David, for having supported and believed in me from the very beginning. Words cannot express how important you have been in shaping the man I am

today. Then, I would like to thank my sister Serena for always keeping me grounded. Despite living our lives like Tom & Jerry, we always look after each other. Overall, we might have lost a few pieces along the way but we are all still part of the same masterpiece.

And last but not least, my most heartfelt acknowledgement goes to Marina. I would like to thank her for her positivity, great patience, and kindness, as well as for reminding me everyday that distance is what makes the heart grow fonder.

Abstract

Hydrogels are among the first materials expressly designed for their use in biomedicine. However, state-of-the-art applications of hydrogels are severely limited because they are typically either too soft or too brittle such that they cannot bear significant loads. Nature, instead, assembles hydrogel-like soft biological tissues displaying unique mechanical properties. These properties are the result of a fine interplay between structural complexity and local composition. Indeed, most biological materials encompass highly ordered, hierarchical structures with locally varying compositions. In an effort to mimic nature complexity, several strategies to reinforce hydrogels and control their internal structure have been thoroughly investigated. However, currently produced manmade hydrogels are still far from reaching mechanical performances similar to that of their biological counterparts.

In the first part of the thesis, I introduce a novel approach to fabricate synthetic load-bearing hydrogels with controlled structure and local varying composition. These properties are obtained through the use of a granular precursor material, referred as the jammed microgel ink, that allows the 3D printing of complex architectures with controlled microstructure and composition. Microgels are produced from monomer-loaded drops, that are then converted into hydrogel particles by a conventional photopolymerization reaction. Owing to their high swelling capacity, microgels are subsequently loaded with another precursor solution. After 3D printing, the precursor solution can be crosslinked to form a second percolating network that stabilizes the 3-dimensional hydrogel construct. This reaction converts the soft jammed paste into a stiff and tough granular material, referred as the double-network granular hydrogel, while maintaining a well-defined microstructure. Furthermore, I discuss the versatility of double network granular hydrogels for the fabrication of recyclable hydrogels. This is achieved by incorporating dynamic covalent crosslinks in the percolating network that allow the on-demand degradation and recycling of the double network granular hydrogel down to its individual microgel components. Furthermore,

I prove that this recycling approach can be extended to hard plastics, thus expanding the potential applications of recyclable double network granular materials.

In the second part of the thesis, I discuss the use of metal-coordination for the local reinforcement of hydrogels. Initially, I show that metal-coordination can be used to selectively reinforce bulk hydrogels by introducing competitive ligands in the crosslinking solution. This strategy allows the fabrication of mechanical gradients within the same material, such that core-shell structures can be obtained. Furthermore, I demonstrate the possibility to combine this reinforcement approach with double network granular hydrogels. This combination allows to independently control microstructure and local reinforcement, thus expanding the degrees of freedom for the design of load-bearing hydrogels. There, I demonstrate the possibility to further improve hydrogel mechanics by fabricating double network granular hydrogels that are reinforced through metal-coordination either in the microgels or in the percolating network.

In the last section, I introduce a novel strategy for the fabrication of synthetic materials whose mechanical properties and structural complexity closely resemble those of their natural counterparts. To achieve this goal, I propose to combine synthetic manmade materials with natural living microorganisms to produce an engineered living biocomposite. The encapsulation of mineralizing bacteria in a granular hydrogel enables their assembly into soft arbitrarily complex structures. Upon mineralization, the local precipitation of biominerals reinforces the scaffold by creating mineral bridges that stabilize the structure. The mineralized granular biocomposite is porous and lightweight, while being able to sustain significant loads. The material shows a unique internal microstructure that closely resemble that of natural bone. Furthermore, I suggest potential applications of this unique material, such as an injectable paste for art restoration.

While drawing my conclusions, I highlight current technological limits that are hindering hydrogel research from reaching its full potential and suggest possible solutions. I believe that overcoming these limitations would help expanding the hydrogel application landscape to more advanced fields, such as that of soft robotics, and smart adaptive materials.

Keywords: *soft materials, hydrogels, 3D printing, engineered living materials*

Abstract (Italian)

Gli idrogeli sono tra i primi materiali espressamente progettati per essere utilizzati in biomedicina. Tuttavia, le applicazioni all'avanguardia degli idrogeli sono fortemente limitate perché in genere sono troppo morbidi o troppo fragili, tanto da non poter sopportare carichi significativi. La natura, invece, assembla tessuti biologici morbidi simili agli idrogeli che presentano proprietà meccaniche uniche. Queste proprietà sono il risultato di una fine interazione tra complessità strutturale e composizione locale. Infatti, la maggior parte dei materiali biologici comprende strutture gerarchiche altamente ordinate con composizioni localmente variabili. Nel tentativo di imitare la complessità della natura, sono state studiate a fondo diverse strategie per rinforzare gli idrogeli e controllare la loro struttura interna. Tuttavia, gli idrogeli attualmente prodotti dall'uomo sono ancora lontani dal raggiungere prestazioni meccaniche simili a quelle delle loro controparti biologiche.

Nella prima parte della tesi, presento un approccio innovativo per fabbricare idrogeli sintetici portanti con struttura controllata e composizione variabile a livello locale. Queste proprietà sono ottenute grazie all'uso di un precursore granulare, denominato inchiostro di microgeli pressati, che consente la stampa 3D di architetture complesse con microstruttura e composizione controllate. I microgeli sono prodotti da gocce caricate con monomeri, che vengono poi convertite in microparticelle di idrogel mediante una reazione di fotopolimerizzazione convenzionale. Grazie alla loro elevata capacità di assorbimento, i microgeli vengono successivamente caricati con un'altra soluzione di precursore. Dopo la stampa 3D, la soluzione precursore può essere reticolata per formare una seconda matrice percolante che stabilizza il costrutto idrogelico tridimensionale. Questa reazione converte la morbida pasta di microgeli pressati in un materiale granulare rigido e resistente, definito idrogel granulare a doppio reticolo, mantenendo una microstruttura ben definita. Discuto, inoltre, la versatilità degli idrogeli granulari a doppio reticolo per la fabbricazione di idrogeli riciclabili. Ciò è possibile grazie all'incorporazione di legami covalenti dinamici nella matrice percolante che consentono la degradazione a livello dei singoli microgeli e

il riciclo dell'idrogel granulare a doppio reticolo. Inoltre, dimostro che questo approccio al riciclaggio può essere esteso alle plastiche convenzionali, ampliando così le potenziali applicazioni dei materiali granulari riciclabili a doppio reticolo.

Nella seconda parte della tesi, discuto l'uso della coordinazione metallica per il rinforzo locale degli idrogeli. Inizialmente, mostro che la coordinazione metallica può essere utilizzata per rinforzare selettivamente gli idrogeli sfusi introducendo ligandi competitivi nella soluzione di ioni reticolanti. Questa strategia consente di creare gradienti meccanici all'interno dello stesso materiale, in modo da ottenere strutture core-shell. Inoltre, dimostro la possibilità di combinare questo approccio di rinforzo con idrogeli granulari a doppio reticolo. Questa combinazione permette di controllare in modo indipendente la microstruttura e il rinforzo locale, ampliando così i gradi di libertà per la progettazione di idrogeli portanti. In seguito, dimostro la possibilità di migliorare ulteriormente la meccanica degli idrogeli fabbricando idrogeli granulari a doppio reticolo che sono rinforzati attraverso la coordinazione di metalli sia nei microgeli sia nella matrice percolante.

Nell'ultima sezione, introduco una nuova strategia per la fabbricazione di materiali sintetici le cui proprietà meccaniche e la cui complessità strutturale ricordano quelle delle loro controparti naturali. Per raggiungere questo obiettivo, propongo di combinare materiali sintetici artificiali con microrganismi viventi per produrre un biocomposito vivente ingegnerizzato. L'incapsulamento dei batteri mineralizzanti in un idrogel granulare consente il loro assemblaggio in strutture morbide e arbitrariamente complesse. Dopo la mineralizzazione, la precipitazione locale di biominerali rafforza l'impalcatura creando ponti minerali che stabilizzano la struttura. Il biocomposito granulare mineralizzato è poroso e leggero, pur essendo in grado di sostenere carichi significativi. Il materiale mostra una microstruttura interna unica che ricorda da vicino quella dell'osso naturale. Inoltre, suggerisco potenziali applicazioni di questo materiale unico, come una pasta iniettabile per il restauro artistico.

Nel trarre le mie conclusioni, sottolineo gli attuali limiti tecnologici che impediscono alla ricerca sugli idrogeli di raggiungere il suo pieno potenziale e suggerisco possibili soluzioni. Ritengo che il superamento di queste limitazioni contribuirebbe a espandere il panorama delle applicazioni degli idrogeli a campi di ricerca più avanzati, come quello della soft robotics e dei materiali adattivi intelligenti.

Parole chiave: *soft matter, idrogeli, stampa 3D, materiali viventi ingegnerizzati*

Resumé

Les hydrogels sont parmi les premiers matériaux spécifiquement conçus pour être utilisés en biomédecine. Toutefois, les applications de pointe des hydrogels sont fortement limitées car ils sont généralement trop mous ou trop fragiles pour résister à des charges importantes. La nature, quant à elle, assemble des tissus biologiques mous semblables à des hydrogels qui présentent des propriétés mécaniques uniques. Ces propriétés sont le résultat d'une interaction fine entre la complexité structurelle et la composition locale. En fait, la plupart des matériaux biologiques comprennent des structures hiérarchiques hautement ordonnées dont la composition varie localement. Dans le but d'imiter la complexité de la nature, diverses stratégies visant à renforcer les hydrogels et à contrôler leur structure interne ont été largement étudiées. Cependant, les hydrogels actuellement produits par l'homme sont encore loin d'atteindre des performances mécaniques similaires à celles de leurs homologues biologiques.

Dans la première partie de cette thèse, je présente une nouvelle approche pour fabriquer des hydrogels synthétiques porteurs avec une structure contrôlée et une composition localement variable. Ces propriétés sont obtenues grâce à l'utilisation d'un précurseur granulaire, appelé encre microgel pressée, qui permet d'imprimer en 3D des architectures complexes dont la microstructure et la composition sont contrôlées. Les microgels sont produits à partir de gouttelettes chargées de monomères, qui sont ensuite transformées en microparticules d'hydrogel par une réaction de photopolymérisation classique. En raison de leur grande capacité d'absorption, les microgels sont ensuite chargés avec une autre solution de précurseur. Après l'impression 3D, la solution précurseur peut être réticulée pour former une seconde matrice percolante qui stabilise la construction tridimensionnelle en hydrogel. Cette réaction transforme la pâte molle des microgels pressés en un matériau granulaire rigide et résistant, appelé hydrogel granulaire à double réseau, tout en maintenant une microstructure bien définie. Je discute également de la polyvalence des hydrogels granulaires à double réseau pour la fabrication d'hydrogels recyclables. Cela est

possible grâce à l'incorporation de liaisons covalentes dynamiques dans la matrice percolante qui permettent la dégradation au niveau des microgels individuels et le recyclage de l'hydrogel granulaire à double réseau. En outre, je démontre que cette approche de recyclage peut être étendue aux plastiques conventionnels, élargissant ainsi les applications potentielles des matériaux granulaires recyclables à double réseau.

Dans la deuxième partie de la thèse, je discute de l'utilisation de la coordination métallique pour le renforcement local des hydrogels. Dans un premier temps, je montre que la coordination des métaux peut être utilisée pour renforcer sélectivement les hydrogels en vrac en introduisant des ligands compétitifs dans la solution d'ions réticulants. Cette stratégie permet de créer des gradients mécaniques au sein d'un même matériau afin d'obtenir des structures core-shell. De plus, je démontre la possibilité de combiner cette approche de renforcement avec des hydrogels granulaires à double réseau. Cette combinaison permet un contrôle indépendant de la microstructure et du renforcement local, élargissant ainsi les degrés de liberté pour la conception d'hydrogels porteurs. Ensuite, je démontre la possibilité d'améliorer encore la mécanique des hydrogels en fabriquant des hydrogels granulaires à double réseau qui sont renforcés par la coordination des métaux à la fois dans les microgels et dans la matrice percolante.

Dans la dernière section, je présente une nouvelle stratégie pour la fabrication de matériaux synthétiques dont les propriétés mécaniques et la complexité structurelle ressemblent à celles de leurs homologues naturels. Pour y parvenir, je propose de combiner des matériaux synthétiques artificiels avec des micro-organismes vivants pour produire un biocomposite vivant. L'encapsulation des bactéries minéralisatrices dans un hydrogel granulaire permet de les assembler en structures souples et arbitrairement complexes. Après la minéralisation, la précipitation locale de biominéraux renforce l'échafaudage en créant des ponts minéraux qui stabilisent la structure. Le biocomposite granulaire minéralisé est poreux et léger, mais capable de supporter des charges importantes. Le matériau présente une microstructure interne unique qui ressemble beaucoup à celle de l'os naturel. En outre, je suggère des applications potentielles de ce matériau unique comme pâte injectable pour la restauration d'œuvres d'art.

En tirant mes conclusions, je souligne les limites technologiques actuelles qui empêchent la recherche sur les hydrogels d'atteindre son plein potentiel et je suggère des solutions possibles. Je pense que le fait de surmonter ces limites permettrait d'élargir le champ d'application des hydrogels à des domaines de recherche plus avancés, tels que la soft robotics et les matériaux intelligentes.

Mots clés: *matière molle, hydrogels, impression 3D, matériaux vivants intelligents*

Resumen

Los hidrogeles se encuentran entre los primeros materiales diseñados específicamente para su uso en biomedicina. Sin embargo, las aplicaciones de vanguardia de los hidrogeles están muy limitadas porque suelen ser demasiado blandos o demasiado frágiles como para soportar cargas importantes. La naturaleza, por su parte, ensambla tejidos biológicos blandos similares a los hidrogeles que presentan propiedades mecánicas únicas. Estas propiedades son el resultado de una fina interacción entre la complejidad estructural y la composición local. De hecho, la mayoría de los materiales biológicos comprenden estructuras jerárquicas altamente ordenadas con composiciones localmente variables. En un intento de imitar la complejidad de la naturaleza, se han estudiado ampliamente diversas estrategias para reforzar los hidrogeles y controlar su estructura interna. Sin embargo, los hidrogeles producidos actualmente por el ser humano aún están lejos de alcanzar un rendimiento mecánico similar al de sus homólogos biológicos.

En la primera parte de esta tesis, presento un enfoque novedoso para fabricar hidrogeles sintéticos de carga con estructura controlada y composición localmente variable. Estas propiedades se consiguen mediante el uso de un precursor granular, llamado tinta de microgel prensado, que permite la impresión en 3D de arquitecturas complejas con microestructura y composición controladas. Los microgeles se producen a partir de gotas cargadas de monómero, que luego se convierten en micropartículas de hidrogel mediante una reacción de fotopolimerización convencional. Debido a su gran capacidad de absorción, los microgeles se cargan posteriormente con otra solución precursora. Tras la impresión 3D, la solución precursora puede reticularse para formar una segunda matriz percoladora que estabilice la construcción tridimensional de hidrogel. Esta reacción convierte la pasta blanda de los microgeles prensados en un material granular rígido y resistente, denominado hidrogel granular de doble red, manteniendo una microestructura bien definida. También hablo de la versatilidad de los hidrogeles granulares de doble red para la fabricación de hidrogeles reciclables. Esto es posible gracias a la incorporación de enlaces covalentes

dinámicos en la matriz percoladora que permiten la degradación a nivel de microgeles individuales y el reciclaje del hidrogel de doble red granular. Además, demuestro que este enfoque de reciclaje puede extenderse a los plásticos convencionales, ampliando así las aplicaciones potenciales de los materiales granulares de doble red reciclables.

En la segunda parte de la tesis, discuto el uso de la coordinación de metales para el refuerzo local de los hidrogeles. Inicialmente, muestro que la coordinación de metales puede utilizarse para reforzar selectivamente los hidrogeles a granel mediante la introducción de ligandos competitivos en la solución de iones de reticulación. Esta estrategia permite crear gradientes mecánicos dentro del mismo material para obtener estructuras core-shell. Además, demuestro la posibilidad de combinar este enfoque de refuerzo con hidrogeles granulares de doble red. Esta combinación permite el control independiente de la microestructura y el refuerzo local, ampliando así los grados de libertad para el diseño de hidrogeles de carga. A continuación, demuestro la posibilidad de mejorar aún más la mecánica de los hidrogeles mediante la fabricación de hidrogeles granulares de doble red que se refuerzan mediante la coordinación de metales tanto en los microgeles como en la matriz percoladora.

En la última sección, introduzco una nueva estrategia para la fabricación de materiales sintéticos cuyas propiedades mecánicas y complejidad estructural se asemejan a las de sus homólogos naturales. Para lograrlo, propongo combinar materiales sintéticos artificiales con microorganismos vivos para producir un biocompuesto vivo de ingeniería. La encapsulación de las bacterias mineralizadoras en un hidrogel granular permite ensamblarlas en estructuras blandas y arbitrariamente complejas. Tras la mineralización, la precipitación local de los biominerales refuerza el andamiaje creando puentes minerales que estabilizan la estructura. El biocompuesto granular mineralizado es poroso y ligero, pero capaz de soportar cargas importantes. El material presenta una microestructura interna única que se asemeja mucho a la del hueso natural. Además, sugiero posibles aplicaciones de este material único como pasta inyectable para la restauración de obras de arte.

Al extraer mis conclusiones, destaco las actuales limitaciones tecnológicas que impiden que la investigación con hidrogeles alcance todo su potencial y sugiero posibles soluciones. Creo que la superación de estas limitaciones ayudaría a ampliar el panorama de aplicaciones de los hidrogeles a campos de investigación más avanzados, como la robótica flexible y los materiales inteligentes.

Palabras claves: *materia blanda, hidrogeles, impresión 3D, materiales vivos inteligentes*

Contents

CHAPTER 1

Introduction

1.1 Nature: An Endless Source of Inspiration

Since the beginning of human history, nature has been the major source of inspiration in the development and maturation of our society. Whether referred as the gift of omnipotent gods or the serendipitous manifestation of unknown forces, natural events were always welcomed as a unique opportunity for technological advancement. First traces of this rudimental biomimetic approach can be found already in Greek mythology with the bird-inspired feathered wings of Daedalus and Icarus, as represented in the fresco in Figure 1.1.

Other examples of biomimetic design can be found across the entire human history. For instance, during the period of the Renaissance, scientists started investigating biological organisms to understand their underlying structural arrangement and compositions, in the attempt to derive constitutive laws that could be translated to manmade processes. One remarkable example is found in Leonardo Da Vinci, who devoted most of his life to the study of human body, with the most famous record being the Vitruvian Man, and derived structure-function relations that led him to the fabrication of rudimental robots, known as Automata, as shown in Figure 1.2.

However, the understanding of nature remained shallow and limited to direct observation for long before major breakthroughs could be recorded. This was mainly due to the lack of advanced technological tools, that limited the investigation of biological organisms at various length scales and from different perspectives. It is only during the 20th century, with the introduction of new microscopy and spectroscopy techniques, that the study of biological systems and structures becomes more rigorous and documented. D'Arcy W. Thompson is considered the first to look at biological systems as engineering structures from which mathematical relationships can be derived [1]. Following the momentum,

Figure 1.1: The Fall of Icarus (Fresco. Domus of the Sacaerdos Amandus, Regio I, Insula 11, Pompeii).

several researchers started investigating natural materials, such as bone [2, 3, 4, 5], wood [6, 7, 8], and living organisms [9, 10, 11, 12, 13].

Since then, the field of biological-based materials science has evolved and branched into a great variety of niches, that can be grouped into three broad interconnected areas:

Biological Materials that refers to the study of biological organism formation

Biomaterials that refers to the use of biosourced materials for manmade applications

Bioinspired Materials Design that refers to the application of biomimetic strategies for the fabrication of synthetic materials

From a materials science perspective, the ability to understand the underlying strategies in biological tissue formation is key for their translation to synthetic manmade materials. As a result, I consider the field of bioinspired materials design of pivotal interest in the advancement of human society [14, 15, 16, 17, 18, 19]. A careful observation of evolutionary strategies, as well as a deep understanding of natural processes, will definitely help tackle the most compelling challenges in modern society, which include the fabrication of smart adaptive, self-healing, and sustainable materials.

Figure 1.2: Left, Vitruvian Man (Leonardo da Vinci. Gallerie dell'Accademia, Venice). Right, Automata (Leonardo da Vinci. Mensch - Erfinder - Genie, Berlin).

In the following, a discussion on the approach and evolution of bioinspired materials design towards more bioinformed solutions will be addressed.

1.2 Building Materials with Extreme Mechanics: A Lesson from Nature

A requirement for most structural materials is the attainment of both strength and toughness. In manmade materials, however, these properties tend to be mutually exclusive [14, 20]. In general, synthetic materials are either stiff and brittle or tough and weak, such that they cannot bear significant loads. Nature, on the other hand, is able to fabricate materials encompassing seemingly counteracting properties, such as a combination of stiffness and toughness. This is due to the complex landscape of interconnected internal and external factors that influence their formation [1], as summarized here:

Self-assembly biological growth is a bottom-up assembly process, where genetic signals, cellular activity, chemo-mechanical cues, and enzymatic activity play a crucial role.

Functionality natural materials commonly possess multiple functionalities, such as struc-

tural support, thermal regulation, and defense.

Hierarchy nature grows its materials and tissues in a controlled hierarchical arrangement, across multiple length scales.

Hydration most biological material properties are dependent on the level of hydration.

Mild synthesis conditions the majority of natural constructs are fabricated under benign conditions with minimal energy consumption.

Evolution, environmental constraints the limited availability of resources, and the environmental conditions dictate the final structure and properties.

As a result, the unique combination of these factors results in biological materials with unique design and mechanical properties, as shown in Figure 1.3.

Understanding the underlying design principles and physicochemical mechanisms that determine the ultimate properties of biological systems at the molecular, cellular, tissue, and organism level, and its relationship to function is the key for the development of bioinspired research [22, 23, 24]. Furthermore, deriving implementation strategies from the observation of nature is of pivotal importance for the advancement of materials research, as it enables the fabrication of structures encompassing unconventional properties that closely resemble those of their natural counterparts. However, the intrinsic architectural and compositional complexity of most natural tissues has hindered the effective translation of biomimetic strategies to synthetic manmade materials. A way to circumvent this shortcoming is to identify simpler organisms to study, such as algae [25, 26], diatoms [27], mollusks [28, 29, 30], and insects [31, 32].

One of the fields of research that benefitted the most from a bioinspired approach is that of soft synthetic hydrogels. Indeed, most biological tissues can be assimilated to hydrated polymeric networks, thus drawing a direct analogy to synthetic hydrogels. Hydrogels are hydrophilic polymeric networks able to retain large amounts of water [33]. Owing to their intrinsic biocompatibility, easiness of fabrication, and versatility, they have been used in several biomedical applications, including drug delivery [34, 35, 36, 37], scaffolds for tissue engineering [38, 39, 40, 41, 42], wound dressing [43, 44, 45, 46], and contact lenses [47, 48]. Furthermore, hydrogels have been the subject of extensive research for their use as synthetic tissue replacements. However, their homogeneous composition and poor control over their internal structure have severely limited their translation to more complex applications. For example, being able to combine high stiffness and toughness would enable the use of hydrogels in a variety of fields including that of prosthetic load-bearing implants and soft robotics.
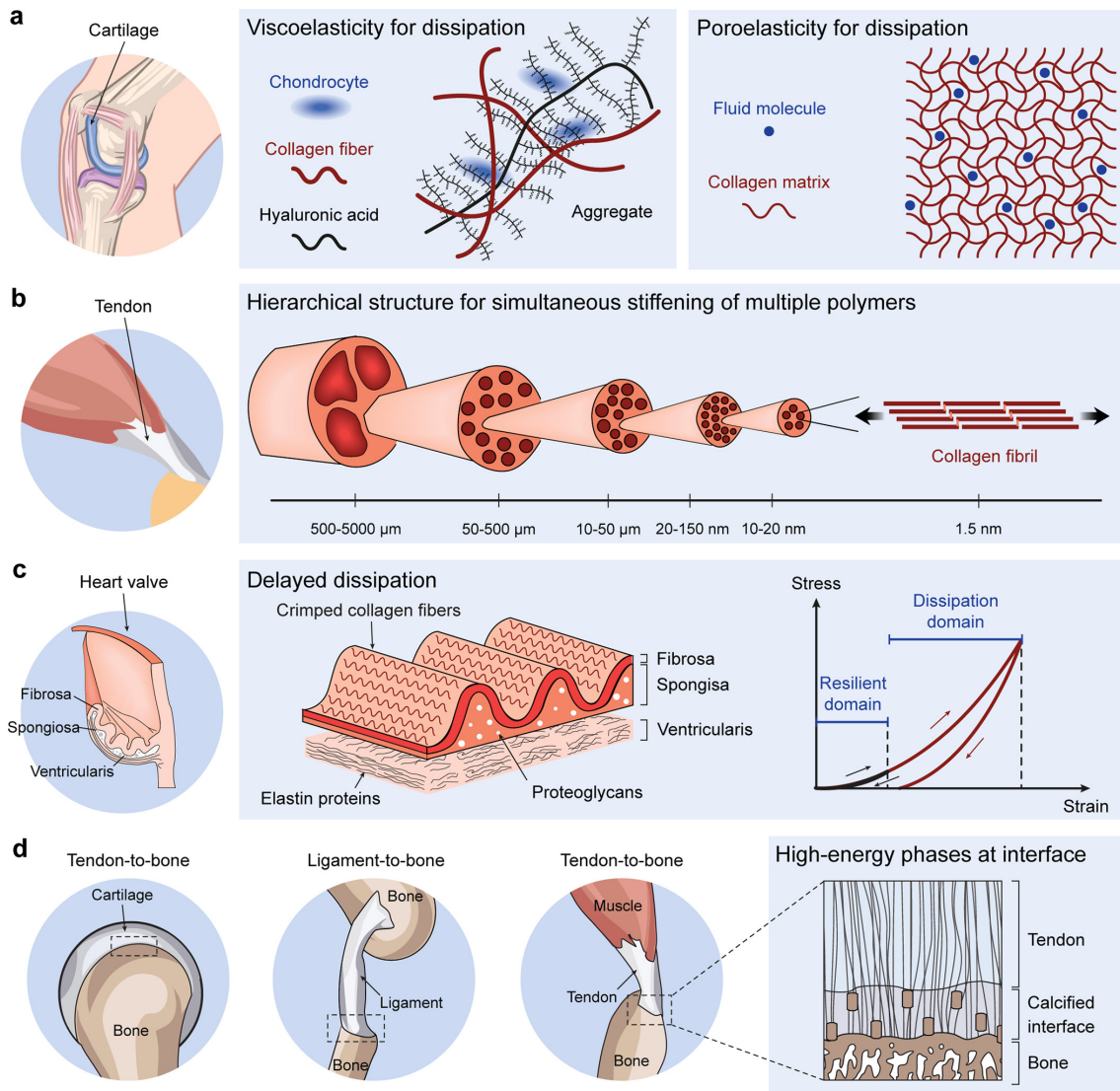
Figure 1.3: Design principles and resulting extreme mechanical properties of various biological tissues. Schematics of (a) cartilage, (b) muscle, (c) heart valve, (d) various tissue interfaces and their mechanical behavior. Reproduced with permission [21]. Copyright 2021, American Chemical Society.

Within this framework, a case in point example of stiff yet tough biological hydrogel is the anchoring thread produced by the mussel, known as the byssus. The mussel byssus is a soft load-bearing acellular tissue that allows the organism to strongly anchor to the rocks and withstand high shear forces due to impacting waves. The unique mechanical properties of the byssus are the result of a fine interplay between internal structure and local varying composition, as detailed in Figure 1.4.

To achieve such an interesting material, the mussel assembles its byssus in the foot groove, through a process that reminds that of injection molding. To obtain the final tissue, precursor-containing vesicles are transported to the desired location and are assembled
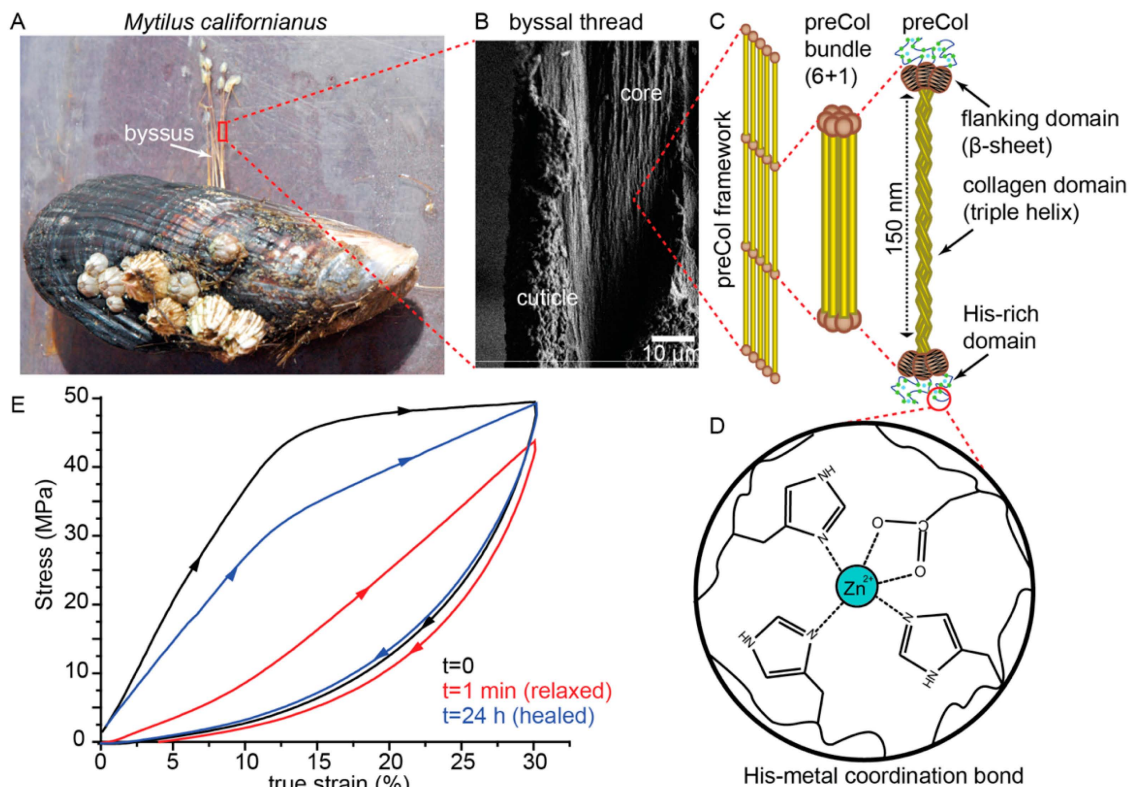
Figure 1.4: Mussel byssus structure and mechanical behavior. (a) Optical phtograph of a *Mytilus californianus*. (b) SEM micrograph of a cross-section of the mussel byssus. (c) Schematic representation of the byssus hierarchical assembly. (d) Schematic representation of the metal-coordination chemistry involved in the byssus extreme mechanics. (e) Tensile curve of the byssal thread displaying extremely high stiffness and toughness, and self-healing properties. Reproduced with permission [49]. Copyright 2019, MDPI.

to form a macroscopic load-bearing material. Interestingly, the use of vesicles provides a unique tool to control the internal structure and local composition of the byssal tissue, hence producing a material with well-defined hierarchical arrangement across multiple length scales.

The ability to mimic this assembly process is of pivotal importance for the design of more complex soft synthetic materials. However, achieving a precise control across multiple length scales in a similar way to that of the mussel is extremely challenging, if not unattainable at the moment. While this might come as disillusioned, the realization of our technological and scientific limits is fundamental for human evolution and it is at the roots of a more engineered approach, known as bioinformation, that aims at studying and abstracting natural strategies to then translate and integrate them to already existing manmade processes [50]. Hence, it becomes clear that nature should not be mimicked but understood to achieve unparalleled results, as it has been demonstrated in several breakthrough innovations made in the past few decades, such as the Shinkansen train,

the Velcro®, and the honeycomb and trabecular structures found in several contemporary buildings.

In the following sections, I will discuss how a bioinformed strategy can be applied to the design of hydrogels, with a particular focus on the use of granular-based assemblies for the fabrication of 3D constructs with heterogeneous structural and compositional properties. Prior to that, a summary of the main concepts of hydrogel design and characterization for load-bearing applications will be discussed.

1.3 Conventional Hydrogel Design and Characterization

Throughout the past few decades, a rich library of polymers and crosslinking strategies has been exploited for the design and fabrication of manmade hydrogels. Depending on their source of origin, these polymers can be categorized as natural or synthetic polymers, as shown in Figure 1.5.

Figure 1.5: Chemical structures and schematics of various (a) natural and (b) synthetic polymers. Reproduced with permission [21]. Copyright 2021, American Chemical Society.

In the following subsections, I will introduce the main building components of conventional

hydrogels and their fundamental properties.

1.3.1   Natural Polymers

Naturally sourced polymers have been extensively used in hydrogel fabrication for biomedical applications owing to their similarity to soft biological tissues and intrinsic biocompatibility. In addition, the body can degrade and absorb many natural polymers through metabolism and tissue remodeling processes. Furthermore, the majority of natural polymers displays chemical reactive groups, that render their modification and crosslinking easier, yet less controlled, than their synthetic counterparts. As a result, natural hydrogels can be endowed with specific biological or mechanical functionalities based on the intended application [21]. A list of common natural polymers is reported below:

Alginate a linear polysaccharide extracted from brown-algae, whose structure is composed of repeating units of D-mannuronic and L-guluronic acid. Conventionally, alginate hydrogels can be crosslinked by exposure to divalent (e.g. Ca^{2+}, Zn^{2+}, etc.) or trivalent (e.g. Fe^{3+}, Al^{3+}, etc.) cationic solutions through a "zip-lock" (or "egg box") mechanism, where two individual chains are held together at their guluronic residues by the intercalating ions.

Hyaluronic acid a linear polymer of disaccharides, D-glucuronic acid and N-acetyl-D-glucosamine. It is found in all mammals, as part of the connective tissue, as space filler, lubricant, and osmotic buffer. Hyaluronic acid can be covalently crosslinked by various hydrazide linkers. Additionally, the abundancy of carboxyl and hydroxyl groups provide room for chemical modifications.

Cellulose the most abundant polysaccharide and the main component of plants and natural fibers. Some bacteria can also produce cellulose. Cellulose is composed of a linear arrangement of D-glucose units and displays a high degree of crystallinity, thus making it difficult to dissolve in water. To improve its solubility several modifications have been developed, thus yielding more hydrophilic cellulose derivatives such as methyl cellulose, carboxymethyl cellulose, and hydroxypropyl cellulose. Cellulose and its derivatives can be crosslinked via covalent, physical crosslinks, or a combination of them. Alternatively, cellulose can be mixed with other natural polysaccharides, such as chitosan, to form interpenetrating polymeric networks with high mechanical performances.

Chitosan a linear polysaccharide composed of D-glucosamine and N-acetyl-D-glucosamine. It is produced from partial deacetylation of chitin, the building material of most crustaceans and insects. Chitosan can form physically crosslinked gels by hydrophobic

interaction, hydrogen bonding, metal coordination, and electrostatic interactions with other polysaccharides, such as cellulose. Similar to other biopolymers, chitosan can be modified to form covalently crosslinkable hydrogels.

Collagen one of the major proteins in animal bodies. Collagen possess a well-defined hierarchical structure, from the individual amino acids, through the triple helix, all the way up to the fibril. In general, the primary repeating unit is always composed of glycine and two amino acids other than glycine. The sequence defines the supramolecular assembly and, hence, the resulting physicochemical properties. Collagen can form physically crosslinked gels by thermal heating, as well as covalently stabilized through chemical crosslinks, such as glutaraldehyde.

Gelatin a single strand of collagen triple-helix structures. They are produced through either acid (type A) or alkaline (type B) hydrolysis of collagen fibers. Gelatin can be easily gelled by cooling down the solution below 37 °C. Alternatively, gelatin can be chemically modified to form covalently crosslinked hydrogels, for example, by methacrylation (gelatin methacryloyl or GelMA).

Overall, natural polymer-based hydrogels are widely used for biomedical applications, owing to their intrinsic biocompatibility, biodegradability, and easiness of fabrication. However, their poor mechanics and lack of long-term stability limit their use for load-bearing applications.

1.3.2 Synthetic Polymers

To overcome the intrinsic limitations of natural biopolymers and expand the set of functionalities available for the fabrication of hydrogels, synthetic polymers have been investigated. As a general strategy, synthetic hydrogels are most frequently formed via free-radical polymerization, through the use of one or more monomers, a crosslinker, and an initiator. A non-exhaustive list of common synthetic polymer is reported below:

Poly(2-hydroxyethyl methacrylate) (PHEMA) can be prepared by free-radical polymerization of 2-hydroxyethyl methacrylate (HEMA), a neutrally charged monomer, in the presence of a crosslinker and a thermal- or photo-initiator. PHEMA hydrogels are optically transparent, mechanically stable, and have limited swelling ability. They are commonly used in ophthalmic applications, for example, in the fabrication of contact lenses.

Poly(ethylene glycol) (PEG) can be end-functionalized with several reactive groups, thus enabling several crosslinking strategies. For example, PEG can be chemically modified at both ends with acrylates, such that it can be polymerized without the

need of any crosslinker. However, the resulting material is rather fragile, such that its use is limited. To overcome that limitation, PEG can also be modified with physically reacting groups, such as host-guest pairs, or metal-coordination motives. Furthermore, PEG can be found with linear, 4-arm, or star-shaped configurations, thus increasing its the degree of control over its structure and intrinsic functionality.

Polyacrylamide (PAM) can be prepared by free-radical polymerization of acrylamide (AM), a neutral monomer, in the presence of a crosslinker and a thermal- or photo-initiator. PAM hydrogels are optically transparent and their mechanical properties and internal porosity can be tuned across a wide range. For this reason, they have been used in applications ranging from load-bearing applications to gel electrophoresis. Furthermore, they are bioinert and can be combined with several other monomers, including acrylic acid (AA), to introduce responsiveness to the system.

Poly(acrylic acid) (PAA) can be prepared by free-radical polymerization of acrylic acid (AA), a negatively charged monomer, in the presence of a crosslinker and a thermal- or photo-initiator. The backbone of PAA presents a large number of carboxylic groups, enabling its crosslinking through physical interactions (e.g. carboxylic groups with Ca^{2+} or Fe^{3+}). Furthermore, the presence of carboxylic groups renders PAA pH responsive. Additionally, PAA is charged under physiologic conditions, and hence can uptake large amounts of water, thus making it a great candidate as superabsorbent materials, for example, in diapers.

Poly(2-acrylamido-2-methylpropane sulfonic acid) (PAMPS) can be prepared by free-radical polymerization of 2-acrylamido-2-methylpropane sulfonic acid (AMPS), a negatively charged monomer, in the presence of a crosslinker and a thermal- or photo-initiator. Similar to PAA, PAMS polymers are utilized as superabsorbent materials and, in combination with ions, for load-bearing applications.

Poly(N-isopropylacrylamide) (PNIPAM) a derivative of AM monomer, hence can be crosslinked with similar strategies as the ones reported for PAM. Its polymeric form presents a coil-to-globule phase transition when the temperature of the environment is raised above a critical temperature (lower critical solution temperature, LCST, of around 34 °C). PNIPAM is a thermo-responsive hydrogel that is suitable for the fabrication of soft actuators.

Overall, depending on the initial polymer chosen, a large variety of hydrogels with either high stiffness or high toughness can be fabricated. This is mainly derived from the crosslinking selection: physical bonds will produce weak yet tough gels, whereas covalent bonds will provide stiff yet brittle materials, as summarized in Figure 1.6.
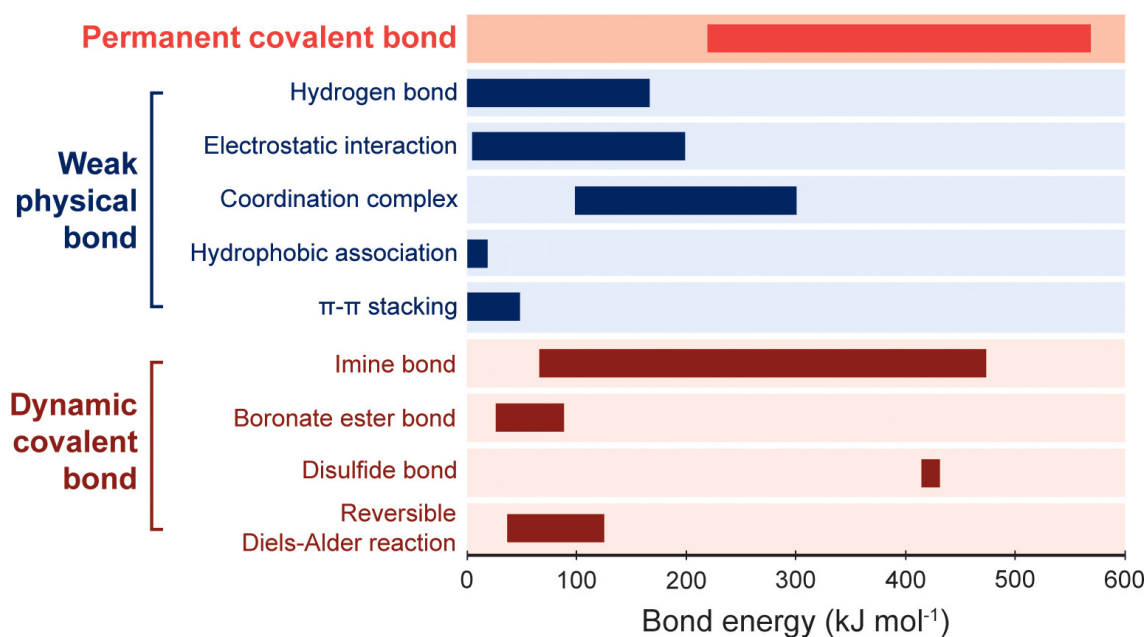
Figure 1.6: Bond energies of various types of permanent covalent, physical, and dynamic covalent crosslinks. Reproduced with permission [21]. Copyright 2021, American Chemical Society.

In the following section, I will discuss the mechanical properties of conventional hydrogel networks, namely stiffness and toughness, as well as the main strategies to reinforce them.

1.4 Controlling Hydrogel Composition: Reinforcement Strategies for Load-Bearing Applications

Covalent bonds can be relatively strong, but do not reform after fracturing. In contrast, reversible bonds are typically weak, but they may reform after breaking. As a result, differences in network topology correlates to differences in mechanical performance [51]. In the following subsections, I will introduce various network topologies and discuss their strengths and weaknesses for load-bearing applications.

1.4.1 Conventional Hydrogels

Conventional hydrogels are generally composed of a single network crosslinked by irreversible covalent crosslinks. These materials display a nearly perfect elastic behavior before fracture, with no dissipation across multiple loading cycles. The hydrogel stiffness can be controlled by varying crosslinker density and the overall polymer content. However, a higher crosslinker density is correlated to a shorter average mesh size, thus strongly reducing the maximum elongation of the system and hence its toughness. As a result, covalently crosslinked hydrogel mechanics generally display a brittle ceramic-like fracture behavior [51].

In contrast, hydrogels composed of a single network crosslinked by reversible crosslinks display a viscoelastic behavior. In such a network, monomers are held together by covalent bonds (e.g. typically a C-C backbone), while the polymer chains are crosslinked into a network by reversible interactions (e.g. electrostatic interactions). As a result, given that intra-chain bonds are much stronger than inter-chain ones, upon load the hydrogel is deformed because the reversible crosslinks break. While deformations can be permanent, physically crosslinked hydrogels might recover their internal damage upon load removal. As opposed to covalent hydrogels, physically crosslinked hydrogels display a ductile fracture behavior [51].

Individually, both strategies offer a limited control over mechanics, thus hindering their use for load-bearing applications. As a result, a combination of reversible and irreversible crosslinks is needed to overcome the intrinsic limitations of the two individual components. The following subsections will discuss unconventional hydrogel networks that have been developed to achieve extreme mechanical properties, as summarized in Figure 1.7.
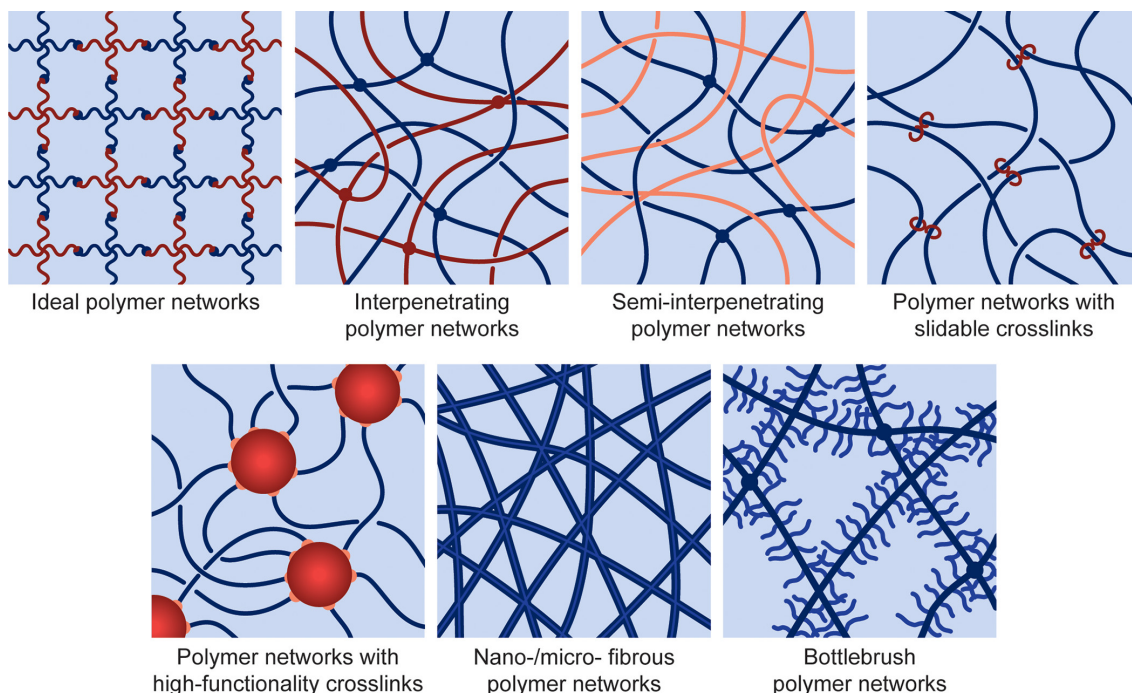
Figure 1.7: Schematics of polymer network architectures used in the fabrication of hydrogels with extreme mechanics. Reproduced with permission [21]. Copyright 2021, American Chemical Society.

1.4.2 Ideal Polymer Networks

Ideal polymer networks are polymer networks that have uniform chain length and functionality, and no defects [52]. As an example, telechelic tetra-arm PEG macromers are reacted to form an ideal hydrogel network. The near-ideal behavior of such gels is the product of crosslinked macromers with uniform arm lengths, that are reacted together at their loose ends producing a defect-free network. However, it should be noted that the large discrepancy between theoretical calculations and experimental validations in conventional hydrogel mechanics is given by the assumption of the material behaving as an ideal network, which is far from reality where a large variability of chain lengths and a considerable defect density negatively affect mechanics.

1.4.3 Double Network Hydrogels

Double network hydrogels, or more generally interpenetrating polymer networks, are gels composed of two interpenetrated networks, that are individually crosslinked and only connected by simple chain entanglements [53]. As a result of the physical entanglements, the two interpenetrated networks cannot be pulled apart unless the two networks are broken. They can be produced sequentially or simultaneously. In the sequential method, a single

network hydrogel is fabricated and immersed in a second gel-forming precursor solution. Then, the gel is exposed to a crosslinking reaction (e.g. UV free-radical polymerization) to form a second percolating network, as shown in Figure 1.8.
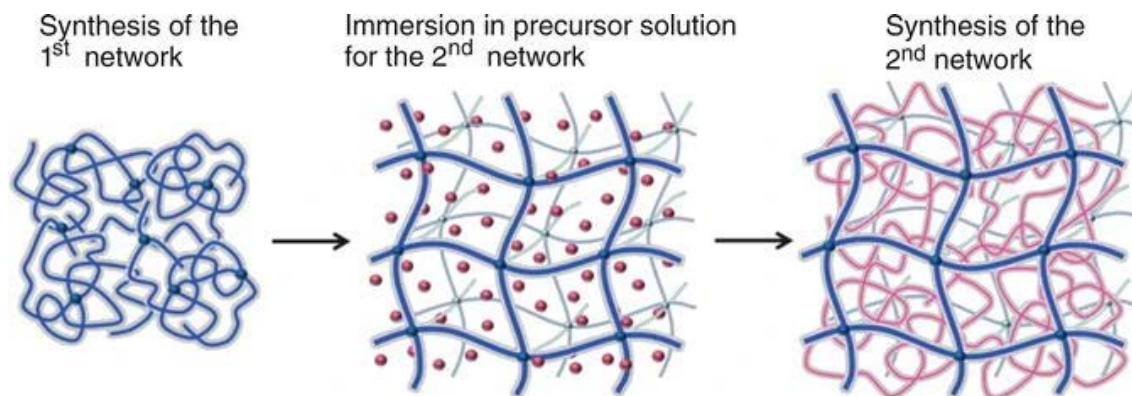
Figure 1.8: Synthesis process of a double network hydrogel. Reproduced with permission [54]. Copyright 2015, Springer-Verlag Berlin Heidelberg.

For example, double network hydrogels have been prepared by swelling PAMPS hydrogels in a solution containing AM monomers, crosslinker, and a photoinitiator, yielding a material with extremely high stiffness and toughness, two seemingly counteracting attributes [53, 55, 56]. In the simultaneous method, instead, two gel-forming solutions, a precursor solution and a polymer solution, are mixed together in a one-pot synthesis and converted into an interpenetrated network hydrogel. One remarkable example of this approach is the one-pot synthesis of PAM-alginate hydrogels with high stretchability and fracture toughness [57, 58]. This strategy is, by far, the most exploited technique for the fabrication of hydrogels with high mechanical performances, owing to the possibility to decouple stiffness and toughness within the same material [54, 59].

The fundamental design requirements to fabricate a stiff and tough double network hydrogel are summarized here [60]:

1. the first network is composed of a rigid and brittle polymer, generally a polyelectrolyte, while the second network is composed of a soft and ductile polymer, generally a neutral polymer

2. the molar concentration of the second network should be 20–30 times higher than that of the first network

3. the first network is highly crosslinked while the second network is loosely crosslinked

The high swelling capacity of a polyelectrolyte allows the uptake of a large volume of solvent. As a result, the first hydrogel network is able to absorb large quantities of the

second network precursor solution. While doing so, the polymer chains of the first network become stretched, thus making the hydrogel stiff and brittle. As a result, the crosslinked double network hydrogel displays an increase in stiffness compared to the pristine single network hydrogel [53, 54, 56], as shown in Figure 1.9.
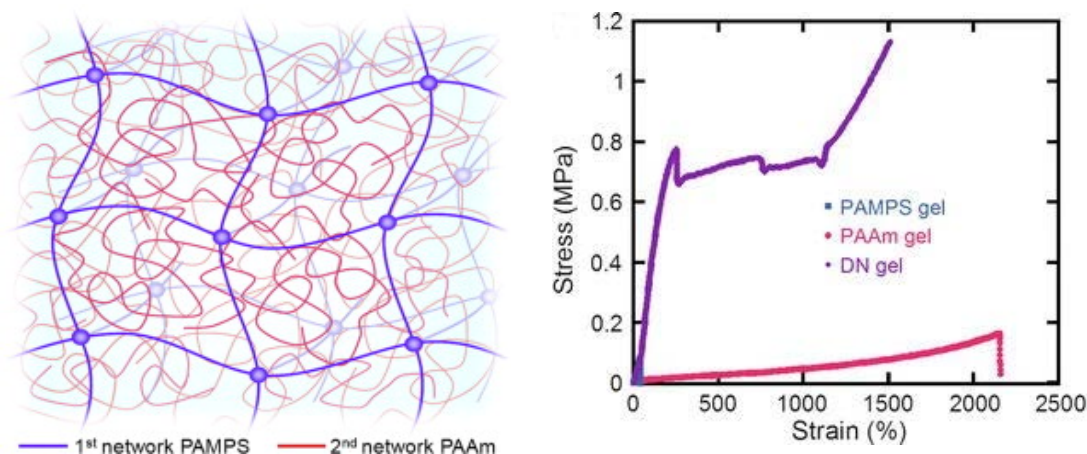
Figure 1.9: Left, Schematic representation of the swelling-induced stiffening of the first network. Reproduced with permission [56]. Copyright 2015, Springer-Verlag Berlin Heidelberg. Right, Stress-strain curve of a double network hydrogel. Synthesis process of a double network hydrogel. Reproduced with permission [54]. Copyright 2015, Springer-Verlag Berlin Heidelberg.

This is attributed to the entropic elasticity of the swollen hydrogel chains that counters the elongation of the material. A characteristic necking is also observed when the sample is stretched above a critical point. This behavior is correlated to a yielding plateau in the tensile curve and is attributed to the stretching of the loosely crosslinked second network that prevents a catastrophic failure of the material. As a result, the double network hydrogel displays a much higher toughness compared to its individual counterparts. Furthermore, when loaded below its ultimate fracture strength, the double network hydrogel displays a significant hysteresis, hinting at an effective stress dissipation within the double network. However, due to the irreversible fracture of the first network, any following cycles will result in a purely elastic behavior similar to that of a single network hydrogel, as shown in Figure 1.10.

Owing to the intrinsic design versatility of a double network hydrogel, a great variety of network combinations have been explored for load-bearing applications [21, 54, 59, 60, 61].

1.4.4 Coordination Complexes

Covalent crosslinks offer a high degree of mechanical stability. Under stress, covalent crosslinks break to dissipate energy. However, the intrinsic irreversibility of covalent
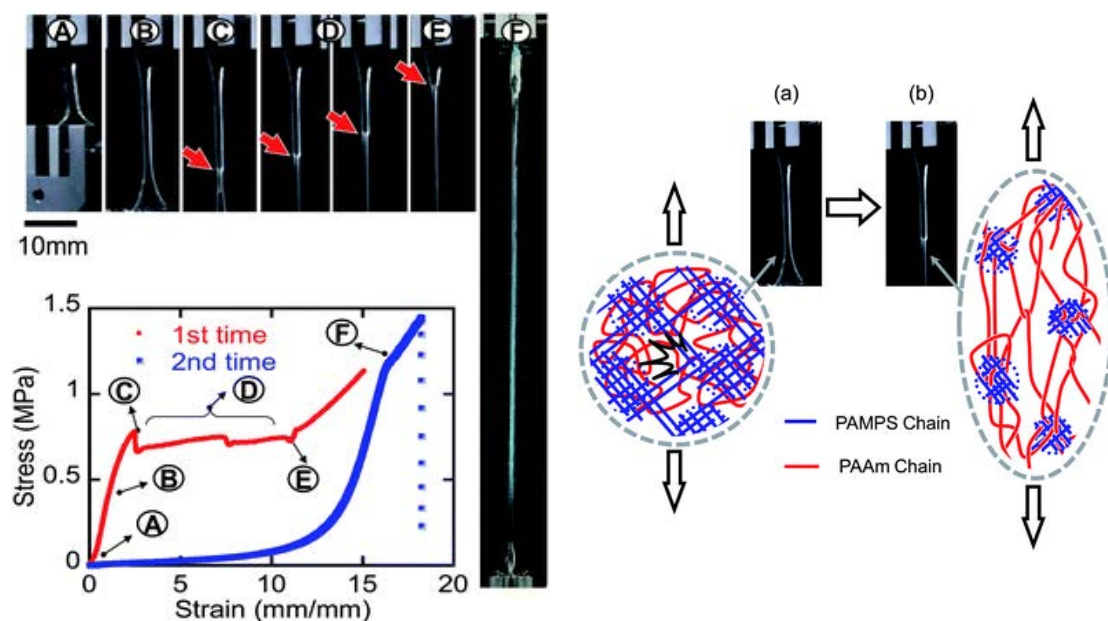
Figure 1.10: Left, Tensile curve of a double network hydrogel and pictures demonstrating the necking process. Right, Schematic representation of the fracture mechanism of double network hydrogels. Reproduced with permission [55]. Copyright 2010, Royal Society of Chemistry

bonds prevents any self-healing of the hydrogel network. Self-healing properties can be implemented in a hydrogel network if dynamic reversible crosslinks, such as coordination complexes, are used. Coordination complexes are a class of physical crosslinks based on the interaction of a metal ion and a surrounding array of organic ligands [62, 63, 64]. Coordination bonds are one of nature's favorite chemistries to build materials from. In general, metal-coordination bonds are formed via the donation of two electrons from the ligand to the metal ion. As a result, compared with traditional covalent bonds, these physical bonds possess increased capacity to break and reform, thus more dynamics, at the expenses of a reduced thermodynamic stability. Hydrogels crosslinked with metal-coordination complexes are conventionally fabricated by functionalization of a polymer backbone with chelating ligands, such as catechols, histidines, and carboxylates. When incorporated in a load-bearing hydrogel network, these bonds enable unique dynamic mechanical properties, owing to their intrinsic capacity to break and reform upon repeated loading. Furthermore, if incorporated in covalently crosslinked hydrogel networks, they can act as sacrificial bonds, thus increasing the overall fracture energy and toughness of the material [2, 65]. Compared to other reversible chemistries, metal-coordination bond strength and dynamic behavior can be more easily tuned by changing the organic ligand, the metal ion or its oxidation state, as well as by adding competitive ligands, thus making the system extremely versatile and useful in several applications [66, 67, 68]. Furthermore, heterogenous and hierarchical mechanical responses can be implemented with

metal-coordination complexes, owing to their high selectivity and specificity [69, 70]. However, coordination complexes are inherently weak such that they cannot bear significant loads and be used for structural applications.

1.4.5 Dynamic Covalent Crosslinks

Similar to physical crosslinks, dynamic covalent bonds can also act as reversible crosslinks. The energy of dynamic covalent bond is similar to that of covalent bonds but they can be cleaved on-demand by external stimuli. As a result, hydrogels built from dynamic covalent linkers are both mechanically robust and adaptable [71, 72]. Typical examples of dynamic covalent crosslinks include imine, boronate ester, and disulfide bonds. For example, PAM hydrogels containing disulfide crosslinkers have been synthesized and demonstrated similar mechanical properties as their conventional non-reversible counterparts [73]. Furthermore, disulfide bonds can be selectively degraded under mild conditions by exposing them to a reducing agent, such as glutathione, and tris(2-carboxyethyl)-phosphine [74]. The combination of the mechanical stability of covalent crosslinks together with their on-demand reversibility endows the material with unique dynamics, thus enabling their use in several applications, such as, for example, recyclable plastics, biomedical implants, or antifouling coating [71, 75, 76, 77, 78].

1.4.6 Other Strategies

Many other types of crosslinking strategies can improve mechanical properties, such as slide-ring crosslinks [79], electrostatic and host-guest interactions [80, 81, 82, 83, 84], or multifunctional crosslinks [66, 85, 86, 87, 88, 89, 90]. Similarly, filler-reinforced [91, 92, 93, 94], or phase separated hydrogels [95, 96, 97, 98] can display unique mechanical properties. All the strategies presented above have successfully expanded the toolbox available for the fabrication of hydrogels with superior mechanical performances. Although widely explored, these solutions have shown limited success in mimicking biological load-bearing tissues, a reason being the poor control over the internal network arrangement. Indeed, most synthetic hydrogels possess a rather homogeneous internal structure, while biological materials display a highly ordered, hierarchical arrangement. As a consequence, it becomes clear that chemistry alone is not enough to replicate nature's complexity. Structure, as well, overlooked for too long, must be taken into consideration. In the following section, I will discuss the main strategies that have been developed and implemented to introduce structural control in synthetic hydrogels.

17

1.5 Controlling Hydrogel Structure: Fabrication of Functionally Graded Materials

Mechanical and biochemical gradients are found throughout the body and provide structural integrity at transitional interfaces of tissues [99]. For example, bone displays a gradient in both radial and longitudinal directions. In the radial direction, bone is composed of a dense outer shell, known as the cortical bone, that evolves into a softer and more porous core, known as the trabecular bone. On the other direction, bone is composed of aligned collagen fibers, that bear the necessary compressive and torsional loads, thus allowing locomotion. By varying its structural properties, bone can withstand more complex loading profiles, while at the same time protecting the internal distribution of nutrients and waste [100]. Furthermore, at the interface between bone and soft connective tissues, such as ligaments and tendons, the material exhibits spatial variations in mineral concentration and collagen fiber orientation that enables an optimal load transfer across the joints. Similarly, articular cartilage possesses a highly graded tissue arrangement where collagen fibers are aligned parallel to the articular surface and are increasingly perpendicular as they approach the bone interface [101]. The design of functionally graded materials has the potential to reproduce the structural complexity found in nature, thus expanding the range of applications that can be achieved with synthetic manmade materials. As such, functionally graded materials, and more specifically graded hydrogels, can open up new frontiers for the fabrication of engineered materials with more complex architectures and locally varying composition. In general terms, this can be achieved by introducing porosity [102, 103, 104], precipitating biominerals [105, 106, 107, 108], or adding anisotropic fillers such as fibers [109, 110, 111, 112, 113], thus affecting material mechanics across multiple length scales, as shown in Figure 1.11.

The combination of these methods enables the fabrication of increasingly complex heterogenous materials, thus advancing the understanding of the influence of structural control in biological materials. In their simplest design, functionally graded materials are composed of two separate phases heterogeneously distributed within the same bulk material. For example, fiber-reinforced hydrogels represent one of the first successful example of composite hydrogels with anisotropic mechanical properties, namely fracture strength and elongation at break[115, 116]. While variations in chemical crosslinks will also result in changes in the nano- and micro-structure of hydrogels, the focus of this section will be exclusively on the design of hydrogels with structural anisotropy through the use of various processing techniques, such as photolithography, electrospinning, microfluidics, and 3D printing.
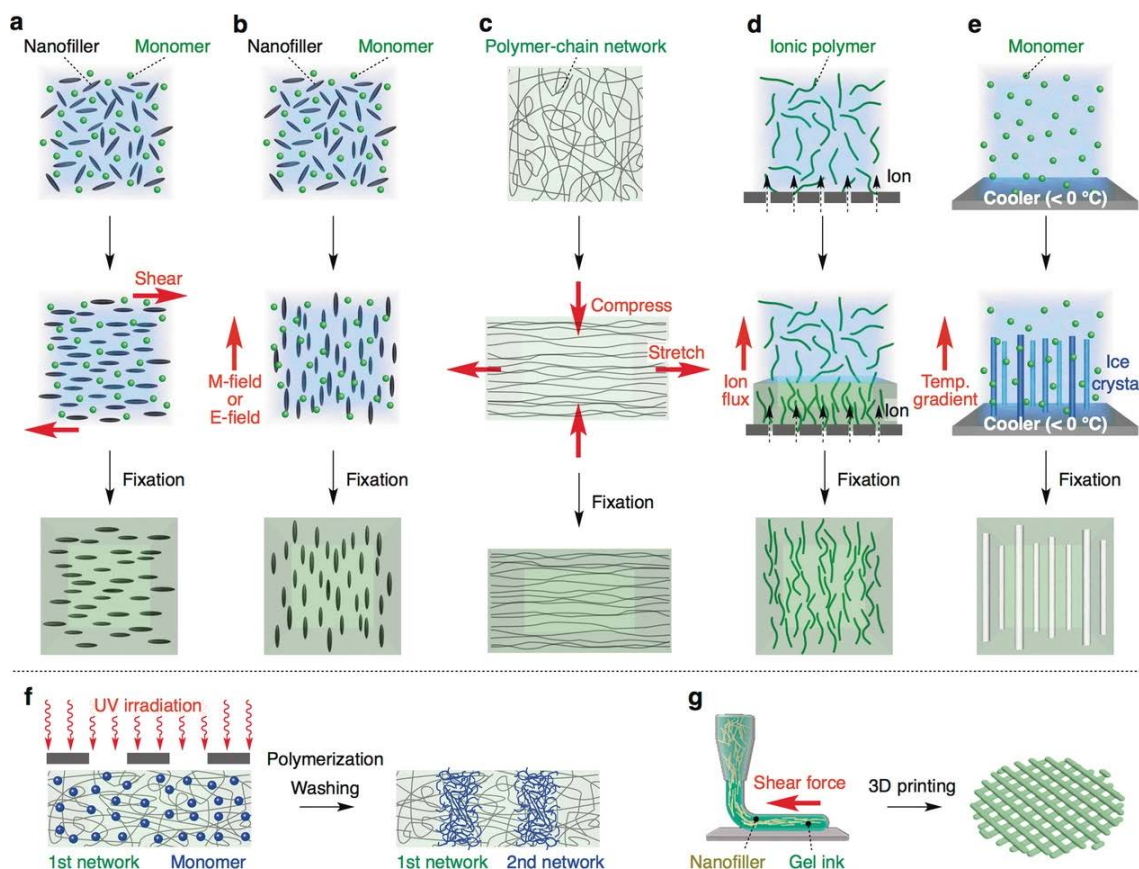
Figure 1.11: Synthesis of graded hydrogels by using (a) shear-aligned or (b) field-aligned anisotropic particles, (c) shear-aligned fibers, (d) ion diffusion, (e) freeze-drying or porogen encapsulation, (f) photolithography, and (g) 3D printing. Reproduced with permission [114]. Copyright 2018, Wiley-VCH.

1.5.1 Photolithography

Photolithography can be used in photosensitive materials to locally trigger a photochemical reaction that forms or destroys chemical bonds. For example, gradient photomasks have been designed with alternating UV-transparent and UV-blocking regions to modulate light transmission in the hydrogel matrix [117]. As an alternative to a fixed photomask, masks can be spatially moved while the material is being illuminated, thus creating spatiotemporal gradients within the hydrogel network. As a result, hydrogels with mechanical gradients can be easily formed [118]. However, such techniques are limited to rather thin samples due to the limited penetration of UV-light inside the hydrogel. A way to circumvent that is to use two-photon photolithography to form gradients within the bulk of the material at localized regions far from the surface [119, 120, 121]. This increased level of spatial control comes at the expense of the throughput.

1.5.2   Electrospinning

Electrospinning relies on the electrostatic repulsion between surface charges to continuously draw nanofibers from a viscoelastic fluid [122]. To obtain a stable fiber production, a high voltage is applied between a syringe loaded with a polymer solution and the collector. Above a critical voltage, a stream of solution is expelled from the fluid surface, forming a stable filament that initiates the drawing of the fiber. Electrospun fibers have been produced from a large variety of materials reaching sizes down to tens of nanometers. Based on the choice of the setup, the resulting fibers can be aligned to achieve hydrogel meshes with complex architectures. Furthermore, functionalities can be added to the spinning solution or after the electropsun scaffold is formed, thus making this technique an appealing choice for the fabrication of functionally graded materials. In a simple operation, several solutions can be spun in a layer-by-layer fashion achieving a structural control down to the single fiber resolution. In more advanced fabrication techniques, electrospinning has been coupled with an interpenetrating network architecture. As a result, aligned electrospun fibers have been embedded in a homogeneous gel matrix yielding a hydrogel fiber composite with anisotropic mechanical properties. The greatest advantages of electrospinning over other processing techniques are the rather inexpensive process and its scalability, thus enabling the fabrication of functionally graded scaffolds at larger scales. However, the high voltage applied to the system can damage cells or microorganisms, thus limiting the effective use of electrospinning for biomedical applications.

1.5.3   Microfluidics

Milder encapsulation of microorganisms and higher degree of structural control can be achieved with the use of microfluidics. Microfluidics exploits the unique dynamics governing fluids under confinement to generate concentration gradients within the same bulk material. For example, microfluidic gradients have been generated using T- or Y-shape junctions, flow-focusing devices, or pneumatic valves [123, 124, 125]. Despite the great control over fluid flow, cell encapsulation, and structural arrangement, microfluidics best performs at small operating volumes, thus making their use case limited to screening and small prototyping. As a consequence, while microfluidics can represent an excellent platform to investigate specific cell–cell or cell–environment interactions, it may not be suited for large scale material processing.

1.5.4 3D Printing

3D printing represents by far the most versatile technique to produce anisotropic heterogeneous materials. Indeed, it allows the fabrication of complex structures from a wide selection of building components, while being able to carefully control their local composition, thus enabling the rational design of heterogenous hydrogel constructs. In the past few decades, 3D printing of hydrogels has been largely investigated and a vast plethora of solutions are now available for the fabrication of functionally graded hydrogels, as summarized in Figure 1.12.
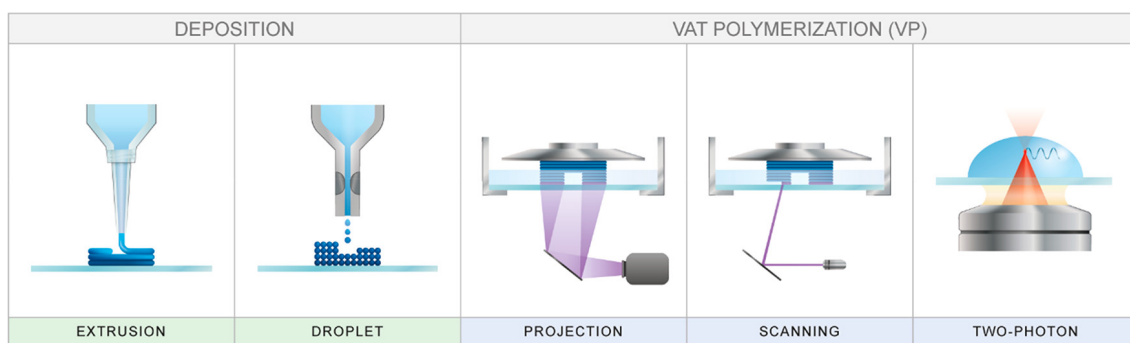
Figure 1.12: Schematic representation of deposition and vat polymerization technologies used for hydrogel 3D printing. Reproduced with permission [126]. Copyright 2020, American Chemical Society.

Deposition-based printing, and especially 3D extrusion, represents the most commonly used technique to fabricate relatively large hydrogel constructs, owing to its easiness of implementation and the relatively mild processing conditions. Furthermore, extrusion techniques allow multi-material printing, while maintaining a high throughput, thus increasing the overall printing complexity [127]. Despite their great potential and versatility, extrusion-based techniques suffer from a limited control over printing complexity, thus limiting their use for the fabrication of convoluted structures, overhangs, and out-of-plane features. To circumvent this, vat polymerization printing has been developed, in which a photosensitive resin is selectively solidified in a reservoir (the vat) through the localized exposure to a light source [126]. Vat polymerization can be used to obtain features with extremely high resolution, ideally down to the size of the illuminating light source. However, this comes at the expense of a reduced printing speed and impossibility to simultaneously print multiple materials, thus limiting its use to relatively small homogeneous constructs. A trade-off is then required when selecting the appropriate printing device.

In the following, I will focus my discussion on 3D extrusion printing. Depending on the setup chosen, this technique can be further catalogued in several different variants [128], as summarized in Figure 1.13 and detailed here:

21

Sacrificial and freeform embedded printing a viscoelastic matrix is used to support the 3D printing of hydrogel solutions with low viscosity. It allows the fabrication of soft hollow structures, such as blood vessels, that are then released from the supporting matrix by simple physical extraction. Owing to the possibility to selectively engineer the ink and the matrix, several combinations of hydrogel inks and supporting baths have been developed.

Co-axial printing based on wet-spinning, where a liquid solution is injected into a coagulation bath to produce fibrous structures, co-axial printing enables the extrusion of hollow fibers by co-extruding a hydrogel ink solution and its corresponding crosslinker solution. Common materials used are alginate or alginate-based mixtures due to the easiness of gelation.

Multi-material printing it generally involves the combination of multiple inks. In a simple configuration, multiple printheads with different inks are sequentially extruded to obtain heterogeneous structures. More complex configurations exploit bundling of various inks into a single nozzle. The different inks can be fed to the nozzle with arbitrary patterns, thus increasing the level of complexity achievable. Microfluidic mixers can also be combined with multi-nozzle printing to increase even more the level of structural control within the same extruded filament.

Continuous chaotic printing the printhead is made of a cylindrical housing encompassing a Kenics static mixer, with two or more ink inlets. As the inks pass through the cylinder, they become increasingly mixed, thus forming a lamellar structure that enlarge the interface between the adjacent inks. This technique enables the formation of highly heterogeneous structures within the same filament, as opposed to conventional extrusion techniques where only an inter-filament heterogeneity can be obtained.
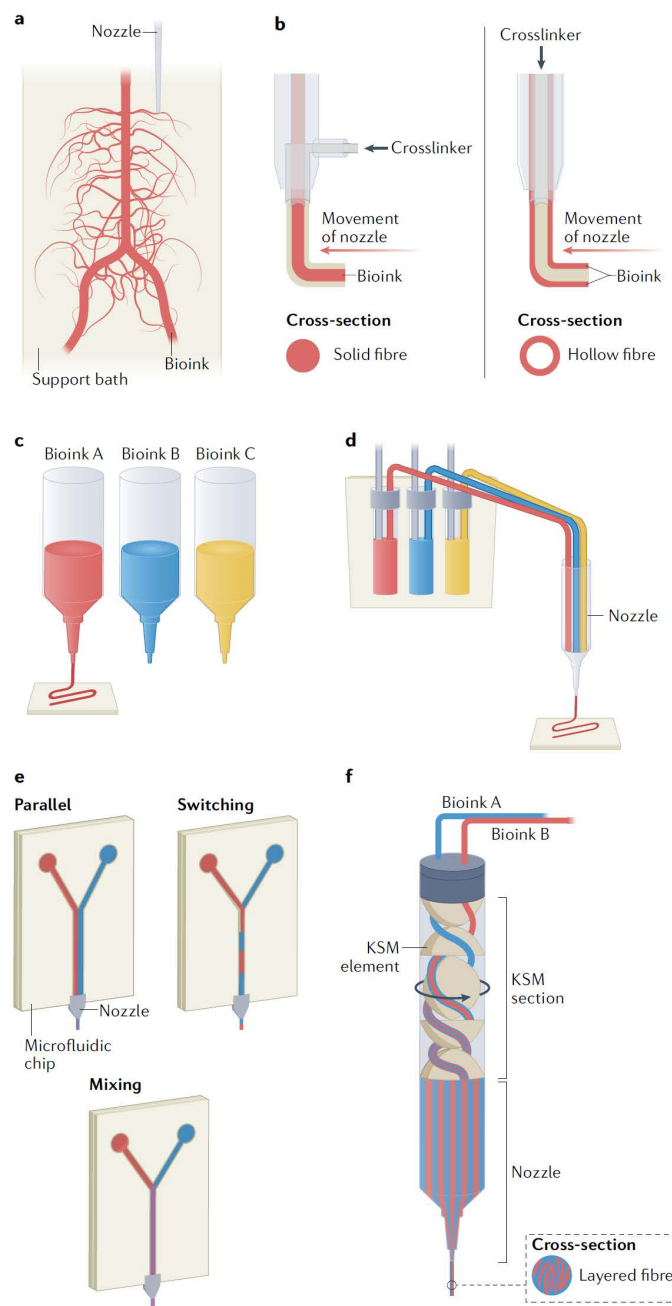
Figure 1.13: Schematic representation of 3D extrusion technologies. (a) Embedded, (b) co-axial, (c) multi-nozzle, (d) multi-material, (e) microfluidic, and (f) chaotic printing. Reproduced with permission [128]. Copyright 2021, Springer Nature.

Printability of an ink is closely related to multiple rheological and non-rheological parameters, such as extrudability, printing uniformity, and shape fidelity. As a whole, printability defines how well a printed object matches the original digital design. Despite the lack of consensus as to how to properly evaluate the printability of an ink, multiple quantitative

approaches have been developed and formally adopted in an attempt to univocally assess the quality of a print, as summarized in Figure 1.14.
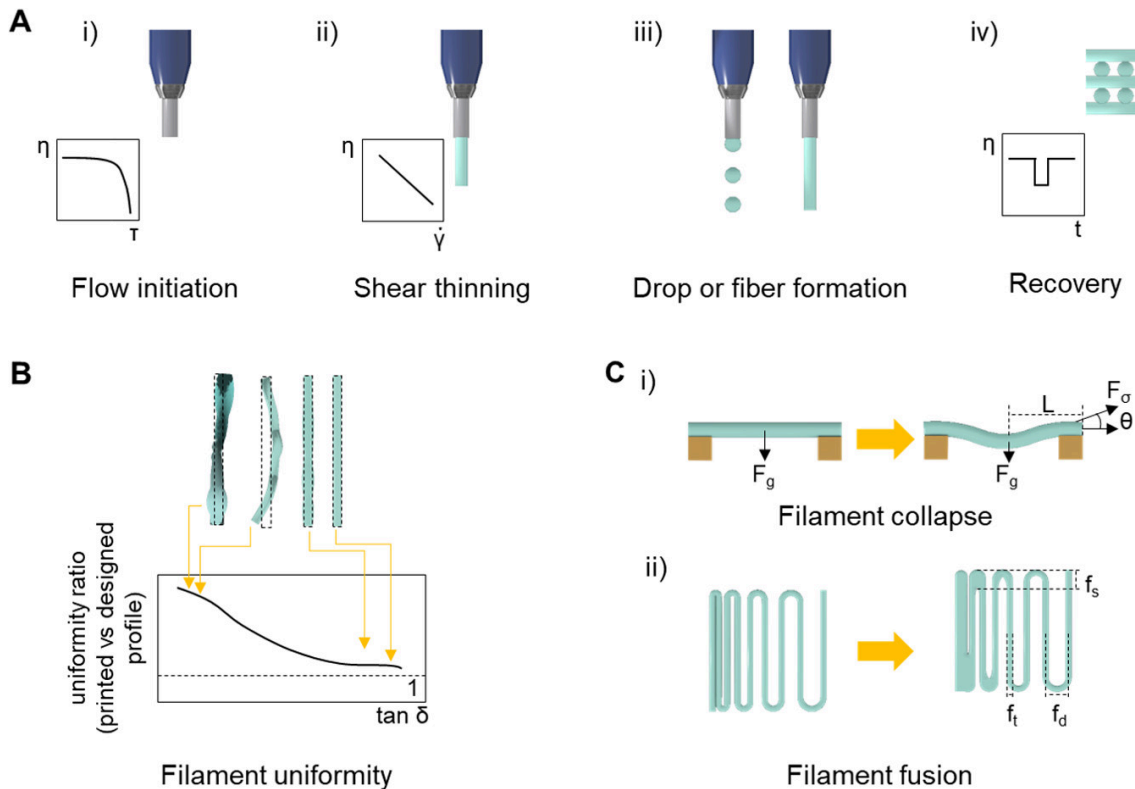
Figure 1.14: Printability design parameters. (a) Rheological and (b,c) non-rheological parameters. Reproduced with permission [127]. Copyright 2020, American Chemical Society.

Among all the possible printability parameters, we differentiate between rheological and physicochemical parameters. Rheological parameters discuss the deformation and flow behavior of materials under the influence of external applied forces. Physicochemical parameters, instead, determine the stability and resolution of the final printed construct. Overall, inks suitable for 3D extrusion should display both flow and shape-retention properties. The most important parameters that quantify an ink performance are discussed below and are divided into rheological parameters (RH), and physicochemical parameters (PC):

Viscoelasticity (RH) the property of displaying a viscous flow under shear and an elastic shape retention at rest. This property can be determined by oscillatory rheology and it is represented by two parameters: the storage modulus G' and the loss modulus G" [129].

Shear-thinning (RH) property of a non-Newtonian fluid, where increasing shear rates

correlate with a decrease in viscosity.

Yield stress (RH) the stress that has to be exceeded for a viscoelastic material to deform. A material yield stress is correlated to the number of crosslinks or entanglements within the ink.
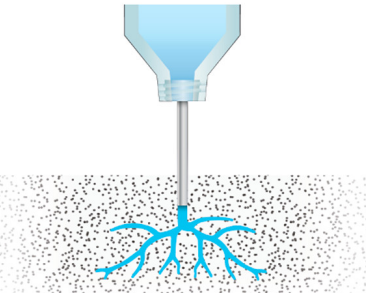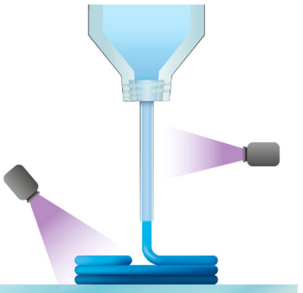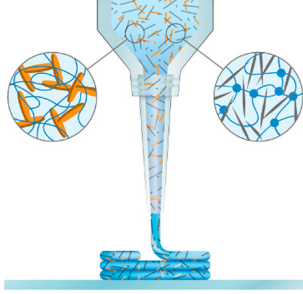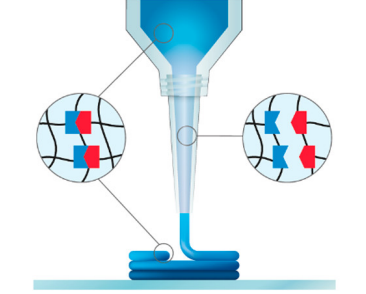
Flow point (RH) the stress that has to be exceeded for a viscoelastic material to flow.

Shear-recovery (RH) property of a viscoelastic material that describes the transition kinetics from a fluid-like (sol) to a solid-like (gel) state upon removal of shear.

Extrudability and filament formation (PC) can be assessed by direct observation of the ink morphology at the nozzle tip. Extrusion force, filament diameter, and extrusion continuity are generally considered to evaluate the quality of an ink.

Printing and shape fidelity (PC) can be assessed by direct observation of the printed construct. Filament shape, pore geometry, and macroscopic shape are generally considered to evaluate the quality of a print.

For proper assessment of an ink performance, all the parameters that influence the extrusion, deposition, and assembly of a printed construct must be carefully evaluated, thus making the design of hydrogel inks for 3D extrusion printing a challenging task. For example, conventional inks based on high molecular weight polymers display a shear-thinning behavior and a relatively low yield stress but poor shape fidelity. A reason behind this is the slow shear-recovery of the ink that causes an overflow of the already extruded material, thus affecting the final printing resolution. To overcome this intrinsic limitation, several strategies have been implemented to improve printability of hydrogel inks, such as the use of a supporting matrix, the simultaneous UV-crosslinking, the addition of inorganic rheological modifiers, the use of host-guest chemistries, or the use of a jammed or entangled precursor solution, as detailed in Figure 1.15.

Figure 1.15: Common strategies to achieve good extrusion printability. Reproduced with permission [126]. Copyright 2020, American Chemical Society.

In the following section, I will discuss how the implementation of a jammed granular solution can achieve both structural control and local varying composition without compromising printing fidelity and overall physicochemical properties of the final construct.

1.6   Combining Structure and Composition: Granular Hydrogel Design

Key to finally bridging the gap between synthetic and natural materials is the ability to synergistically combine structural control and local varying composition. Inspired by nature, especially by the unique formation mechanism of the mussel byssus, scientists have developed a new approach to produce heterogeneous hydrogels with precise control over

their internal structure and local composition down to the tens of μm. This technique utilizes micrometer-sized hydrogel particles, known as microgels, that are assembled into macroscopic materials, referred as granular hydrogels [130].

Microgels may be produced into a range of shapes and sizes utilizing methods that can be compatible with the encapsulation of various biological moieties, including cells and drugs [131]. Furthermore, they can be created from both natural and synthetic polymers, thus extending the range of possible applications. Their most competitive advantage resides in their physical behavior: compared to polymers in solution, where the dynamic is controlled by thermal fluctuations, microgel behavior is dominated by gravity and frictional forces, thus facilitating their handling and increasing their versatility. As a result, they can be utilized as individual components in suspension, embedded in a second matrix as fillers, or jammed together to form a granular macroscopic material. Hydrogel microparticles possess a set of unique properties compared to bulk hydrogels that renders them appealing for their use in biomedical and materials science applications. On one hand, their small size and interparticle interaction lead to a shear-thinning behavior, that enables extrusion and injection without any chemical modification [132]. On the other hand, microgels are inherently modular, such that particles with different sizes, shapes, and compositions can be mixed together to form highly heterogeneous materials. In the following, I will introduce the methods used to fabricate microgels, with a particular focus on size, distribution, and throughput. Then I will discuss the requirements and emerging properties of jammed granular hydrogels, with a particular focus on rheology, and mechanics. Finally, I will focus on the use of microgels for 3D printing applications, highlighting the unique potential of such materials to attain a better control over both structure and composition.

1.6.1 Microgel Fabrication Techniques

Microgels can be produced from several fabrication techniques, including batch emulsification, microfluidics, lithography, spraying, and mechanical fragmentation, as shown in Figure 1.16. As a general concept, hydrogel particles are produced from precursor-loaded droplets, that are converted into microgels through various crosslinking mechanisms, including UV- or T-induced free-radical polymerization, enzymatic crosslinking, and click-chemistry.

Each fabrication technique imposes constraints on the precursor formulation, the throughput, and the final microgel properties. For instance, batch emulsion and mechanical fragmentation offer the simplest yet fastest way of producing polydisperse microgels from a greater variety of precursors. By contrast, microfluidics and lithography trade in the production speed in exchange for a more controlled particle size and shape. As a result, the
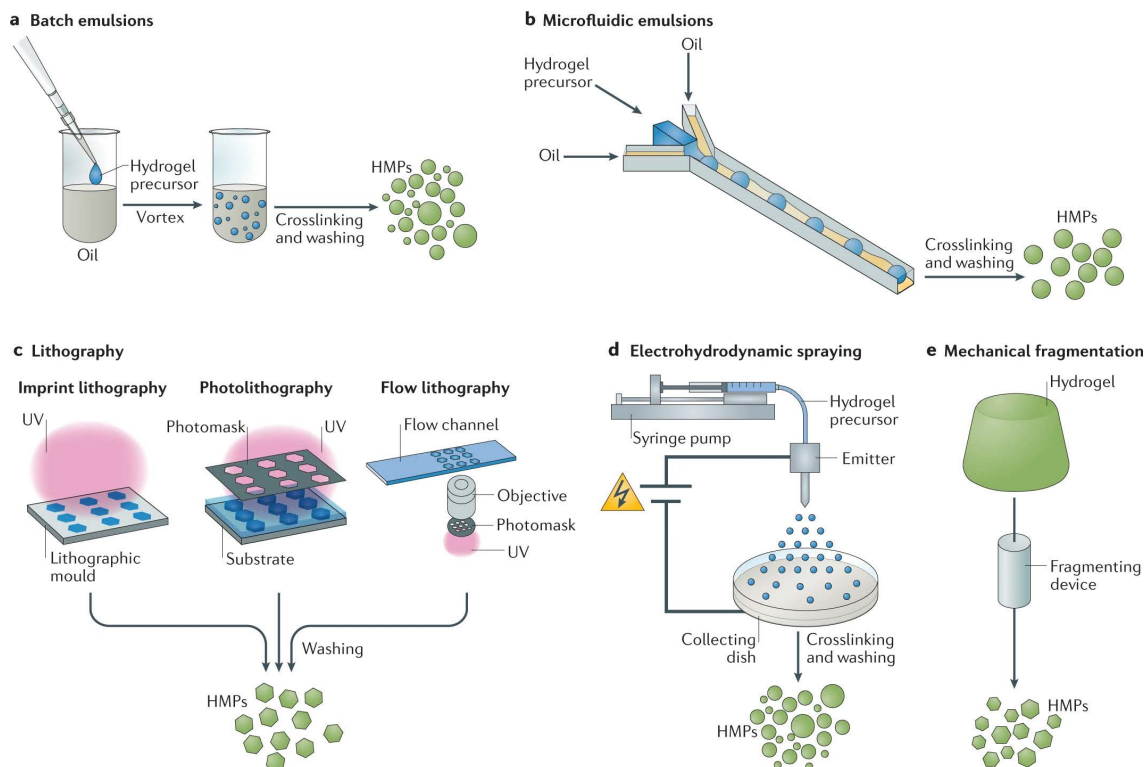
Figure 1.16: Microgel fabrication techniques. Microgels can be fabricated through (a) batch or (b) microfluidic emulsification, (c) lithography, (d) spraying, or (e) mechanical fragmentation. Reproduced with permission [131].Copyright 2019, Springer Nature.

appropriate production technique should be chosen based on the microgel final attributes and intended applications.

Batch-Emulsion Techniques

Emulsion-based microgel production utilizes precursor-loaded water-in-oil emulsions that are converted into particles. In a batch process, the hydrogel precursor solution (i.e. monomers, crosslinker, and initiator) is added in a container together with oil and surfactant and mixed to obtain a kinetically stable emulsion. The energy required to break down the aqueous solution in individual droplets can be provided to the system by several means, including shaking, vortexing, stirring, and sonication. The duration and extent of mixing, as well as the precursor viscosity and surfactant concentration, can influence the size and polydispersity of the resulting droplets. Once the stable emulsion is produced, the individual droplets are converted into particles, and the oil phase is discarded. In general, several cycles of washing, centrifugation, and filtration are required to obtain a solution containing microgels.

The main advantages of batch emulsification techniques are their easiness of implementation, the high throughput, and the wide material and crosslinking chemistry selection. On the other hand, their main limitations are the intrinsic polydispersity, batch-to-batch variations, and the rather cumbersome purification process.

Microfluidic Emulsion Techniques

Controlled droplet formation can be achieved through the use of microfluidic setups, such as flow-focusing [133, 134, 135], step-emulsification [136, 137], and millipede devices [138, 139]. In these systems, the aqueous phase is injected in a channel that intersects with a continuous flow of the oil phase. A combination of hydrophobic interactions and shear forces at the intersection of the two flows is responsible for the break down of the water phase in individual droplets. Furthermore, the geometry of the microfluidic channels and the flow rate can be controlled to obtain various droplet sizes, while maintaining a narrow size distribution. In addition, different crosslinking profiles allow for the fabrication of hexagonal prismatic [140] or anisotropic rod-shape particles [134, 141], thus expanding the range of properties attainable with particles produced in such devices.

The main advantages of microfluidics are the precise control over the final droplet size and the extremely low dispersity index. On the other hand, the requirements for the precursor solution are more stringent to ensure a continuous production of monodisperse droplets. As a result, low viscosity solutions with rather fast gelation mechanisms are preferred to ensure good quality of the final product. Furthermore, compared to conventional batch emulsification techniques, microfluidics production rates are relatively low, with few remarkable exceptions [136, 137, 138].

Lithography

Lithographic techniques are less commonly used than the techniques previously discussed. To achieve more complex microgel shapes, various lithographic techniques can be applied. For instance, with imprint lithography, a hydrogel precursor is casted on a templated mold and crosslinked to obtain the negative of the design. In photolithography, instead, a photomask is used to transfer a pattern to the hydrogel precursor.

The main advantage of lithographic techniques is the ability to precisely control the geometrical features of the masks, thus resulting in superior control over the shape and monodispersity of the microgels. The great advancements in microfabrication techniques have increased the level of particle complexity that can be obtained with such processes.

The main drawbacks of such techniques are the relatively low throughput and the initial cost of mask fabrication.

Spraying Techniques

Spraying techniques are a set of processes where the hydrogel precursor is sprayed or nebulized in air and then crosslinked on the flight or by exposure to a gelling bath. For instance, electrohydrodynamic spraying consists of a syringe with a voltage applied, where the precursor is extruded from a metal needle and broke into small emulsions [142, 143]. The resulting droplet size is a function of the applied voltage, needle diameter, and polymer flow rate. Surface acoustic wave spraying, instead, exploits a piezoelectric nebulizer that breaks down the precursor solution thanks to the formation of in-plane surface acoustic waves [144]. There, the droplet size is a function of the frequency applied to the device.

The main advantage of spraying techniques is the high production rate of relatively small droplets and the possibility to obtain a stable gelation in air, thus avoiding the need of a continuous oil phase. However, tight constraints are posed in terms of precursor viscosity.

Mechanical Fragmentation Techniques

The easiest way to produce large quantities of micrometer-sized hydrogel particles is through the use of mechanical fragmentation methods. In this approach, a preformed bulk hydrogel is broken into particles by various routes, such as sieving, milling, and blending [145, 146]. For example, hydrogels have been sieved through a nylon mesh to obtain hydrogel microstrands [147]. In another example, bulk hydrogels have been reduced into small particles by cryogrinding [148].

The main advantages of mechanical fragmentation are the unparalleled throughput, the solvent-less production method, and the wide material selection. The major limitations are the poor control over the shape and size of the produced particles, as well as the rather harmful process if cells are encapsulated in the gel.

1.6.2 Properties of Jammed Microgels

Regardless of their fabrication route, microgels can be used as building blocks for the fabrication of macroscopic granular materials. Under certain stress and temperature conditions, individual microgels can be concentrated above a certain particle-volume fraction (φ) to achieve a jamming transition [130]. The easiest way to obtain a jammed particle

state is by removing the excess continuous phase that surrounds the microgels [132, 149]. The resulting paste behaves as a collective macroporous solid-like material possessing a shear-thinning behavior, as summarized in Figure 1.17.
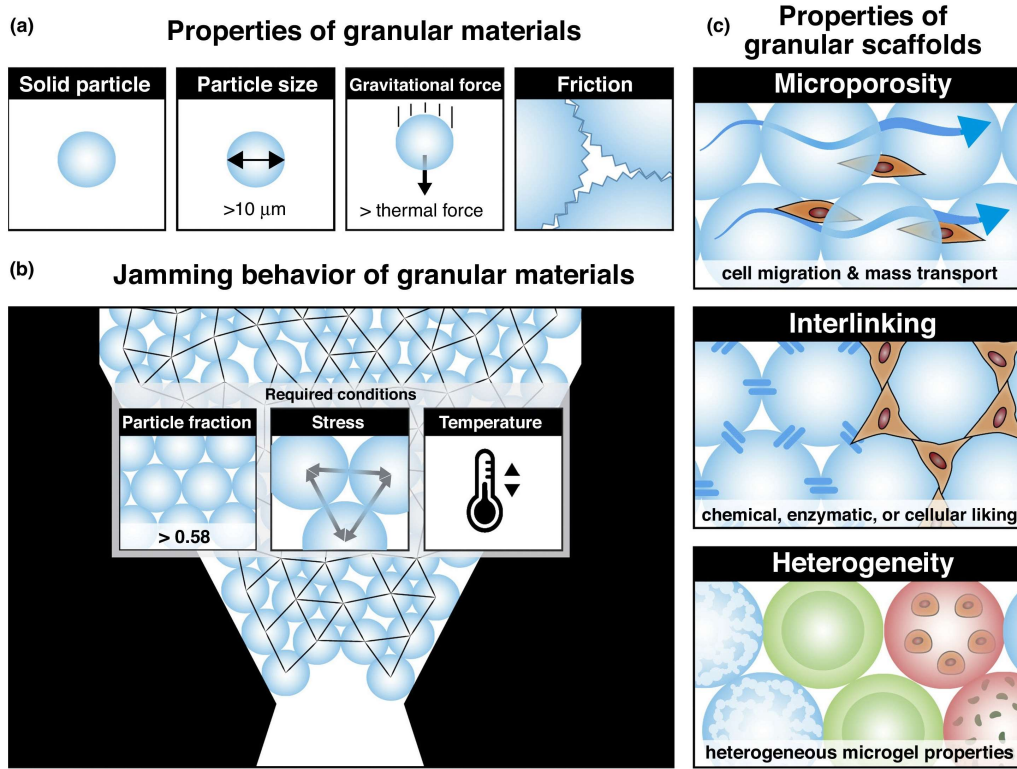
Figure 1.17: Properties of microgel-based materials. (a) Properties of granular materials, (b) properties of jammed microgels, and (c) properties of granular scaffolds. Reproduced with permission [130]. Copyright 2019, Elsevier.

Conventionally, jamming of hard spheres can be categorized into: random loose packing ($\varphi > 0.58$), random close packing ($0.58 < \varphi < 0.64$), and perfect packing ($\varphi \approx 0.74$). Jammed microgels would lie in a random close packing configuration. However, owing to their intrinsic deformability, interparticle friction, polydispersity, and shape, microgels could concentrate to $\varphi > 0.74$, up to an ultraclose packing configuration ($\varphi \approx 1$) [150], as shown in Figure 1.18.

The collective behavior of jammed microgels gives rise to unconventional properties that cannot be found in traditional synthetic hydrogels, namely injectability, macroporosity, and heterogeneity.

Injectability the shear-thinning behavior and the relatively small microgel size allow

a Polymer network   Hydrogel microparticle   Granular hydrogel

nm   µm   mm

b Loose packing   Close packing   Ultraclose packing

Increasing particle-packing fraction
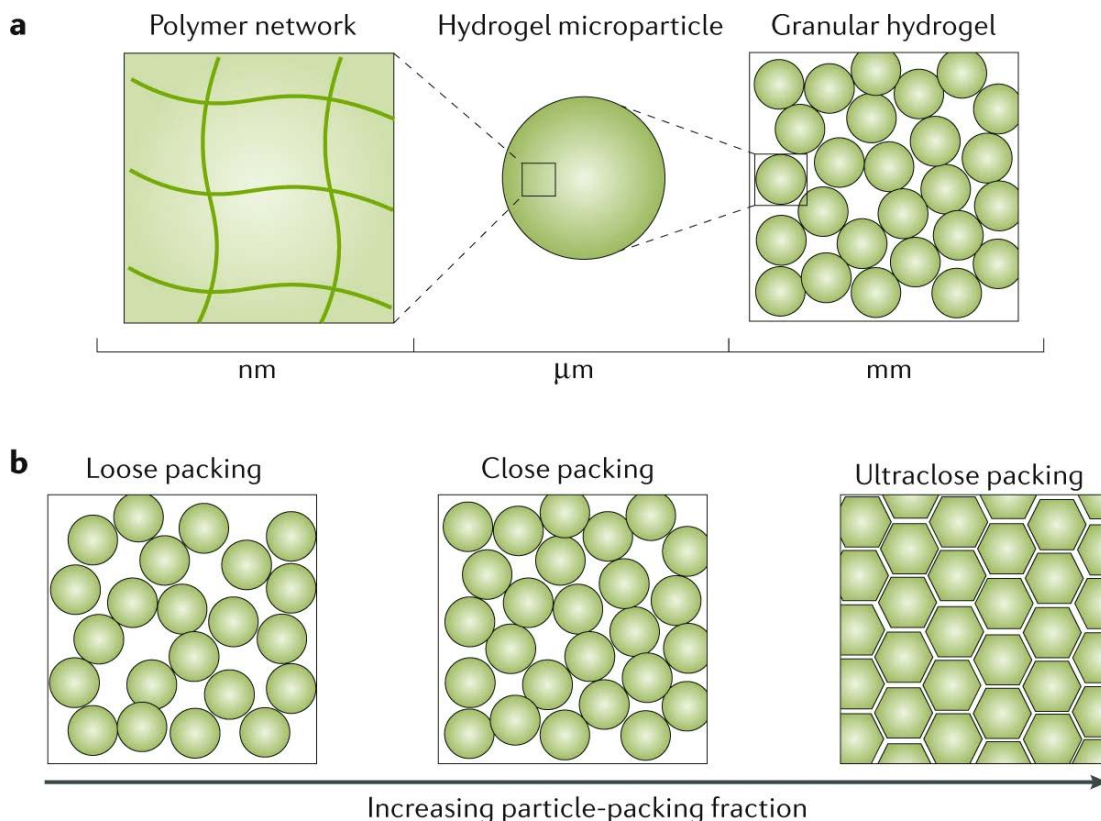
Figure 1.18: Granular hydrogels. (a) Length scales in granular hydrogels. (b) Packing of jammed microgels. Reproduced with permission [131]. Copyright 2019, Springer Nature.

particle flow at low pressures, followed by an almost instantaneous recovery of the solid-like behavior upon release. This enables their extrusion through syringe needles or catheters, thus making them suitable for minimally invasive injections, cavity filling, and 3D printing.

Macroporosity the interstitial space among microgels endows the granular hydrogel with porosity proportional to the particle size, thus producing micrometer-sized pores compared to the nanometer-sized one found in conventional bulk hydrogels. This additional porosity allows a faster mass transport across the scaffold, as well as an easier cell invasion in a biological environment.

Heterogeneity microgels of different species (e.g. chemistry, shape, and cargo) can be mixed together, until uniformly distributed, or extruded to achieve controlled local varying composition in a macroscopic construct.

All these properties contribute to the additional degrees of freedom that granular materials possess compared to more homogeneous conventional hydrogels. Furthermore, such physicochemical properties are key for the application of granular hydrogels to various

fields, including drug delivery [151], tissue engineering [152, 153, 154], load-bearing applications [155, 149], and 3D printing [147, 156, 157, 158, 159, 160]. While all worth mentioning, the following paragraphs of this section will be devoted to the discussion of their use in additive manufacturing, as well as on their application as load-bearing materials.

1.6.3 Additive Manufacturing of Granular Hydrogels

Microgels display a shear-thinning behavior if concentrated above their jamming threshold. Solely given by the granular nature of the precursor, this property has attracted great interest in the field of additive manufacturing due to its material versatility and easiness of implementation. Whether used as supporting bath [161, 162, 163, 164] or as inks [165, 154, 166, 167], granular hydrogels represent a powerful tool that allows to decouple physical and chemical requirements of the final product, thus enabling the processing of a larger variety of precursors, including those with a low viscosity. For instance, commercially available microgels (Carbopol ETD 2020) were used as supporting bath for the fabrication of complex structures made from a variety of materials, including silicones, hydrogels, colloids, and cells [161], as shown in Figure 1.19.
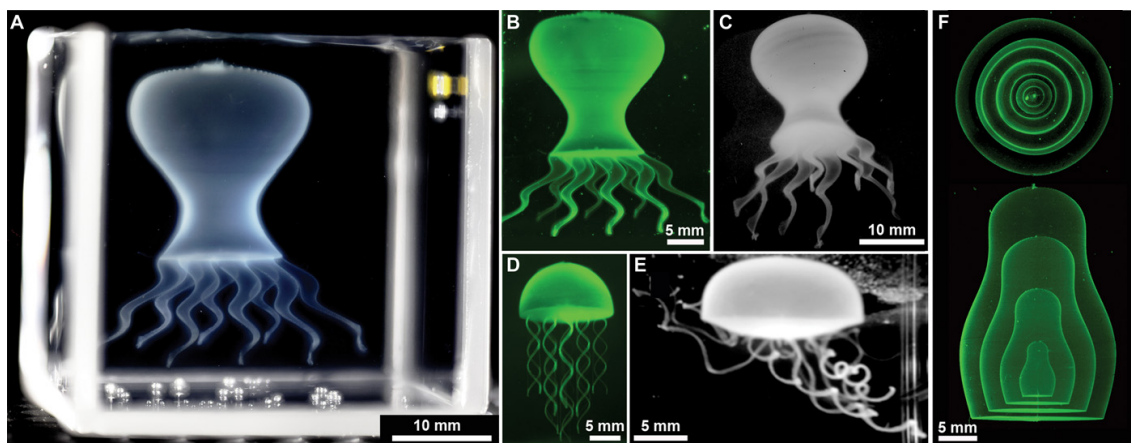
Figure 1.19: Examples of 3D embedded printing. Reproduced with permission [161]. Copyright 2015, Science.

The success of granular hydrogels has been even greater with their application as building materials (i.e. inks). Indeed, upon jamming, microgels can be extruded with relatively low pressure and under mild conditions (e.g. temperature) through conventional 3D printing machines, thus making them suitable for the fabrication of soft scaffolds for tissue engineering. Furthermore, microgels can be used as vectors for the encapsulation and local delivery of biologics, including therapeutics and living cells, thus making them much more

versatile and appealing compared to conventional hydrogel inks [168, 169]. For example, jammed microgel inks, referred as granular bioinks, have been used for the fabrication of granular scaffolds with high cell viability [170, 154, 166, 171]. Remarkably, this strategy allows the fabrication of heterogeneous scaffolds across different length scales, thus increasing the structural complexity of the final printed construct.

1.6.4 Reinforcement Techniques for Granular Hydrogels

Despite the favorable properties demonstrated by the use of a granular precursor, granular hydrogels fail to meet the minimum mechanical requirements, namely high stiffness and toughness, needed for their application as load-bearing materials. This failure is due to the fact that microgels are held together by weak interparticle adhesion, such that minimal forces cause their relative displacement, with subsequent loss of mechanical integrity. Current hydrogel applications demand for more advanced physicochemical properties, including high mechanical performances. To achieve a synergistic combination of structural control, local varying composition, and load-bearing properties, novel strategies to reinforce granular hydrogels have been derived, such as the use of interparticle crosslinking, back-filling, and secondary interpenetrating networks [172], as summarized in Figure 1.20.

Based on the type of reaction involved, we can classify them as interfacial, embedded, or interpenetrated networks.

Interfacial Crosslinked Networks

Microgels can be synthesized or functionalized such that they present reactive species on their surface. Upon extrusion, granular hydrogels can be mechanically reinforced by crosslinking adjacent particles either by chemical reactions or supramolecular interactions, such as free-radical polymerization, click chemistry, enzymatic reaction, metal-coordination, and electrostatic interactions. In free-radical polymerization, acrylated monomers or polymers are used to form the initial hydrogel particles. Once the construct has been assembled, the unreacted moieties left in the microgel network are exploited to form interparticle crosslinks. However, their poor control and intrinsic toxicity limit their application to non-biological systems. Alternatively, click chemistry reactions can be implemented in a granular hydrogel to covalently crosslink adjacent particles with high specificity and under mild conditions. For example, thiol-ene click chemistries and Michael addition have been used to stabilize 3D printed constructs, thus making them free-standing and insoluble in water. Yet, their mechanics is far from sufficient for load-bearing applications. A similar behavior is observed if interparticle crosslinks are introduced with the help

of enzymes. For instance, peptide-based microgels have been enzymatically crosslinked in a mechanically stable granular hydrogel through the interfacial reaction of lysine- and glutamine-rich domains. Microgels can also be reversibly linked through non-covalent interactions, such as metal-coordination or electrostatic coupling, thus forming tougher, self-healing constructs. This is achieved, for example, through the surface functionalization of hydrogel particles with chemical moieties that are responsive to certain metal ions (i.e. Fe^{3+}, Al^{3+}, etc.) and can direct the formation of physical crosslinks among individual particles. Another alternative consists in fabricating zwitterionic microgels or combining hydrogel particles with opposing electrostatic charges to increase their degree of interaction, thus enhancing the overall mechanical integrity of the granular hydrogel. However, all the proposed solutions provide minor improvements to the mechanical performances of granular hydrogels, most likely due to the relatively short interparticle crosslinks compared to the actual microgel size.

Embedded Networks

To further improve mechanics of granular hydrogels, microgels can be embedded in a gel-forming precursor solution, such that they can be reinforced with more conventional bulk techniques. Whether they constitute the majority of the ink or they act as rheological modifiers, microgels can be premixed and extruded with various polymers, such as alginate, gelatin metacryloyl (GelMA), or poly(vinyl alcohol) (PVA). As a result, the final construct will benefit from the favorable shear-thinning behavior of microgels, as well as the reinforcement effect of bulk hydrogels. However, this comes at the expenses of a reduced porosity. For example, a granular hydrogel composed of gelatin microgels and a gelatin matrix has been produced displaying an 8-fold increase in Young's modulus compared to their homogeneous counterpart. While these solutions offer a better control over mechanics, their range of tunability remains relatively limited, such that they cannot be used for load-bearing applications.

Interpenetrated Networks

A more recent strategy to reinforce granular hydrogels utilizes the high swelling property of microgels to load a second gel-forming precursor solution inside preformed hydrogel particles. Once assembled, a secondary crosslinking locks the structure in shape, thus enabling the formation of an interpenetrated hydrogel network. This solution is reminiscent of the well-known process for the fabrication of double-network hydrogels, where a second precursor solution is loaded in a pre-existing hydrogel network and then crosslinked to

reinforce it. As a result, a granular hydrogel with high mechanical integrity can be easily fabricated, expanding its use to more structural applications. Furthermore, the ability to trigger the on-demand formation of the second network provides a better control over printing and stabilization compared to conventional 3D printed materials. Remarkably, the secondary crosslinking is independent of the assembly process, allowing the fabrication of structures with isotropic mechanical performances, an attribute impossible to obtain with most conventional 3D printing inks. The strong improvement in mechanical properties is attributed to the efficient load transfer from the secondary network to the primary microgel network. As a result, the use of an interpenetrated network overcomes the limitations of previously discussed strategies, namely the poor interfacial adhesion of neighboring hydrogel particles.
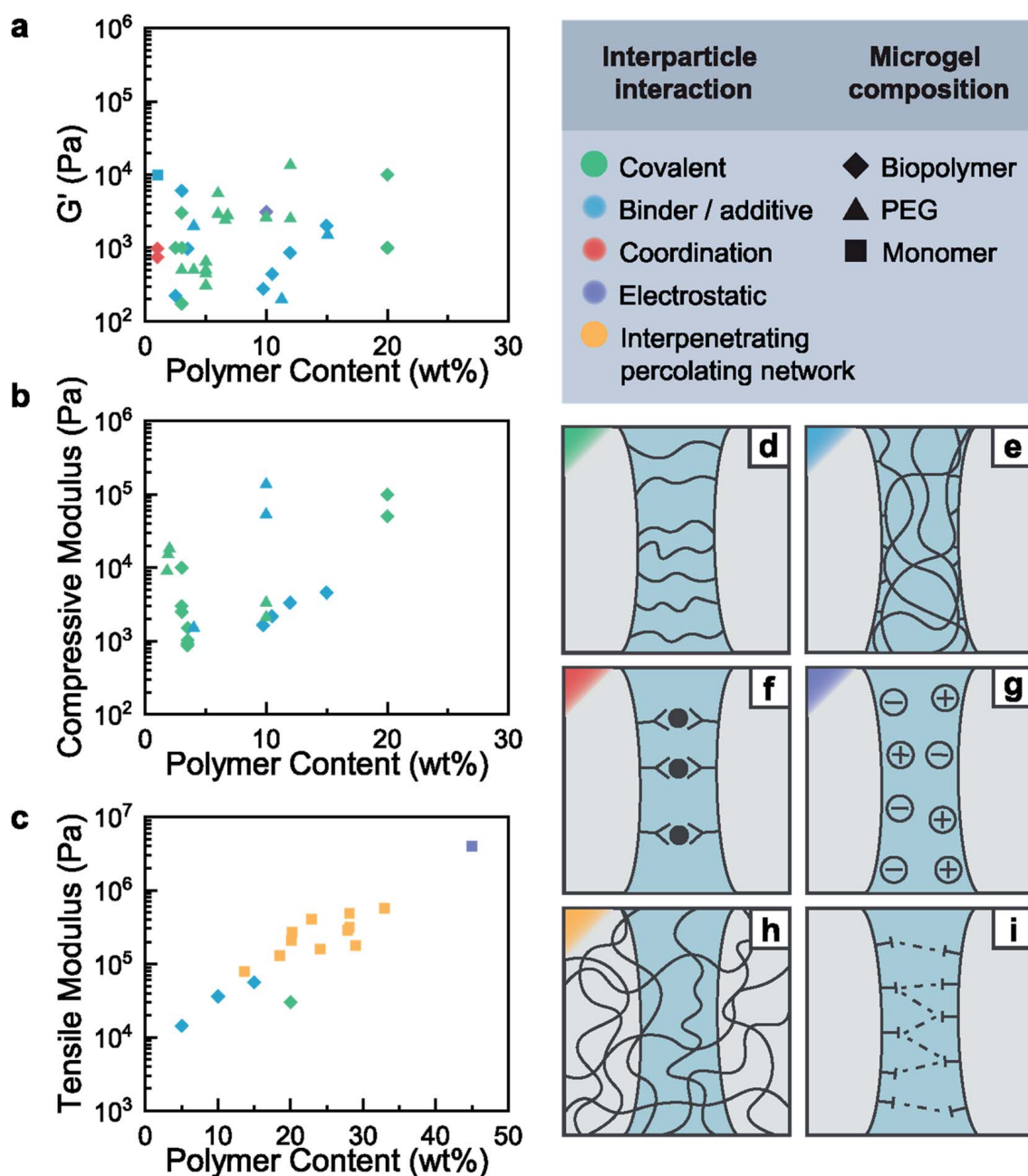
Figure 1.20: Reinforcement techniques for granular hydrogels. Ashby plots of (a) G', (b) compressive modulus, and (c) tensile modulus of various granular hydrogels as a function of their polymer content. Granular hydrogels can be reinforced with (d) covalent, (e) small molecule binding, (f) coordinating, (g) electrostatic, (h) interpenetrated, or (i) hydrophobic crosslinks. Reproduced with permission [172]. Copyright 2022, Royal Society of Chemistry.

1.7 Beyond Bioinspired Materials:
The Next-Generation of Engineered Living Materials

Despite the great improvement in hydrogel design and mechanical performances discussed in the previous sections, the last step to finally bridging the gap between natural and synthetic soft materials has yet to be made. The fundamental mismatch that still exists pertains to the last, almost unexplored dimension: time. Indeed, manmade materials, and especially hydrogels, show an intrinsic lack of self-regulation and adaptation that strongly hinders their real-life applications. Most synthetic constructs are immanent by definition: the scientist designs the material with certain properties, manufactures it, and deploys it for operation. However, there is little to no room for the introduction of adaptive or self-growing features, that would allow the material to self-regulate to sustain environmental changes. This is in stark contrast with biological materials, where nature is able to grow, renew, and adapt in response to external stimuli.

A strategy that would render synthetic hydrogels responsive to changes in the external environment, thus introducing a certain degree of compliance to the material, could push the boundaries of hydrogel design and could finally enable more complex applications in the field of soft robotics and tissue engineering. In this regard, a new approach for the fabrication of smart responsive hydrogels has emerged, where synthetic materials are combined with living microorganisms that are able to transform their environment with unprecedented control [173, 174, 175]. This combination constitutes a paradigm shift as nature is no longer a source of inspiration but it is the actual maker. As a result, engineered living hydrogels possess the ability to grow and adapt to a dynamic environment with greater complexity than ever reported before.

Engineered living hydrogels are a new class of living systems comprising a microorganism and a scaffold [173]. This combination increases the degrees of freedom for the design of synthetic materials. In general, the microorganism can be engineered to display certain properties, such as sensing, chemical production, and resource transformation, while the hydrogel matrix can be designed to exert mechanical or chemical gradients, or to serve as barrier to spatially separate different microbial populations. Based on the processing technique and microbial cell chosen, an almost limitless selection of engineered living materials can be fabricated, with many applications, as exemplified in Figure 1.21.

The main goals of engineered living material research include encoding for a wide variety of functional materials, drawing on many environmental sources of energy and matter, directing the assembly of complex structures across multiple length scales, and spatial and temporal environment adaptation [175]. In the following paragraphs, I will discuss
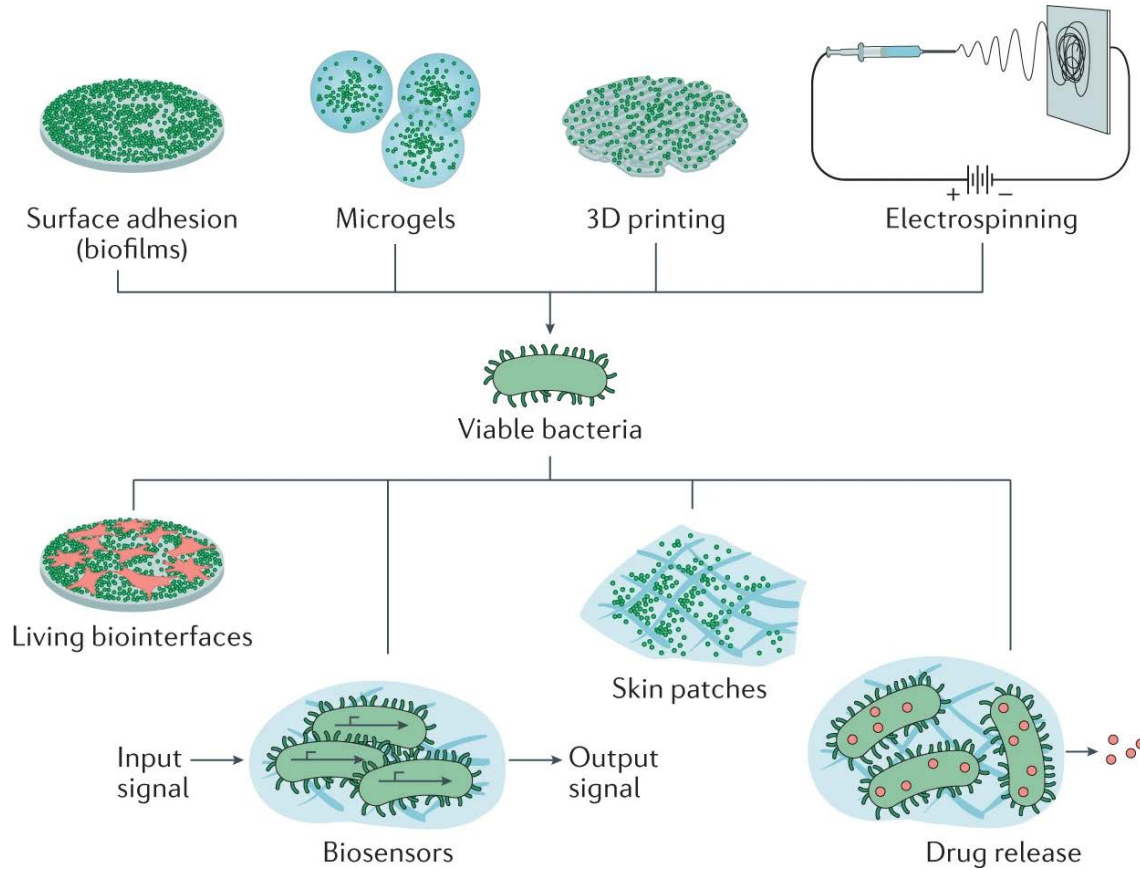
Figure 1.21: Engineered living materials. Reproduced with permission [176]. Copyright 2021, Springer Nature.

matrix-cell interactions and restrict my discussion to technologies where living cells (i.e. bacteria) partially fabricate or direct the assembly of the bulk material. I will focus the discussion on engineered living hydrogels based on bacteria that are not directly related to tissue engineering or regenerative medicine.

1.7.1 The Living in the Material: Bacteria for Engineering Living Hydrogels

The core concept of engineered living materials is the idea that microorganisms are the main character in play and are responsible for the material synthesis, self-organization, and adaptation of the structure in response to external stimuli. A straightforward translation of this statement can be made if bacteria are selected as the powerhouse for material fabrication. Indeed, most bacteria proliferate at high rates, can be easily genetically engineered, and can secrete several extracellular matrix components, such as polysaccharides, and proteins [177]. Polysaccharides are produced by most species of bacteria in a wide

variety of compositions and structural organizations. In general, they serve as an adhesive interface, as well as a physical barrier to protect the microorganism from the external environment. Modification of their chemical configuration and production remains a challenge, due to their poorly defined structure. Extracellular proteins are also a common component in the extra cellular matrix in the form of amyloid fibers, pili, and flagella. As opposed to polysaccharides, proteins can be easily engineered to impart different functionalities to the material. As a result, specific structures and amino acids sequences can be encoded in the bacteria genome for the production of engineered proteins, either by metabolic or genetic engineering, as shown in Figure 1.22.
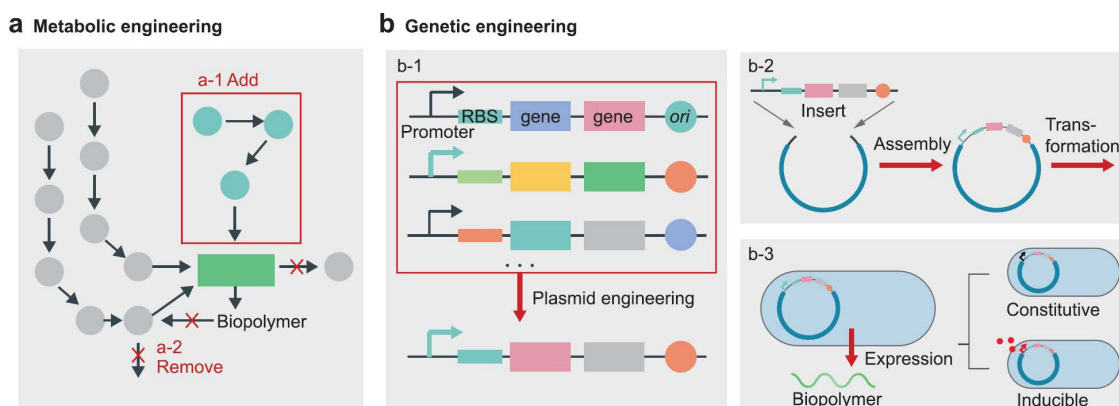
Figure 1.22: Engineering pathways. Bacteria can be modified by (a) metabolic or (b) genetic engineering. Reproduced with permission [173]. Copyright 2022, Wiley-VCH.

Among the various polysaccharides produced by bacteria, the most attractive for materials engineering is cellulose. Bacterial cellulose possess several unique properties compared to other naturally occurring polymers, such has high crystallinity and hence extremely high stiffness [178, 179]. Without any modifications, bacterial cellulose produced by the *Gluconacetobacter xylinus* is commonly used in medical and food applications. To enhance biopolymer production or alter its chemical composition, metabolic engineering strategies have been established in the past decades. In parallel to more traditional engineering approaches discussed so far, novel strategies involving directed evolution have also been investigated [180, 181]. Besides bacterial cellulose, protein-based amyloid fibers are produced by microorganisms, such as *Escherichia coli* [182]. All these biologically produced materials contribute to the formation of stable 3D biological composites, as schematically shown in Figure 1.23.

Another fundamental property of microorganism-produced materials is their ability to self-repair in response to structural damages. For example, microbial cells have been mixed in concrete or soil to heal cracks and prevent structural failure by inducing carbonate pre-
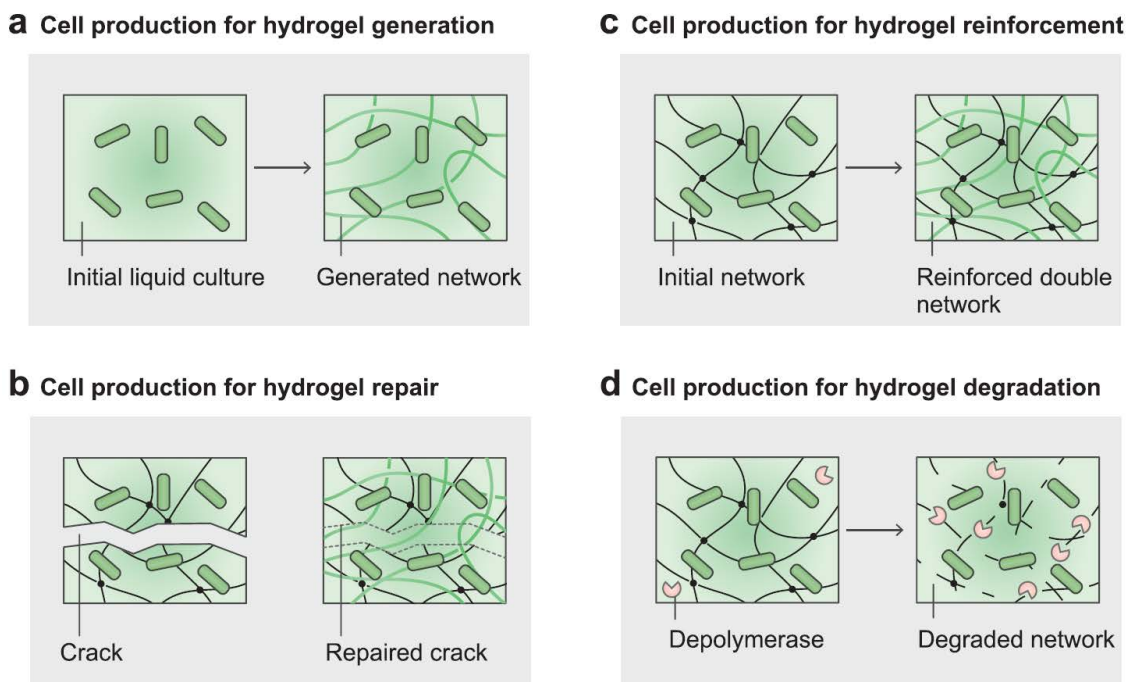
Figure 1.23: Bacteria-matrix interactions. (a) Bacteria can autonomously form their hydrogel matrix. Alternatively, bacteria can be embedded in a hydrogel to endow the engineered material with (b) self-healing, (c) local reinforcement, or (d) degradation abilities. Reproduced with permission [173]. Copyright 2022, Wiley-VCH.

cipitation as part of their metabolic activity [183, 184]. In addition to regeneration and self-repair, materials can be reinforced by living microorganisms. For instance, microbial cells can secrete chemical compounds, such as monomers, that can react and form an interpenetrated polymer network within the already existing matrix, thus mechanically strengthening the composite material [185]. Lastly, microorganisms can induce the degradation of their scaffold material. The degradation can be triggered either by mechanical instabilities, such as the growth-induced network deformation [186, 187], or by chemical cues, such as the naturally occurring decomposition of biopolymers [188] or the enzymatic degradation of synthetic petroleum-based polymers [189].

Besides the reciprocal influences between living microbial cells and hydrogel matrices discussed above, the engineered living material can also interact with the external environment, thus enabling their use in several applications [190, 191], as summarized in Figure 1.24.
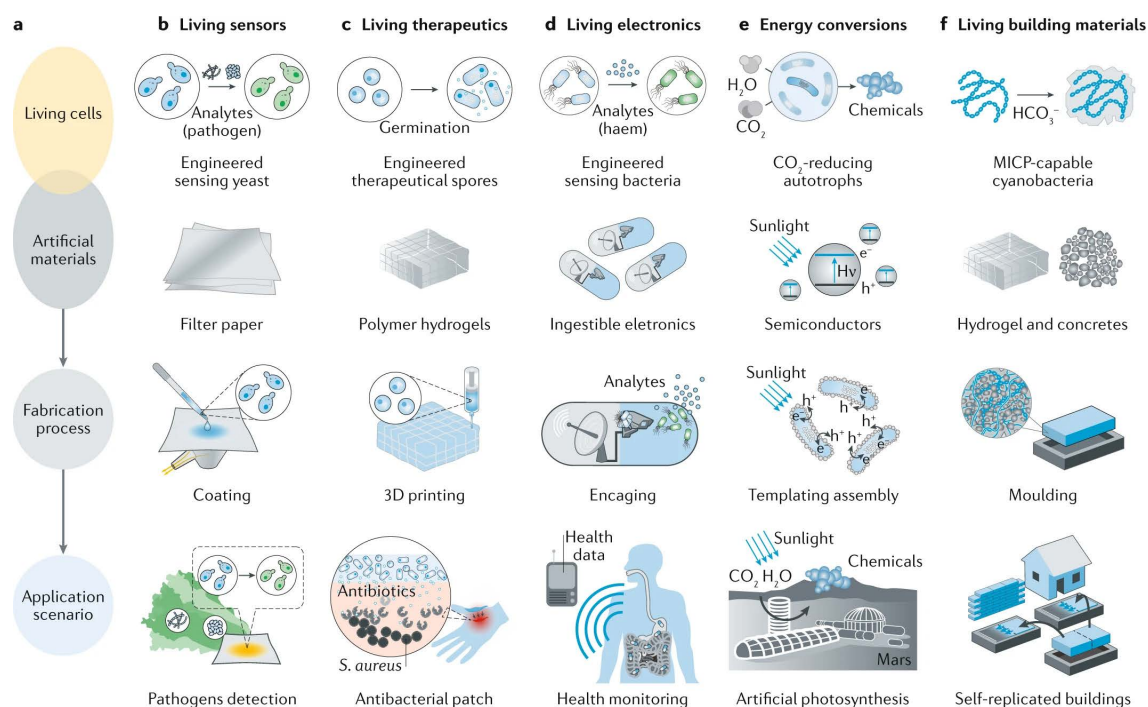
Figure 1.24: Applications of engineered living materials. Engineered living materials have been developed for their application as (b) sensors, (c) therapeutics, (d) electronics, (e) energy conversion, and (f) building materials. Reproduced with permission [190]. Copyright 2021, Springer Nature

In the following section, I will discuss the combination of engineered living materials with 3D printing technologies for the fabrication of responsive living scaffolds.

1.7.2   3D Printing of Engineering Living Materials

3D printing technologies are relatively well-established for printing mammalian cells for tissue engineering, thus being referred to bioprinting. Recently, novel applications that use microbial cells as living components in combination with a gel scaffold have been reported. Extrusion-based bioprinting has become the preferred technique due to its simplicity, high cell viability, and compatibility with several ink formulations [192]. Furthermore, the microbial-loaded ink, known as the bioink, should possess sufficient viscosity to allow a good printing resolution, as well as a rapid gelation to retain the intended geometry [176]. For example, a solution of alginate and *Escherichia coli* was extruded in a printing bath loaded with calcium chloride to trigger alginate gelation upon contact [193]. In another example, a bioink composed of hyaluronic acid, κ-carrageenan, fumed silica, and a photoinitiator was employed to 3D print *Pseudomonas putida* and *Acetobacter xylinum* [194]. Similarly, a pluronic-based bioink has been used to fabricate catalytically active living materials [195], as shown in Figure 1.25.
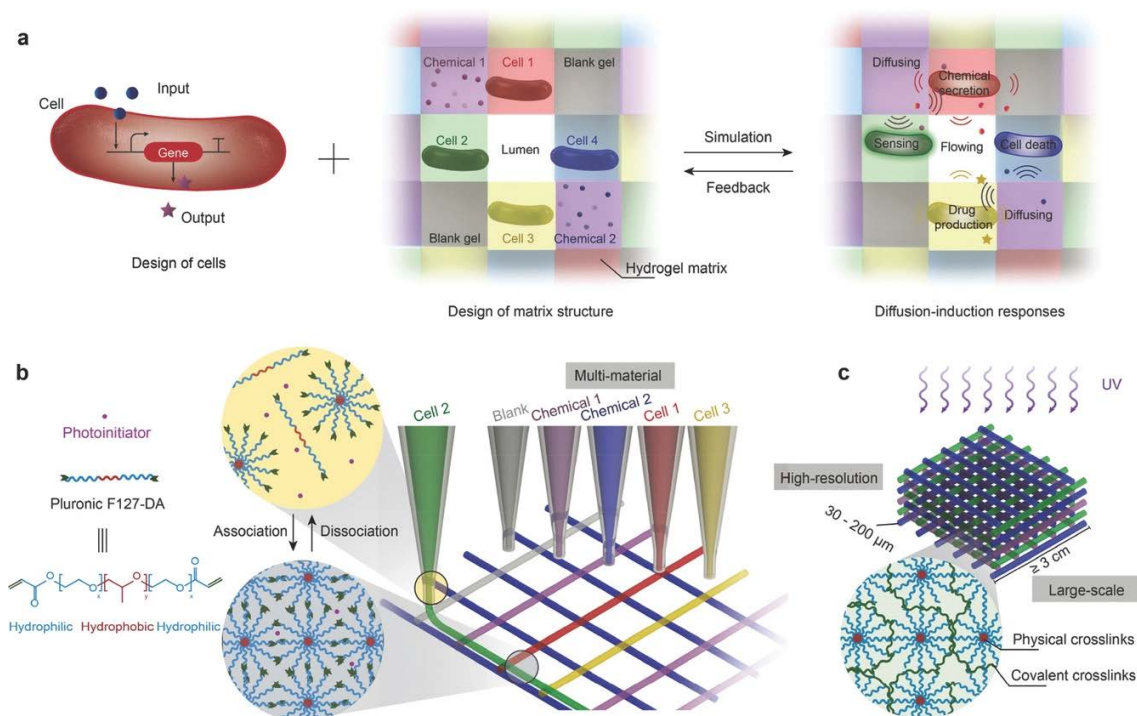
Figure 1.25: Design and 3D printing of large-scale, high-resolution living responsive materials. Reproduced with permission [195]. Copyright 2017, Wiley-CH.

This field of engineered living materials has bloomed in the past couple years owing to the wide range of bioinks and microbial cells available [176, 196, 197, 198]. Furthermore, the competitive economical advantage of rapid prototyping makes 3D bioprinting extremely appealing for the design of engineered living materials. However, none of the reported examples so far have fully leveraged the living contribution of bacteria to rationally control the mechanical properties of the final construct. This breakthrough would be advantageous for the fabrication of more sustainable load-bearing materials, especially in resource-poor environments. This would push the emerging field of engineered living materials to uncharted territories.

CHAPTER 2

Scope of the Thesis

Hydrogels are among the first biomaterials expressly designed for their use in biomedicine. However, state-of-the-art applications of hydrogels are severely limited because of their mechanical properties. Most hydrogels are rather soft such that the range of mechanical properties that is attainable with them is limited. To overcome this shortcoming, several techniques to reinforce hydrogels have been introduced in the past decade. Despite this great improvement in mechanics, composition and structural complexity found in soft natural tissues remain yet to be matched. Indeed, soft natural materials possess locally varying compositions and structures that are well-defined over many length scales. By contrast, synthetic hydrogels typically have an ill-defined microstructure and their composition is most often homogeneous. In this thesis, I discuss a novel approach to control the microstructure and composition of synthetic hydrogels through the use of 3D granular printing. I believe that the findings reported in my work can effectively contribute to the narrowing of the gap between synthetic and natural soft materials in terms of mechanical properties and I hope it will help shaping future research in the field.

Thesis Structure

This thesis is organized in eight chapters. In Chapter 3, I will introduce the materials and methods used to establish the following discoveries. Chapter 4 will discuss the implementation of a double-network granular hydrogel for the fabrication of 3D printed load-bearing hydrogels. In Chapter 5, I will propose a way to introduce recyclability into a granular material, to achieve repeated regeneration cycles without major losses in mechanical performance. Chapter 6 will provide a preliminary investigation of metal-coordination as a reinforcement strategy for bulk hydrogels. Chapter 7 will combine the structural control of granular hydrogel printing together with the selective reinforcement of

metal-coordination to achieve heterogeneous shape-morphing and load-bearing hydrogels. An additional chapter (Chapter 8) discusses the possibility to attain even more complex structures and compositions if engineered living materials are used. Finally, in Chapters 9 and 10, I will draw the conclusions along with some outlooks on the problems that are yet to be tackled in the field.

CHAPTER 3

Materials and Methods

3.1   Materials

All reagents are used as received: Acrylamido-2-methylpropane sulfonic acid (AMPS) (Sigma-Aldrich, 282731), Acrylamide (AM) (Sigma-Aldrich, A4058), N,N'-Methylene bis-acrylamide (MBA) (Carl Roth, 7867.1), 2-Hydroxy-2-methylpropiophenone (PI) (Sigma-Aldrich, 405655), Mineral oil light (Sigma-Aldrich, 330779), Span80 (TCI Chemicals, S0060), Sulforhodamine B sodium salt (Sigma-Aldrich, S1402), Fluorescein disodium salt (Carl Roth, 5283.1), Ethanol (Sigma-Aldrich, 459844), N,N'-Bis(acryloyl)cystamine (BAC) (Alfa Aesar, J66893), Tris(2-carboxyethyl)phosphine HCl (TCEP) (Combi-Blocks, OR-5119), Methylene blue hydrate (Acros Organics, 229801000), Carboxymethyl cellulose sodium salt (CMC) (90'000 Da, Sigma-Aldrich, 419273), Glycidyl methacrylate (GMA) (Sigma-Aldrich, 779342), Acrylic acid (AA) (Sigma-Aldrich, 147230), n-Hexane (Sigma-Aldrich, 32293), Ammonium peroxydisulfate (APS) (Sigma-Aldrich, 248614), 2-Ketoglutaric acid (KGA) (Sigma-Aldrich, 75890), Citric acid (CA) (Sigma-Aldrich, 251275), Iron(III) chloride (Sigma-Aldrich, 157740), Aluminum chloride (Sigma-Aldrich, 206911), *Sporosarcina pasteurii* (strain designation ATCC 11859, CCOS), Gelatin Type-A from porcine skin (gel strength 300, Sigma-Aldrich, G2500), Alginic acid sodium salt (low viscosity, Sigma-Aldrich, A1112), Phosphate buffered saline (PBS) (Gibco), Calcium chloride 98% (Roth, CN93.1), Yeast extract (PanReac, A1552), Urea (Sigma-Aldrich, 51456), Calcium carbonate 99% (Sigma-Aldrich, 239216), and Deionized water (Direct-Q®) with a resistivity of 18.2 MOhm·cm^{-1}.

3.2   Double Network Granular Hydrogels

3.2.1   Preparation of PAMPS Microgels

An aqueous solution containing 30 wt% AMPS, 3.5 mol% MBA, and 3.5 mol% PI is prepared, unless specified differently. The aqueous phase is emulsified with a mineral oil solution containing 2 wt% Span80. The volume fraction of water is set to 25%. The water-in-oil emulsion is stirred for 5 min while being illuminated with UV light (OmniCure S1000, Lumen Dynamics, 320-390 nm, 60 mW·cm^{-2}) to convert drops into microgels. The resulting PAMPS microgels are transferred into ethanol and centrifuged at 4700 rpm for 15 minutes (Mega Star 1.6R, VWR) to remove the oil. The supernatant is discarded, and the process is repeated three times with ethanol and three times with water. Clean PAMPS microgels are resuspended in water for storage. To render microgels fluorescent, we add 0.05 mg of sulforhodamine B sodium salt or fluorescein disodium salt per mL of microgel solution.

3.2.2   Preparation of Jammed PAMPS Microgel Ink

The solution containing dispersed PAMPS microgels is centrifuged and the supernatant is exchanged with excess aqueous solution containing 20 wt% AM, 0.2 mol% MBA, and 1.5 mol% PI. Microgels are soaked overnight. The solution containing PAMPS microgels is vacuum filtrated (Steriflip® 50 mL tube, 0.22 µm, Millipore) to yield a jammed microgel ink.

3.2.3   Preparation of Molded DNGHs

The granular ink is casted into Teflon molds of cylindrical (d = 8 mm, h = 2 mm) or rectangular (15 x 5 x 2 mm^3) shape, for compression and tensile measurements respectively. The samples are crosslinked for 5 min under UV light (UVP CL-1000, Analytik Jena, 365 nm, 2 mW·cm^{-2}).

3.2.4   Preparation of Bulk Double Network Hydrogels

An aqueous solution containing 30 wt% AMPS, 3.5 mol% MBA, and 3.5 mol% PI is prepared. The AMPS solution is casted into Teflon molds for tensile measurements. The samples are crosslinked for 5 min under UV light (UVP CL-1000, Analytik Jena, 365 nm, 2 mW·cm^{-2}). PAMPS hydrogels are immersed overnight in an aqueous solution

containing 20 wt% AM, 0.2 mol% MBA, and 1.5 mol% PI. Soaked samples are exposed to UV illumination for 5 minutes to trigger the polymerization of the PAM second network.

3.2.5 3D Printing of DNGHs

The jammed microgel ink is loaded in a 3 mL Luer lock syringe. To remove trapped air, the syringe is sealed and centrifuged at 4700 rpm for 1 min. Additive manufacturing of jammed microgels is performed with a commercial 3D bioprinter (Inkredible+^{TM}, Cellink). The granular ink is extruded from a conical nozzle (410 µm) through a pressure driven piston (30 kPa). Printing is controlled through G-code commands that are generated by a built-in machine software (Cellink HeartWare). Printing is performed on a glass substrate with a starting gap of 0.1 mm. Printed structures are crosslinked by exposing them to UV light (UVP CL-1000, Analytik Jena, 365 nm, 2 mW·cm^{-2}) for 5 min.

3.2.6 Rheology of Jammed PAMPS Microgels

Rheology is performed on a DHR-3 TA Instrument with an 8 mm diameter parallel plate steel geometry. All measurements are performed at 25°C, with an 800 µm gap. Frequency dependent viscosity measurements are made at 0.5% strain. Amplitude sweep is performed at 1.0 rad·s^{-1} oscillation. Self-healing measurements are performed at 1.0 rad·s^{-1}, alternating 200 s at 1% strain, with 200 s at 30% strain. Samples are allowed to relax for 200 s at the set temperature before a measurement starts. Stress relaxation measurements are made for crosslinked and uncrosslinked microgels with an initial step strain of 10% and measured for 10 s. The gelation measurement is done at 1% strain and 10 rad·s^{-1} frequency for 250 s. The liquid sample is loaded on the rheometer, and the UV lamp is switched on at t = 25 s to initiate the polymerization reaction.

3.2.7 Mechanical Characterization of DNGHs

Tensile measurements are performed with a commercial machine (zwickiLine 5 kN, 100 N load cell, Zwick Roell). Rectangular DNGH are mounted and stretched at a constant velocity of 100 mm·min^{-1}. The Young's modulus is calculated as the slope of the initial linear region (from 5% to 15% strain). The toughness is calculated as the area below the stress-strain curve of an un-notched sample until fracture. The quantity is expressed as the energy absorbed until fracture per unit volume (J/m^3). Compression measurements are performed on a rheometer equipped with a parallel plate geometry (DHR-3, 50 N load cell, TA Instrument). Cylindrical DNGH are compressed at a constant velocity of 1.2 mm·min^{-1} until 60% strain is reached.

3.2.8 Dry Polymer Content and EWC

Dry Polymer Content and EWC. The dry polymer content of AMPS microgels and DNGHs is calculated as the ratio of dry sample weight over as-prepared weight ($W_d/W_{ap} \cdot 100$). The equilibrium water content (EWC) is calculated as the ratio of dry sample weight over fully swollen sample weight ($W_d/W_s \cdot 100$).

3.3 Recyclable Double Network Granular Hydrogels

3.3.1 Preparation of PAMPS Microgels

PAMPS microgels were prepared following the protocol described in section 3.2.1. Briefly, an aqueous solution containing 25 wt% AMPS, 3.5 mol% MBA, and 3.5 mol% PI is prepared, unless specified differently. The aqueous phase is emulsified with a mineral oil solution containing 2 wt% Span80. The volume fraction of water is set to 25%. The water-in-oil emulsion is stirred while being illuminated with UV light (OmniCure S1000, Lumen Dynamics, 320-390 nm, 60 mW·cm^{-2}) for 5 min to convert drops into microgels. The resulting PAMPS microgels are transferred into ethanol and centrifuged at 4700 rpm for 15 min (Mega Star 1.6R, VWR) to remove the oil. The supernatant is discarded, and the process is repeated three times with ethanol and three times with water. Clean PAMPS microgels are resuspended in water for storage.

3.3.2 Preparation of rDNGHs

The solution containing dispersed PAMPS microgels is centrifuged at 4500 rpm for 10 min and the supernatant is exchanged with excess aqueous solution containing 30 wt% AM, 0.1 mol% BAC, and 1.5 mol% PI. The solution containing PAMPS microgels is centrifuged at 4700 rpm for 15 minutes and further jammed over filter paper. The granular paste is casted into dog-bone shaped Teflon molds and crosslinked under UV irradiation (UVP CL-1000, Analytik Jena, 365 nm, 2 mW·cm^{-2}) for 5 min.

3.3.3 3D Printing of rDNGHs

The jammed microgel ink is loaded in a 3 mL Luer lock syringe. To remove trapped air, the syringe is sealed and centrifuged at 4700 rpm for 1 min. 3D printing of jammed microgels is performed with a commercial 3D bioprinter (BIO X^{TM}, Cellink). The granular

ink is extruded from a conical nozzle (410 µm) through a pressure driven piston (30 kPa).
Microgels are dyed with 0.001 mg·mL^{-1} methylene blue for visualization.

3.3.4   Degradation and Recycling of rDNGHs

Crosslinked rDNGH samples are immersed in 50 mM TCEP aqueous solution at pH 9,
unless specified differently. The solution is left to stir at 300 rpm until complete rDNGH
dissolution is observed. Degradation kinetics is monitored through gravimetric analysis.
Dispersed microgels are recovered through centrifugation at 4700 rpm for 15 min. Re-
covered particles are washed in excess water and centrifuged. The process is repeated
three times. The recovery yield is calculated as the weight of recovered microgels with
respect to the initial microgel weight. Cleaned microgels are reused as pristine ones for
the preparation of new rDNGH samples.

3.3.5   Printing Resolution Characterization

The granular ink was extruded in a grid structure ($10 \times 10 \times 1$ mm^3) with a grid spacing
of 1.05 mm. The spreading coefficient and the filament resolution were calculated as:

$$\text{Spreading Factor } (\%) = \frac{A_P - A_T}{A_T} \cdot 100 \tag{3.1}$$

where A_P is the actual measured area, and A_T is the theoretical area of a printed cell.
The filament resolution is calculated as:

$$\text{Filament Resolution } (\%) = \frac{D_P - D_T}{D_T} \cdot 100 \tag{3.2}$$

where D_P is the actual measured filament diameter, and D_T the nominal needle diameter
(20 G, DT = 603 µm). Results are representative of at least 50 independent replicates.

3.3.6   Resonance Raman Characterization

Samples are characterized using a Renishaw Raman spectrometer, equipped with a confo-
cal microscope, a 785 nm laser line, a 1200 l·mm^{-1} grating and a Renishaw camera. Each
spectrum is taken as the average of 500 exposures of 1 s at 125 mW laser power.

3.3.7 Rheology of Pristine and Recycled PAMPS Microgels

Rheology is performed on a DHR-3 TA Instrument with an 8 mm diameter parallel plate steel geometry. All measurements are performed at 25 °C, with an 800 µm gap. Amplitude sweeps are performed at 1.0 rad·s^{-1} oscillation.

3.3.8 Mechanical Characterization of rDNGHs

Tensile measurements are performed with a commercial machine (AllroundLine Z005, 50 N load cell, Zwick Roell). Dog-bone shaped rDNGHs are mounted and stretched at a constant velocity of 100 mm·min^{-1}. The Young's modulus is calculated as the slope of the initial linear region (from 5% to 15% strain). Three-point bending measurements are performed on rectangular beams (20.0 x 10.2 x 1.4 mm^3). The load is applied by a central roller (d = 3 mm) at a displacement rate of 1 mm·min^{-1}. The sample is placed on two cylindrical rollers (d = 3 mm) spaced 16 mm apart. The flexural modulus is calculated as the slope of the initial linear region (from 0.1% to 0.3% strain).

3.4 Hydrogel Reinforced Through Metal-Coordination

3.4.1 Preparation of CellMA Polymer

2 g of CMC were dissolved in 200 mL of deionized water and the pH was adjusted to 5.5. Subsequently, the solution was heated to 40 °C and 2.5 mL of GMA were added to the solution. The mixture was allowed to react for 8 h at 40 °C. Then, the product (CellMA) was purified with excess hexane to remove unreacted GMA. Finally, the CellMA solution was frozen at -20 °C, lyophilized, and stored at -20 °C until further use. ^{1}H-NMR was performed to evaluate the successful outcome of the synthesis reaction, as shown in Figure 3.1.

3.4.2 Preparation of One-Pot CellMA-PAA-Fe Hydrogels

An aqueous solution containing 18 wt% AA, 2 wt% CellMA, 1 wt% APS, and 0.5, 1, 2, or 4 mol% of FeCl$_3$ was prepared and casted into cylindrical Teflon molds (r = 4 mm, h = 2 mm). The samples were allowed to react at 40 °C for 1 hour.
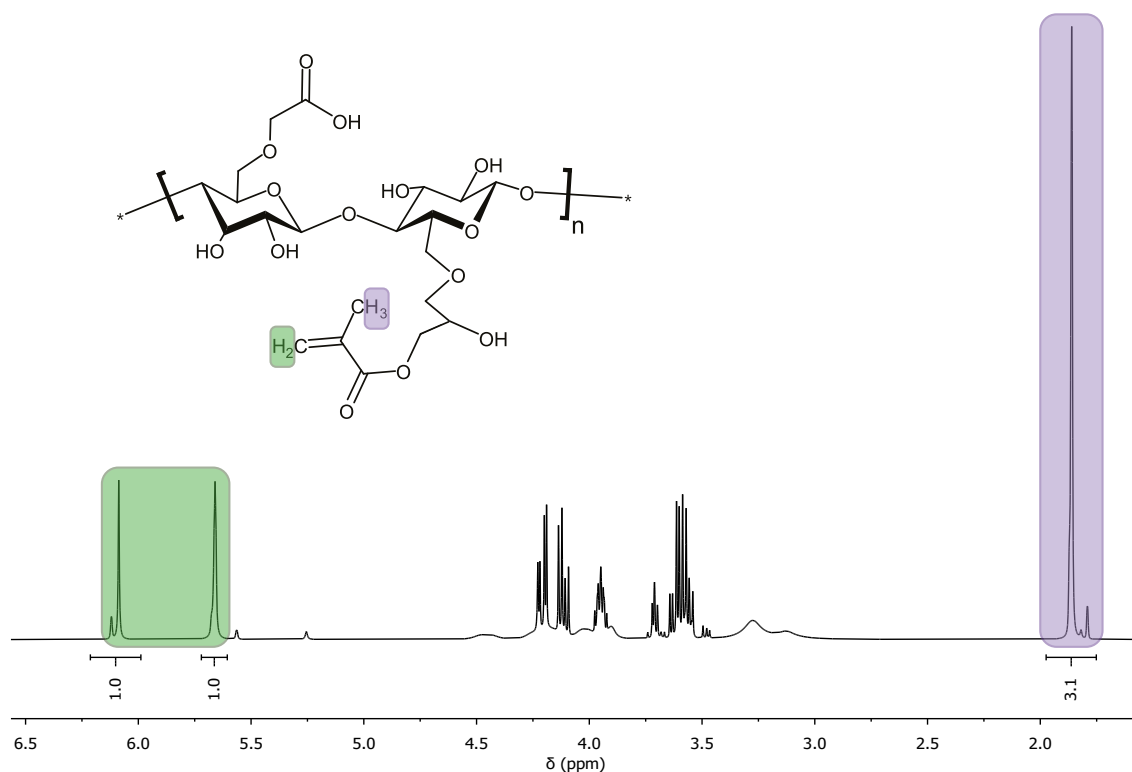
Figure 3.1: ^{1}H-NMR measurement of CellMA in D_2O. ^{1}H-NMR (400 MHz, Deuterium Oxide) δ 6.09 (s, 1H), 5.66 (s, 1H), 1.86 (s, 3H). The successful grafting of methacrylate groups onto cellulose is shown by the appearance of the peaks at 6.09, 5.66, and 1.86 ppm. Reproduced with permission [69]. Copyright 2021, Royal Society of Chemistry.

3.4.3 Preparation of Two-Step CellMA-PAA-Fe Hydrogels

An aqueous solution containing 18 wt% AA, 2 wt% CellMA, 1 wt% KGA was prepared and casted into cylindrical Teflon molds (r = 4 mm, h = 2 mm). The samples were crosslinked for 5 min under UV light (UVP CL-1000, Analytik Jena, 365 nm, 2 mW·cm^{-2}). Subsequently, CellMA-PAA hydrogels were immersed in DI water until swelling equilibrium was reached. Then, the samples were transferred into an aqueous solution containing varying mol% of $FeCl_3$ and CA.

3.4.4 Rheology of CellMA-PAA Hydrogels

Rheology was performed on a DHR-3 TA Instrument with a 8 mm diameter parallel plate steel geometry. All measurements were performed at 25 °C, with a 2 mm gap. Frequency sweep measurements were made at 1% strain. Amplitude sweeps were performed at 1.0 rad·s^{-1} oscillation frequency. Stress relaxation measurements were carried out with an initial step strain of 10% and measured for 100 s.

3.4.5 Mechanical Characterization of CellMA-PAA Hydrogels

Compression measurements were performed on a commercial machine (zwickiLine 5 kN, 100 N load cell, Zwick Roell). Molded cylindrical samples (r = 5 mm, h = 10 mm) were compressed at a constant velocity of 1.2 mm·min^{-1}. The compressive modulus was calculated as the slope of the initial linear region (from 5% to 15% strain).

3.4.6 EDX Mapping of CellMA-PAA-Al/Fe Hydrogels

Images for characterization were acquired using a Zeiss Merlin FE-SEM equipped with an Oxford Inst. EDX detector and operated at 7 kV and 180 pA. To prevent EDX artifacts, the sample was polished and left uncoated. EDX signals were averaged over the entire measurement area and extracted for a quantitative comparison. The horizontal axis represents the distance from the sample edge.

3.4.7 Nanoindentation of CellMA-PAA-Al/Fe Hydrogels

Nanoindentation measurements were conducted on an Anton Paar NHT^3 tester mounted with a Berkovich indenter. The experiment was performed in a displacement control mode with a maximum indentation depth of 20 μm and a displacement rate of 10 nm·s^{-1}.

3.4.8 Statistical Analysis

All data are expressed as the mean $\pm$ standard deviation (SD). For all the experiments, each test was repeated five times to determine reproducibility.

3.5 Metal-Coordinated Double Network Granular Hydrogels

3.5.1 Preparation of PAA and PAM Hydrogels

An aqueous solution containing 30 wt% of monomer (AA or AM), 1 wt% MBA crosslinker and 5 mg·mL^{-1} of PI is prepared. The solution is poured in a Petri dish (d = 20 cm) and it is polymerized at room temperature for 5 min in a UV oven (UVChamber-365-100, UWave, 25mW·cm^{-2}) yielding a bulk hydrogel.

3.5.2 Preparation of Microfragments

The bulk hydrogel is crushed and dispersed in water to reach swelling equilibrium. Next, hydrogel fragments are further milled in LN2 with an oscillatory cryomill (Cryomill, Retsch) using 12 stainless steel balls (d = 10 mm). The cryomilling protocol is as follows: 3 min of pre-cooling; 5 milling cycles of 3 min at 30 Hz; 30 s at 5 Hz between each cycle, unless stated differently. The resulting microfragments are suspended in water and filtered with a nylon filter of 100 μm mesh size to remove bigger fragments. The microfragments are freeze-dried and stored in powder form until further use.

3.5.3 Preparation of Microgels

An aqueous solution containing 30 wt% AA, 1 wt% MBA, and 5 mg·mL^{-1} PI is prepared. The aqueous phase is emulsified with a mineral oil solution containing 2 wt% Span80. The water-in-oil emulsion is stirred while being illuminated with UV light (OmniCure S1000, Lumen Dynamics, 320-390 nm, 60 mW·cm^{-2}) for 5 min to convert drops into microgels. The resulting PAA microgels are transferred into ethanol and centrifuged at 4500 rpm for 10 min (Mega Star 1.6R, VWR) to remove the oil. The supernatant is discarded, and the process is repeated three times with ethanol and three times with water. Clean PAA microgels are resuspended in water for storage.

3.5.4 Rheology of Microfragments

Rheology measurements are performed on a DHR-3 TA Instrument with an 8 mm diameter parallel plate steel geometry. All measurements are performed at 25 °C, with an 800 µm gap. The samples are allowed to relax for 200 s before each measurement starts. Frequency dependent viscosity measurements are performed at 0.5% strain. Amplitude sweep is performed at 1.0 rad·s^{-1} oscillation. Self-healing measurements are performed at 1.0 rad·s^{-1}, alternating 200 s at 1% strain, with 200 s at 100% strain.

3.5.5 3D Printing of Microfragments

The jammed microfragment paste is loaded in a 3 mL Luer lock syringe. The syringe is sealed and centrifuged at 4500 rpm for 5 min, to remove trapped air bubbles that would affect the printing quality. 3D printing is performed with a commercial 3D bioprinter (BIO X, Cellink). The granular ink is extruded from a conical nozzle (22 G) through a pressure driven piston.

3.5.6   Preparation of mfDNGH

PAA microfragments are suspended in an aqueous solution containing 30% AM, 0.5 wt% MBA and 5 mg·mL^{-1} of PI. After centrifuging at 4500 rpm for 10 min and removing the supernatant, a jammed paste is obtained. The paste is casted into dog-bone shaped molds (cross-section 5 x 2 mm^2) or cylindrical molds (d = 5 mm, t = 5 mm), and it is crosslinked for 5 min under UV irradiation (UVChamber-365-100, UWave, 25mW·cm^{-2}).

3.5.7   Preparation of mxDNGH

PAM microfragments are suspended in an aqueous solution containing 30% AA, 0.5 wt% MBA and 5 mg·mL^{-1} of PI. The same procedure used to prepare mfDNGH is applied.

3.5.8   Mechanical characterization of mfDNGH and mxDNGH

Mechanical measurements are performed with a commercial machine (zwickiLine 5 kN, 50 N load cell, Zwick Roell). Compression tests are performed on cylindrical samples, compressed at a constant velocity of 3 mm·min^{-1} until fracture or 80% strain is reached. The compressive modulus is calculated as the slope of the region from 0% to 5% strain. Tensile tests are performed on dog-bone shaped samples, stretched at a constant velocity of 100 mm·min^{-1}. The Young's modulus is calculated as the slope of the initial linear region, from 0% to 5% strain. The work of fracture (WOF) is calculated as the area below the stress-strain curve.

3.6   Biomineralization of Bacteria-Loaded Microgels

3.6.1   Preparation of Bacteria-Loaded Microgels

To prepare bacteria-loaded gelatin microgels, a PBS solution containing 25 wt% gelatin is prepared and maintained at 37 °C to prevent gelation. 1 wt% of freeze-dried *S. pasteurii* is added to the gelatin solution. The gelatin-S. pasteurii solution is emulsified by adding mineral oil with 2 wt% Span80 in a 3:1 volume ratio. The emulsion is gelled at 4 °C for 30 min and then centrifuged at 3000 rpm for 15 minutes at 20 °C (Mega Star 1.6R, VWR) to remove the majority of the oil. To remove the remaining oil and surfactant, the obtained microgels are resuspended in PBS, centrifuged, and the supernatant is discarded. The process is repeated five times. The microgels are stored at -20 °C prior to further use.

3.6.2 Preparation of BactoInk

To prepare the BactoInk, a PBS solution containing 5 wt% alginate is prepared and mixed with the bacteria-loaded microgels at a 4:1 weight ratio. The suspension is centrifuged at 3000 rpm for 15 minutes at 20 °C and the supernatant is discarded. The obtained BactoInk is stored at -20 °C prior to further use.

3.6.3 3D Printing of BactoInk

The BactoInk is loaded in a 3 mL Luer-Lock syringe and trapped air is removed by centrifugation at 3800 rpm for 1 min at 20 °C. 3D printing of BactoInk is performed with a commercial 3D bioprinter (BIO X, Cellink). The BactoInk is extruded through a 21 G needle, through a pressure driven piston at 70 kPa with 10 mm·s^{-1} printing speed. Printed samples are gelled in a 1 M CaCl$_2$ solution for 30 min.

3.6.4 Preparation of Molded BactoInk

To mold-cast the BactoInk, a negative mold is prepared using Quickform mold making material (Glorex) and a 3D-printed master mold (Prusa MK3S). The BactoInk is casted in the mold using a syringe and subsequently gelled in a 1 M CaCl$_2$ solution for 30 min.

3.6.5 Rheology of BactoInk

Rheology is performed on a DHR-3 TA Instrument with an 8 mm diameter parallel plate steel geometry. All measurements are performed at 25 °C, with an 800 µm gap. Frequency dependent viscosity measurements were made at 0.5% strain. Amplitude sweep is performed at 1.0 rad·s^{-1} oscillation. Samples are allowed to relax for 200 s at the set temperature before a measurement starts. Rheology is performed on samples with and without bacteria.

3.6.6 Biomineralization of BactoInk

Prior to biomineralization, two stock solutions of 1 M CaCl$_2$ and 1.5 M urea with 0.8 wt% yeast extract are prepared respectively. The two solutions are mixed in 1:1 volume ratio before use. The gelled BactoInk sample is added to initiate the biomineralization. The solution is exchanged every 24 h for four days. After the fourth day, samples are removed from the biomineralization solution, soaked in ethanol for 30 min, and dried in vacuum at room temperature for 48 h.

3.6.7 Preparation of Pre-mixed CaCO$_3$-Hydrogel Composite

To obtain a mixed CaCO$_3$-hydrogel composite, a PBS solution containing 25% w/w gelatin and 75% w/w of CaCO$_3$ powder is prepared at 37 °C. The obtained solution is mixed with a PBS solution containing 5 wt% alginate. The mixture is centrifuged at 3800 rpm for 15 minutes at 20 °C and the supernatant is discarded. The obtained paste is molded and gelled in a 1 M CaCl$_2$ containing aqueous solution for 30 min.

3.6.8 TGA Measurement of Biomineralized Samples

Biomineralized samples are finely grinded in a mortar before testing with TGA (TGA 4000, PerkinElmer). The measurement is performed from 30 °C to 950 °C at a heating rate of 10 °C·min^{-1} with a nitrogen flow rate of 20 mL·min^{-1}. The CaCO$_3$ weight percentage (wt%CaCO$_3$) is computed via the following formula:

$$wt\%_{CaCO3} = \frac{(\Delta wt\%)}{m_{wCO2}} m_{wCaCO3} \qquad (3.3)$$

Where Δwt% is the weight percentage loss calculated between 600 °C and 900 °C, m$_{wCO2}$ is the molecular weight of CO$_2$ (44.102 g·mol^{-1}) and m$_{wCaCO3}$ is the molecular weight of CaCO$_3$ (100.1 g·mol^{-1}). Measured data are representative of at least three independent samples and are reported as mean $\pm$ SD.

3.6.9 XRD Measurement of Biomineralized Samples

XRD analysis (Malvern Panalytical, Empyrean) is performed on biomineralized powdered samples with 2θ ranging from 10° to 60°, with a scan rate 0.03° 2θ·min^{-1}. The radiation source is Cu Kα with wavelength 1.5405 Å and the generator is operated at 40 keV, 40 mA. Baseline removal and peak search is performed using the Peak Analyzer function in OriginPro2021. To evaluate the Ic/Iv ratio, the intensity of the main peak is measured for calcite and vaterite at 29.7° and 33°, respectively. Measured data are representative of at least three independent samples and are reported as mean $\pm$ SD.

3.6.10 SEM Imaging of Biomineralized Samples

SEM imaging is performed on a Zeiss Gemini 300, with a working distance of 6 mm, using a secondary electron detector. Samples are coated with 5 nm of gold.

3.6.11 Optical density measurement of bacteria-loaded microgels

The viability of bacteria after the encapsulation process is assessed by incubating 0.5 g of bacteria-loaded microgels in 50 mL of a 0.4 wt% yeast and 0.75 M urea solution at 30 °C for 4 days. The optical density is measured with a UV-Vis spectrophotometer at a wavelength of 600 nm.

3.6.12 Mechanical Characterization of Biomineralized Samples

Compressive measurements are performed with a commercial machine (AllroundLine Z005, 5 kN load cell, Zwick Roell). Cylindrical samples are prepared in a silicone mold (d = 8 mm, t = 8 mm) and compressed at a constant velocity of 1.2 mm·min^{-1} until 40% strain is reached. The compressive modulus is calculated as the slope of the initial linear region (from 0% to 1% strain).

3.6.13 µCT Imaging and 3D Reconstruction of Biomineralized Samples

X-Ray µCT is performed with an Ultratom micro tomography system (RX-SOLUTIONS). The sample is scanned at a voxel resolution of 1.05 µm, with a voltage of 45 kV and a current of 166 µA. Amira-Avizo v.2019.4 software is used for reconstruction, segmentation, and visualization.

CHAPTER 4

3D Printing of Strong and Tough Double Network Granular Hydrogels

In this chapter, I introduce a novel microgel-based ink for the 3D printing of strong and tough load-bearing structures. The ink is composed of jammed polydispersed microgels that are loaded with a second hydrogel-forming solution. After printing, the construct is exposed to an UV source to trigger the formation of a percolating network, thus solidifying the structure. The resulting material, referred as DNGH, is able to withstand significant loads without major damage. This approach demonstrates the possibility to combine the optimal rheological behavior of jammed granular inks with the unparalleled mechanical performances of double network hydrogels, thus enabling the 3D printing of complex load-bearing structures.

This chapter is adapted from the paper entitled "3D Printing of Strong and Tough Double Network Granular Hydrogels" authored by Matteo Hirsch, Alvaro Charlet, and Esther Amstad. M. Hirsch, and A. Charlet are equally contributing co-first authors and both included this chapter in their thesis. M. Hirsch, A. Charlet, and E. Amstad designed the experiments. M.Hirsch performed the tensile tests and 3D printing studies. A. Charlet performed the rheological experiments. M. Hirsch, A. Charlet, and E. Amstad analyzed the data and wrote the manuscript.

Contents

4.1   Abstract

Many soft natural tissues display a fascinating set of mechanical properties that remains
unmatched by manmade counterparts. These unprecedented mechanical properties are
achieved through an intricate interplay between the structure and locally varying com-
position of these natural tissues. This level of control cannot be achieved in soft syn-
thetic materials. To partially address this shortcoming, we introduce a novel 3D printing
approach to fabricate strong and tough soft materials, namely double network granu-
lar hydrogels (DNGHs) from compartmentalized reagents. This is achieved with an ink
composed of microgels that are swollen in a monomer-containing solution; after the ink
is 3D printed, these monomers are converted into a percolating network, resulting in a
DNGH. These DNGHs are sufficiently stiff to repetitively support tensile loads up to 1.3
MPa. Moreover, they are more than an order of magnitude tougher than each of the pure
polymeric networks they are made from. We demonstrate that this ink enables printing
macroscopic strong and tough objects that can optionally be rendered responsive with a
high shape fidelity. The modular and robust fabrication of DNGHs opens up new possi-
bilities to design adaptive strong and tough hydrogels that have the potential to advance,
for example, soft robotic applications.

4.2   Introduction

Most hydrogels that must retain their 3D structure and bear some load are covalently
crosslinked and hence, if swollen, they are inherently brittle. As discussed in section 1.4.4,
their toughness can be strongly increased, if reversible crosslinks that rely on non-covalent

interactions [67, 199], slide-ring structures [79], host-guest interactions [200], nanoparticle fillers [86], or a combination of them [201] are introduced. Indeed, this strategy enables the design of extremely tough hydrogels that can be stretched up to 50 times [92, 202, 203]. However, these tough hydrogels are typically rather soft such that they cannot bear significant loads under tension. To overcome this shortcoming, double network (DN) hydrogels composed of two interpenetrating polymeric networks have been introduced. These DN hydrogels are composed of a highly crosslinked network, the filler, that imparts stiffness to the hydrogel and a second loosely crosslinked one, the matrix, that imparts toughness to it [53]. This advance enabled engineering the mechanical properties of DN hydrogels to be similar to those of certain natural tissues such as cartilage [204, 205].

Despite the great improvement in mechanics, manmade hydrogels are typically inert and hence, cannot adapt their properties in response to external stimuli, in stark contrast to many natural counterparts. An important difference between these two types of materials is their structure and local composition. Soft natural materials possess locally varying compositions and structures that are well-defined over many length scales. By contrast, synthetic hydrogels typically have ill-defined microstructures and their composition is most often homogeneous. Variations in the composition can be introduced using magnetic nanoparticle gradients [206], UV patterning [207], micro-molding [208], photo-triggered chemical crosslinkers [203], or micro-phase separation [96]. However, these methods are often labor intense such that they cannot fabricate macroscopic soft materials with structures that are similar to those of natural models. A contributing reason for the discrepancy in the structure and local composition of soft natural versus synthetic materials is the difference in their processing. Nature produces many of its strong and tough materials from compartmentalized reagents. For example, most marine mussels fabricate their byssus from precursor-containing vesicles that are released on demand and self-assemble into well-defined structures [28, 209]. By contrast, synthetic hydrogels are typically fabricated by mixing reagents in bulk. This technique offers an excellent control over the overall composition of the hydrogels. However, it lacks control over the local composition and microstructure. Complex 3D structures can be achieved through patterned droplet networks [210] or jammed microgels for example using additive manufacturing techniques [132, 154, 170, 211]. However, monodisperse spherical microgels have a small contact area such that the resulting superstructures are weak [147]. The mechanical properties of these granular materials can be improved if the surfaces of the microgels are modified with thiols [166] or metal-coordinating groups [212], through covalent crosslinking of adjacent microgels [213], or by means of a percolating second network [214, 215]. However, the increased adhesion between microgels compromises the stretchability of the materials, thereby reducing their toughness. Methods to fabricate strong and tough complex 3D

hydrogels that have the potential to be used, for example, as load bearing parts of soft robots, remain to be established.

Here, we introduce a new ink that can be additive manufactured into strong and tough DNGHs with locally varying compositions. The ink is composed of polyelectrolyte-based microgels that are swollen in a monomer-loaded solution. This monomer-loaded solution can be converted into a percolating network after the ink has been processed into macroscopic materials. The new two-step approach separates the fabrication of microgels and their annealing. Thereby, it combines the advantages of jammed granular solutions such as injectability and printability with the excellent mechanical properties of DN hydrogels. Importantly, the mechanical properties of the additive manufactured materials can be tuned with the composition of the ink and are independent of the printing parameters such as the printing direction. Because this new technology employs a microgel-based ink, it significantly extends the choice of materials that can be additive manufactured such that the range of mechanical properties that can be accessed with 3D printed hydrogels is much wider. Our new DNGH promise to bridge the gap between structural complexity and mechanical performance that is key in the advancement of soft materials for load-bearing applications. These features will likely enable the design of new, functional, responsive hydrogels that can be used for soft robots and actuators, and membranes for wastewater treatment.

4.3   Experimental Section

Experimental details are reported in Chapter 3 from Section 3.2.1 on page 48 to Section 3.2.8 on page 50.

4.4   Results and Discussion

4.4.1   Microgel Ink Design and Fabrication

To maximize the contact area between adjacent microgels and minimize interstitial spaces, we synthesize microgels possessing a high swelling capacity. Polyelectrolyte-based microgels have been shown to fulfil these requirements. Hence, we select AMPS as a model system and fabricate PAMPS microgels from reagent-loaded water in oil emulsion drops, as sketched in Figure 4.2a and detailed in section 3.2.1. To test if the size of the microgels we produce scales with that of the emulsion drops, we quantify this parameter from optical microscopy images. Drops and crosslinked microgels are nearly identical in

size, as shown in Figure 4.1. After having been crosslinked, microgels are washed several times in ethanol and deionized water to remove unreacted molecules, as sketched in Figure 4.2b. To ensure good inter-particle adhesion, which is key for obtaining good mechanical properties, we swell the microgels in a solution containing reagents that can be converted into a percolating network after the microgels have been 3D printed. Here, we swell the microgels in an aqueous solution containing AM monomers, as sketched in Figure 4.2c. To avoid any dilution effects from the water exchange, we soak microgels in the monomer solution for 24h in large excess of the second network precursor solution. The degree of swelling of the microgels strongly depends on the crosslinker concentration of the microgels: microgels containing 14 mol% crosslinker have an average diameter of 40 µm whereas those containing 3.5 mol% crosslinker have a diameter of 120 µm, as shown in Figure 4.1.

An important feature of our technique is the processing of individually dispersed microgels into macroscopic materials with structures that are well-defined over the millimeter up to the centimeter-length scales. This structural control is achieved through 3D printing. To enable 3D printing of the dispersed microgels, we jam them using vacuum filtration, as shown in Figure 4.2d. The resulting ink is 3D printed into complex structures, as schematically presented in Figure 4.2e. The printed construct is post-cured by exposing it to UV light to allow the formation of a percolating second network, as exemplified on Figure 4.2f.

4.4.2   Rheological Characterization of Microgel Inks

A prerequisite for inks to be 3D printed into macroscopic complex structures is their shear thinning behavior, which is a common property of bioinks [216, 217] and jammed microgels [218]. To ensure a reproducible jamming of the microgels, we measure the solid polymer content of samples swollen in deionized water, as reported in Table 4.1. The results suggest a good reproducibility of our jamming process, where the AMPS polymer content accounts for 4.83 wt% of the resulting ink. The standard deviation of the solid fraction is as low as 0.22 wt%.

As expected, our jammed microgels are shear thinning, as demonstrated by oscillatory rheology in Figure 4.3a. The viscosity of the jammed PAMPS microgels can be tailored with the crosslinker concentration; it increases from 100 to 1000 Pa·s at a shear rate of 10 s^{-1}, if the crosslinker concentration is increased from 3.5 to 14 mol%. To enable precise dosing, the solid granular ink should possess a low flow point. This requirement is fulfilled by our jammed PAMPS microgels, as shown in Figure 4.3b. Indeed, the flow point is in the range of 10% for all the different formulations. Furthermore, we observe no influence of the monomer loading on the flow point of our granular ink, as shown in Figure 4.4.
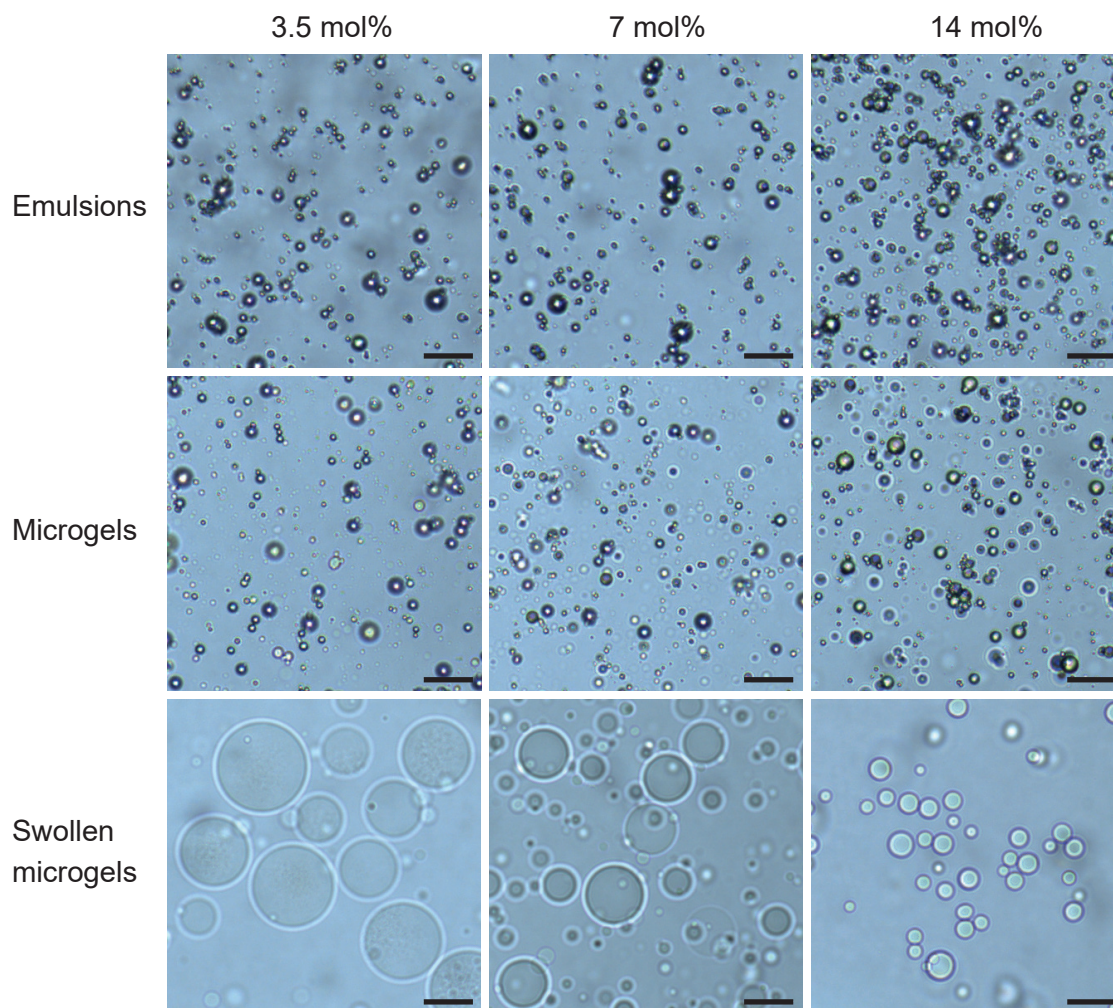
Figure 4.1: Influence of crosslinker concentration on the swelling of microgels. Optical micrographs of (top) emulsions (middle) after the reagents have been crosslinked to form microgels, and (bottom) microgels swollen in an AM-containing solution. Microgels contain (left) 3.5 mol%, (middle) 7 mol%, and (right) 14 mol% crosslinker. The average diameter of emulsion drops is 20 μm, that of swollen microgels containing 3.5 mol% crosslinker 120 μm, those containing 7 mol% crosslinker have an average diameter of 65 μm, and those containing 14 mol% crosslinker have a diameter of 40 μm. Scale bars are 100 μm. Reproduced with permission [149]. Copyright 2022, Wiley-VCH.

Microgel ink preparation

DNGH 3D printing and post-curing
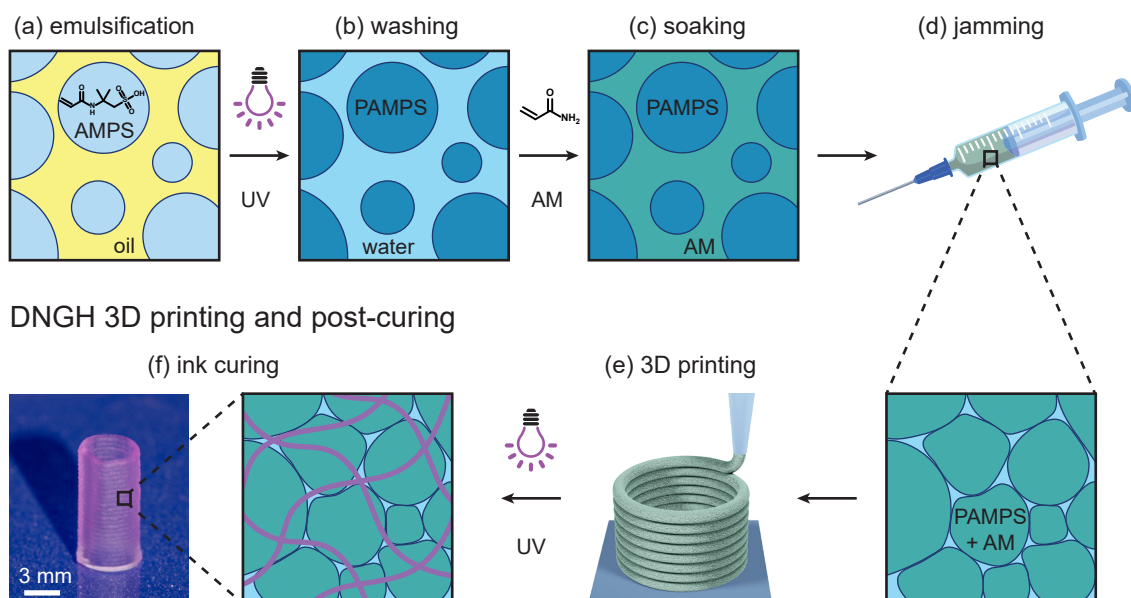
Figure 4.2: Additive manufacturing of DNGHs. Schematic representation of microgel fabrication. a, A monomer-containing aqueous solution is processed into a water-in-oil emulsion. b, AMPS-loaded drops are converted to PAMPS microgels through an UV-induced polymerization. c, Microgels are soaked in an AM monomer-containing solution. d, Monomer-loaded microgels are jammed to yield a printable ink. e, Jammed microgels are extruded as a continuous filament that displays fast shear recovery, enabling the printing of granular hydrogels possessing high aspect ratios with a high shape fidelity. f, The 3D printed objects are post-cured through an exposure to UV light that initiates the polymerization of the AM monomers to form a percolating network, as exemplified by the 3D printed cylinder. Reproduced with permission [149]. Copyright 2022, Wiley-VCH.

Table 4.1: Dry polymer content of jammed microgels. Solid polymer content of water swollen and jammed microgels prepared from a 30 wt% AMPS solution. The standard deviation of the weight fraction of jammed microgels calculated from nine independent measurements is 0.22 wt%, indicating that this procedure is reproducible.

30wt% PAMPS microgel sample	Solid Content (wt%)
#1	4.45
#2	4.78
#3	4.49
#4	4.78
#5	4.85
#6	5.02
#7	4.97
#8	5.04
#9	5.06
Average	4.83
+/- SD	0.22

To obtain a good printing resolution, the ink must rapidly solidify after it has been extruded, which is the case if it displays fast stress healing properties. Indeed, our jammed
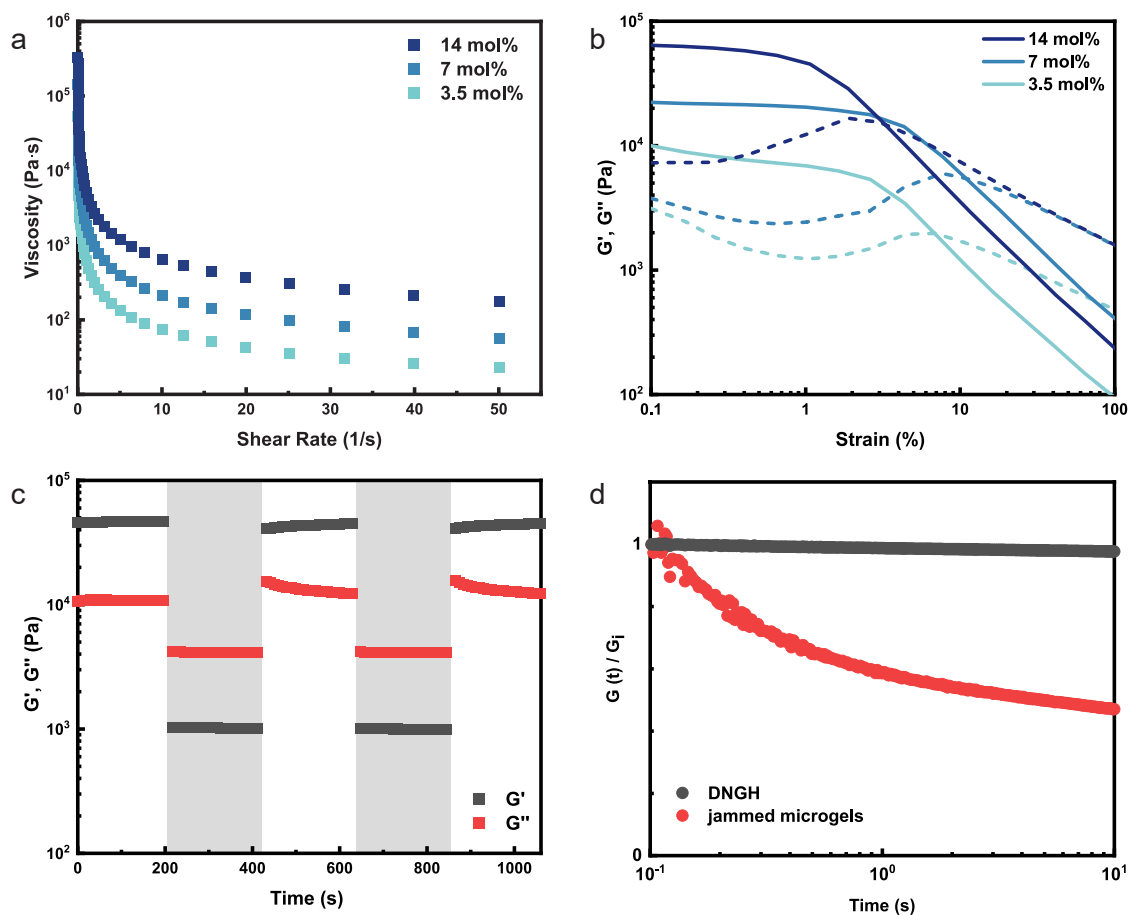
Figure 4.3: Rheology of jammed microgels. a-b, Frequency dependent viscosity (a) and amplitude sweep (b) of jammed microgels containing different cross-linker concentrations. All three samples display a characteristic shear-thinning behavior and a low yield strain. c, Self-healing behavior of jammed microgels containing 3.5 mol% cross-linker. The material transitions from a solid-like to a liquid-like state when subjected to high shear ($\gamma = 30\%$). The jammed solution recovers rapidly to its initial condition at low shear ($\gamma = 1\%$). The process can be repeated cyclically without deterioration of the ink performance. d, Step strain relaxation of a DNGH and jammed microgel ink. The difference in relaxation time is due to the presence of the second percolating network in DNGH. Reproduced with permission [149]. Copyright 2022, Wiley-VCH.
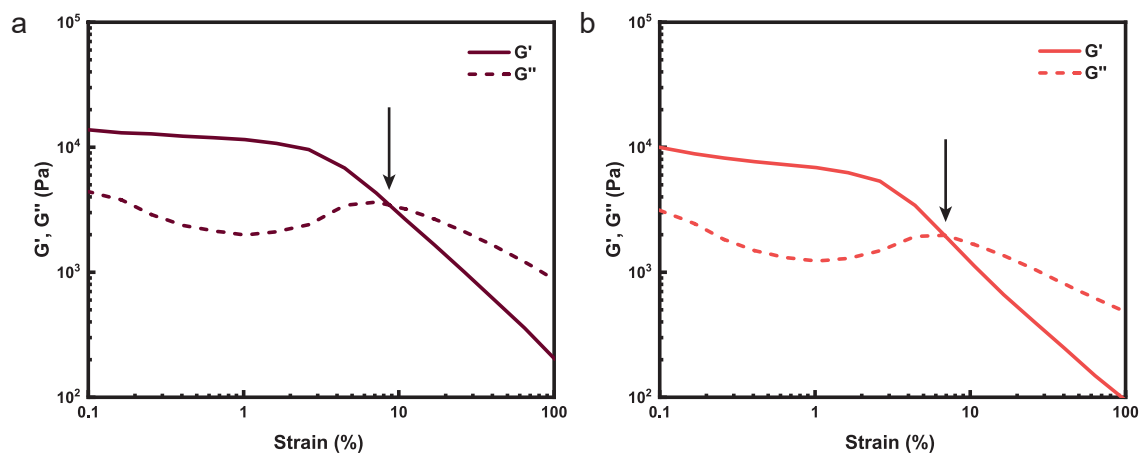
Figure 4.4: Rheological behavior of jammed microgels. Amplitude sweep of microgels swollen (a) directly in a monomer containing solution and (b) in water before they were swollen again in a monomer containing solution. The flow point, represented by an arrow, is within experimental error the same for the two samples. Therefore, the two samples can be extruded with similar printing parameters. Reproduced with permission [149]. Copyright 2022, Wiley-VCH.

PAMPS solution recovers almost immediately and repetitively, from a liquid-like state at high strains, to a solid-like state at low strains, as shown in Figure 4.3c. To test if this behavior is temperature-dependent, we perform step strain relaxation measurements at temperatures varying between 5 °C and 45 °C. The relaxation time of our jammed microgels remains the same between 5 °C and 45 °C, as shown in Figure 4.5a, indicating that these microgels can be easily processed within this temperature range. This behavior is inherent to jammed microgels that behave as solid-like materials because their linear elasticity is governed by the microgel composition [218]. Hence, our results indicate that the jammed microgels possess rheological properties that are well-suited for additive manufacturing.

Jammed microgels can form macroscopic, porous materials that retain their structure [154, 170, 213]. However, the lack of covalent adhesion between particles makes them mechanically weak such that they cannot bear significant loads. To overcome this shortcoming, we transform jammed microgels into a mechanically robust material by forming a second percolating network within the jammed microgels. This is achieved by exposing the granular construct to UV light to initiate the polymerization of the AM monomers. To follow the gelation kinetics of the percolating second network, we perform time-dependent oscillatory rheology measurements. Results suggest that gelation plateaus around 150 s, as shown in Figure 4.5b. As a result of the formed percolating PAM network, the DNGH retains its integrity, in stark contrast to jammed microgels that relax stress over time, as shown in Figure 4.3d.
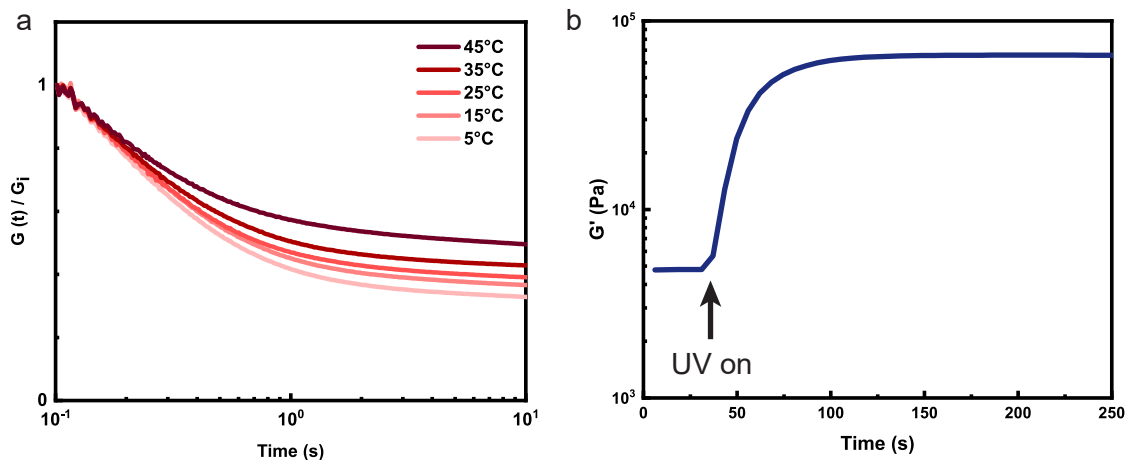
Figure 4.5: Temperature-dependent rheology of jammed microgel ink and its gelation kinetics. a, Step strain relaxation of the jammed microgel ink at 5, 15, 25, 35, and 45 °C. The relaxation time of all measurements is almost independent of temperature within the measured temperature range. b, Gelation kinetics of the DNGH. The jammed microgel ink is subjected to an oscillatory strain of 1% at constant frequency of 10 rad·s^{-1}. Starting from t = 25 s, the sample is continuously illuminated with UV light. The increase in storage modulus is attributed to the polymerization of the percolating second network (PAM). Reproduced with permission [149]. Copyright 2022, Wiley-VCH.

4.4.3 Mechanical Characterization of DNGHs

The mechanical properties of hydrogels are strongly influenced by the weight fraction of the polymers. To characterize the polymer fraction of our DNGHs, we compare the weight of DNGHs as prepared and that of dried DNGHs as a function of their composition. Depending on the composition of our DNGHs, their dry polymer content ranges from 13.6 wt% to 45.7 wt%, as summarized in Figure 4.6a. To predict their swelling behavior, we compare the dry polymer content with the equilibrium water content (EWC) of our DNGHs. EWCs range from 81.5 wt% to 98.0 wt% depending on the DNGH composition, as summarized in Figure 4.6b.

Granular hydrogels inherently possess locally varying compositions. In our case, grains are composed of PAMPS that are reinforced by PAM and hence, they constitute DN hydrogels. By contrast, the grain boundaries are composed of PAM only. To test the influence of the composition of our hydrogels on their mechanical properties under tension, we perform tensile tests on as-prepared DNGHs composed of PAMPS microgels fabricated from a 30 wt% monomer solution and a second network made from a solution containing 20 wt% AM. The granular hydrogel is significantly stiffer and tougher than bulk hydrogels composed of either PAMPS or PAM. The Young's modulus of the DNGH is 5-fold higher than that of PAMPS and 3-fold higher than that of PAM. We attribute the high stiffness of the DNGHs to the chain entanglements that are topologically constrained between PAM chains and the microgel network, such that they cannot be easily displaced [155]. However, our DNGHs
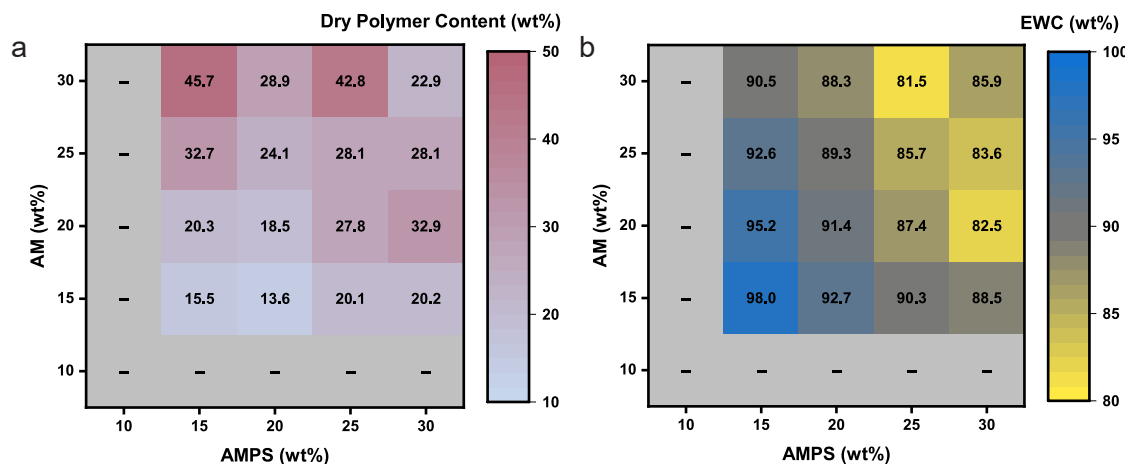
Figure 4.6: Dry polymer content and EWC measurements. a, Dry polymer content of DNGHs with varying network concentrations. The values are calculated as the dried sample weight divided by the as prepared sample. The dry polymer content increases with increasing secondary network concentration. b, EWC of the same DNGHs concentration combinations. Reproduced with permission [149]. Copyright 2022, Wiley-VCH.

are two-fold softer than unstructured DN counterparts, as summarized in Figure 4.8a. We assign this difference to the PAMPS network that is not percolating the entire DNGHs but is only present within the microgels, in stark contrast to the bulk unstructured DNs presented in section 1.4.3.

A key requirement for the use of hydrogels for load bearing applications is that they are tough such that they do not fail catastrophically if deformed within a well-defined range. To assess the toughness of our DNGHs, we quantify their fracture strength. The fracture strength of the DNGH is more than 10-fold higher than that of bulk PAMPS and PAM. Remarkably, the fracture strength of DNGHs is even three-fold higher than that of the unstructured DN counterparts, despite of its lower Young's modulus, as shown in Figure 4.8a. We attribute the corresponding increase in toughness to a stress concentration at the poles of the microgels due to a substantial mismatch in elasticity of the two interpenetrating networks, as has been described for microgel reinforced hydrogels [219]. These results demonstrate the potential of granular hydrogels possessing locally varying compositions for load-bearing applications and as dampers.

Most soft natural materials are subjected to complex loading profiles [220]. To test if our DNGH is sufficiently robust to sustain more demanding loading profiles, we perform compression measurements on DNGH, PAMPS, and PAM samples. The compressive modulus of the DNGH is 2-fold higher than that of PAM, as shown in Figure 4.7a. The compressive stress increases even more: it reaches 0.8 MPa at 60% strain which is 3 times higher than that of the PAM network. Furthermore, we test its ability to lift a 1 kg weight through a folded rectangular stripe with a cross section of 10 mm x 2 mm, as shown in
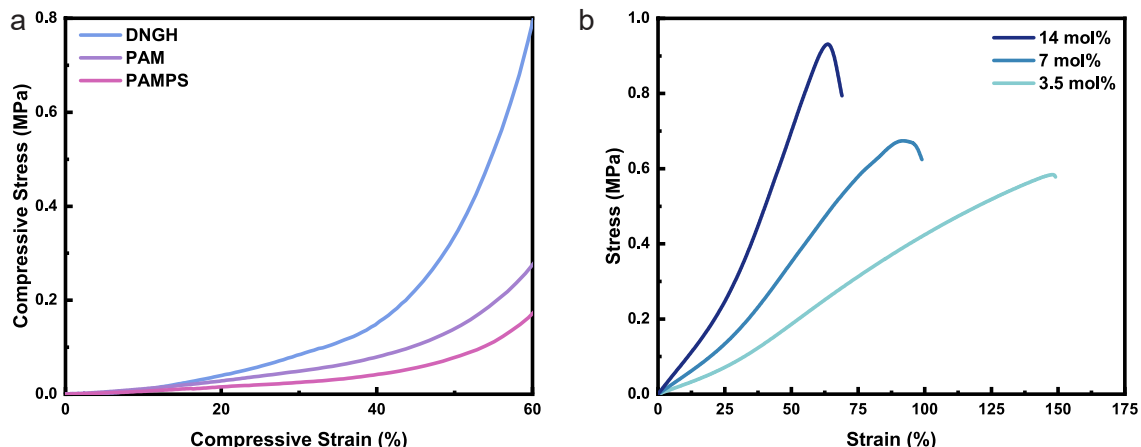
Figure 4.7: Mechanical characterization of DNGHs. a, Compression measurements of DNGH and those of bulk corresponding PAM and PAMPS single network hydrogels. The compressive strength of the DNGH is at least 3-fold higher than that of both bulk hydrogels. b, Tensile measurements of DNGHs with different primary network crosslinker densities. The material shows an increase in elasticity with no significant change in toughness. Reproduced with permission [149]. Copyright 2022, Wiley-VCH.

Figure 4.8b. Remarkably, the stripe is able to support the applied load for at least 5 loading cycles with no appreciable weakening. These results demonstrate the potential of our DNGHs to be used for load bearing applications.

The elasticity of DN hydrogels depends on the initial polymer content and crosslinker concentration of the first network [53]. To test if this is also the case for our DNGH where the first network is not percolating, we fabricate microgels containing different polymer contents and perform tensile tests on them. Indeed, the Young's modulus of the DNGH increases from 0.10 MPa to 0.48 MPa with increasing polymer content until it reaches a plateau at 25 wt% AMPS, as shown in Figure 4.8c. The lower mechanical performance of the DNGH at 30 wt% AMPS is related to the poor swelling of the microgels in the second AM solution. A similar behavior is observed if we fix the polymer content of the AMPS microgels and vary the crosslinker concentrations. For example, DNGHs prepared with 14 mol% MBA crosslinker possess a Young's modulus four-fold higher than the corresponding sample containing only 3.5 mol% MBA, as shown in Figure 4.7b. However, the increase in the microgel crosslinker density decreases the fracture strain of the DNGH from 150% to 65%. To ensure good elasticity of the printed construct while maintaining good mechanical integrity, we keep the crosslink density of the microgels constant at 3.5 mol% in the following experiments.

Our results indicate that the mechanical properties of DNGHs strongly depend on the polymer content of the microgels and the second percolating network. To determine the best combination of the polymer contents of the microgels and the percolating network, we systematically and independently vary these two parameters and quantify the Young's
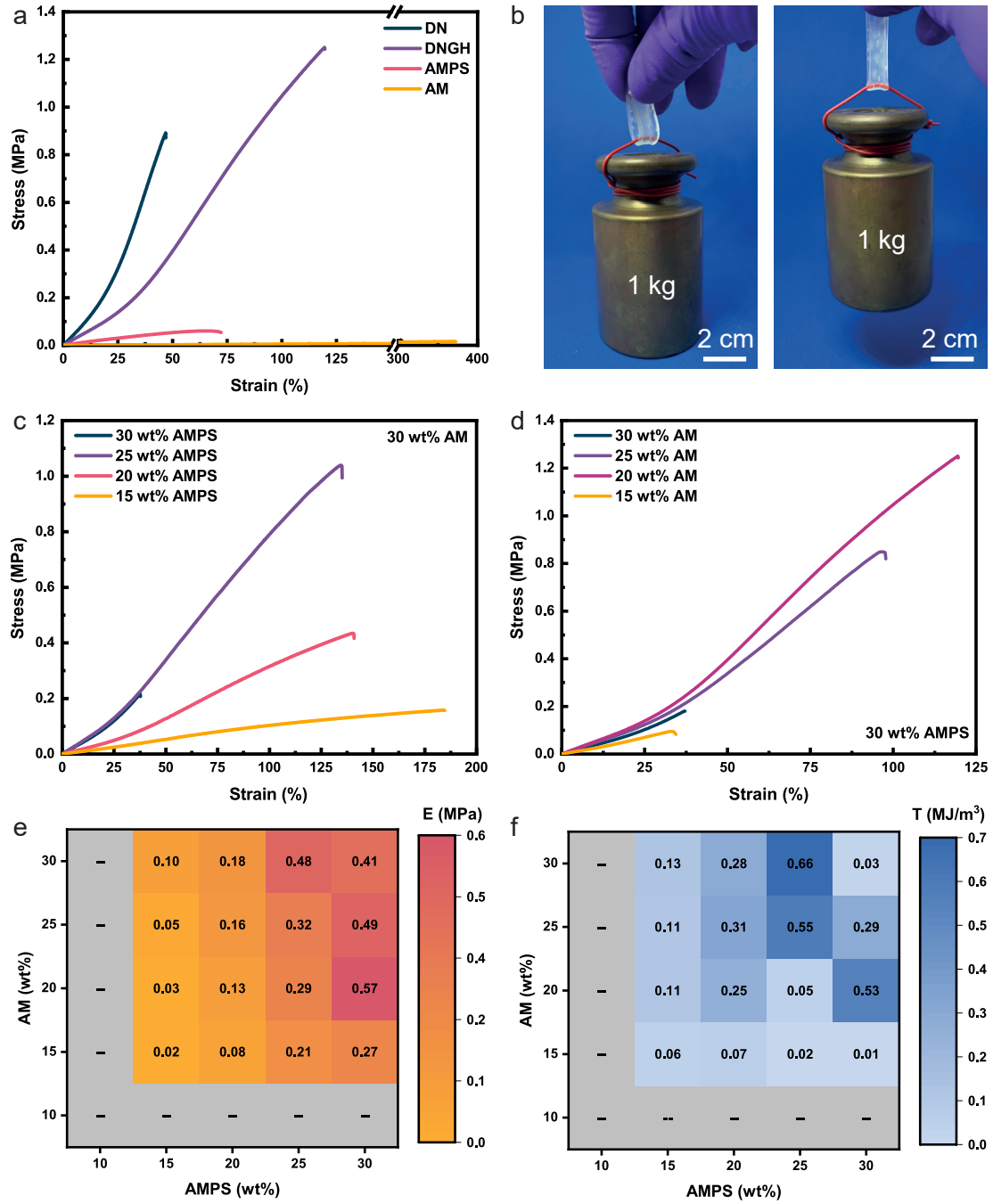
Figure 4.8: Mechanical characterization of DNGHs. a, Tensile tests of DNGHs are compared to those of bulk PAMPS-PAM DN, single PAM and PAMPS hydrogels. The granular material displays a toughening behavior typical of DN hydrogels that is threefold higher than the bulk DN counterpart. b, Photograph of a hydrogel stripe with a cross section of 10×2 mm^2 that has been loaded with a 1 kg weight. c, Tensile measurements of DNGHs prepared with 30 wt% AMPS microgels and a PAM second network made from varying AM concentrations. The toughness of the samples increases

Figure 4.8: with increasing AM concentration until it peaks at 25 wt% AM. d, Tensile measurements
of DNGHs made of PAMPS microgels synthesized with varying AMPS concentrations that are embedded in
a percolating network made from 30 wt% AM. The elasticity of the DNGHs increases with increasing AMPS
concentration. e-f, Color maps of the Young's moduli (e) and toughness (f) calculated as the area under the
stress–strain curve of DNGHs as a function of the concentration of AMPS contained in the microgels and
that of AM that forms the second percolating network. Reported values represent the mean of five repeated
measurements. Reproduced with permission [149]. Copyright 2022, Wiley-VCH.

modulus and toughness of the resulting materials from tensile tests. The Young's modulus
of our DNGHs increases with increasing AMPS concentration, independent of the AM
concentration used to form the second percolating network, as summarized in Figure
4.8e. This finding is in agreement with unstructured DN where the elasticity is mainly
determined by the first network [205, 221]. The Young's modulus of our DNGHs can reach
values up to 0.57 MPa if they are composed of 30 wt% AMPS and 20 wt% AM.

The toughness of unstructured DNs is mainly determined by the loosely crosslinked sec-
ondary network [205, 221]. To test if this is also the case for our DNGHs, we quantify
the toughness, calculated as the area under the stress-strain curve, for all the tested sam-
ples. Indeed, the toughness of our DNGHs increases with increasing AM concentration,
as summarized in Figure 4.8d. The one clear exception to this trend presents the stiffest
DNGHs that we formed, that also displays a high toughness of 0.53 MJ·m^{-3}. The max-
imum toughness of 0.66 MJ·m^{-3} is achieved for DNGHs prepared with 25% AMPS and
30% AM, as summarized in the color map in Figure 4.8f. The color maps of the Young's
moduli and toughnesses of DNGHs nicely show that their mechanical properties can be
tuned over a wide range by adjusting the concentrations of monomers used to form the
microgels and the secondary network respectively.

An additional parameter that strongly influences the mechanical properties of unstruc-
tured DNs is the crosslinker density of the second network. To test if this is also the
case for our DNGHs, we fabricate DNGHs with two different AM crosslinker densities and
test them under tension. At 0.02 mol% crosslinker concentration, the material displays
the yielding behavior that is characteristic for conventional DN hydrogels, as shown in
Figure 4.9a. However, because of the low crosslink density, the bonds between microgels
are weak such that the material easily ruptures along the grain boundaries, as shown in
Figure 4.9b. These results suggest a weak interparticle adhesion. The toughness strongly
increases, if we increase the AM crosslink density: by increasing it ten-fold, the fracture
strength increases from 50 kPa to 600 kPa. Importantly, the increase in toughness does
not compromise the stiffness of the DNGH: the Young's modulus remains unchanged at
0.28 MPa. As a consequence, the fracture toughness of the DNGH increases more than
10-fold if we increase the AM concentration to 0.2 mol%. These results demonstrate that
the mechanical properties of DNGH can be tuned with the crosslink density of the perco-
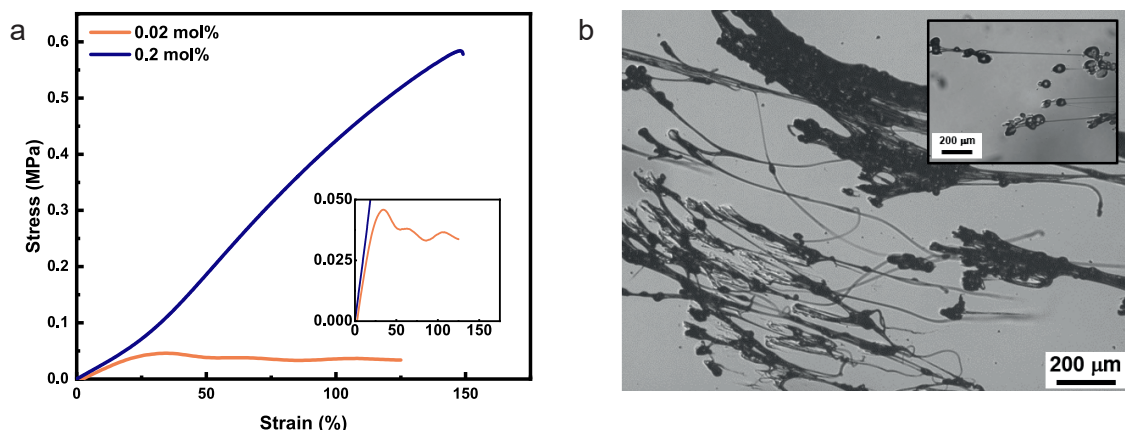
Figure 4.9: Influence of the crosslink density of the percolating second network on the mechanical properties of DNGH. a, Tensile measurements performed on DNGH with a crosslink density of the secondary network of 0.02 mol% (orange) and 0.2 mol% (blue). The Young's modulus of both samples is 0.28 MPa. DNGHs containing 0.02 mol% crosslinker display a typical yielding behavior, as illustrated in the inset. b, Optical micrograph of a fractured sample containing 0.02 mol% crosslinker. The loosely crosslinked secondary network hinders good interparticle adhesion such that individual PAMPS microgels are bridged by fibrous PAM filaments, as highlighted in the inset. Reproduced with permission [149]. Copyright 2022, Wiley-VCH.

lating network, by analogy to DN materials that contain individually dispersed microgels in them [155]. However, by contrast to the DN materials, our DNGH can be 3D printed into complex shapes. To ensure good shape-retaining properties of the ink and a good stability of the additive manufactured materials, we employ the formulation containing 0.2 mol% crosslinker for the following experiments.

4.4.4 Printability and Post-Curing Stability of DNGHs

An important asset of our DNGHs is their fabrication from jammed microgels that shear thin and rapidly recover when stress is relieved. We expect this rheological behavior to render our jammed microgels well-suited inks for 3D printing. When the ink is extruded through a 410 µm diameter nozzle, it is subjected to significant shear stresses that lower the viscosity of the ink locally. The fast recovery of the elastic properties upon relaxation of the stress allows extruding a stable filament whose diameter is similar to that of the nozzle, as shown in the photograph in Figure 4.10a. Importantly, the extruded filament maintains the characteristic granularity of the ink, as evidenced form the fluorescent micrograph in Figure 4.10b.

Macroscopic 3D structures are typically printed by depositing multiple layers on top of each other. To ensure good integrity of the 3D printed structures, subsequent layers must partially merge. Our ink is fundamentally different in that it is composed of jammed microgels that can re-arrange before a second percolating network is formed such that we
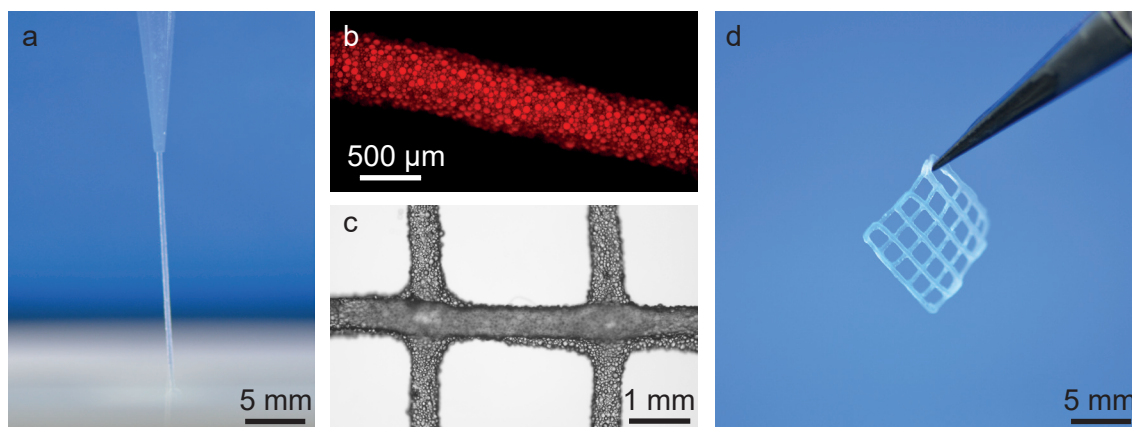
Figure 4.10: Printing of jammed microgels. a, Photograph of the jammed microgel filament while it is extruded from a 410 μm conical nozzle. The material can be printed continuously without rupture yielding a filament with high shape fidelity. b, Fluorescent micrograph of the extruded granular filament. Microgels are labeled with sulforhodamine B sodium salt. The resulting granular filament has an average diameter of 500 μm. c, Optical micrograph of a printed grid demonstrating the high shape-retaining properties of the extruded layers. The curvature between crossing filaments suggests partial merging of subsequent layers. d, Photograph of a free-standing DNGH grid. Upon UV curing, the printed object can be removed from the substrate while retaining its shape, demonstrating the good interconnectivity between layers that is caused by the percolating second PAM network. Reproduced with permission [149]. Copyright 2022, Wiley-VCH.

expect it to enable printing junctions with good interconnections. To test our expectation, we print two perpendicular filaments in a grid-like geometry. Indeed, the junctions display good interconnectivity between adjacent layers already before the second percolating network is formed, as shown in Figure 4.10c. After the second percolating network is formed, the grid retains its shape and integrity even if removed from the substrate, as shown in Figure 4.10d.

The mechanical properties of additive manufactured materials are typically inferior to those of the corresponding bulk materials. This discrepancy is often related to a weak adhesion between sequentially deposited layers. Our ink offers an elegant possibility to overcome this limitation as the second, percolating network is formed after the ink is 3D printed. Therefore, we expect the interfaces between sequentially deposited layers to be equally strong as the grain boundaries within the printing plane. To test this hypothesis, we print a solid DNGH rectangular stripe where the printing direction is along its length and one where the printing direction is perpendicular to it, as schematically shown in Figure 4.11a. Remarkably, we do not observe any significant influence of the printing direction on the mechanical properties of these stripes, as shown in Figure 4.11b. This is in stark contrast to polymers that are 3D printed using conventional, homogeneous inks [222]. Indeed, the Young's modulus is the same as the one measured for molded samples, 0.28 MPa. Interestingly, the additive manufactured samples possess a higher toughness than the corresponding molded ones: DNGH printed stripes reach a fracture strength of
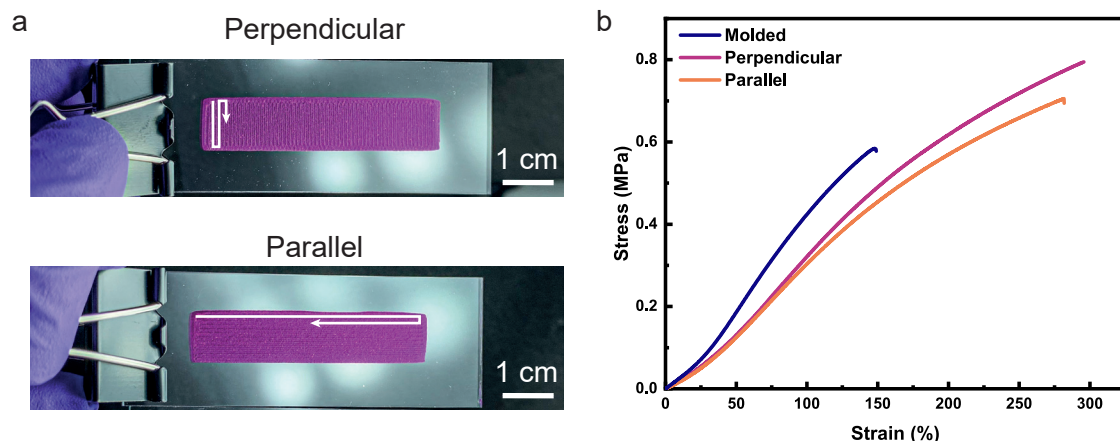
Figure 4.11: Effect of printing direction on mechanical properties. a, Photograph of DNGH stripes printed with perpendicular (top) or parallel (bottom) filament orientation. Microgels are labeled with sulforhodamine B sodium salt for visualization. b, Tensile measurements of DNGH stripes printed parallel and perpendicular to the long axis of the stripe. We cannot observe any influence of the printing direction on the mechanical properties. The toughness of additive manufactured DNGHs is significantly higher than that of molded samples. Reproduced with permission [149]. Copyright 2022, Wiley-VCH.

more than 0.8 MPa, and a maximum elongation of around 290%, compared to the molded samples whose fracture strength is 0.6 MPa and the maximum elongation is 150%. The superior mechanical properties are likely related to the more homogeneous distribution of microgels in printed samples and the lower density of defects such as air inclusions.

To put the mechanical performance of our 3D printed DNGHs in perspective with previously reported 3D printed hydrogel, we compare the Young's moduli of these systems. Our DNGHs are stiffer than any of the previously reported formulation, as summarized in Figure 4.12 [166, 223, 224, 225, 226, 227, 228, 229, 230]. We assign this difference to the processing: our DNGHs are fabricated from jammed microgels such that we can independently optimize the rheological properties of the ink and the composition of the microgels. This is in stark contrast to most 3D printed hydrogels where these two parameters are closely coupled. Taking advantage of this important aspect, we can combine the extraordinary mechanical properties of DN hydrogels with an additive manufacturing process, without compromising the printability and resolution of the ink.

4.4.5 Potential Applications of DNGHs

Our results suggest that jammed microgels soaked in a monomer solution are well-suited inks to 3D print strong and tough hydrogels. This is an asset that has been difficult to achieve with previously reported 3D printed hydrogels [231, 232, 233]. To exploit this new feature, we 3D print our jammed microgels into high aspect ratio hollow cylinders, as shown in Figure 4.13a. Indeed, the additive manufactured DNGH structure can be
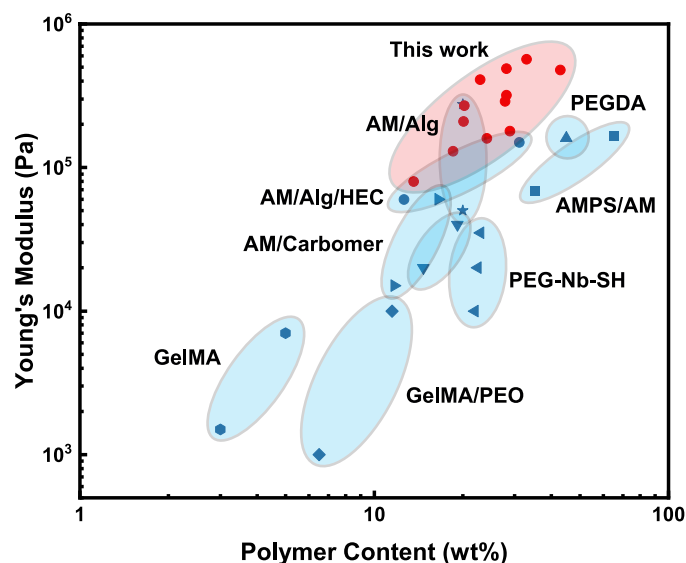
Figure 4.12: Ashby plot. Young's moduli of various hydrogel inks plotted as a function of the total polymer content. DNGHs reported here are stiffer than any other previously reported 3D printed hydrogel. Reproduced with permission [149]. Copyright 2022, Wiley-VCH.

repetitively compressed up to 80%, where it buckles, and retains its initial shape when the stress is released. Importantly, we do not observe any signs of damage, even after samples have been unloaded, as shown in Figure 4.13b. The exceptional shape fidelity and mechanical stability of the construct hints at the potential of the jammed microgel-based ink to design mechanically robust granular materials possessing complex geometries.

A key feature of the ink introduced here is its ability to vary the composition of 3D printed objects locally without risking the introduction of weak interfaces that would sacrifice their mechanical properties. This feature can be achieved if materials are 3D printed from multiple inks, each one composed of jammed microgels possessing a well-defined composition that varies between the different inks and all microgels are soaked in the same type of monomer solution. This ink formulation allows covalent crosslinking of adjacent microgels even if these microgels originate from different types of inks and hence possess different compositions after they have been processed into complex 3D structures. To demonstrate feasibility, we print an ink containing red microgels and one containing green microgels into a grid where the two types of hydrogels remain spatially separated, as illustrated in Figure 4.13c. To demonstrate the importance of the second percolating network for the mechanical stability of the DNGHs, we print the EPFL logo from a structural ink composed of microgels that are soaked in a monomer-containing solution and fill the interstices with a sacrificial ink, namely one composed of jammed microgels that do not contain any monomers. After the second percolating network is formed through exposure to UV-light, we selectively remove the sacrificial ink by immersing the 3D printed

structure into an aqueous solution. We obtain an integral material possessing well-defined cm-sized structures, as illustrated in Figure 4.13d.

To demonstrate the advantage of co-printing inks composed of microgels possessing different properties we 3D print shape-morphing DNGHs. Shape-morphing properties can be imparted to complex structures if they display anisotropic swelling behaviors [234, 235, 236]. To obtain this property, we employ microgels with different crosslink densities such that their swelling behavior varies. Indeed, if we print a flower whose first layer is composed of microgels possessing a lower crosslink density than those contained in the second layer, the flower folds into opposite directions upon drying and soaking, as exemplified in Figure 4.13e. This example demonstrates the power and versatility of the presented method to fabricate responsive, smart soft materials that are sufficiently strong and stiff to bear significant loads.
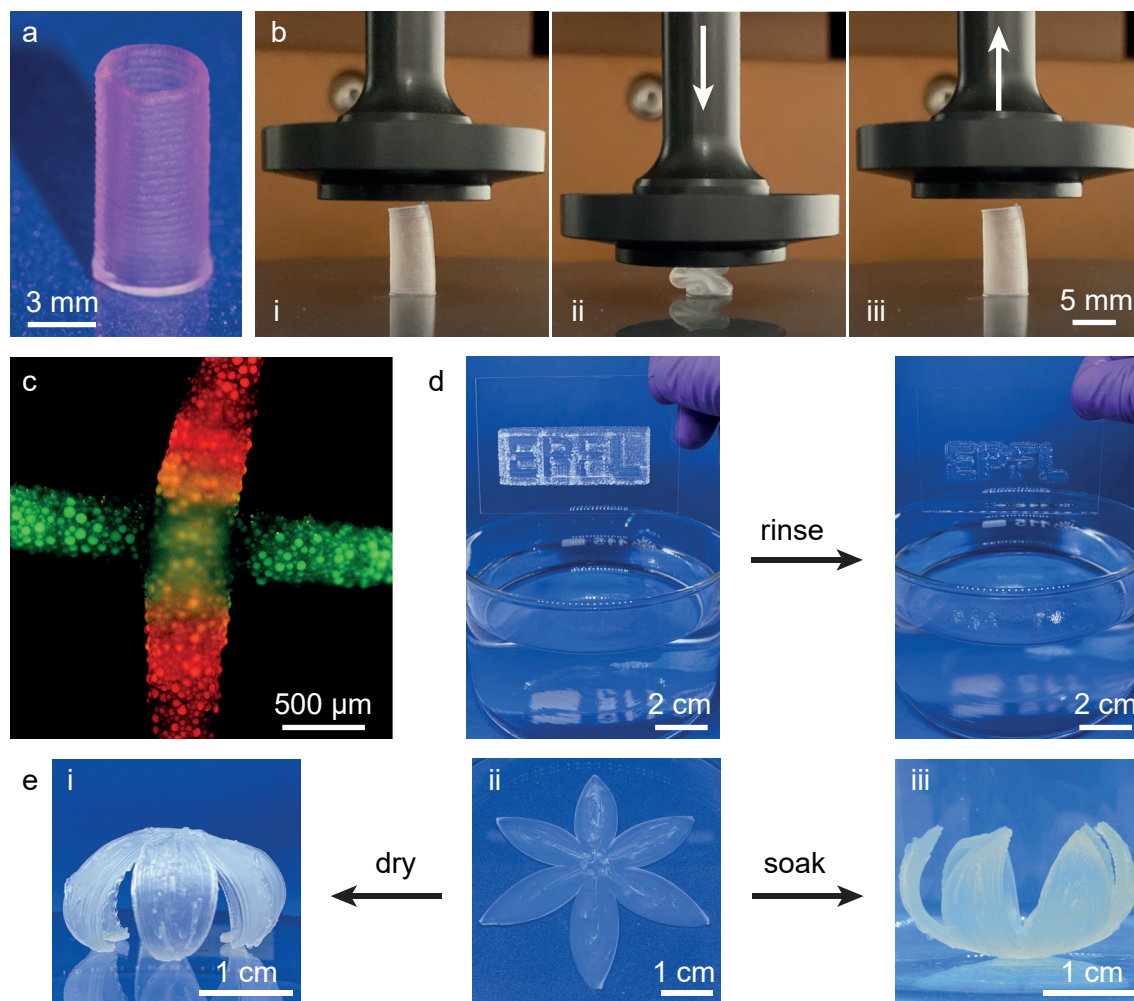
Figure 4.13: 3D printing of DNGHs. a, Photograph of a hollow cylinder with an aspect ratio of 2 that can be printed with high shape fidelity. Microgels are labeled with sulforhodamine B for better visualization. b, Photographs of the hollow DNGH cylinder under compression. While compressed, the cylinder experiences strong deformation and buckling. The good elasticity of DNGHs allows the cylinder to return to its initial shape when the stress is released. c, Fluorescent micrograph of two filaments labeled with different dyes, demonstrating the ability to control the composition locally. d, Photographs of an object that has been 3D printed with a structural and sacrificial ink. The sacrificial ink can be removed after the secondary network of the structural ink has been formed by immersing the material into an aqueous solution. e, Photographs of dual-ink printing of a shape-morphing flower. The object is fabricated from two layers with different swelling behaviors. The first layer is composed of microgels containing 3.5 mol% cross-linker, the microgels contained in the second layer contain 14 mol% cross-linker. As a result of the different swelling behaviors of the microgels and the secondary network, that ensures a good integrity of the overall structure, the DNGH flower can repetitively fold in opposite directions upon drying and immersion in water. Reproduced with permission [149]. Copyright 2022, Wiley-VCH.

4.5 Conclusion

We introduce a modular, versatile method to 3D print strong and tough complex hydrogels. The hydrogels are composed of jammed microgels that are connected through a second covalently crosslinked percolating network. Our approach combines the advantageous rheological properties of jammed microgels with the excellent mechanical properties of double network hydrogels to additive manufacture strong and tough granular hydrogels that can optionally be rendered adaptive. Because adjacent microgels are embedded in a percolating 3D network, the mechanical properties of the 3D printed materials are isotropic and independent of the printing direction. Importantly, the two-step approach to fabricate DNGH is not limited to hydrogel particles but can be extended to a broad range of materials that can be processed into porous particles. Thereby, it significantly enlarges the range of materials that can be 3D printed into complex mechanically robust materials. The flexibility in the granular ink design and excellent control over the micrometer length scale structure opens up new possibilities to design the next generation of strong and tough soft robots and implants that can adapt their properties locally in response to external stimuli.

CHAPTER 5

3D Printing of Recyclable Double Network Granular Hydrogels

In this chapter, I introduce a modification from the protocol reported in Chapter 4 that enables the fabrication of recyclable double network granular hydrogel. In this work, non-degradable microgels are held together by a degradable percolating second network, that enables the on-demand recycling of the constructs. The system is based on covalent reversible crosslinks that can be degraded under benign conditions. This approach combines the optimal printability of jammed granular inks with the controlled degradation of disulfide linkages, allowing the fabrication of recyclable load-bearing granular hydrogels with mechanical properties compared to their non-degradable counterparts. Furthermore, the process can be translated to similar hard plastics and is shown to be reversible over several cycles, thus holding great potential for the field of sustainable materials.

This chapter is adapted from the paper entitled "3D printing of Recyclable Double Network Granular Hydrogels" authored by Alvaro Charlet, Matteo Hirsch, Sanjay Schreiber, and Esther Amstad. M. Hirsch, and A. Charlet are equally contributing co-first authors and both included this chapter in their thesis. M. Hirsch, A. Charlet, and E. Amstad designed the experiments. A. Charlet performed the Raman spectroscopy. M. Hirsch carried out the 3D printing of the material. All remaining experiments, including degradation, rheology, and mechanics are performed by M. Hirsch and A. Charlet jointly. S. Schreiber performed preliminary experiments that were essential to establish the final protocol used in this work. M. Hirsch, A. Charlet, and E. Amstad analyzed the data and wrote the manuscript.

Contents

5.1 Abstract

Sustainable materials, such as degradable and recyclable polymers, become increasingly
important as they are often environmentally more friendly than their one-time-use coun-
terparts. In parallel, the trend towards more customized products demands for fast pro-
totyping methods that allow processing materials into well-defined 3D objects that are
mechanically sufficiently robust to bear significant loads. Soft materials that satisfy the
two rather contradictory needs remain to be shown. Here, we introduce a material that
simultaneously fulfills both requirements, a 3D printable and recyclable double network
granular hydrogel (rDNGH). This hydrogel is composed of PAMPS microparticles that are
covalently crosslinked through a disulfide-based percolating network after they have been
3D printed. The possibility to independently degrade the percolating network, with no
harm to the primary network contained within the microgels, renders the recovery of the
microgel paste efficient. As a result, the recycled material pertains mechanical properties
that are similar to those of the pristine material. Importantly, this process can be ex-
tended to the fabrication of recyclable hard plastics made of, for example, dried rDNGHs.
We envision this approach to not only benefit the field of soft materials but also serve as
foundation for a paradigm shift in the design of new sustainable plastics.

5.2 Introduction

Plastic pollution represents one of the largest sources of environmental threat [237]. Every
year, more than 40 million tons of plastic waste is released into the environment [238].

Because the majority of these materials cannot be degraded, the plastic rapidly accumulates. To address the urgent need to reduce plastic waste, a lot of work has been devoted towards recyclable plastics [239, 240, 241, 242]. For example, the increased awareness of the environmental impact of plastic waste motivated excellent work devoted to degradable and recyclable elastomers [243, 244], and hydrogels [72, 78, 245]. The ability to degrade hydrogels also offers new possibilities to use them as adhesive layers between other hydrogels and biological tissues or synthetic substrates where the adhesive layer selectively degrades over time, thereby enabling a safe removal of the coating [246, 247, 248, 249]. Unfortunately, these degradable hydrogels cannot be used for load-bearing applications because they are mechanically too weak. Another approach to reduce the ecological impact of plastic and hydrogel waste is the use of novel processing technologies that enable shorter and more localized value chains [250]. In this context, additive manufacturing has gained tremendous interest in the field of hydrogel for its efficient use of resources, fast prototyping capability, and on-demand production [251]. Among various manufacturing techniques, extrusion printing has been widely adopted thanks to its easy implementation and low material waste [168, 252, 253, 254].

As was presented in chapter 4, the use of jammed microgels enables the 3D printing of strong and tough double network granular hydrogels. Here, we introduce a double network granular hydrogel, which can be selectively degraded and recycled several times. This is achieved by synergistically combining the favorable 3D printing properties of jammed microgels, the high mechanical performance of double-network hydrogels, and the degradability of covalent reversible bonds. Our material is composed of microgels loaded with a second precursor that contains cleavable crosslinks. Once printed, the granular structure is stabilized by initiating the polymerization reaction of the second precursor to form a percolating network that interpenetrates the microgels and simultaneously crosslinks them. The resulting rDNGH can bear loads up to 0.7 MPa. At the end of its life, it can be disassembled into its microgel components upon exposure to an aqueous solution containing an agent that degrades the dynamic covalent bonds of the second percolating network, TCEP, as described in section 1.4.5. The ability to recover the microgels, that can then be reused for the preparation of a new rDNGH ink, renders this process thrifty and sustainable. Our new rDNGHs demonstrate the possibility to combine good mechanical properties and recyclability. We envision this material to serve as a source of inspiration for the fabrication of the next generation of additive manufactured sustainable hydrogel materials and maybe even for more sustainable plastic replacements.

5.3   Experimental Section

Experimental details are reported in Chapter 3 from Section 3.3.1 on page 50 to Section 3.3.8 on page 52.

5.4   Results and Discussion

5.4.1   Microgel Ink Design and rDNGH Fabrication

To decouple the rheological properties of the hydrogel precursor solution from that of the 3D printable ink, we produce microgels in a similar way to what was presented in chapter 4. Briefly, microgels are produced from aqueous emulsion drop templates that contain AMPS precursors and a photoinitiator. They are converted into microparticles by initiating the polymerization reaction of the precursors using UV illumination. The microgels are washed and transferred into an aqueous solution containing AM, N,N′-bis(acryloyl)cystamine (BAC), and 2-hydroxy-2-methylpropiophenone that serves as a photoinitiator (PI) before they are jammed to obtain the rheological properties required for 3D printing. The 3D printed structure is solidified by initiating the polymerization reaction of AM and BAC which form a percolating network that interpenetrates the microgels and simultaneously crosslinks them, as schematically illustrated in Figure 5.1a.

The key novelty of our system is its ability to be recycled at the end of its life. Importantly, the disassembly of 3D printed materials can be done under benign conditions in an aqueous solution: the intrinsic reversibility of disulfide linkages enables selective de-crosslinking of the secondary network, while the microgel primary structure is preserved, as schematically shown in Figure 5.1b. The microgels can be purified from the de-crosslinked PAM chains, loaded with new AM, BAC, and PI and jammed such that they can be used as a new ink, as shown in Figure 5.1c. This process can be iterated several times without major microgel deterioration thus making this material suitable for recycling, as detailed in Figure 5.1d.

5.4.2   Dynamic Covalent Bonds as Degradable Crosslinks

For recyclable materials to be truly useful, they must degrade upon exposure to an externally controllable trigger [256]. Furthermore, the degradation process should occur under benign conditions. To satisfy these requirements, we introduce a degradation protocol that bases on a naturally occurring hydrolysis. We employ a covalently crosslinked percolating network that entails disulfide bonds, each of which is hydrolyzed into two thiol moieties by
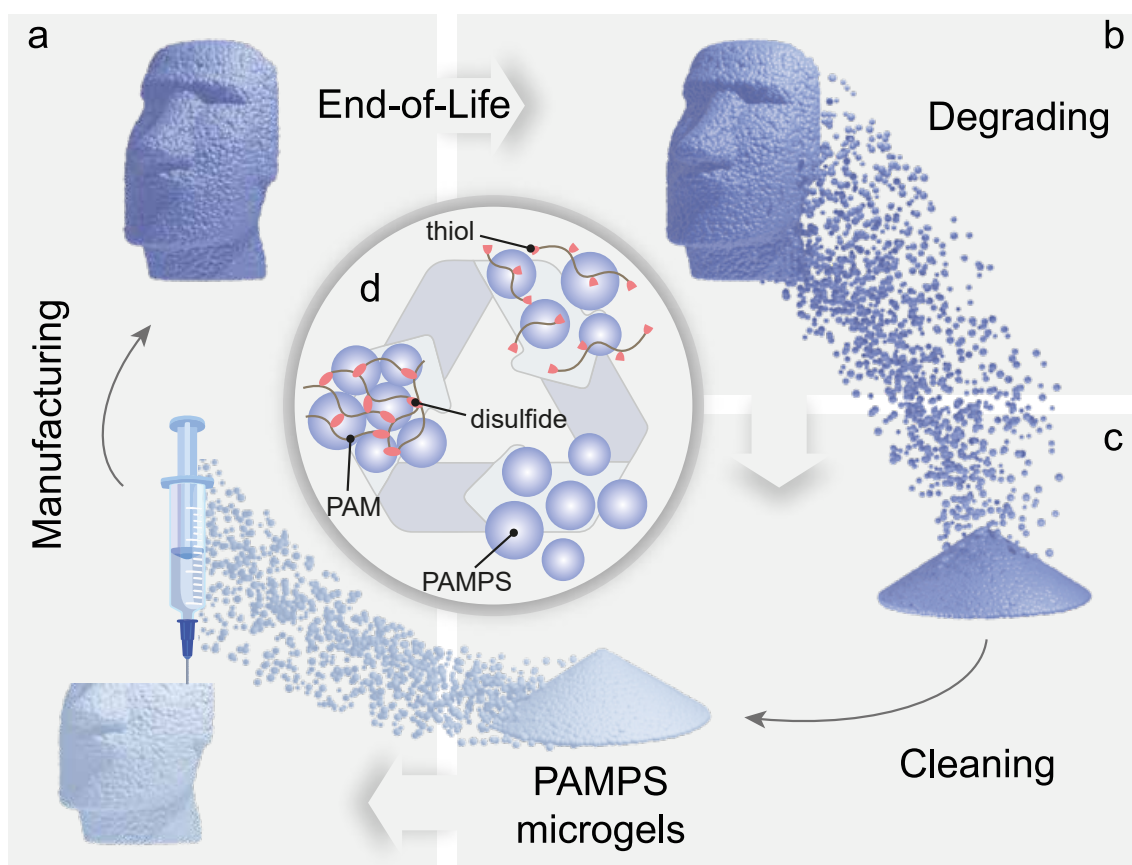
Figure 5.1: Life cycle of rDNGHs. a, Schematic representation of the manufacturing process of rDNGHs. Jammed microgels loaded with AM monomers and the degradable crosslinker BAC are 3D printed or molded into an arbitrary shape, and stabilized through UV exposure. b, Upon object failure or wear, the structure can be disassembled into its microgel components by a green degradation reaction, performed in an aqueous environment. c, The recovered microgels are washed to remove the former percolating network. The purified microgels are recycled into a fully functional ink by re-soaking them in a monomer-containing solution. d, The inset shows a schematic representation of the degradable and recyclable crosslink mechanism. Microgels (blue) are held together by a percolating PAM network (brown) crosslinked by a cleavable disulfide linkage (red). Reproduced with permission [255]. Copyright 2022, Wiley-VCH.

immersing the material in a TCEP containing aqueous solution, as schematically shown in Figure 5.2a. Hence, we expect that rDNGHs decompose into individual microgels if immersed in such a solution. To test this expectation, we attach a 100 g weight to one of the ends of a rDNGH thread and immerse it in an aqueous solution containing 50 mM of TCEP. Indeed, within 10 min, the weight is released because the rDNGH starts to degrade, as shown in Figure 5.2b. To demonstrate that the degradation of the rDNGH is caused by the hydrolysis of the disulfide bonds, we immerse a rDNGH that is again loaded with a 100 g weight into deionized water. We do not observe any sign of degradation, even after 3 hours, as shown in Figure 5.3. We verify that the decomposition of the rDNGH is caused by the hydrolysis of disulfide bonds by monitoring their conversion into individual
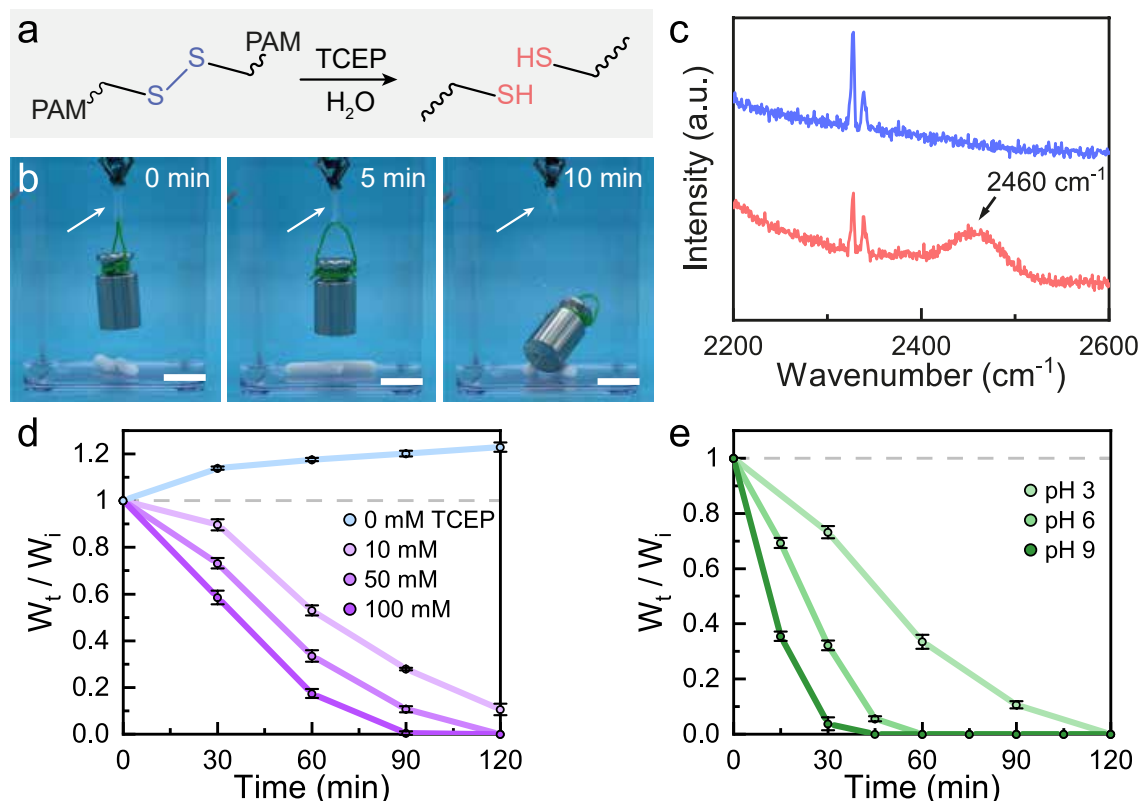
Figure 5.2: Degradability of rDNGHs. a, Schematic representation of the degradation reaction. Upon rDNGH immersion in a TCEP solution, the disulfide bonds are reduced into individual thiols, thus breaking the percolating network. b, Time lapse of a rDNGH thread holding a 100 g weight in a solution containing 50 mM TCEP. After 10 min incubation, the hydrogel thread breaks, releasing the weight. Scale bars are 20 mm. c, The degradation mechanism is confirmed with Raman spectroscopy, by the appearance of the characteristic -SH peak at 2460 cm^{-1} in the degraded sample (red), that is absent in the pristine rDNGH (blue). d, Degradation kinetics of rDNGHs as a function of the TCEP concentration. Samples immersed in solutions containing increasing TCEP concentrations are monitored through gravimetric analysis over time. In the absence of TCEP, swelling is observed resulting in an increased weight. With increasing TCEP concentrations the degradation rate increases. e, Degradation kinetics of rDNGHs in 50 mM TCEP as a function of pH. Increasing pH results in faster degradation. Reproduced with permission [255]. Copyright 2022, Wiley-VCH.

thiol groups using resonance Raman spectroscopy. Indeed, upon 30 min incubation of the rDNGH in the TCEP containing solution, we observe the appearance of a peak at 2460 cm^{-1} which is attributed to the vibration of thiol groups [257], as shown in Figure 5.2c.

An important factor that determines the potential of recyclable materials to be broadly used is the time needed for recycling: this time should be similar or shorter than currently used commercial recycling processes. To assess this parameter, we measure the recycling time of our material as a function of the TCEP concentration. If rDNGHs are immersed in an aqueous solution containing 100 mM TCEP, they degrade within 90 min. A two-fold reduction in the TCEP concentration prolongs the degradation by 30 min. The material can be decomposed under even more benign conditions: if immersed in aqueous solutions
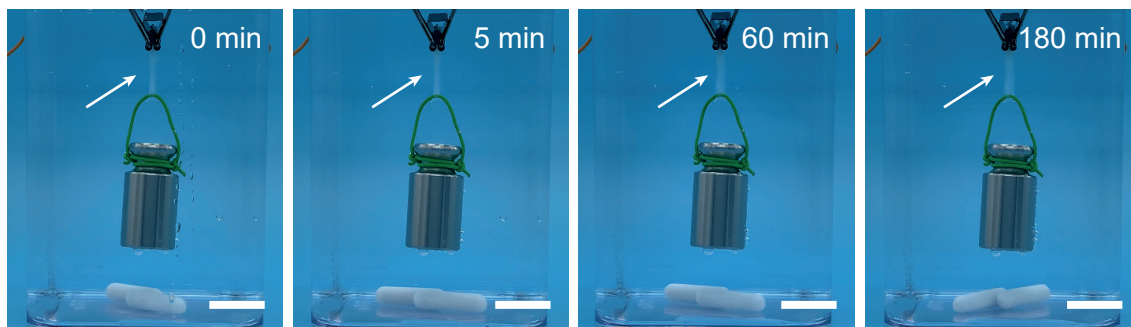
Figure 5.3: Stability in aqueous environment of rDNGH. Time lapse of a rDNGH thread holding a 100 g weight in deionized water. Scale bars are 20 mm. Reproduced with permission [255]. Copyright 2022, Wiley-VCH.

containing only 10 mM TCEP, they still degrade within the experimental observation time of 120 min, as shown in Figure 5.2d. Note that the degradation kinetics also depends on the solution pH: if we keep the TCEP concentration constant at 50 mM and increase the pH from 3 to 9, we reduce the degradation time from 120 to 45 min, as shown in Figure 5.2e. This degradation time is much faster than the time needed to degrade biodegradable plastic, which can take up to 6 months, illustrating the potential of our material [258].

5.4.3 Mechanical Characterization of rDNGHs

Another key parameter for the quality of a recyclable material is its recovery yield. To evaluate this property, we quantify the microgel amount that is recovered as a function of the number or recycles the microgels have been subjected to. After each recycle, the process is monitored by weighing the purified microgels and evaluated by normalizing this value with the original microgel weight. We recover close to 100% of the microgels such that we obtain a recovery yield close to 1, as shown in Figure 5.4a. We assign this very high recovery yield to the size of our microgels: they have diameters of order 10-100 µm such that they readily sediment if centrifuged at 4500 rpm and thus, can easily be extracted from the solution.

Recyclable materials are only truly useful if their mechanical properties do not deteriorate upon recycling [239]. In a first approximation, we expect the mechanical properties of our rDNGH to be independent of the number of recycles the microgels have been subjected to. To test this expectation, we quantify the mechanical properties of pristine rDNGHs and compare them to recycled counterparts using tensile tests. The stiffness of rDNGHs containing microgels made from a 25% AMPS solution remains unchanged. By contrast, their maximum elongation decreases after the first recycle by approximately 30% and after the following four recycles by another 30%, as shown in Figure 5.4b. The decrease in max-
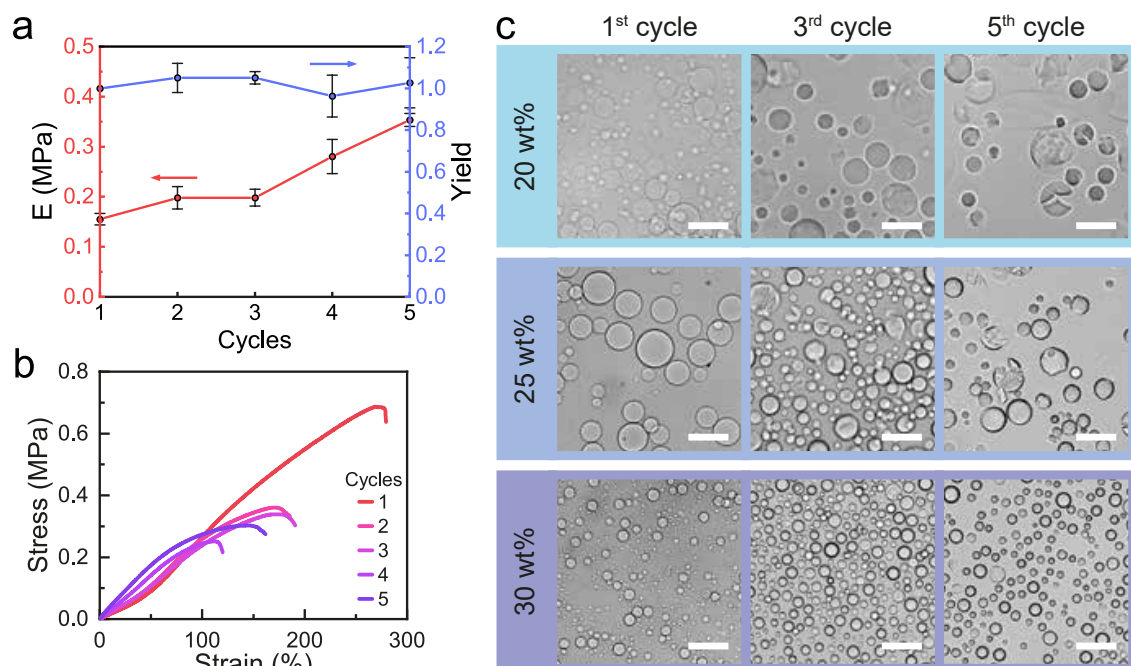
Figure 5.4: Mechanical performance of rDNGHs. a, The Young's modulus of the rDNGHs (red) and recovery yield of the microgels (blue) as a function of the number of recycles microgels have been subjected to. The small increase in Young's modulus is attributed to AM residues that are crosslinked during recycling. The resulting recycled microgels have a higher polymer content that results in a higher stiffness of the double network. The recovery yield of the degraded microgels, measured by gravimetry, is close to 100 % even after 5 cycles. b, Tensile curves of rDNGHs containing microgels prepared from an aqueous solution containing 25 wt% AMPS as a function of recycling. c, Optical micrographs of PAMPS microgels with varying polymer contents as a function of the degradation cycle. Microgels prepared from solutions containing 20 wt% monomers are damaged as they are recycled multiple times. With increasing polymer content, the microgels display better shape fidelity and reduced damage over multiple recycling iterations. Scale bars are 100 μm. Reproduced with permission [255]. Copyright 2022, Wiley-VCH.

imum elongation with increasing recycles hints at a non-perfect removal of the degraded PAM chains. We assign the hindered removal to the physical entanglement of PAM chains within the microgels such that part of these degraded chains remain trapped in the microgel network, thus increasing the overall crosslink density. As a result, subsequent cycles suffer from reduced diffusion of the secondary precursor solution which yields rDNGHs with lower maximum elongation.

The stiffness of double network granular hydrogels is dictated by the polymer content and crosslink density of the microgels [155, 219, 259, 260]. We observe an increase in stiffness of the rDNGHs with increasing number of recycles, as shown in Figure 5.4a. To test if this increase is indeed caused by the increase in microgel stiffness, we fabricate microgels from solutions containing different concentrations of AMPS and assess the mechanical properties of rDNGHs made from them. Indeed, rDNGHs containing microgels produced from an aqueous solution containing 20 wt% AMPS possess a lower stiffness compared to
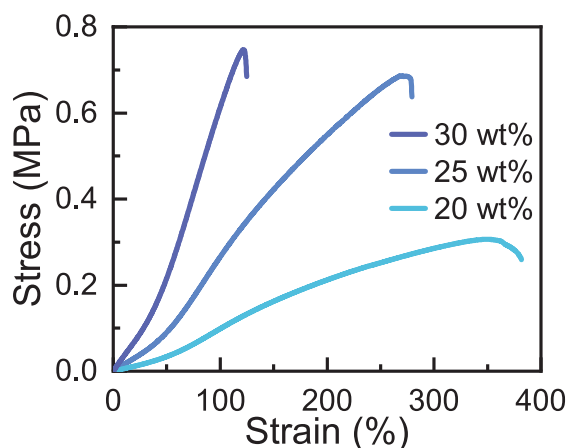
Figure 5.5: Mechanical performance of rDNGHs. Tensile curves of rDNGHs as a function of microgel polymer content.
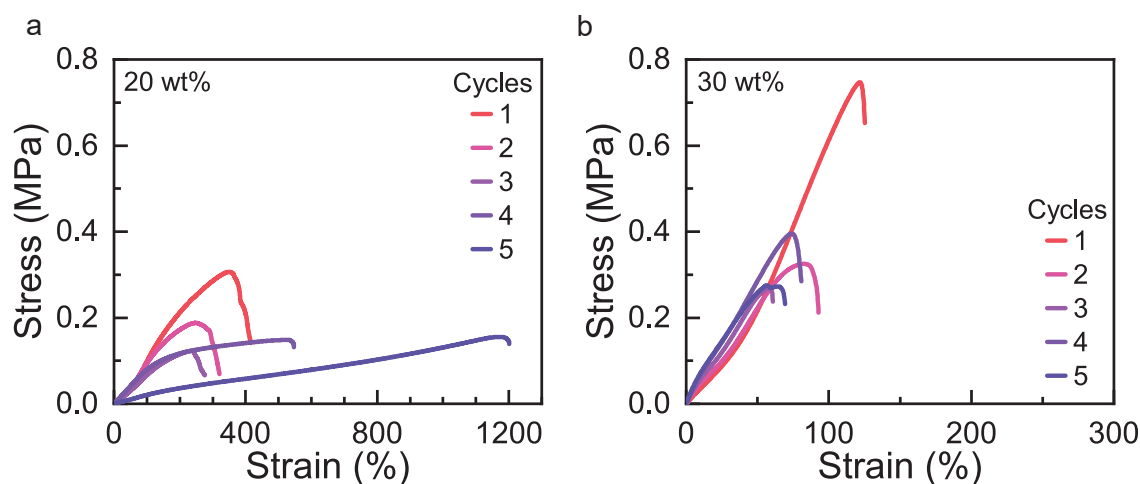
Figure 5.6: Mechanical performance of rDNGHs. a, Tensile curves of rDNGHs containing microgels prepared from an aqueous solution containing 20 wt% AMPS as a function of recycling. b, Tensile curves of rDNGHs containing microgels prepared from an aqueous solution containing 30 wt% AMPS as a function of recycling. Reproduced with permission [255]. Copyright 2022, Wiley-VCH.

those containing microgels made from an aqueous solution containing 25 wt% AMPS, as already established in chapter 4. The stiffness is further increased if we fabricate rDNGHs containing microgels produced from a 30% AMPS containing solution, as shown in Figure 5.5. Upon recycling, we observe a decrease in stiffness for rDNGHs made from a solution containing 20 wt% AMPS with increasing number of recycles, as shown in Figure 5.6a. By contrast, rDNGHs containing microgels made from 30 wt% AMPS solutions show no appreciable stiffness change throughout cycles, as shown in Figure 5.6b. This difference in stiffness of rDNGHs composed of microgels made from a 20 wt% AMPS solution is attributed to an ever-increasing internal damage of these microgels, that influences the mechanical performance of rDNGHs throughout the cycles, as observed from the optical

91

images in Figure 5.4c. The internal damage is much lower for recycled microgels that have been prepared from a 25 wt% AMPS solution, and almost no damage is observed for recycled microgels prepared from a 30 wt% AMPS solution. While rDNGHs prepared from a 30 wt% AMPS solution appear to be the least damaged throughout the recycles, the high polymer content within the microgels limits their swelling capability and therefore their capacity to load AM precursor. As a result, the density of PAM within 30 wt% AMPS rDNGHs is lower, resulting in lower maximum elongation in the pristine sample, as shown in Figure 5.6b. Hence, the maximum elongation must be traded off with the structural integrity. For this reason, we fix the AMPS concentration in the solution used to make microgels to 25 wt% for the following experiments.

5.4.4 3D Printing of rDNGHs

As investigated in Chapter 4, jammed microgels are well-suited for 3D printing because they are shear thinning and display a low yield stress [130, 146]. To test, if this is also the case for our ink based on AM and BAC precursors, we assess its rheological properties. As expected, our jammed microgels are shear thinning and have a yield stress as low as 5 kPa. Note that the rheological properties are independent of the number of recycles the microgels have been subjected to, as shown in Figure 5.7a, suggesting that the recycling does not affect the 3D printability of the ink.

The ease to 3D print depends on the pressure required to extrude the ink through the nozzle. This parameter is determined by the characteristic rheological flow point, defined as the crossover between storage modulus (G') and loss modulus (G"), beyond which the material will flow through the nozzle. Furthermore, the quality of the 3D printed object depends on its shape fidelity, a parameter that is determined by the amplitude of the plateau G' at low strain [132, 149, 261]. To assess whether the recycling affects the ease of printing and the quality of the resulting object, we monitor the characteristic rheological flow point and the plateau storage modulus at 0.1% as a function of the recycles. We observe no appreciable change in these two parameters even if microgels are recycled up to 5 times, as shown in Figure 5.7b, indicating that the ease and precision of the 3D printing remains unchanged even if microgels are recycled several times. To highlight this feature, we print a 3D rDNGH construct representing a Moai head, as displayed in Figure 5.7c. We subsequently degrade the Moai head, recover the microgels, and re-print another rDNGH construct representing a boat that displays a similar printing resolution, as seen in Figure 5.7d.

Key to the performance of 3D printable inks is the printing resolution they offer. To assess this parameter, we 3D print square lattices (10 x 10 $\times$ 1 mm^3) with a grid spacing of 1.05
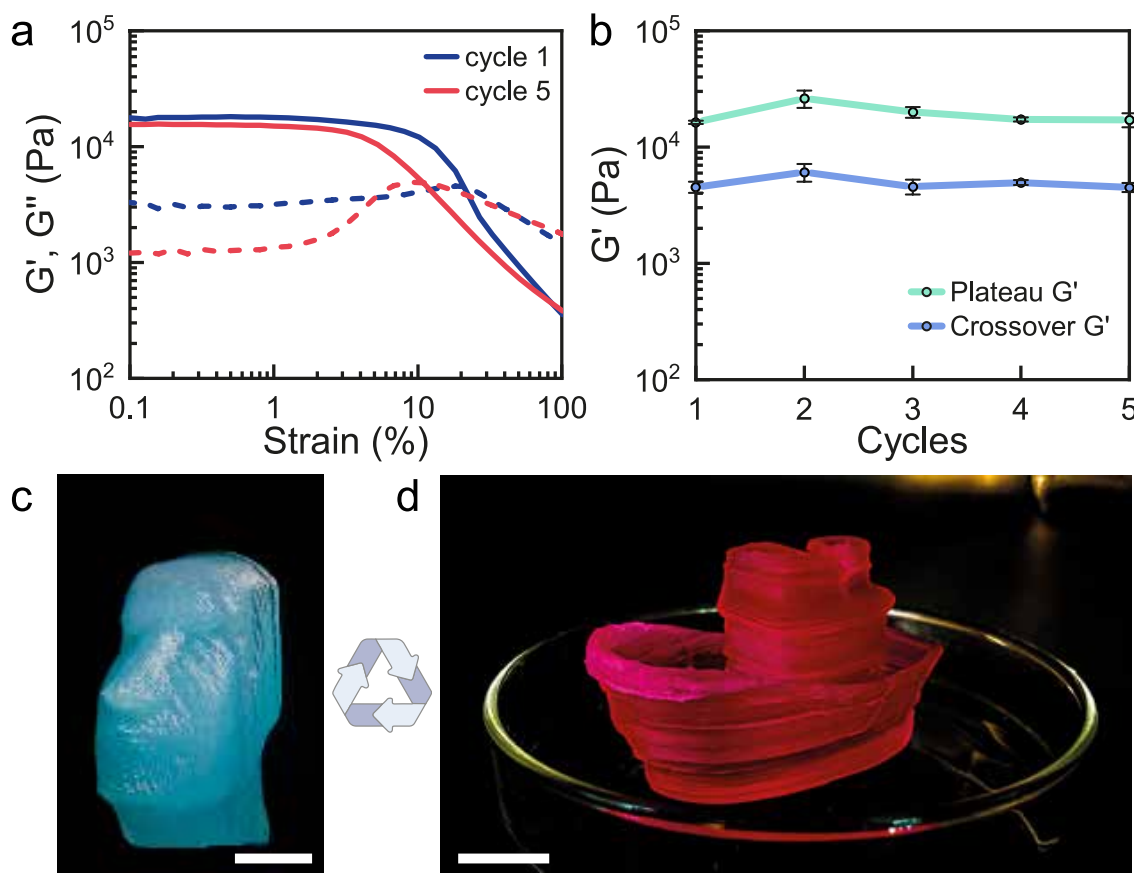
Figure 5.7: Printing and recycling of rDNGHs. a, Rheological characterization of pristine and recovered jammed microgels. The amplitude sweep shows good printability of the jammed microgels even after 5 cycles. b, Storage modulus (plateau G') and flow point (crossover G' with G") demonstrate no appreciable decrease in rheological performance over several recycling iterations. c, Pristine jammed microgels are printed into a Moai figure, and polymerized into a rDNGH. Microgels are colored with methylene blue for visualization. Scale bar is 10 mm. d, After degradation of the Moai figure, the recovered microgels can be regenerated into a fully functional ink and 3D printed again. To better elucidate the recycling process, a boat is chosen as the new print. Scale bar is 10 mm. Reproduced with permission [255]. Copyright 2022, Wiley-VCH.

mm, as shown in Figure 5.8a. The spreading factor, defined as the relative difference between the practical area (A_P) and the theoretical area (A_T) of a single grid cell [159], does not significantly increase throughout the recycles, as shown in Figure 5.8b. Similarly, the filament resolution, defined as the normalized difference between the filament and nozzle diameters, does not significantly change with the number of recycles, as detailed in Figure 5.8c. These results demonstrate that the printing fidelity remains unchanged even if the ink is recycled up to 5 times. As a result, continuous filaments can be printed into a grid with well-defined internal structure, as summarized in Figure 5.9.
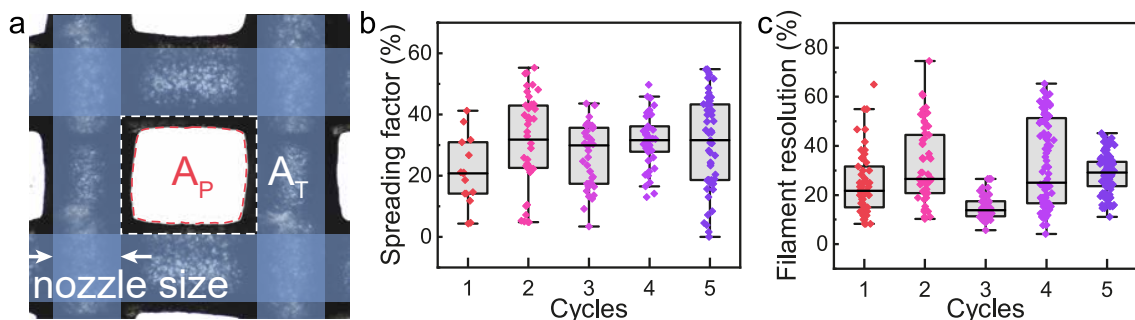
Figure 5.8: Printing resolution as a function of rDNGH recycles. a, 3D printed rDNGH grid. Light blue bands represent the nominal nozzle printing lines. A_T refers to the theoretical area of an ideal print, A_P to the measured area. b, Spreading factor as a function of recycles. We do not observe any significant increase in the spreading factor throughout the recycles. c, Filament resolution as a function of recycles. We do not observe significant changes of the filament resolution with recycles, indicating that the printing resolution remains unchanged even if the ink has been recycled up to five times. Reproduced with permission [255]. Copyright 2022, Wiley-VCH.

5.4.5 Dried rDNGHs as Recyclable Plastics

Hydrogels are well-suited for biomedical applications. However, their mechanical properties can only be tuned over a limited range. To demonstrate the versatility of our material and extend the range of mechanical properties that can be accessed with our rDNGHs, we 3D print a light yet mechanically strong honeycomb structure that we subsequently dehydrate in a vacuum chamber, as shown in Figure 5.10. The obtained hard integral plastic is much stiffer than its hydrated counterparts, such that it can lift a 1 kg weight without noticeable deformation, as shown in Figure 5.11a. This result is well in agreement with existing literature on dehydrated polyelectrolyte gels [262]. The mechanical properties of the resulting material are assessed using three-point bending. Dried rDNGHs display a bending modulus as high as 1.92 GPa with a maximum flexural stress of 130 MPa at 6% strain. These values are similar to those of commercial plastics, such as acrylonitrile butadiene styrene (ABS), polyethylene (PE), and polyethylene terephthalate (PET) [263]. To recycle the material at the end of its life, we immerse it in an aqueous solution containing TCEP until it is fully degraded, which takes approximately 2 hours. The recovered material is swollen in an aqueous solution containing acrylamide before it is processed into a new rDNGH sample. After drying, the bending modulus increases by 10% whereas the flexural strain decreases by 50%, as shown in Figure 5.11b. We assign the changes in mechanical properties to the increase in the PAM density within the microgel that stiffens them.

To demonstrate the potential of the dried rDNGHs to act as load-bearing materials, we fabricate a wrench to screw in a stainless-steel nut. Like in conventional manufacturing processes, poor design can result in an unfunctional tool, as shown in Figure 5.11c. Thanks
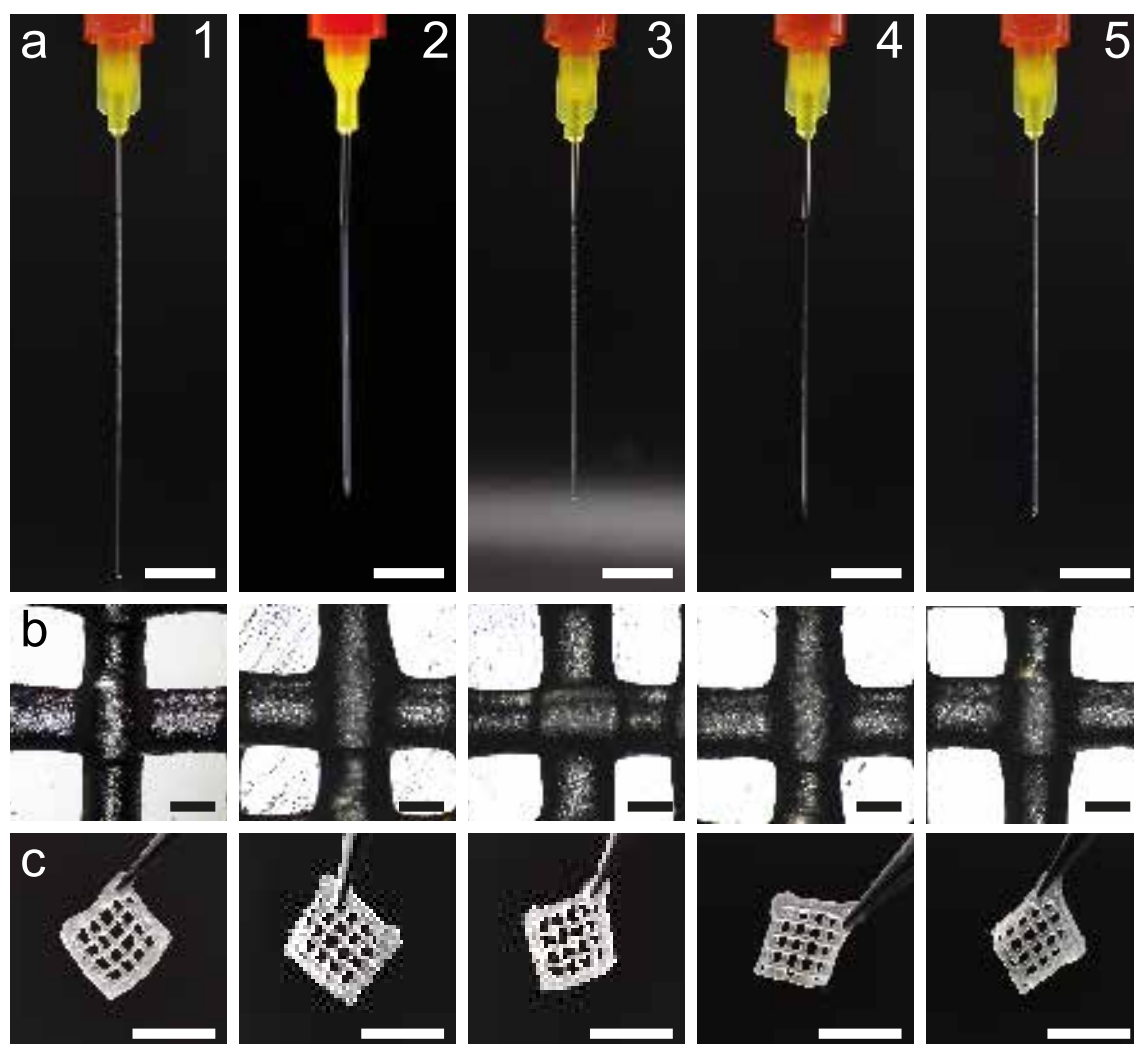
Figure 5.9: Printing resolution of rDNGHs as a function of their recycles. a, Pictures of extruded stable filaments. Scale bars are 1 cm. b, Micrographs of cross-points when printing a grid structure. Scale bars are 500 µm. c, Pictures of free-standing grids after curing. Scale bars are 1 cm. Reproduced with permission [255]. Copyright 2022, Wiley-VCH.
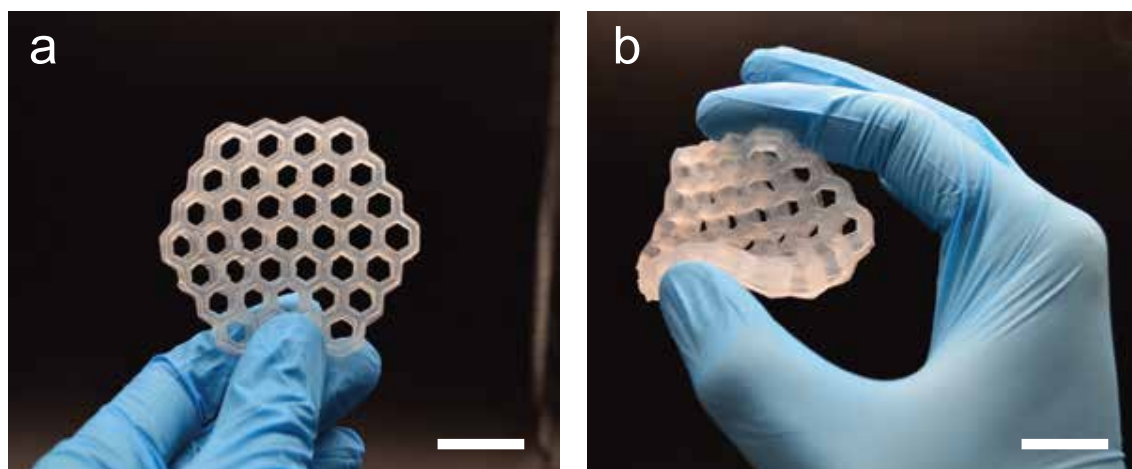
Figure 5.10: 3D printing of a honeycomb structure. Photograph of (a) a cured rDNGH honeycomb structure that is freestanding and (b) a bent rDNGH honeycomb demonstrating its high ultimate tensile strain that enables the fabrication of flexible yet strong 3D printed structures. Scale bars are 2 cm. Reproduced with permission [255]. Copyright 2022, Wiley-VCH.
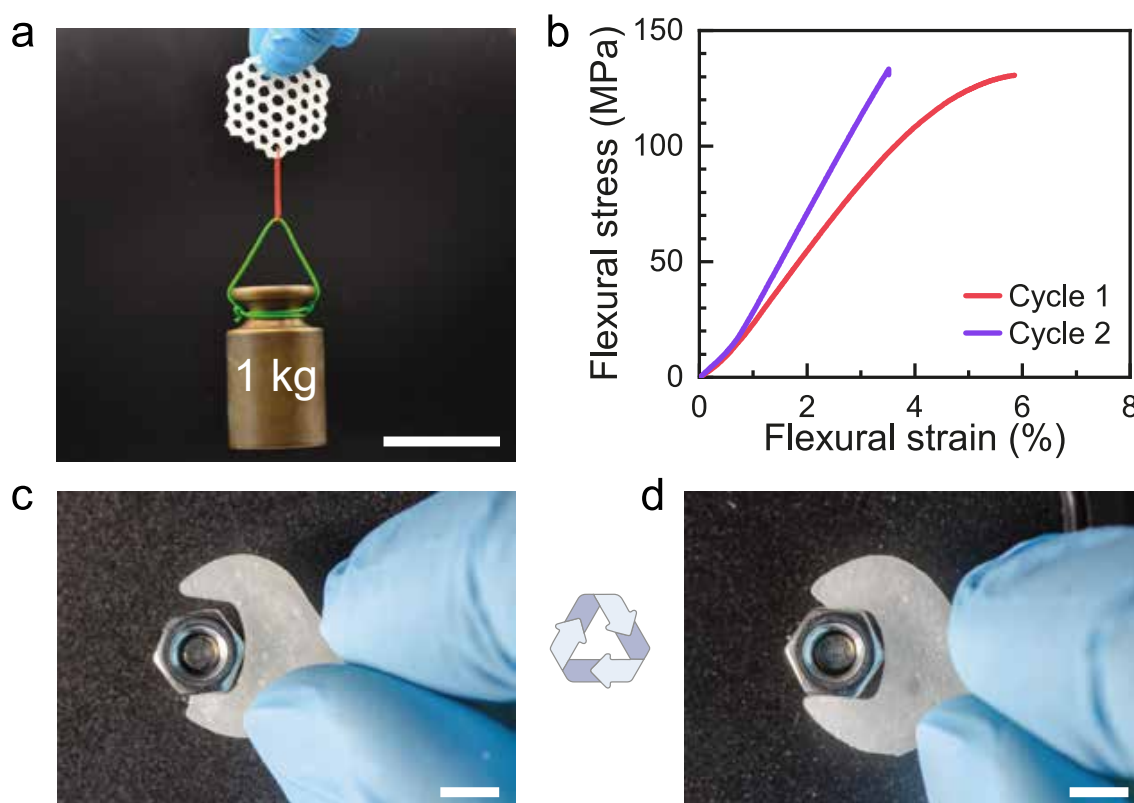
Figure 5.11: The new paradigm of rDNGH-based plastics. a, Picture of a 3D printed dried rDNGH honeycomb structure. Scale bar is 5 cm. b, Flexural stress–strain curves of dried pristine and recycled rDNGH. The solid material behaves as a hard plastic with a flexural modulus of 1.92 GPa. The recycled material displays an increase in modulus of 10% with respect to the pristine sample, while the flexural strain decreases by 50%. c-d, Proof of concept of fast prototyping of dried rDNGHs. As an example, a M5 molded wrench cannot tighten a M4 bolt (c). The wrench is therefore recycled and casted into a new M4 wrench, enabling us to tighten the bolt (d). Scale bars are 5 mm. Reproduced with permission [255]. Copyright 2022, Wiley-VCH.

to the intrinsic recyclability of our material, it is possible to reprocess our plastic within the same day and adapt the design to better fit the nut, as shown in Figure 5.11d. As a result, the final tool can easily tighten the nut to the bolt.

5.5   Conclusion

We introduce a 3D printable, recyclable double network granular hydrogel that can bear loads up to 0.7 MPa. The material is composed of microgels that are connected through a degradable covalently crosslinked network that interpenetrates the microgels and covalently crosslinks them. The ability to selectively degrade the percolating secondary network enables a fast, benign material disassembly. The microgels can be recovered at a yield close to 1, purified and loaded with new reagents, before they are again processed into a rDNGH whose mechanical properties closely resemble those of the pristine counterpart. Importantly, the degradation procedure is not limited to hydrogels or disulfide-based linkers but can be extended to a broader range of materials and reversible chemistries, thus making this process generalizable. Finally, we showcase a proof of concept for the translation of rDNGHs to the fabrication of recyclable hard plastics. We envisage this approach to have the potential to shift the paradigm of recyclable polymeric materials and serve the bigger purpose of fighting global environmental pollution.

CHAPTER 6

Load-Bearing Hydrogels Ionically Reinforced Through Competitive Ligand Exchanges

As discussed in Chapter 4 and Chapter 5, DNGHs display remarkable improvements in terms of structural control and mechanics. However, their mechanical performances remain too low compared to their natural counterparts, thus limiting their use for load-bearing applications. A possibility to increase stiffness and toughness of such materials would be to reinforce them with metal ions.

To enable this, I first introduce a metal-coordination technique to reinforce hydrogels in bulk to gain a fundamental understanding of the influence of metal ions, distribution, and concentration on the hydrogel mechanics. In this chapter, I discuss the metal-reinforcement of single network hydrogels through a competitive ligand exchange approach. Once crosslinked, the hydrogel is immersed in a solution containing free metal ions and a ligand with affinity similar to that of the hydrogel network. As a result, I can control the homogeneous distribution of metal-coordination within the network, thus achieving a controlled reinforcement effect. Additionally, I can exploit the dynamic nature of competitive ligand exchanges to selectively remove metal ions from the network surface to obtain heterogeneous core-shell structures. This novel approach offers a new degree of control over the local composition of soft materials, and shows great potential for the fabrication of synthetic materials that closely resemble natural ones.

M. Hirsch, and E. Amstad analyzed the data and wrote the manuscript.

Contents

6.1   Abstract

Fast advances in soft robotics and tissue engineering demand for new soft materials whose mechanical properties can be interchangeably and locally varied, thereby enabling, for example, the design of soft joints within an integral material. Inspired by nature, we introduce a competitive ligand-mediated approach to selectively and interchangeably reinforce metal-coordinated hydrogels. This is achieved by reinforcing carboxylate-containing hydrogels with Fe^{3+} ions. Key to achieving a homogeneous, predictable reinforcement of the hydrogels is the presence of weak complexation agents that delay the formation of metal-complexes within the hydrogels, thereby allowing a homogeneous distribution of the metal ions. The resulting metal-reinforced hydrogels show a compressive modulus of up to 2.5 MPa, while being able to withstand pressures as high as 0.6 MPa without appreciable damage. Competitive ligand exchanges offer an additional advantage: They enable non-linear compositional changes that, for example, allow the formation of joints within these hydrogels. These features open up new possibilities to extend the field of use of metal reinforced hydrogels to load-bearing applications that are omnipresent for example in soft robots and actuators.

6.2 Introduction

Hydrogels are networks composed of synthetic or nature-derived polymers that are infiltrated with large quantities of water. They are often used for moistening purposes, for example in wound healing [43], food packaging [264], soil moisturizing [265], and drug delivery [35], owing to their ability to absorb up to 98 wt% of water. The properties and functionalities of synthetic hydrogels can be tuned over a wide range with the choice of monomers and oligomers they are made from. It is much more difficult to tune the properties and functionalities of natural hydrogels because they are fabricated from nature-derived hydrophilic high molecular weight polymers whose structure and composition cannot easily be adjusted. However, their intrinsic biocompatibility, bioactivity, and biodegradability renders them attractive scaffolds for soft biological tissues and sustainable soft materials.

The stiffness of synthetic covalently crosslinked hydrogels depends on their crosslink density. Unfortunately, highly crosslinked, stiff hydrogels that can bear significant loads are typically rather brittle. Their toughness can be improved with the introduction of sacrificial bonds, leading to multi-network designs [53, 266]. Sacrificial bonds can consist of hydrophobic interactions [267], reversible covalent crosslinks [78], metal coordination [63, 268], host-guest interactions [200], nanoparticle-based crosslinkers [86], or a combination of them [201]. However, the increase in toughness of these reinforced hydrogels typically comes at the expense of their stiffness such that they cannot be used for load-bearing applications. Reinforcing carboxylic acid-based covalently crosslinked hydrogels with trivalent cations (e.g. Fe^{3+}, Al^{3+}) promises great potential to obtain hydrogels that combine mechanical stiffness and high toughness [68, 266, 269, 270, 271, 272]. However, infiltration of these hydrogels with metal ions typically results in non-homogeneous structures that are difficult to control and hence, the mechanical properties of the resulting materials are poor. Hydrogels have recently been homogeneously reinforced with ligand-mediated ion infiltration [273, 274]. However, this strategy was not exploited to deliberately and non-linearly change the hydrogel composition.

Nature produces soft materials possessing fascinating mechanical properties that are achieved through well-defined non-linearly changing compositions [28, 275]. The composition of soft synthetic materials can be controllably locally varied [99] for example if they are formed from solutions that undergo phase separations [96], through mineral infiltration [204], or magnetic actuation [206]. However, the ability to selectively and non-linearly remove or modify the graded composition is still lacking. The introduction of nature-derived hydrogels possessing adjustable non-linear composition gradients that render them sufficiently stiff and tough to bear significant loads without catastrophically failing, by repeatedly

modifying their internal structure and composition would open up new possibilities to use
them, for example, as cartilage replacements [223, 276, 277], artificial muscles [278, 279],
and soft actuators [280].

We introduce strong hybrid hydrogels composed of the nature-derived methacrylate-functionalized
carboxymethyl cellulose (CellMA) and synthetic acrylic acid (AA). In its dormant state,
the network is covalently crosslinked and can be reversibly stiffened and hardened *in situ*
through the addition of ions that form reversible bonds. We introduce competitive lig-
and exchanges to obtain controlled non-linear compositional gradients that harden and
toughen the material. This approach integrates conventional synthetic design principles
into biologically relevant materials, thereby enabling the design of non-linear composi-
tional changes that result in an unprecedented control over the mechanical properties of
hybrid hydrogels. The ability of this hybrid material to bear pressures of up to 0.6 MPa
in compression opens up new possibilities to build the next generation of implants in or-
thopedics if made from biocompatible materials. Similarly, they have the potential to be
used as soft robots that can change their mechanical properties *in situ.*

6.3   Experimental Section

Experimental details are reported in Chapter 3 from Section 3.4.1 on page 52 to Section
3.4.8 on page 54.

6.4   Results and Discussion

6.4.1   CellMA-PAA Hydrogel Synthesis Process

Carboxymethyl cellulose (CMC)-based hydrogels are typically used for drug delivery [281,
282] and tissue engineering [40] owing to their intrinsic biocompatibility, biodegradability,
and low cost. However, pure CMC hydrogels are rarely used for load-bearing applications
because they are soft and possess a limited stretchability such that they catastrophically
fail if excessively stretched [283]. To increase the toughness of CMC, we chemically modify
it with methacrylate groups to form CellMA. Unfortunately, when gelled alone, CellMA
hydrogels are rather fragile because the crosslinks between individual cellulose chains are
relatively short, as shown in Figure 6.1. This result is well in agreement with other
reports on covalently crosslinked cellulose [284]. However, this chemical modification
allows to exploit the biopolymer as macromolecular multifunctional crosslinker for the
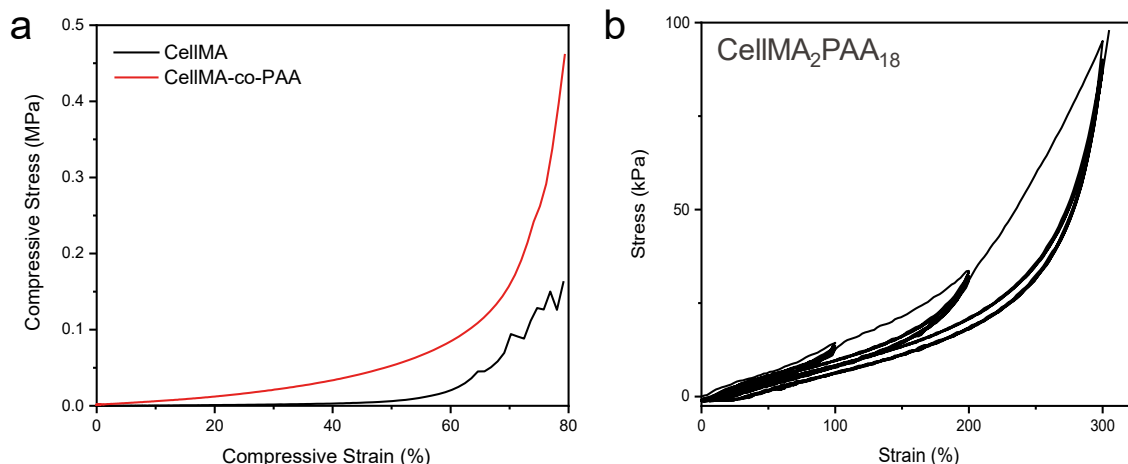
Figure 6.1: Compressive curves of CellMA and CellMA-PAA hydrogels. a, The curves show a clear toughening of the sample when CellMA is crosslinked with acrylic acid. b, Cyclic tensile loading reveals a Mullin's behavior of the hydrogel. Upon a first cycle, a hysteresis loop is present due to the irreversible deformation of the network. The following cycles that are performed to the same maximum elongation display a purely elastic behavior. Reproduced with permission [69]. Copyright 2021, Royal Society of Chemistry.

free radical polymerization of a synthetic monomer, AA, as schematically shown in Figure 6.2a [282, 285].

6.4.2 One-pot CellMA-PAA-Fe Hydrogel Fabrication

The toughness of hydrogels usually increases if reversible bonds are introduced [57, 202, 286, 287]. We leverage this behavior to increase the toughness of CellMA-based hydrogels by adding Fe^{3+} ions to form ionic crosslinks between carboxylic groups that are presented by adjacent CellMA molecules. The intensity of the red color within the hydrogels increases with increasing Fe^{3+} concentration present in the initial solution, as shown in Figure 6.3a, hinting at an increasing concentration of Fe^{3+} ions within the hydrogels. If these ions are added during the thermal radical polymerization reaction of the CellMA, as is typically done [286, 288], the toughness of the hydrogels only modestly increases from 20 kJ·m^{-3} to 40 kJ·m^{-3}. We assign the small increase in hydrogel toughness to the reduced density of covalent crosslinks. Such an effect is caused by the competitive formation of redox reactions between Fe^{3+} ions and the radical initiator, that strongly affects the polymerization efficiency of CellMA [289, 290]. Indeed, if we add as much as 4 mol% FeCl$_3$, the resulting hydrogels cannot retain their shape, indicating that the density of covalent crosslinks is very low, as shown in Figure 6.3a.

To minimize the effect of Fe^{3+} on the density of covalent bonds that form, we limit its concentration to 1 mol%. Cyclic compression tests performed on the resulting hydrogels reveal that they soften after the first cycle, as shown in Figure 6.3b. We observe a
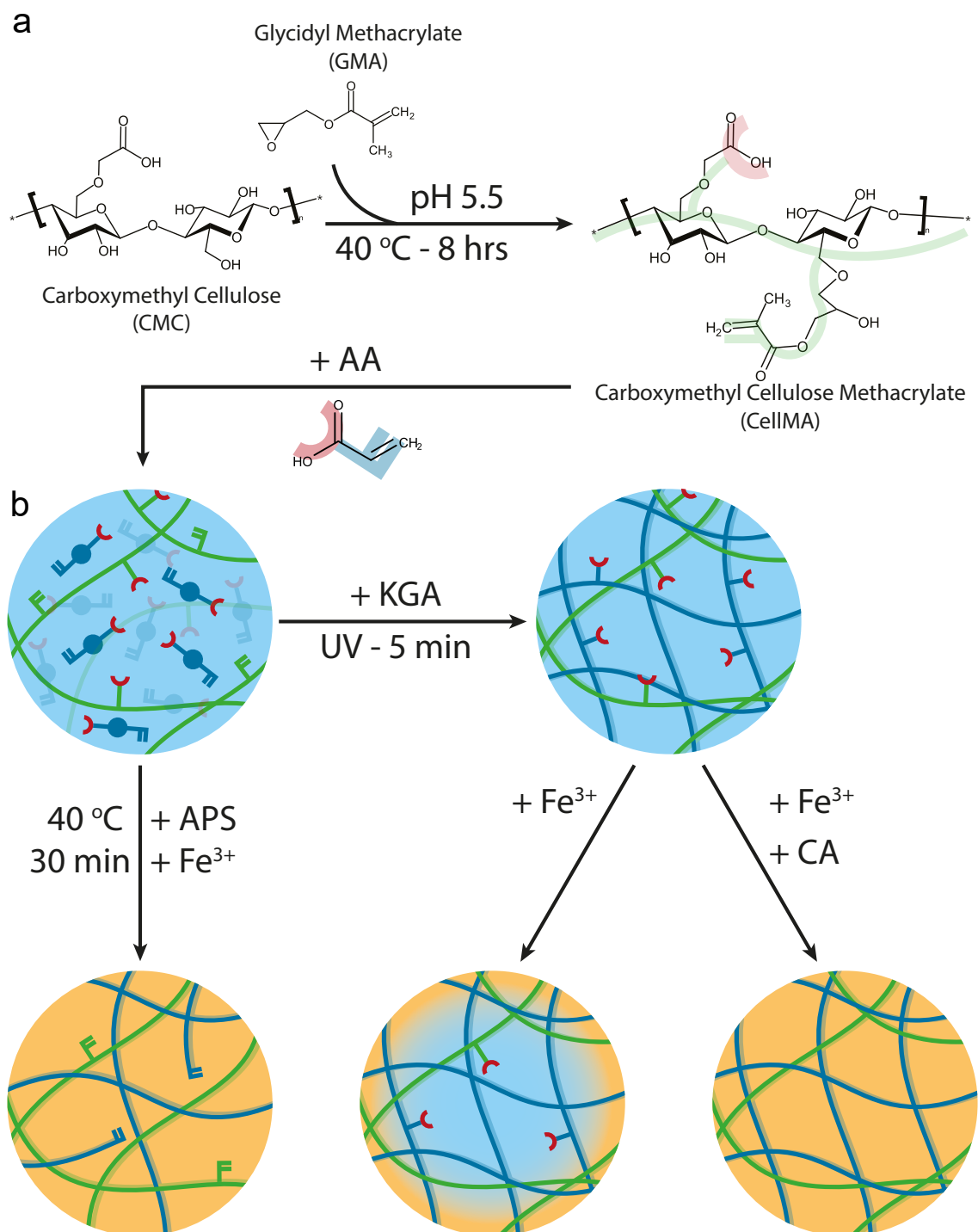
Figure 6.2: Preparation of CellMA-PAA-Fe hydrogels. a, Schematic representation of the grafting process used to produce CellMA polymers. b, Schematic representation of the one-pot (left) and two-step (right) synthesis routes for the preparation of CellMA-PAA-Fe hydrogels. In the one-pot approach, AA is added to a solution containing 2 wt% CellMA, $FeCl_3$, and APS prior to crosslinking. In the two-step process, AA and CellMA are mixed with KGA and the polymerization is carried out under UV exposure. After crosslinking, the hydrogels are immersed in a $FeCl_3$ containing solution to form the secondary ionic crosslinks. Samples exposed to a combination of $FeCl_3$ and CA are more homogeneous and stronger. Reproduced with permission [69]. Copyright 2021, Royal Society of Chemistry.

similar behavior for CellMA-PAA hydrogels that are not ionically crosslinked, indicating that part of the covalent network is irreversibly damaged when compressed. As expected, the ionic crosslinks increase the hysteresis of the stress-strain curve, as summarized in Figure 6.4. Note that this hysteresis remains high for ionically crosslinked hydrogels also during all the subsequent cycles, in stark contrast to purely covalently crosslinked CellMA-PAA hydrogels. These results demonstrate that Fe^{3+} ions significantly increase the toughness of CellMA-PAA hydrogels. Indeed, ions increase the energy dissipated during a cyclic compression test two-fold from 19 kJ·m^{-3} for pure CellMA-PAA hydrogels to 39 kJ·m^{-3} for CellMA-PAA counterparts that are ionically crosslinked with 1 mol% Fe^{3+} (CellMA-PAA-Fe). These results are in good agreement with findings in metal-reinforced carboxylic-containing purely synthetic and hybrid hydrogels [57, 291, 292]. Despite the clear influence of metal coordination on the toughness of our material, no additional information can be derived from cyclic tensile measurements of CellMA-PAA samples. Hence, we limit the characterization of the mechanical properties of our hydrogels to the static compression tests.

Our results indicate that the Fe^{3+} concentration influences the mechanics of the CellMA-PAA-Fe hydrogels. To investigate the reason for this behavior, we perform frequency sweeps on CellMA-PAA-Fe hydrogels as a function of the Fe^{3+} concentration. In the absence of any crosslinking ions, CellMA-PAA displays a purely elastic behavior, as shown in Figure 6.3c. Upon addition of 1 mol% Fe^{3+}, the mechanics of the hydrogel includes a viscoelastic component, as indicated by the change in slope of the loss modulus, G". We attribute the viscoelastic component to the reversible bonds that form between the carboxyl groups of the CellMA-PAA hydrogel and the Fe^{3+} ions. Note that the storage modulus, G', of samples produced from solutions containing 4 mol% Fe^{3+} is significantly lower than that of samples produced from solutions containing lower ion concentrations, supporting our hypothesis that the presence of Fe^{3+} ions decreases the density of covalent crosslinks. Nevertheless, G' is still higher than G" confirming the presence of a weak percolating network that renders the material solid.

The mechanical properties of ionically crosslinked hydrogels strongly depend on the dissipation times of the ionic crosslinks [63, 199]. To estimate the dissipation times of the ionic bonds involved in our hydrogels, we perform stress relaxation tests and compare them to a pure CellMA-PAA hydrogel. The slope of the normalized shear modulus, G(t)/G$_0$, increases with increasing Fe^{3+} concentration suggesting an increase in dissipation times, as shown in Figure 6.3d. The increase in dissipation times is accompanied by a moderate increase in strength and toughness of the ionically crosslinked CellMA-PAA hydrogels. Hence, it would be highly advantageous to increase the Fe^{3+} concentration within CellMA-PAA hydrogels without compromising their covalent network. Unfortunately, Fe^{3+} ions
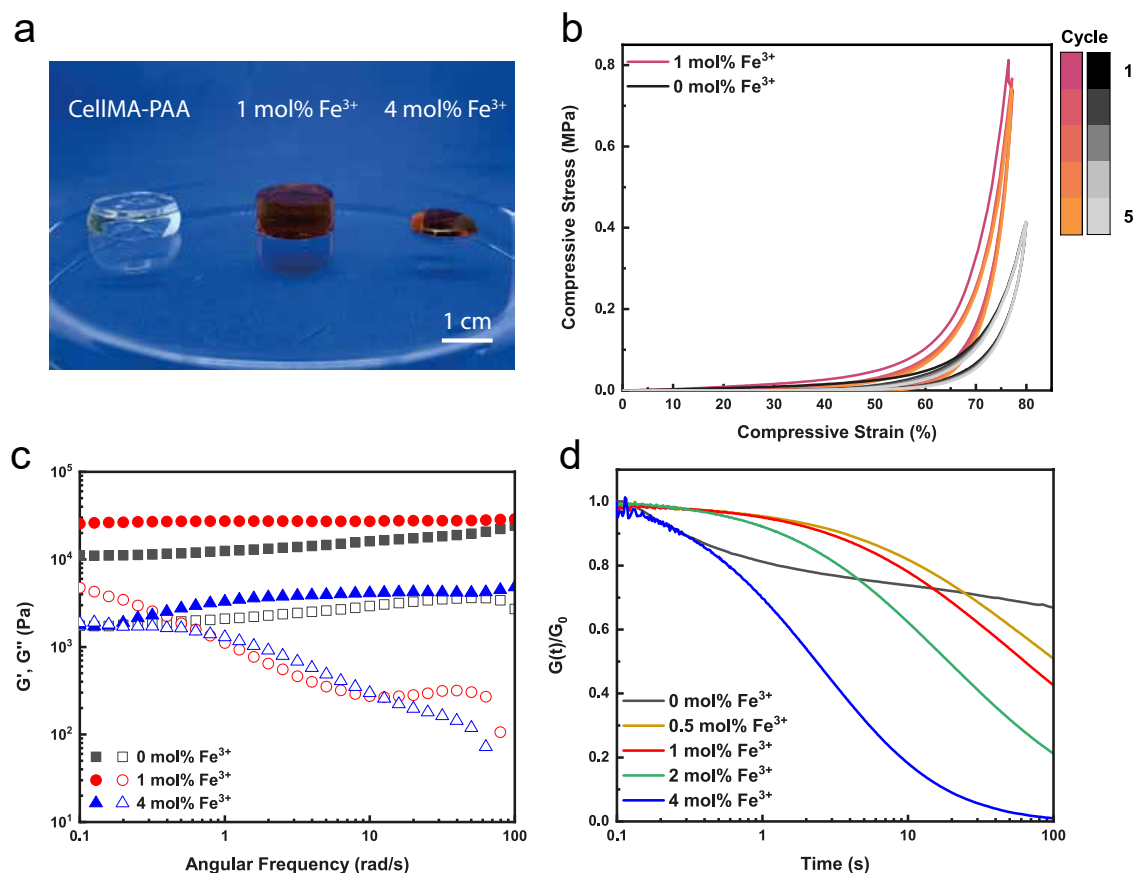
Figure 6.3: Mechanical and rheological characterization of one-pot CellMA-PAA-Fe hydrogels. a, Photograph of the as-prepared CellMA-PAA hydrogels reinforced with 0, 1, and 4 mol% Fe^{3+}. At high iron concentrations, the polymerization is hindered and the sample cannot retain its shape after demolding. b, Cyclic compression tests of CellMA-PAA containing 0 and 1 mol% Fe^{3+}. The Fe^{3+}-reinforced sample shows a higher modulus and hysteresis throughout all the cycles. c, Frequency sweep measurement of CellMA-PAA hydrogels reinforced with 0, 1, and 4 mol% Fe^{3+}. The sample produced with 4 mol% Fe^{3+} displays a lower storage modulus (G') than Fe^{3+}-free samples, and those reinforced with 1 mol% Fe^{3+}. Moreover, it displays a crossover point at 0.2 rad/s suggesting a more viscoelastic behavior. d, Stress-relaxation measurements performed on CellMA-PAA hydrogels reinforced with 0, 0.5, 1, 2, and 4 mol% Fe^{3+} reveal a decrease in relaxation times with increasing iron content. Reproduced with permission [69]. Copyright 2021, Royal Society of Chemistry.

interfere with the radical polymerization reaction, thereby limiting the range of mechanical properties that can be achieved with CellMA-PAA-Fe hydrogels produced through a one-pot approach.

6.4.3 Two-Step CellMA-PAA Hydrogel Fabrication

To extend the range of mechanical properties CellMA-PAA-Fe hydrogels can display, we must temporally decouple the formation of the covalent network from the formation of ionic crosslinks. To do so, we initially form the covalent network through an UV-light
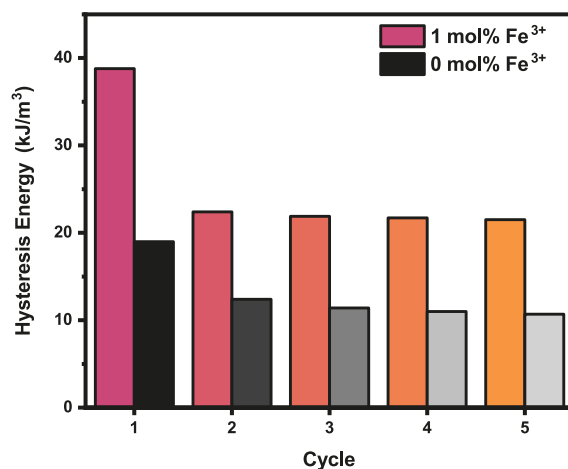
Figure 6.4: Hysteresis energies for CellMA-PAA and CellMA-PAA-Fe. Extracted hysteresis energy of CellMA-PAA hydrogels prepared in a one-pot approach crosslinked with 0 and 1 mol% Fe^{3+}. Values are calculated from 5 repeated compressive cycles. The sample reinforced with 1 mol% Fe^{3+} displays a 2-fold higher hysteresis energy than the non-reinforced counterpart.

initiated radical polymerization reaction between the CellMA and AA to form CellMA-PAA hydrogels in the absence of any Fe^{3+} ions. We subsequently expose the covalently crosslinked hydrogels to an aqueous solution containing $FeCl_3$ to form the second, ionic network. This procedure offers the distinct advantage that the covalent and ionic networks can be independently tuned. We expect the stiffness of our CellMA-PAA hydrogels to be mainly determined by the rather rigid CellMA polymers such that it should increase with increasing CellMA concentration. To test our expectation, we vary the CellMA concentration from 1 to 5 wt% while keeping the total polymer content constant at 20 wt% and assess the mechanical properties of the resulting CellMA-PAA hydrogels with compression tests. As expected, the compressive modulus increases with increasing CellMA concentration from 30 kPa for 1 wt% to 100 kPa for 5 wt%, as shown in Figure 6.5a, and summarized in Figure 6.5b. We assign the stiffening to an increase in the physical crosslink density that is caused by the higher CellMA concentration, a shortening of the PAA crosslinking chains, that is caused by the reduction in PAA concentration, or a combination of the two parameters. However, the increase in stiffness is accompanied with an increase in viscosity of the precursor solution, which makes the sample preparation more difficult. To trade-off the stiffness of the hydrogels with the viscosity of the hydrogel solution and hence its processability, we fix the CellMA concentration to 2 wt% for the following experiments.

Cellulose chains contained in cellulose-reinforced hydrogels gradually fracture such that these hydrogels display a stress dissipation behavior [109]. To test if cellulose chains contained in our hybrid hydrogels also gradually fracture, we subject the CellMA-PAA hydrogels to cyclic tensile tests. Indeed, our hydrogels display a strong hysteresis during
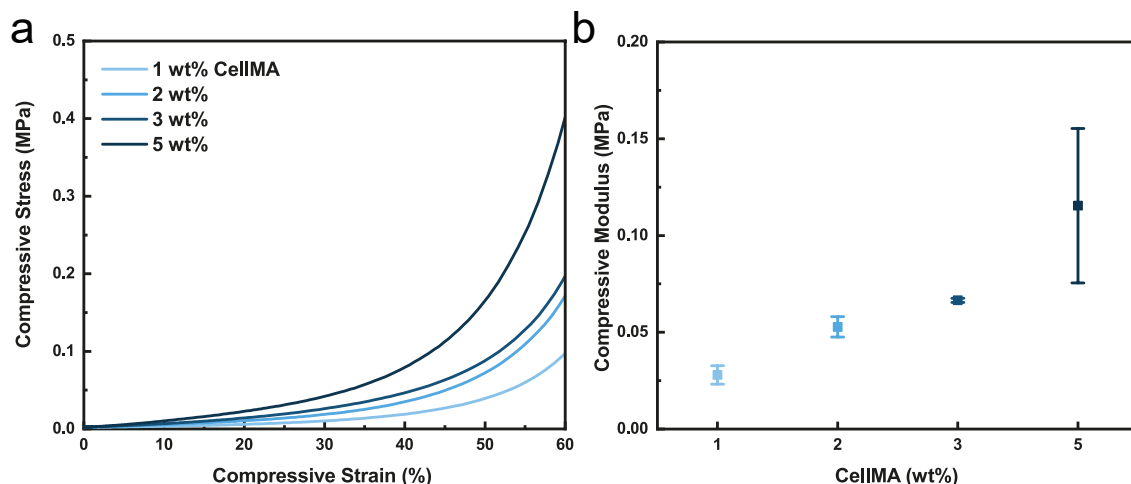
Figure 6.5: Mechanical characterization of CellMA-PAA hydrogels. a, Compression curves of CellMA-PAA hydrogels whose total polymer content was fixed to 20 wt%. The stiffness and toughness of these hydrogels increase with increasing CellMA concentration. b, Compressive moduli of CellMA-PAA hydrogels measured in a. The compressive modulus increases with increasing CellMA content. Data points are presented as mean $\pm$ standard deviation. Each data point is the result of 5 independent measurements. Reproduced with permission [69]. Copyright 2021, Royal Society of Chemistry.

the first cycle, as shown in Figure 6.1. These results indicate that our hydrogels dissipate a significant amount of energy during the first cycle most likely because part of the cellulose polymers break. Remarkably, the hydrogel exhibits a nearly elastic behavior during the next 10 cycles. We obtain a similar result if we increase the stretch magnitude from 100% to 300%, as shown in Figure 6.1. This phenomenon is usually referred as the Mullins effect, and has been reported for interpenetrating network hydrogels [57, 109, 293] and filled elastomers [221, 294, 295].

6.4.4 Hydrogel Reinforcement Through Dynamic Ligand Exchanges

To test the influence of Fe^{3+} on the mechanical properties of CellMA-PAA hydrogels that are produced in a two-step process, we soak our covalently crosslinked sample in a Fe^{3+} containing solution. The resulting CellMA-PAA-Fe hydrogels display an uneven ion distribution: the Fe^{3+} concentration is high in proximity to the surface of the hydrogel and gradually decreases towards its center. We attribute this heterogeneous distribution of Fe^{3+} ions to their strong interaction with carboxylic groups that captures a high concentration of Fe^{3+} ions at the hydrogel surface. As a result, free Fe^{3+} ions that attempt to infiltrate the hydrogel after this first layer has been formed encounter a hydrogel that has a significantly higher crosslink density and hence, is less permeable to them. In addition, arriving Fe^{3+} ions are electrostatically repelled by the Fe^{3+} ions that are already complexed by the carboxylic groups. Both effects reduce the ion diffusion into the hydrogel

core.

The ion gradient present within the hydrogel that displays a core-shell structure imparts a strong osmotic pressure to it such that it collapses, as shown in Figure 6.6a. To overcome this limitation, we complex Fe^{3+} with a weak ligand, citric acid (CA). The binding affinity of CA towards Fe^{3+} is similar to that of the carboxylic groups contained in CellMA-PAA [248]. As a result, we expect the two systems to compete for Fe^{3+} ions to form coordination complexes, thereby slowing down the interaction between ions and chelators, as has been shown for Ca^{2+} crosslinked alginate [296, 297]. We expect this delay in ion-chelator interactions to result in a more homogeneous Fe^{3+} distribution. To test our expectation, we soak CellMA-PAA hydrogels in a solution containing 1 mol% Fe^{3+} and vary the concentration of CA. Remarkably, hydrogels immersed in an aqueous solution containing 1 mol% Fe^{3+} and 1.5 mol% CA are 10-fold stiffer than counterparts that are immersed in a Fe^{3+}-containing but CA-free aqueous solution: hydrogels that are soaked in a solution containing Fe^{3+} and CA display a compressive modulus of 0.87 MPa, compared to those soaked in an Fe^{3+}-containing, CA-free solution, whose modulus is 0.08 MPa. An increase of CA to 3 mol% moderately decreases the stiffness of the hydrogel while improving the homogeneity of Fe^{3+} ions contained within it, as shown in Figure 6.7. Note that a further increase in the CA concentration strongly decreases the compressive modulus, as shown in Figure 6.6b. The decrease in Young's Modulus is attributed to an excess of carboxylic groups in solution that compete with those contained within the hydrogel and hence, reduce the number of Fe^{3+} ions complexed within the hydrogel. Hence, there is an optimum CA concentration that is sufficiently high to complex the majority of free Fe^{3+} ions, thereby preventing a fast formation of a rather stiff skin at the hydrogel surface, and sufficiently low to avoid scavenging Fe^{3+} ions from the hydrogel.

Our results demonstrate that the stiffness of CellMA-PAA hydrogels increases up to 10-fold if they are infiltrated with Fe^{3+} that is initially complexed with CA. These results are in good agreement with our previous observation and confirm that the CA present in solution competes with the Fe^{3+} complexation of the carboxy groups contained in the hydrogels. Indeed, the benefit of competitive ligand exchange is lost if the molar ratio of carboxylic groups in solution ([-COOH(CA)]) to that attached to the hydrogel ([-COOH(AA)]) exceeds 1, suggesting that in this case, the majority of Fe^{3+} ions is complexed by CA and remains in solution, as shown in Figure 6.6c.

We expect the distribution of Fe^{3+} ions and hence, the local differences in mechanical properties within the hydrogels to depend on the CA : Fe^{3+} ratio. To test this expectation, we vary the CA : Fe^{3+} ratio from 1.5 to 6 by independently varying the CA and Fe^{3+} concentrations. The compressive modulus of all tested hydrogels reaches a maximum if the CA : Fe^{3+} molar ratio is 1.5, as shown in Figure 6.6d. For instance, the compressive
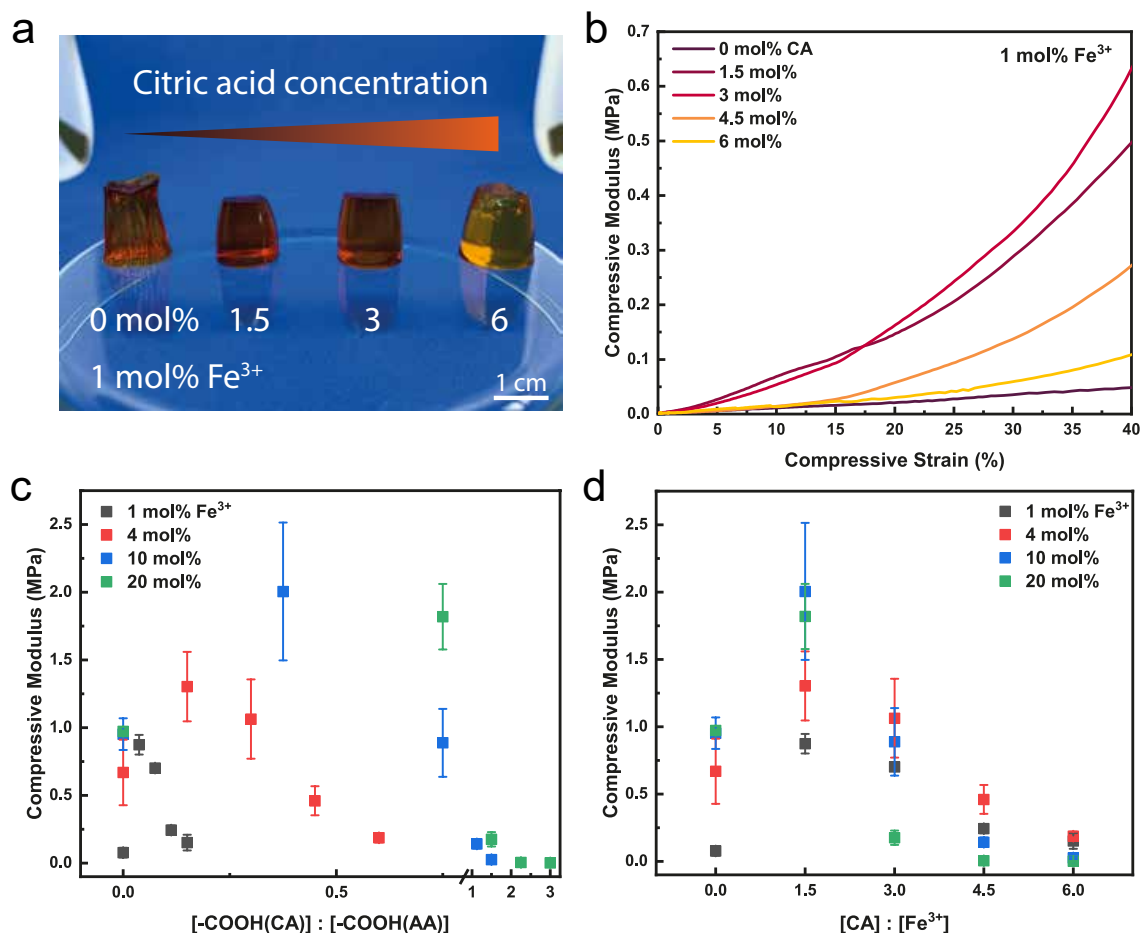
Figure 6.6: Mechanical characterization of two-step CellMA-PAA-Fe hydrogels. a, Photograph of CellMA-PAA-Fe prepared with 1 mol% Fe^{3+} and various amounts of CA. In the absence of CA, hydrogels display a hard and brittle surface and a soft core. With increasing CA concentration, the homogeneity of hydrogels increases until a critical threshold is reached. Above this threshold, the chelation is hindered and the hydrogel remains soft. b, Compression curves of CellMA-PAA-Fe reinforced with 1 mol% Fe^{3+} and various amounts of CA. The stiffness and toughness of the hydrogel increase with the CA concentration until it exceeds 3 mol%. c, Compressive modulus of CellMA-PAA-Fe hydrogels as a function of the [-COOH(CA)] : [-COOH(AA)] molar ratio. When the ratio reaches 1 the benefit of the competitive ligand exchange is lost. d, Compressive modulus of CellMA-PAA-Fe hydrogels as a function of the [CA] : [Fe^{3+}] molar ratio. Independent of the amount of Fe^{3+} initially contained in the solution, the optimal CellMA-PAA-Fe reinforcement is obtained at a [CA] : [Fe^{3+}] molar ratio of 1.5. Reproduced with permission [69]. Copyright 2021, Royal Society of Chemistry.

modulus reaches its maximum value of 2 MPa at 10 mol% Fe^{3+} and 1.5 CA : Fe^{3+} molar ratio. These results demonstrate that the mechanical properties of CellMA-PAA hydrogels can be independently tuned with the Fe^{3+} and CA concentrations. In our case, the mechanical properties of CellMA-PAA-Fe hydrogels are best if we incubate them in a solution containing 10 mol% Fe^{3+} and 15 mol% CA, such that we use this protocol for the remaining experiments.
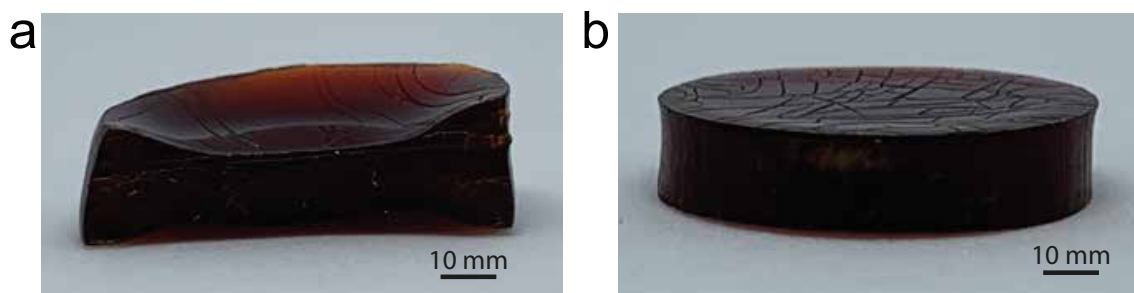
Figure 6.7: Optical photograph of CellMA-PAA-Fe hydrogels. Photographs of CellMA-PAA hydrogels reinforced with 1 mol% Fe^{3+} in the presence of 1.5 mol% (a), and 3 mol% (b) CA. At lower CA concentrations, the Fe^{3+} concentration is heterogeneous, creating an osmotic pressure that deforms the sample. Reproduced with permission [69]. Copyright 2021, Royal Society of Chemistry.

6.4.5 Core-Shell CellMA-PAA Hydrogels

Key to obtaining good mechanical properties of CellMA-PAA-Fe hydrogels is a homogeneous distribution of the Fe^{3+} ions within the hydrogel. The limited diffusion of Fe^{3+} ions within ionically crosslinked hydrogels necessitates the use of complexation agents to obtain a homogeneous distribution. However, the limited diffusivity of ions within hydrogels can also be used as an asset: It enables introducing core-shell structures into hydrogels. To demonstrate this feature, we exploit the same ligand exchange principle we used to form homogeneous CellMA-PAA-Fe hydrogels: We expose CellMA-PAA-Fe hydrogels possessing a homogeneous Fe^{3+} distribution to an aqueous solution containing an excessive CA concentration overnight. Taking advantage of the limited diffusivity of CA in the hydrogel, we confine its scavenging effect to the hydrogel surface. As a result of the ion depletion that primarily occurs in proximity to the hydrogel surface, only this surface softens. To prevent further scavenging, the concentration of CA in the solution is kept to low, at 2 mol%. If we incubate these hydrogels in an Al^{3+} containing solution, the freed carboxylic groups of the CellMA-PAA-Fe hydrogel can bind these new ions to form a core-shell structure, as schematically shown in Figure 6.8a. To verify that we indeed formed a core-shell structure, we perform energy dispersive X-ray spectroscopy (EDX) on a cross-section of our sample. To account for topographic artifacts, we compare ion profiles of Al, and Fe to the C signal. The results evidence a high concentration of Al ions within the first 100 µm from the surface of the hydrogel, while Fe and C are homogeneously distributed, as shown in Figure 6.8b, and Figure 6.9. These results confirm the core-shell structure of our sample. Aluminum ions possess a higher binding affinity to carboxylated polymers than Fe^{3+} [298, 299] such that the Al-reinforced shell should be harder. Indeed, nanoindentation measurements reveal a hardness of 20.7 MPa for the Al-reinforced shell and 3.6 MPa for the Fe-crosslinked core, as shown in Figure 6.8c. However, the increased hardness of the core-shell system renders the material more rigid.
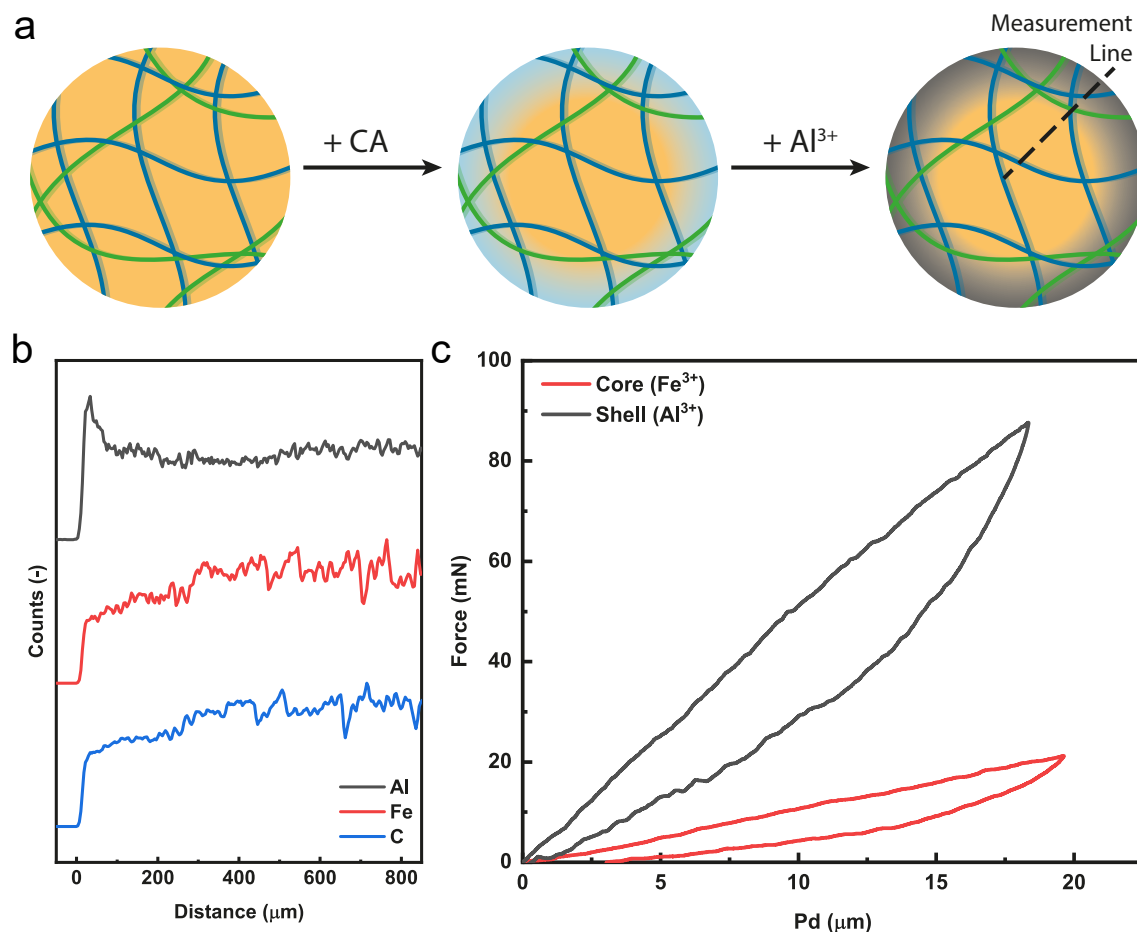
Figure 6.8: Fabrication of core-shell structures. a, Schematic representation of the fabrication of CellMA-PAA hydrogels displaying a Fe^{3+} reinforced core and a Al^{3+} reinforced shell. b, EDX line scans for Al, Fe, and C measured along a cross-section of a CellMA-PAA core-shell hydrogel. The data confirm a high concentration of Al at the interfaces ($\approx$100 µm), while Fe and C are homogeneously distributed within the entire cross-section. c, Nanoindentation measurement of a CellMA-PAA core-shell hydrogel. The shell displays a hardness of 20.7 MPa, while the core is 7-fold softer. Reproduced with permission [69]. Copyright 2021, Royal Society of Chemistry.
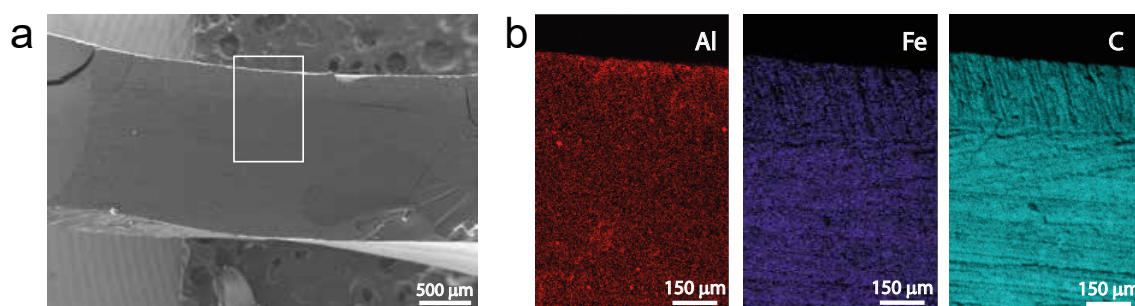
Figure 6.9: SEM and EDX micrographs. a, SEM micrograph of a core-shell CellMA-PAA hydrogel and the corresponding EDX area (white box). b, 2D EDX maps displaying the distribution of Al, Fe, and C respectively. Reproduced with permission [69]. Copyright 2021, Royal Society of Chemistry.

6.4.6 Fabrication of Conformable Dynamic Hydrogel Structures

The ligand-dependent mechanical properties of our hybrid hydrogels render them appealing for the design of conformable shape-retaining structures. To demonstrate this feature, we cast a cross-shaped hydrogel sheet that is molded into a stool-like structure before it is reinforced with Fe^{3+} ions, as shown in Figure 6.10a(i). The Fe^{3+}-reinforced hydrogel stool is strong enough to withstand a 1 kg weight, corresponding to a pressure of 0.6 MPa, with no appreciable shape deformation or damage, as shown in Figure 6.10a(ii). Upon immersion in a CA-containing solution, the stool softens and the structure collapses due to the applied load, as shown in Figure 6.10a(iii). This process can be repeated at least 5 times, demonstrating the robustness of this material.

Our approach enables local changes in mechanical properties that are predestined to form joints within a single integral hydrogel sheet. To demonstrate this asset, we cast a rectangular sheet with dimensions of 50 x 17 x 2 mm^3 and soak it in an aqueous bath containing $FeCl_3$ and CA to reinforce it. The resulting hydrogel is rigid and able to hold up to 100 g, corresponding to a pressure of 0.03 MPa, applied to one extremity without bending, as shown in Figure 6.10b(i). When the middle section of the bar is exposed to a CA containing solution, it locally softens to form a joint that bends if one of its extremity is loaded with 100 g, as shown in Figure 6.10b(ii). To demonstrate the reversibility of the process, we immerse the entire bar again in a Fe^{3+} containing solution to stiffen it and thereby to lock its shape. Indeed, the resulting L-shaped piece can again hold the 100 g weight applied to one of its extremities without deforming, as shown in Figure 6.10b(iii). These results indicate the potential of our hydrogel to serve as a load-bearing material that can be rendered locally flexible to serve as a joint, a feature, that is of increasing importance especially in the field of soft actuators and robots.
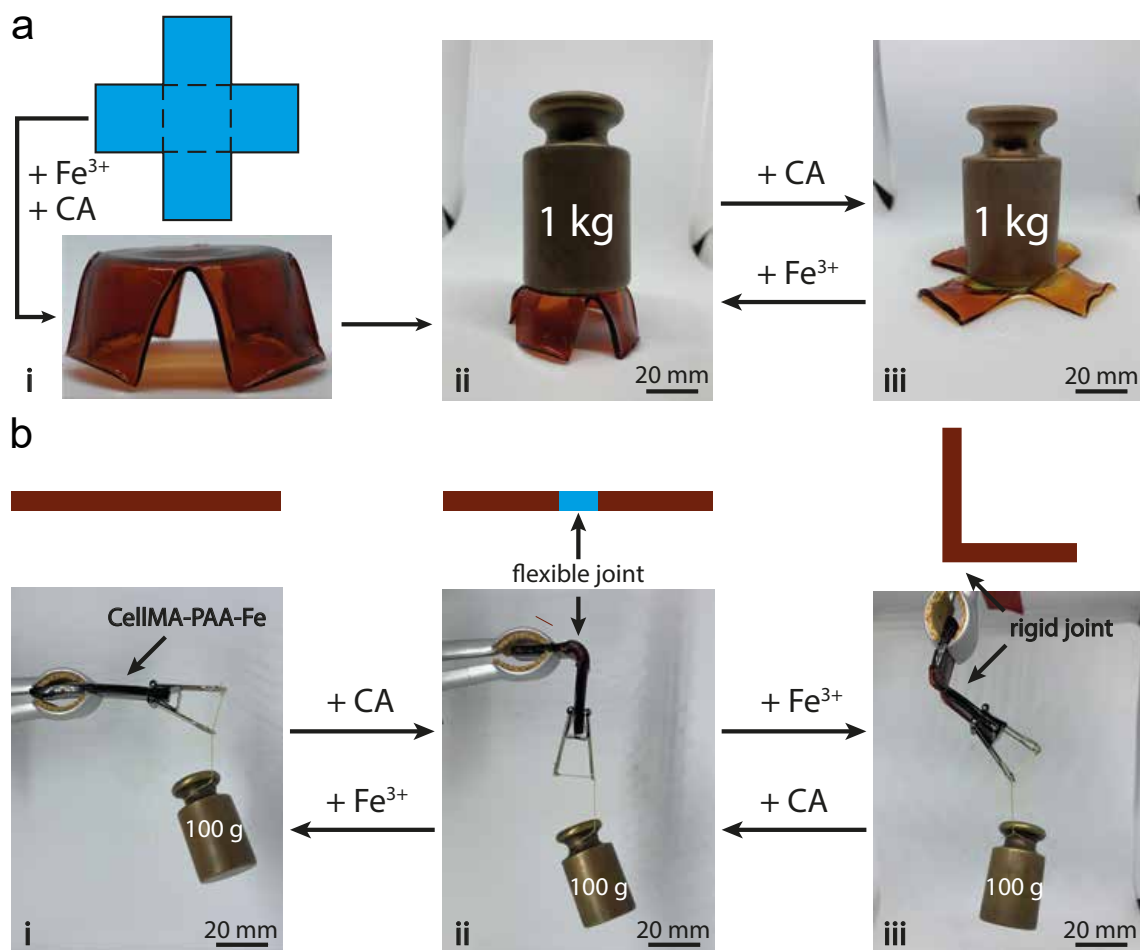
Figure 6.10: Fabrication of conformable load-bearing structures through competitive ligand exchanges. a, (i) A cross-shaped CellMA-PAA hydrogel is exposed to a Fe^{3+}-CA containing solution to lock its shape to that of a stool. (ii) The obtained stool can support a 1 kg weight without buckling or failure, corresponding to a pressure of 0.6 MPa. (iii) Upon exposure to a CA solution, the structure softens and the hydrogel collapses. This process can be repeated several times without noticeable losses in the load-bearing capacity of the CellMA-PAA-Fe hydrogel. b, (i) A CellMA-PAA-Fe sheet holds a weight of 100 g that is attached to one of its extremities. (ii) Upon exposure to CA, the sheet locally softens, thus creating a flexible joint. (iii) if immersed in a Fe^{3+} containing solution, the sheet stiffens such that it can again hold a 100 g weight at one of its extremities. Reproduced with permission [69]. Copyright 2021, Royal Society of Chemistry.

6.5 Conclusion

We introduce a two-step process to fabricate metal-reinforced load-bearing hybrid hydrogels that are sufficiently strong to bear loads up to 1 kg under compression. The unprecedented mechanical properties are achieved by ionically reinforcing the covalent CellMA-PAA network with Fe^{3+}. We leverage the limited diffusivity of ions and ligands such as Al^{3+} and citric acid within the hydrogels to introduce non-linear compositional gradients that enable the formation of joints within integral hydrogel sheets. Importantly, the mechanical properties of this hybrid hydrogels can be reversibly tuned with the addition of Fe^{3+} and citric acid respectively, thereby opening up new possibilities to use these hydrogels as soft actuators. These advancements promise to expand the current application window of hybrid hydrogels to load bearing applications.

3D Printing of Metal-Reinforced Double Network Granular Hydrogels

In this chapter, I discuss the possibility to combine the double network granular printing, introduced in Chapter 4, with the mechanical reinforcement of metal-coordination, introduced in Chapter 6. Here, poly(acrylic acid) microgels are produced by mechanical fragmentation to ensure a reproducible and scalable process. These microgels are loaded with a second precursor solution to enable their conversion into a double network granular hydrogel after 3D printing. The resulting double network granular hydrogel is responsive to ions, such that it can be locally reinforced either in the microgels or in the percolating secondary network. As a result, heterogeneously reinforced granular hydrogels can be fabricated displaying mechanical properties that have been unmatched before, namely extremely high stiffness and high toughness. These results bring us a step closer to finally mimicking nature's complexity.

This chapter is adapted from an unpublished work entitled "3D Printing of Ionic-Reinforced Double Network Granular Hydrogels" authored by Matteo Hirsch, Livia D'Onofrio, and Esther Amstad. M. Hirsch, and E. Amstad designed the experiments. M. Hirsch and L. D'Onofrio performed the experiments. M. Hirsch, and E. Amstad analyzed the data and wrote the manuscript.

Contents

7.1 Abstract

Recent developments in soft actuation demand for new resilient materials that can bear
significant loads yet, whose mechanical properties can be changed with a high spatial
resolution. A technique that offers tight control over the composition of a wide variety
of materials on length scales down to 100 µm is extrusion-based 3D printing. However,
the number of inks that enable 3D printing of hydrogel-based materials is limited and
those that can be 3D printed yield in weak hydrogels that prevent bearing significant
loads. This shortcoming can be addressed by formulating hydrogels into microparticles,
so-called microgels, that can be up-concentrated until they are jammed. These jammed
microgels display a rheological behavior that is ideal for 3D printing. However, the weak
inter-particle interactions typically again yield soft 3D printed granular hydrogels that
cannot bear significant loads. Granular hydrogels can be mechanically reinforced through
a percolating hydrogel network that is formed after they have been processed into the
appropriate shape, resulting in double network granular hydrogels (DNGHs). Yet, these
hydrogels are rather brittle. To address this limitation, we introduce 3D printable metal-
reinforced double network granular hydrogels that can bear loads up to 3 MPa while
displaying a fracture energy up to 12 MJ·m^{-3}, a value that exceeds those of previously
3D printed hydrogels 20-fold. By selectively reinforcing only certain regions of DNGHs,
we locally vary their degree of swelling, thereby introducing shape morphing properties
to them without compromising their mechanical performance. We anticipate the freedom
in varying the mechanical properties of 3D printable DNGHs locally without the need to
change the material system and hence, to introduce joints that hamper miniaturization
and compromise the durability of this system to present a paradigm shift in the design of
soft actuators.

7.2 Introduction

Since the beginning of human evolution, the natural world has been a tremendous source of inspiration for the design of functional materials [50]. Excellent work performed in this area allowed us to gain a much better understanding of the chemistry and structure-function relationship of natural materials [28, 300]. For instance, the analysis of soft biological tissues revealed that nature provides self-healing and dynamic stress response to their constructs through non-covalent interactions [49, 301, 302]. One remarkable example is the mussel byssus, a soft load-bearing acellular tissue that allows the organism to strongly anchor to the rocks to even withstand the shear of impacting waves. The unique design of the byssus enables them to repetitively withstand stresses up to 40 MPa and recover their initial state upon release of the load [300]. Inspired by nature, soft synthetic materials have been mechanically reinforced through non-covalent reversible interactions [21, 172, 303], such as host-guest [304, 305] or hydrophobic interactions [267, 306], metal coordination [66, 68, 69, 307], and covalent reversible crosslinkers [255, 308]. Despite the substantial improvement in mechanics of synthetic soft materials, nature remains unmatched. A fundamental reason behind this mismatch in performances is that manmade constructs typically possess homogeneous structures and compositions compared to the well-defined hierarchical structure and abruptly changing composition of their natural counterparts [24, 23, 6]. Recently, several strategies have been implemented to control the structure of soft synthetic materials at different length scales [21, 99, 131, 156], including directed self-assembly [309, 310, 311, 312], phase separation [96, 97, 224, 313, 314], microfluidics [125, 140], and 3D printing [103, 216, 315, 316, 317]. However, attempts to better mimic soft natural tissues have been limited by a poor control on the assembly and resolution. Recently, a novel class of 3D printable materials, jammed microgels, has been developed to increase the level of control over the microstructure and local composition in manmade soft materials [132, 140, 141, 146, 154, 166, 318]. Microgels are micrometer-sized hydrogel particles that undergo jamming when concentrated above a certain critical volume fraction [130, 131]. They can be fabricated from emulsion drop templates produced through batch emulsification [149], or if a tighter size-control is warranted through microfluidics [133, 134, 136, 319]. However, these water-in-oil emulsions must be stabilized with surfactants that, together with the oil, must be removed through several washing steps after the microgels have been produced, thereby limiting the throughput of this technique and increasing the production costs [146]. Microgels can also be made through precipitation polymerization[320] or spray emulsification [144], yet with more stringent requirements in terms of material selection and precursor viscosity. A way to circumvent these shortcomings is to mechanically fragment bulk hydrogels [145, 146, 147, 148] for

example using blenders [321], or sieves [147]. Many more materials can be mechanically fragmented through cryomilling [148], which allows the processing of any material whose T_g is above the temperature of liquid nitrogen (-196 °C), independent on its mechanical properties. Thereby, even hydrogels can be broken into micro-sized particles, so called microfragments at high throughputs [148]. Key to bridging the gap in mechanical performance between synthetic and natural materials is the ability to synergistically combine structural control and local variations in composition. To combine microstructural control with a good stiffness, we introduced 3D printable double network granular hydrogels (DNGHs) made of microparticles that are firmly connected through a second hydrogel network that interpenetrates and covalently crosslinks them [149, 255]. Yet, these materials displayed a limited toughness. Here, we introduce 3D printable metal-coordinated DNGHs whose fracture energy exceeds those of any 3D printed hydrogel reported thus far by at least 20-fold. This is achieved by forming microfragments from poly(acrylic acid) (PAA) that can be ionically reinforced with a wide range of cations. We demonstrate that the stiffness of DNGHs made by covalently crosslinking these microfragments with a percolating PAM hydrogel increases to 0.12 MPa, whereas their work of fracture increases to 0.02 MJ·m^{-3}. The work of fracture of DNGHs increases much more, up to 12 MJ·m^{-3}, if the percolating network is ionically reinforced, as demonstrated on DNGHs composed of polyacrylamide (PAM) microfragments that are connected through a metal-reinforced PAA network. We demonstrate the potential of these materials in soft actuation by 3D printing shape morphing structures. This is achieved by locally reinforcing certain areas to vary the degree of swelling of the hydrogels, that triggers their change in configuration upon exposure to an aqueous solution containing metal ions.

7.3 Experimental Section

Experimental details are reported in Chapter 3 from Section 3.5.1 on page 54 to Section 3.5.8 on page 56.

7.4 Results and Discussion

7.4.1 Metal-Reinforced Double Network Granular Hydrogel Design and Fabrication

To controllably vary the composition of our hydrogels on a 100 μm length scale, we render a bulk PAA hydrogel, 3D printable by cryomilling it into microfragments. The resulting
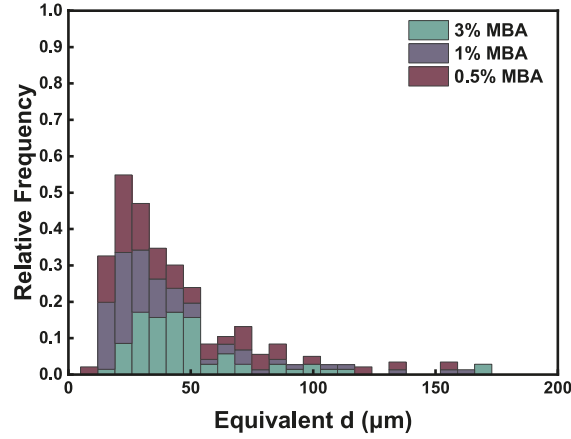
Figure 7.1: Microfragment size distribution. Particle size distribution of cryomilled PAA hydrogels as a function of their crosslinker density. The cryomilling process is independent of the physicochemical properties of the initial bulk hydrogel.

microfragments are non-spherical with an equivalent diameter (d*) of 45 µm, that is independent of the precursor formulation, as shown in Figure 7.1.

To firmly connect the microfragments and thereby impart mechanical stability to the final product, we soak them in an aqueous solution containing acrylamide before they are jammed to enable their 3D printing, as schematically shown in Figure 7.2a. After the ink has been 3D printed, we firmly connect microfragments by crosslinking the acrylamides contained in them to form a percolating network that interpenetrates and crosslinks them, as shown in Figure 7.2b. The granular nature of DNGHs allows for the selective reinforcement of the individual grains, thus enabling the fabrication of heterogeneously reinforced DNGHs, as schematically shown in Figure 7.2c. Alternatively, DNGHs can be composed of polyacrylamide-based microfragments that are connected through a PAA network. In this type of DNGHs, the percolating network can be selectively reinforced with ions, as schematically shown in Figure 7.2c. The ability to control the DNGH structure through 3D printing together with the ability to selectively reinforce it allows the design of shape morphing structures that are of great interest for the field of soft robotics, as schematically shown in Figure 7.2d.

7.4.2 Optimization of Microfragment Size Distribution

The microstructure of our DNGH is determined by the size and morphology of the microfragments. The fragment size and polydispersity depend on the cryomilling parameters, including the milling frequency, size of the milling spheres, and number the of cycles [148]. For better printability, we aim at obtaining fragments that are smaller than 100 µm while at maintaining a high throughput. To test the influence of the milling cycles on the mi-
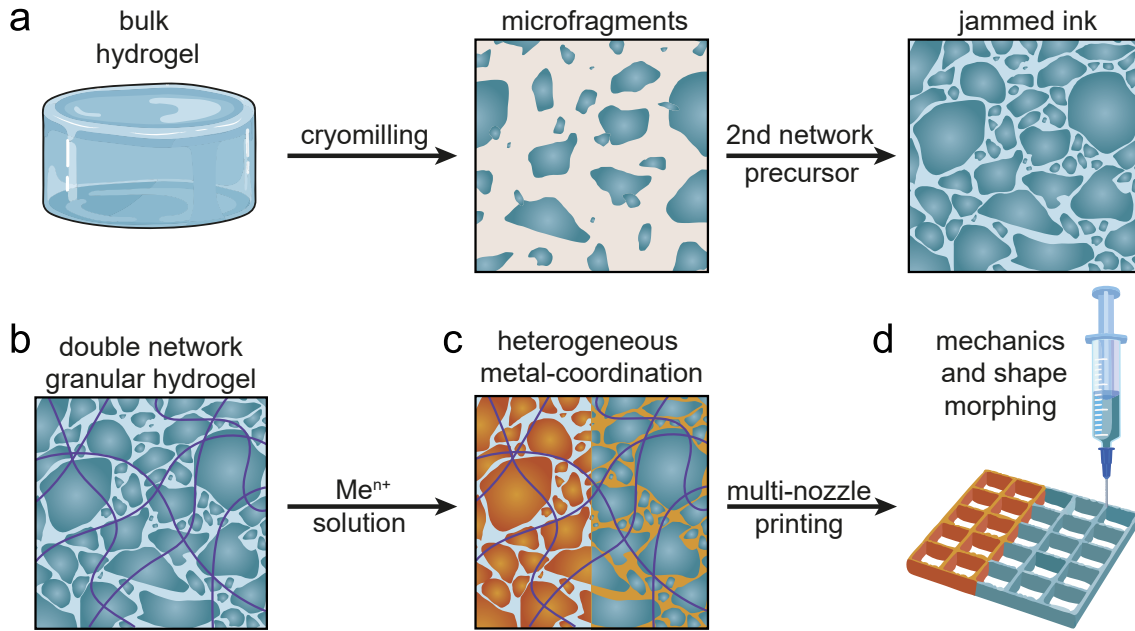
Figure 7.2: Fabrication of metal-coordinated DNGHs. a, A bulk hydrogel is cryomilled to produce polydisperse prismatic microfragments. The obtained microfragments are freeze-dried and resuspended in a monomer-containing solution prior to jamming, yielding a 3D printable ink. b, The jammed microfragment paste can be additive manufactured and converted into load-bearing DNGHs by UV illumination. c, Once crosslinked, the DNGHs are immersed in an ion-containing solution to trigger the mechanical reinforcement either in the microfragments or in the matrix. d, The intrinsic heterogeneity of this system can be harnessed for the fabrication of shape-morphing structures, through the use of a multi-nozzle printing approach.

crofragment size, we fix the size of the milling ball to 20 mm and the frequency to 30 Hz, and measure the dimensions of microfragments as a function of milling cycles. The average microfragment size decreases with increasing number of milling cycles, reaching a minimum average size of 45 µm after 5 cycles, as shown in Figure 7.3b. Unfortunately, even if we subject microfragments to 5 milling cycles, approximately 20% of the microfragments still have at least one dimension above 100 µm, as shown in Figure 7.3c. These microfragments risk clogging the printing nozzle, resulting in a discontinuous extrusion, thus affecting the printing resolution. To overcome this limitation, we filter microfragments that have been subjected to 5 milling cycles with a 100 µm nylon mesh to remove bigger particles, as shown in Figure 7.3a. The sieved solution contains particles with a lower average size of 20 µm, a more homogeneous size distribution, and hardly any particles with dimensions above 100 µm are left, as shown in Figure 7.3d. Note that despite the filtering process, we still find a few particles with at least one dimension above 100 µm in the solution. We attribute the presence of these rather large particles to their anisotropic shape that lets them penetrate the sieve if favorably aligned. However, thanks to the shear alignment of anisotropic particles, we expect them to minimally impact the printability [134, 141]. Due to the favorable combination of polydispersity and throughput, filtered
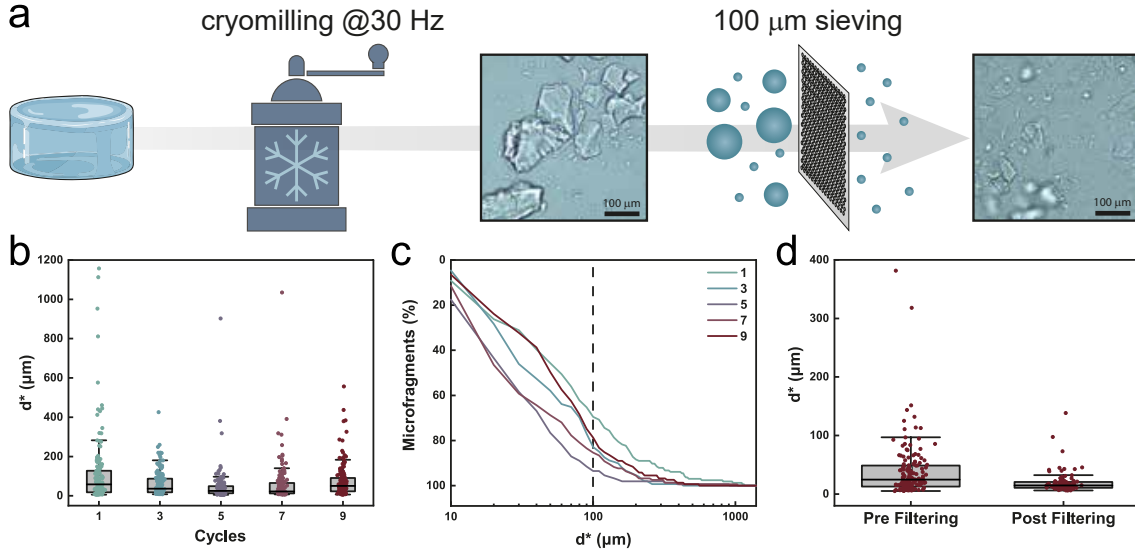
Figure 7.3: Cryomilling process of the hydrogel microfragment. a, A bulk gel is cryomilled at 30 Hz for a certain number of cycles, yielding polydisperse prismatic microfragments. In a second step, the microfragments are filtered through a nylon mesh to remove particles bigger than 100 µm, that would risk clogging the nozzle during the printing process. b, Equivalent diameter (d*) of microfragments as a function of the milling cycles. An average d* of 45 µm is measured for gels milled more than 5 cycles. No major improvement is observed after 5 repeated cycles. c, Cumulative frequency of microfragment sizes as function of the milling cycles. Despite the decrease in average d* with increasing milling cycles, around 20% of the microfragments possess diameters larger than 100 µm. d, Equivalent diameter of microfragments pre and post filtering. The average d* decreases from 45 µm to 20 µm upon filtration, thus confirming removal of bigger particles.

microfragments obtained with 5 cycles of cryomilling will be used for all the remaining experiments. The microfragments are freeze-dried prior to further use to ensure longer shelf-life and a better control over their jamming behavior.

To produce an ink composed of jammed microfragments, we resuspend dried microfragments in a solution containing a second precursor solution. Jammed microgel inks possess rheological properties that are optimal for extrusion-based 3D printing, namely they display a low yield stress, a shear-thinning behavior, and a fast shear recovery [126, 132, 149, 192]. To evaluate if this is also the case for jammed microfragments, we perform shear rheology on our ink. We vary the microfragment content contained in it from 10 wt% to 16 wt%, based on the dry polymeric weight. To assess the shear-thinning behavior, we perform a frequency sweep as a function of the microfragments weight fraction. All tested samples display a shear-thinning behavior, independent of the microfragment content, shown in Figure 7.5a.
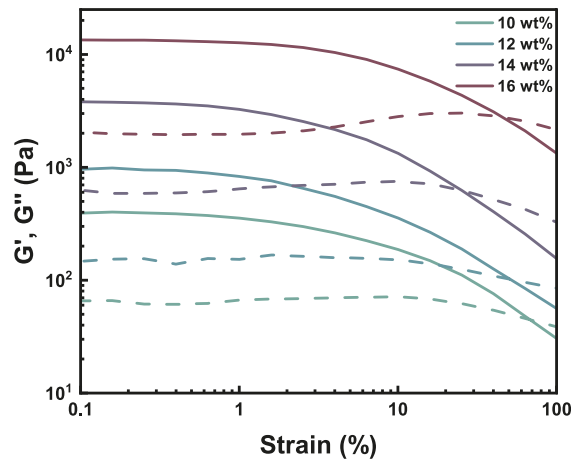
Figure 7.4: Rheology of microfragments and microgels. Amplitude sweeps of microfragment inks as a function of the microfragment content.

7.4.3 Printability of Jammed Microfragments

Key to obtain good printability is a low extruding pressure. To achieve this goal the ink must possess a low yield stress [128]. To measure the yielding behavior of our inks as a function of the microfragment content contained within it, we perform amplitude sweeps. All samples display a relatively low yield stress, with values that increase from 46 Pa to 2630 Pa, if we increase the microfragment content from 12 wt% to 16 wt%, as shown in Figure 7.5b and Figure 7.4.

We assign the increase in yield stress with increasing microfragment content to the increased polymer content in the jammed pastes. Interestingly, the yield point of all measured inks is higher compared to that of inks containing the same weight fraction of jammed spherical microgels discussed in Chapter 4. This difference in yield point is attributed to the mechanical interlocking that is much more pronounced between non-spherical microfragments than between spherical microparticles, thereby increasing inter-particle friction forces [146].

To achieve a high printing fidelity, the ink must quickly recover its solid-like properties upon removal of the shear. To evaluate this property, we perform alternating shear recovery cycles at 1% and 100% strain for 200 s each. All the analyzed inks rapidly transition from the solid-like to the liquid-like state and vice versa with no major changes in G' values, as shown in Figure 7.5c. As a result of the favorable rheological properties, the ink can be 3D printed in a grid shape with minimal loss in resolution, as exemplified for an ink containing 16 wt% microfragments in Figure 7.5d. To quantify the printing resolution of the microfragment ink, we measure the cross-section of the filament and the area enclosed in the grid as a function of the microfragments concentration. The higher
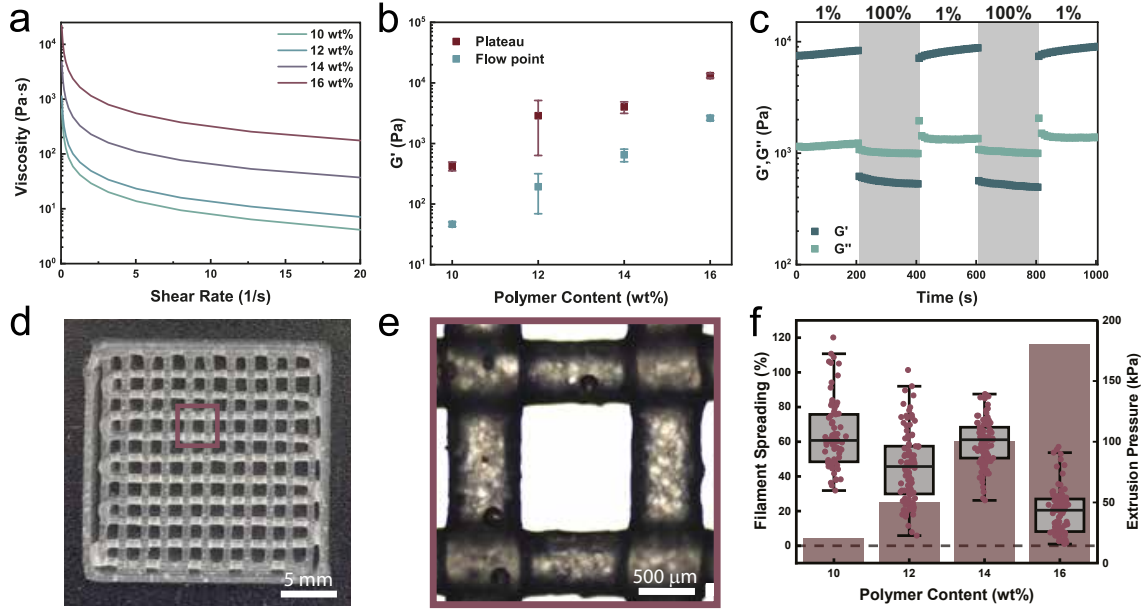
Figure 7.5: Printability of jammed microfragments. a, Frequency measurement of jammed microfragment inks as a function of their microfragment content. All the samples display a decrease in viscosity with increasing shear rate, thus confirming a shear-thinning behavior. b, Storage plateau modulus (G') and flow point of jammed microfragment inks as a function of their microfragment content. c, Shear recovery measurement. A Self-healing behavior of jammed microfragments containing 16 wt% of PAA. The material transitions from a solid-like to a liquid-like state when subjected to high shear ($\gamma = 100\%$). The jammed solution recovers rapidly to its initial condition at low shear ($\gamma = 1\%$). The process can be repeated cyclically without deterioration of the ink performance. d, Optical micrograph of a 3D printed grid produced with a jammed ink containing 16 wt% of PAA. e, Optical micrograph of a unit cell of the 3D printed mesh. f, Filament spreading (left) and extrusion pressure (right) as a function of the ink microfragment content. An increase in microfragment content of the ink is correlated to a decrease in filament spreading, thus demonstrating a better printing resolution. Simultaneously, an increase in microfragment content renders the ink more solid, thus increasing the pressure needed to extrude the material.

the microfragment concentration, and hence, the higher the degree of jamming, the better is the printing resolution, as shown in Figure 7.5e and 7.5f. However, the higher printing resolution obtained at higher microgel contents requires a higher extrusion pressure to push the ink through the nozzle, as shown in Figure 7.5f. We do not have any pressure sensitive component in our ink that would limit the maximum printing pressure we can apply to it. Hence, we will maximize the printing resolution by using inks containing 16 wt% of microfragments for the remainder of this study.

7.4.4 Mechanics of Metal-Reinforced Double Network Granular Hydrogels

Key in the use of hydrogels for load-bearing applications is their ability to withstand significant loads under compression and tension [53, 57]. To assess this parameter we
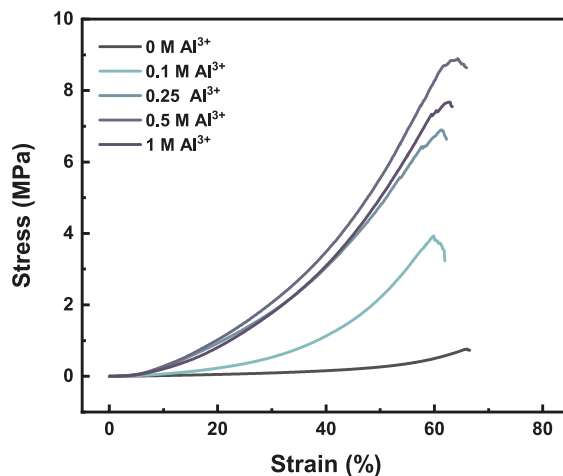
Figure 7.6: Compression measurements of mfDNGHs. Compression curves of mfDNGHs as a function of the Al^{3+} concentration. The compressive modulus and fracture strength increase with increasing Al^{3+} concentration.

quantify the stiffness and work at break of DNGHs composed of PAA microfragments that are firmly connected through an acrylamide network. To transform the rather fragile microfragment-based structure into a mechanically stable 3D DNGH that can bear significant load, we initiate the polymerization of the precursors contained within the microfragments after they have been processed into the appropriate shape. This is done by exposing the structure to UV light to initiate the radical polymerization reaction of the precursors [149]. The resulting DNGH is soaked in DI water until it reaches swelling equilibrium. The material is relatively soft with a stiffness of 0.16 MPa, and work of fracture of 0.05 MJ·m^{-3}. The work at break of bulk hydrogels typically increases upon ionic reinforcement [68, 322, 323]. PAA has a high affinity to certain cations such that it can be ionically reinforced. To test if ionic reinforcement also increases the work at break of our DNGHs, we expose the DNGH to an aqueous solution containing Al^{3+}, as schematically shown in Figure 7.10a. Indeed, under compression, microfragment-reinforced DNGHs (mfDNGHs) with Al^{3+} display a 10-fold increase in compressive modulus, reaching values as high as 1.5 MPa, as shown in Figure 7.10b and Figure 7.6. Similarly, the Young's modulus measured under tension increases 25-fold upon reinforcement with Al^{3+}, reaching values as high as 4 MPa, as shown in Figure 7.7a. The compressive and tensile moduli increase even more, up to 25-fold and 50-fold, respectively, if we reinforce mfDNGHs with Fe^{3+}, as shown in Figure 7.10b and Figure 7.7a. The great improvement in stiffness is paired with a 16-fold increase in work of fracture with respect to non-reinforced DNGHs, reaching values as high as 0.8 MJ·m^{-3}, as shown in Figure 7.7b.

Super-elastic, anti-fatigue hydrogels can be obtained if divalent cations are used in combination with carboxylic ligands [108, 324]. By contrast, we do not observe a significant
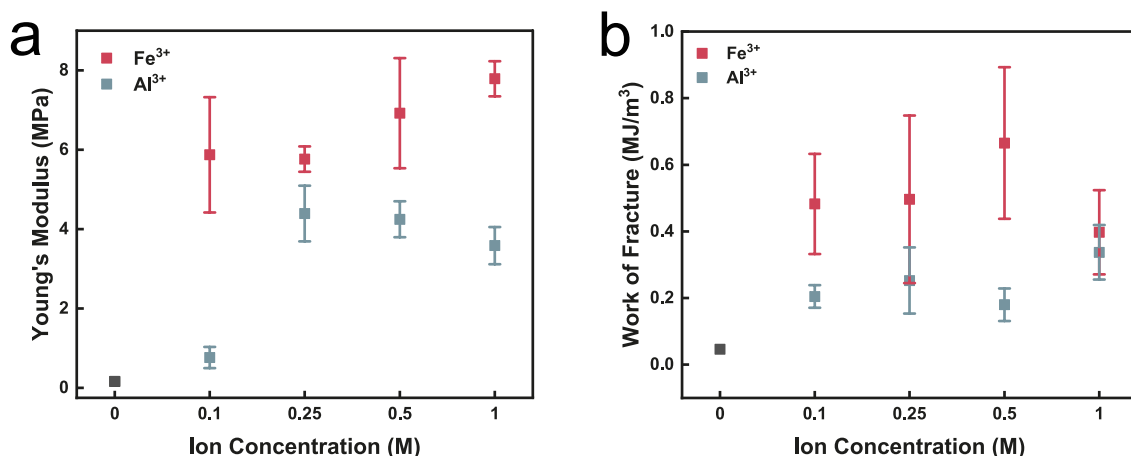
Figure 7.7: Tensile measurement of mfDNGHs. a, Young's modulus of mfDNGHs as a function of the ion concentration. mfDNGHs reinforced with Fe^{3+} display an increase in stiffness with increasing ion concentration, whereas mfDNGHs reinforced with Al^{3+} show a fairly constant modulus if the Al^{3+} concentration exceeds 0.25 M. b, Work of fracture of mfDNGHs as a function of the ion concentration. mfDNGHs reinforced with Fe^{3+} display an increase in fracture energy with increasing ion concentration, until it reaches a maximum of 0.8 $MJ \cdot m^{-3}$ for 0.5 M of Fe^{3+}. mfDNGHs reinforced with Al^{3+} show a fairly constant fracture energy if the Al3+ concentration exceeds 0.1 M.

increase in mechanics if we reinforce our mfDNGHs with divalent ions, as shown in Figure 7.10b. This result is surprising as bulk PAA hydrogels have been reported to be reinforced with divalent cations [108]. We attribute the absence of mechanical reinforcement of mfDNGHs upon addition of divalent ions to a stronger complexation between -COOH and -NH$_2$ groups present in the DNGH, that hinder the complexation of Ca^{2+}, and Zn^{2+}. As expected, Ag^+ ions, being monovalent, do not display any reinforcement effect.

A homogeneous metal reinforcement of bulk hydrogels is difficult as the diffusivity of metal ions is limited by the fast formation of a metal-coordinated hydrogel shell that slows down ion diffusion within this area of the hydrogel. In addition, the complexed metal ions electrostatically repel free metal ions, thereby further hindering their infiltration into the hydrogel. As a result, there are often gradients in ion concentration within bulk hydrogels that have been ionically reinforced, compromising their mechanical properties [69]. This limitation can, at least to some extent, be overcome by complexing metal ions with weak ligands that undergo competitive ligand exchanges [69]. To test if we can increase the extent of ion reinforcement by weakly complexing Fe^{3+} in solution, we incubate our DNGHs in an aqueous solution containing FeCl$_3$ and varying amounts of citric acid (CA), as shown in Figure 7.10c, and Figure 7.8. Surprisingly, mfDNGHs display a decrease in compressive modulus with increasing CA concentration, as shown in Figure 7.10d. A similar trend is observed under uniaxial tensile load, as shown in Figure 7.9. This trend is in stark contrast with previously reported bulk metal-reinforced hydrogels, where CA favors a more homogeneous distribution of the ions and thereby improves the overall
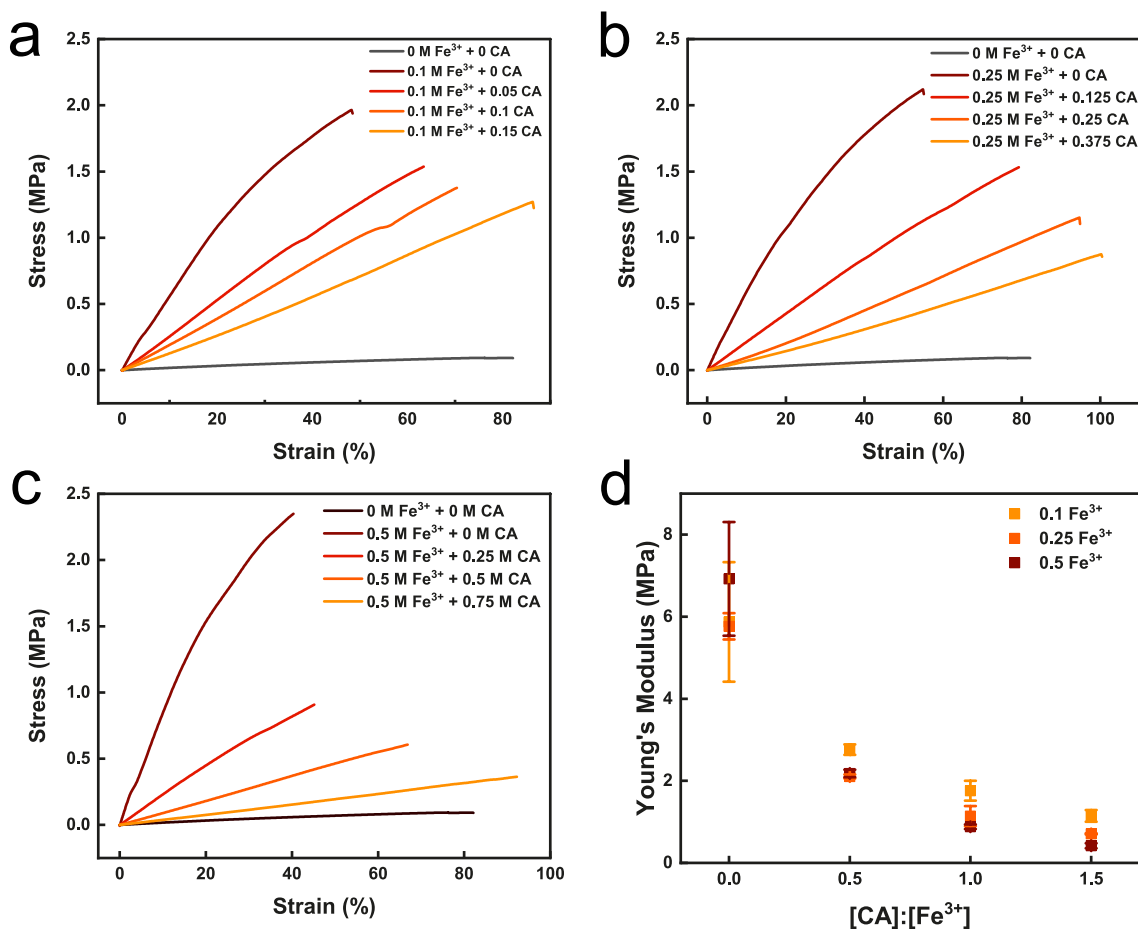
Figure 7.8: Tensile measurement of mfDNGHs reinforced with Fe^{3+} and CA. Tensile curves of mfDNGHs reinforced with (a) 0.1 M, (b) 0.25 M, and (c) 0.5 M Fe^{3+} as a function of the CA concentration. An increase in CA concentration is paired with a decrease in tensile strength and an increase in elongation at break. d, Young's modulus of mfDNGHs reinforced with Fe^{3+} as a function of the CA content. An increase of CA content correlates with a decrease in stiffness.

mechanical performance of these hydrogels [69]. We assign this difference in behavior to the granular structure of our gel: ions can more easily diffuse in uncharged PAM networks compared to the charged PAA networks. In between the microfragments, our DNGHs are exclusively composed of PAM whereas within the microfragments PAA and PAM networks are present. Hence, we expect ions to more readily diffuse within the PAM single network and hence, between the microfragments. The diffusion path within the microfragments is short such that ions can homogeneously reinforce bulk mfDNGHs with dimensions up to 1 cm without the need for any competitive ligand exchanges. This result demonstrates one of the main advantages of the granular structure: an enhanced diffusivity of charged moieties.

Competitive ligand exchanges are typically used to mechanically reinforce hydrogels. This
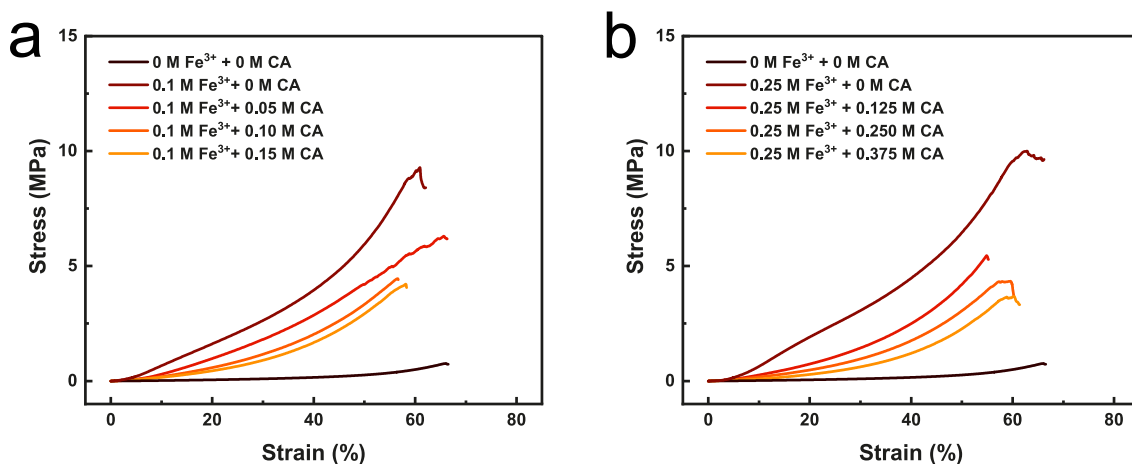
Figure 7.9: Compression measurement of mfDNGHs. Compression curves of mfDNGHs reinforced with (a) 0.1 M, and (b) 0.25 M Fe^{3+} as a function of the CA concentration. An increase in CA concentration is paired with a decrease in tensile strength and stiffness.

trick is not needed in our system. However, we still can take advantage of competitive ligand exchanges to selectively remove coordinated Fe^{3+} ions to restore the initial mechanical behavior of DNGHs, as exemplified in Figure 7.10e. The mfDNGHs can be repetitively ionically reinforced by incubating in a solution containing Fe^{3+} and weakened to restore their initial state by exposing them to a solution containing CA, as shown in Figure 7.10e. Indeed, the stiffness of mfDNGHs does not significantly change even after they have been subjected to 5 cycles of reinforcement and weakening, as shown in Figure 7.10e. The combination of metal-coordination and competitive ligand exchange offers a precise control over the mechanical behavior of mfDNGHs, thus expanding their use for load-bearing applications.

Our results indicate that the metal reinforcement of mfDNGHs strongly increases their stiffness. However, its effect on the work of fracture is limited. The work of fracture of bulk double network is typically predominantly determined by the second network [55, 205]. To test if we can increase the work of fracture of DNGHs by ionically reinforcing the matrix network, we fabricate microfragments composed of polyacrylamide (PAM) and soak them in an aqueous solution containing acrylic acid. The microfragments are processed into matrix-reinforced double network granular hydrogels (mxDNGHs) using the protocols we established for mfDNGHs, as schematically shown Figure 7.18a and detailed in the experimental section. The compressive modulus of mxDNGHs increases 8-fold if reinforced with Al^{3+} and 4-fold if reinforced with Fe^{3+}, as shown in Figure 7.18b. Similarly, the Young's modulus measured under tension reaches values as high as 9 MPa if reinforced with Al^{3+}, corresponding to a 75-fold increase relative to non-reinforced DNGHs. Similarly, the stiffness increases to 3 MPa, if reinforced with Fe^{3+}. Hence, the
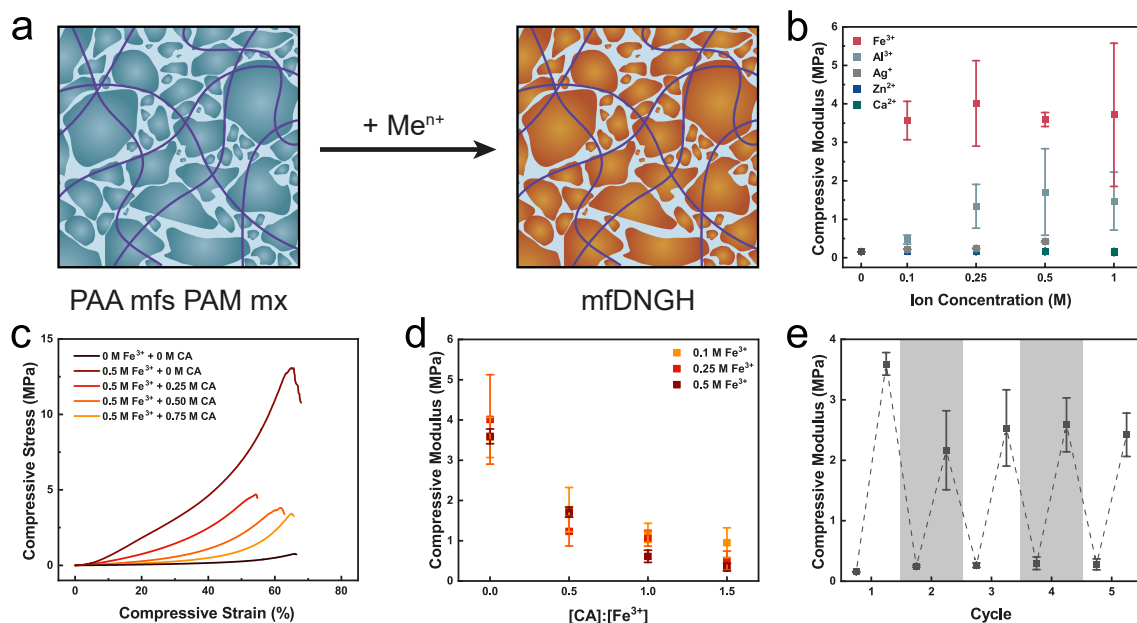
Figure 7.10: Mechanical characterization of mfDNGHs. a, A DNGH is produced form PAA microfragments and a PAM matrix. The material can be selectively reinforced in the individual grains, yielding a mfDNGH. b, Compressive modulus of mfDNGHs reinforced with various ions. Exposure to Fe^{3+} and Al^{3+} solutions results in a strong increase in stiffnes, whereas no appreciable changes are observed for mfDNGHs reinforced with Ca^{2+}, Zn^{2+}, and Ag^{+}. c, Compression curves of Fe-reinforced mfDNGHs as a function of the CA concentration. An increase in CA concentration is correlated with a decrease in mechanics. d, Compressive modulus of Fe-reinforced mfDNGHs as a function of the CA concentration. An increase in CA concentration is paired with a decrease in compressive modulus. e, Reversibility test of Fe-reinforced mfDNGHs. mfDNGHs can be repeatedly reinforced and weakened by exposure to alternating solutions containing Fe or CA. An effective weakening is observed upon exposure to a CA solution. After the first cycle, a lower degree of reinforcement is observed, suggesting a non-optimal removal of the CA left in the matrix.

stiffness of Fe-reinforced mxDNGHs increases 25-fold relative to non-reinforced DNGHs, as shown in Figure 7.11.

Upon incubation of mxDNGHs in an Fe^{3+} containing solution, samples become colored. However, we observe a clear color gradient along the cross-section of mxDNGHs, in stark contrast to mfDNGHs, as shown in Figure 7.18c. The color gradient hints to the formation of a core-shell structure. This hypothesis is supported by the compression curves of mxD-NGHs samples reinforced with Fe^{3+} or Al^{3+} that display two distinctly different slopes, as shown in Figure 7.18d and Figure 7.12. Color gradients in bulk hydrogels, which are indicative of gradients in ion concentration within the hydrogel, can be minimized upon complexing ions with CA. To test if this is also the case for our mxDNGHs, we incubate them in an aqueous solution containing Fe^{3+} and varying concentrations of CA. If incubated in a solution containing 0.5 M Fe^{3+} and 0.75 M CA, samples are homogeneously colored. These results suggest that the complexation of Fe^{3+} with CA increases the homogeneity of Fe^{3+} ions within the mxDNGHs. This suggestion is supported by the increase
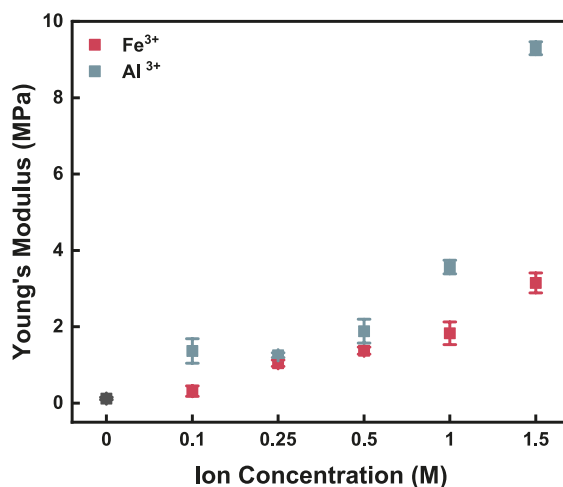
Figure 7.11: Young's modulus of mxDNGHs. mxDNGHs display an increase in stiffness with increasing ion concentration, reaching values as high as 8 MPa when reinforced with 1.5 M Al^{3+}.
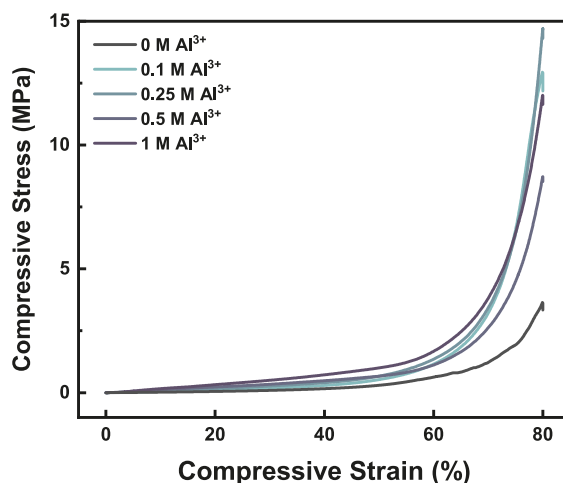
Figure 7.12: Compression measurement of mxDNGHs reinforced with Al^{3+}. The curves show a clear two-slope behavior, characteristic of a core-shell structure.

in compressive modulus with increasing CA concentration contained in the incubating solution until it reaches 3 MPa, as shown in Figure 7.18e. An analogous behavior is observed under tensile testing, where the stiffness of mxDNGHs increases when CA is added, until it reaches Young's moduli as high as 25 MPa, as shown in Figure 7.13.

Interestingly, when the molar ratio of [CA] : [Fe^{3+}] exceeds 0.5, the Young's modulus decreases again. This behavior is attributed to the large excess of carboxylic groups in the CA solution with respect to the carboxylic groups in the PAA network. Furthermore, the increase in stiffness is paired with a strong decrease in strain at break, as shown in Figure 7.14. In general, this counteracting effect influences the toughness of soft materials rendering them more fragile. To test if this is also the case for our system we extract
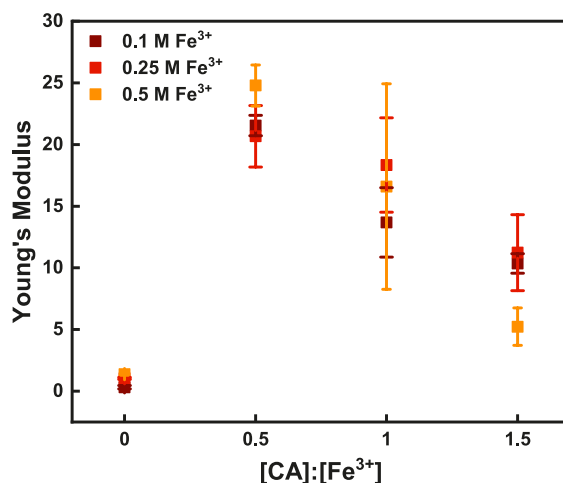
Figure 7.13: Young's modulus of Fe-reinforced mxDNGHs as a function of CA concentration. An increase in CA concentration is paired with a steep increase in Young's modulus. The CA slows down the ionic complexation, thus producing stiffer, more homogeneous structures.
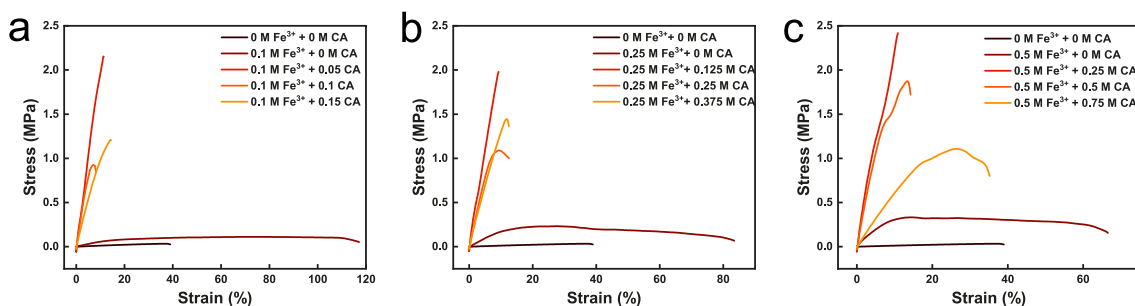
Figure 7.14: Tensile measurement of mxDNGHs reinforced with Fe^{3+} as a function of the CA concentration. a, Tensile curves of mxDNGHs reinforced with 0.1 M Fe^{3+} as a function of the CA concentration. b, Tensile curves of mxDNGHs reinforced with 0.25 M Fe^{3+} as a function of the CA concentration. c, Tensile curves of mxDNGHs reinforced with 0.5 M Fe^{3+} as a function of the CA concentration. All the curves show a clear stiffening behavior with increasing CA concentration at the expense of a strong decrease in strain at break behavior.

the work of fracture as a function of the molar ratio of [CA] : [Fe^{3+}]. Interestingly, the work of fracture remains almost unchanged with values of 0.20 MJ·m^{-3}. This result is in agreement with previously reported literature on metal-reinforced bulk hydrogels [69].

Metal-coordination increases the stiffness and toughness of dually crosslinked hydrogels by introducing physical crosslinks in a pre-existing covalent network [65]. However, the increased crosslink density comes at the expense of the water content: upon metal-reinforcement, hydrogels typically undergo syneresis, resulting in their shrinkage. To assess to what extent that is true for our metal reinforced DNGHs, we quantify their water content by gravimetric analysis as a function of ion concentration. As expected, an increase in ion concentration is paired with a decrease in water content, reaching values as low as 24 wt% when mxDNGHs are exposed to 1.5 M of AlCl$_3$, as shown in Figure 7.15.
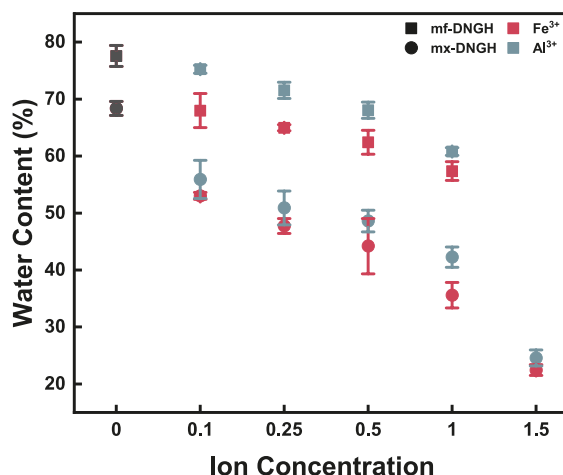
Figure 7.15: Equilibrium water content of metal-reinforced DNGHs. The water content decreases with increasing ion concentration.

Our results indicate that an increased density of ionic crosslinks is directly correlated with a reduction in water content within these hydrogels. While this behavior can be detrimental for cell work, it can be exploited as an asset in the fabrication of load-bearing tough hydrogels. Indeed, the shrinkage induced by the secondary crosslinking with metal ions forces the polymer chains to collapse, thus increasing their hidden length, and hence, the fracture toughness of the hydrogel [21]. Nature frequently leverages this behavior to build hydrogel-based materials displaying an unparalleled toughness [2, 28, 49]. To test if we can promote this behavior in our mxDNGHs, we reinforce them with Fe^{3+} in the absence of CA to create a stiff shell that shrinks, thereby mechanically forcing the core contained within the shell to also collapse. Upon tensile testing, mxDNGHs reinforced with Fe^{3+} display an initial stiff behavior followed by a clear yielding plateau, confirming the core-shell structure of the material, as shown in Figure 7.18f and 7.18g. A similar behavior is observed when mxDNGHs are reinforced with Al^{3+}, as shown in Figure 7.16. Overall, the fracture strength and strain at break increase with increasing ion concentration, resulting in values of stiffness as high as 9 MPa and work of fracture as high as 12 MJ·m^{-3}, as shown in Figure 7.11 and 7.17.

To evaluate the overall mechanical performance of mfDNGHs and mxDNGHs, we compare our material with state-of-the-art load-bearing hydrogels. Remarkably, our material possesses values of stiffness and work of fracture that are higher than any previously reported 3D printed hydrogels, as shown in Figure 7.19a. The Ashby plots reveal that our material outperforms any previously reported one, setting a new all-time high for the field. Furthermore, we compare our formulations as a function of polymer content, as shown in Figure 7.19b and Figure 7.19c. We observe that even under similar polymer contents our materials still perform better than any reported bulk or 3D printed hydrogel, bringing us
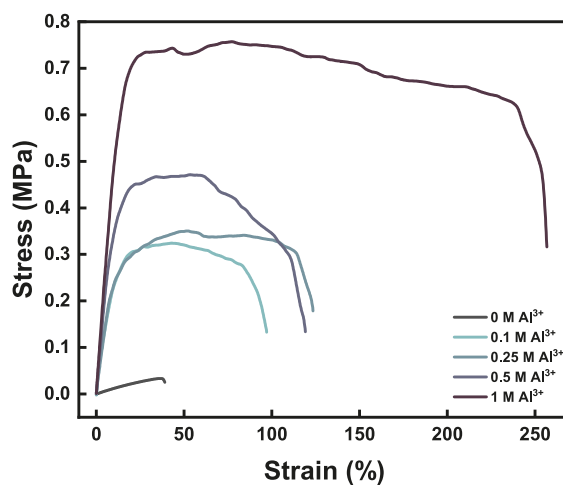
Figure 7.16: Tensile curves of mxDNGHs as a function of their Al^{3+} concentration. Higher Al^{3+} contents results in a more pronounced yielding plateau, characteristic of the formation of a core-shell structure.
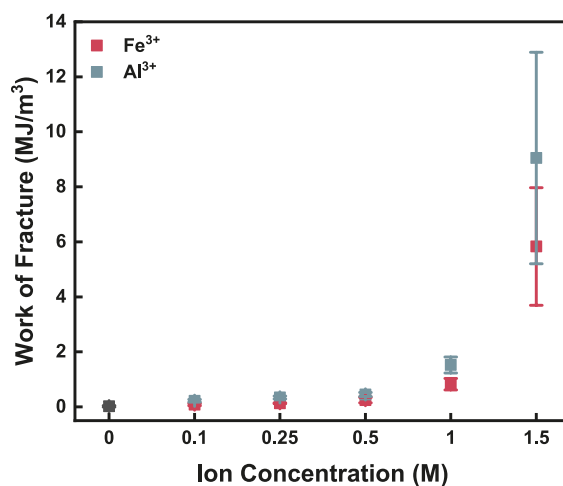
Figure 7.17: Work of Fracture of mxDNGHs. mxDNGHs display an increase in work of fracture with increasing ion concentration, reaching values as high as 12 MJ·m^{-3} when reinforced with 1.5 M Al^{3+}.

a step closer to finally mimicking soft load-bearing natural materials.
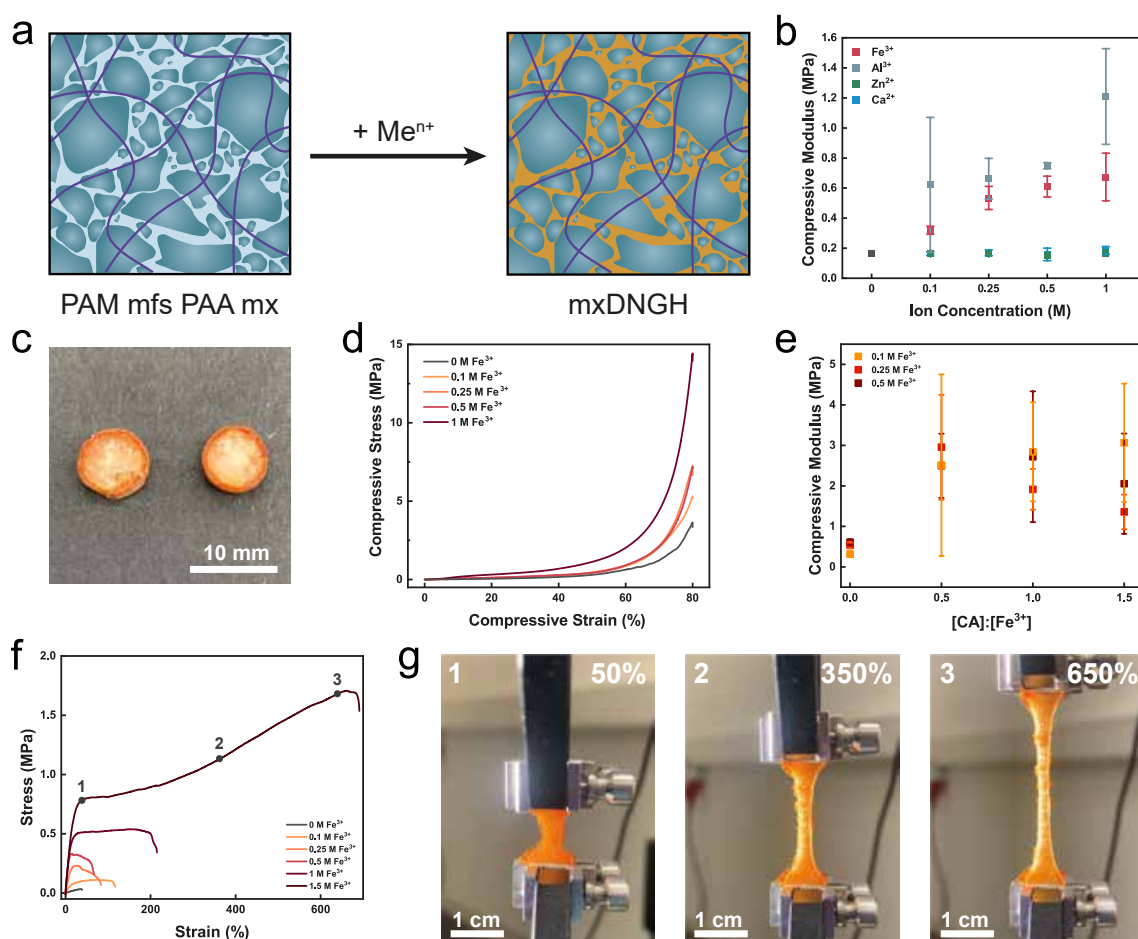
Figure 7.18: Mechanical characterization of mxDNGHs. a, A DNGH is produced form PAM microfragments and a PAA matrix. The material can be selectively reinforced in the matrix, yielding a mxDNGH. b, Compressive modulus of mxDNGHs reinforced with various ions. Exposure to Fe^{3+} and Al^{3+} solutions results in a strong increase in mechanics, whereas no appreciable changes are observed for mxDNGHs reinforced with Ca^{2+}, Zn^{2+}, and Ag^+. c, Optical photograph of a mxDNGH cylinder. The color gradient is a clear indication of a non-homogeneous ionic reinforcement. d, Compression curves of Fe-reinforced mxDNGHs as a function of the Fe^{3+} concentration. All curves display an initial soft behavior, followed by a stiffening. This indicates the formation of a hard shell and a soft core. e, Compressive modulus of Fe-reinforced mxDNGHs as a function of the CA concentration. An increase in CA concentration is paired with a steep increase in compressive modulus. The CA slows down the ionic complexation, thus producing stiffer, more homogeneous structures. f, Tensile curves of mxDNGHs as a function of their Fe^{3+} concentration. Higher Fe^{3+} contents result in a more pronounced yielding plateau, characteristic of the formation of a core-shell structure. g, Time lapse of a Fe-reinforced mxDNGH. Initially the sample displays a homogeneous texture (1). Once the mxDNGH is pulled above its yielding point, the hard shell starts cracking (2), and a softer stretchy core is revealed (3).
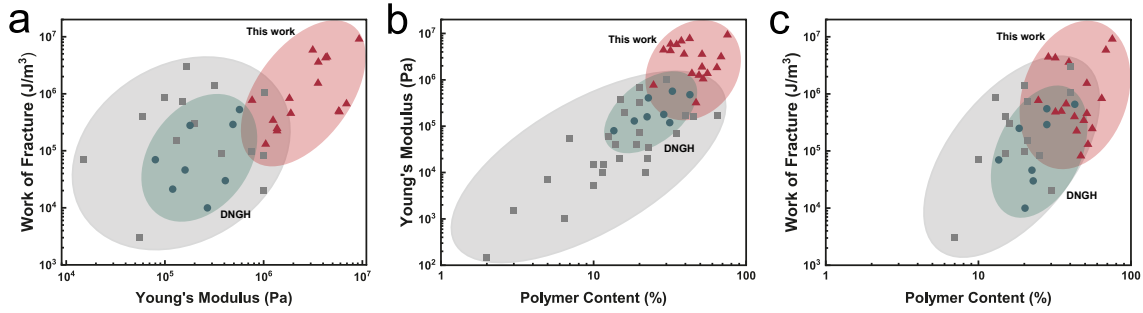
Figure 7.19: Ashby plots of 3D printed hydrogels. a, Ashby plot of the work of fracture of 3D printed hydrogels as a function of their Young's modulus. Our material possesses a synergistic combination of high stiffness and high work of fracture, a seemingly counteracting set of properties. b, Ashby plot of the Young's modulus of 3D printed hydrogels as a function of their polymer content. Both mf- and mxDNGHs display higher stiffnesses compared to any previously reported material. c, Ashby plot of the work of fracture of 3D printed hydrogels as a function of their polymer content. Both mf- and mxDNGHs display higher fracture energies compared to any previously reported material.

7.5   Conclusion

We introduce 3D printable metal reinforced DNGHs that display a stiffness that exceeds previously reported 3D printed hydrogels by 9-fold and their work of fracture by 20-fold. We can tune the mechanical properties of these DNGHs to be similar to those of their natural counterparts. The fabrication of microfragments through cryomilling holds great potential thanks to its scalability and the possibility to process a wide range of materials. The ink composed of jammed microfragments can be 3D printed with no appreciable changes with respect to inks composed of jammed spherical microgels, thus rendering it an ideal candidate for extrusion-based printing. The introduction of responsive materials within the granular construct adds an extra degree of control to the system, allowing the fabrication of complex materials with engineered local variations in composition. The selective binding of metal ions with PAA enables a selective, targeted reinforcement of the 3D printed structure without the need to trade off stiffness or toughness. We envisage the combination of granular printing with responsive materials to be of pivotal importance for the development of the next generation of 3D printable soft load-bearing materials, providing new fuel that brings us a step closer to successfully mimicking soft natural tissues.

3D Printing of Living Structural Biocomposites

In this chapter, I present a novel approach to fabricate structural biocomposite materials from a living granular hydrogel precursor. Here, I encapsulate ureolytic bacteria, known as *Sporosarcina pasteurii*, in gelatin microgels and jam them to form a living granular ink, referred as BactoInk. This process, extensively discussed in Chapter 4, enables their 3D assembly by conventional extrusion printing. The 3D printed granular hydrogel is stabilized by exposure to an Alginate-Ca^{2+} solution, yielding a soft, yet fragile hydrogel scaffold. The scaffold is inserted into a solution containing urea and $CaCl_2$ to trigger its biomineralization. The resulting biocomposite is free-standing and load-bearing, displaying structural and mechanical properties similar to those of trabecular bone. In the final part of the chapter, I present potential applications of the BactoInk for marine reef remediation, and art restoration.

This chapter is adapted from the submitted paper entitled "3D Printing of Living Structural Biocomposites" authored by Matteo Hirsch, Lorenzo Lucherini, Ran Zhao, Alexandra Clarà , and Esther Amstad. M. Hirsch, and E. Amstad designed the experiments. M. Hirsch and L. Lucherini are equally contributing co-first authors. L. Lucherini performed the bacteria encapsulation, the biomineralization, and the TGA analysis. M. Hirsch performed the 3D printing, molding, and injection of the material. M. Hirsch, and L. Lucherini performed all the remaining experiments collectively. M. Hirsch, L. Lucherini, A. Clarà Saracho, and E. Amstad analyzed the data and wrote the manuscript.

Contents

8.1 Abstract

Nature fabricates organic/inorganic composites under benign conditions, yet, in many cases, their mechanical properties exceed those of the individual building components it is made from. The secret behind the evolutionary pivot is the unique ability of nature to control structure and local composition of its materials. This tight control is often achieved through compartmentalization of the reagents that can be locally released. Inspired by nature, we introduce an energy-efficient process that takes advantage of the compartmentalization to fabricate porous $CaCO_3$-based composites exclusively comprised of nature-derived materials whose compressive strength is similar to that of trabecular bones. The unique combination of nature-derived materials, 3D printability, and good mechanical properties is achieved through the formulation of these materials: We combine microgel-based granular inks that inherently can be 3D printed with the innate potential of engineered living materials to fabricate bacteria-induced biomineral composites. The resulting biomineral composites possess a porous trabecular structure that comprises up to 93 wt% $CaCO_3$ and thereby can withstand pressures up to 3.5 MPa. We envisage this system to have the potential to be used in art restoration, serve as artificial corals to help the regeneration of marine reefs, and, with additional work, might even allow the reparation of broken or partially disintegrated natural mineral-based materials such as certain parts of bones.

8.2 Introduction

Nature is able to produce biocomposites of high structural complexity and mechanical integrity using a limited number of elements. These biocomposites are often fabricated under benign conditions and with a minimum amount of energy input [325]. The unparalleled mechanical properties of these natural materials, such as nacre [13], sea urchin spikes [10], and stomatopod dactyl clubs [326] result from the unique interplay between hierarchical structure and locally varying composition [24]. For example, 95% of the weight of nacre can be assigned to hexagonal aragonite platelets that are assembled in a layered structure. These inorganic platelets are held together by a polymeric matrix that increases the overall material toughness up to 40-fold compared to platelets alone [11, 327, 328]. In contrast, synthetic composites lack any micrometer length-scale structure because the vast majority of them is fabricated by mixing materials possessing different mechanical properties in bulk [329, 330]. Despite the higher energy cost of the production of most synthetic composites, the combination of stiffness and toughness some natural materials display remains unmatched by synthetic counterparts possessing a similar composition. This shortcoming can at least partially be assigned to the inferior control over the microstructure and local composition of synthetic materials [14, 331].

Inspired by nature, techniques that offer a superior control over the local composition and hence result in composites with superior mechanical properties have been introduced. These methods include reinforcing composites with ions [69, 273, 332] or particle-based fillers [333, 334, 335], controlling the mineralization through enzymes [107, 336, 337], or *in situ* precipitation of minerals [106, 276, 338, 339]. Similarly, additive manufacturing methods that offer control over the mm length scale structure have been introduced [149, 340, 341, 255]. However, by analogy to the bulk methods mentioned above, many of these more involved procedures offer a limited control over the micrometer length scale structure of the materials that negatively impacts their mechanical properties. Sustainable solutions to fabricate stiff and strong composites under benign conditions and using minimal amounts of energy remain elusive [342].

The introduction of engineered living materials presented a paradigm shift in the biocomposite field from the design of synthetic, inert biomaterials to biologically-active, self-growing ones. Recent studies have demonstrated the possibility to combine conventional geotechnical processing with a microbially-induced calcium carbonate precipitation (MICP) for the mechanical stabilization and reinforcement of soil [184, 343], and for the production of self-healing concrete [344, 345], because of its simplicity and high efficiency [346]. Furthermore, MICP by urea hydrolysis has been previously demonstrated in the context of living construction materials [183], heritage restoration [347], and deep-seabed

applications [348]. Generally, ureolytic bacteria used for such geo-environmental and construction applications must have a reliable, high urease activity, while being harmless to humans and pose low risk to the local ecosystem. In this regard, *Sporosarcina pasteurii* has been often selected owing to its high-urease activity and biosafety [349]. Similarly, other microorganisms have been embedded in soft organic materials to form engineered living materials [176, 183, 350]. For instance, bioinks have been supplemented with unicellular green algae to enable the 3D printing of cellular scaffolds displaying a homogeneous degree of oxygenation [26]. Similarly, hydrogel-based inks have been functionalized with bacteria that degrade phenolic compounds for bioremediation and those that produce bacterial cellulose for biomedical applications [194]. Bacteria have also been used to precipitate inorganic materials into organic matrices. For example, 3D printed acrylate-based, inert polymeric structures have been exposed to a MICP environment to trigger the precipitation of calcite within the empty space of the printed mesh. The formed calcite particles served as fillers, thereby increasing the stiffness and mechanical strength of the composite [351]. Yet, to achieve this effect, the composite had to be annealed at 70 °C.

Recent advances in additive manufacturing of cell-laden inks have highlighted the unparalleled printing potential of granular systems over their conventional biopolymer counterparts [132, 136, 154]. However, the advantages offered by granular systems in terms of their processability have never been leveraged to 3D print bacteria-loaded biosourced materials that can subsequently be stiffened and strengthened through a controlled bacteria-initiated mineralization of the organic scaffold. Here, we introduce a method that enables 3D printing of bacteria-loaded microgels that can be converted into biomineral composites possessing up to 93 wt% $CaCO_3$ and bearing loads up to 3.5 MPa. This is achieved by fabricating gelatin microgels containing ureolytic bacteria, *Sporosarcina pasteurii*. These microgels are jammed to form a 3D printable granular bioink (BactoInk) that can be converted into load-bearing biocomposites through microbially-induced calcium carbonate precipitation. We obtain a homogeneous mineralization within microstructured composites with dimensions as large as 10 cm and mineral contents up to 93 wt%. We demonstrate that the compressive strength increases with the degree of mineralization until it attains values as high as 3.5 MPa, similar to those of the human trabecular bone [352]. The potential and versability of the environmentally friendly BactoInk is showcased by 3D printing it into cm-sized statues, injected into defects for art restoration and casting it into artificial corals that might help restoring marine reefs.

8.3 Experimental Section

Experimental details are reported in Chapter 3 from Section 3.6.1 on page 56 to Section 3.6.13 on page 59.

8.4 Results and Discussion

8.4.1 BactoInk Design and Fabrication

Due to the similarity of hydrogels to naturally-produced extracellular matrices and biofilms, they have been widely used for the encapsulation of microorganisms in the form of films [353], particles [156, 166, 183], capsules [354], fibers [147, 83], and bulk structures [314, 355]. Extrusion-based 3D printing of hydrogels is limited to those made of precursor solutions that fulfill the rheological requirements inherent to this process [168, 316]. Unfortunately, these hydrogels typically are rather soft or fragile [172]. A much wider range of hydrogels can be 3D printed if formulated as microparticles, so-called microgels, that are jammed [46, 131, 136, 154, 318]. Yet, microgels that were thus far 3D printed did not contain microorganisms that precipitate materials which can change the mechanical properties of the resulting composite such that they were inherently soft [136, 146, 166]. To overcome this limitation and enable 3D printing of stiff biominerals from soft microgel-based inks, we produce microgels that are loaded with bacteria which can induce $CaCO_3$ precipitation. Bacteria-loaded microgels are fabricated by dispersing freeze-dried *S. pasteurii* in a gelatin solution at 37 °C, emulsifying the aqueous solution with mineral oil under vigorous stirring, and cooling the emulsion to room temperature. The resulting microgels are washed several times with phosphate buffered saline (PBS) to remove the oil and any unreacted moieties before they are resuspended in a solution containing alginate that serves as a stabilizer for our printed scaffolds, as summarized in Figure 8.1a. The suspended bacteria-loaded microgels are jammed by centrifugation yielding our BactoInk. To stabilize the 3D printed granular structure, we expose it to a calcium chloride ($CaCl_2$) solution that ionically crosslinks alginate, thereby strengthening inter-particle links. The resulting polymeric scaffold is soft, yet self-sustaining, as shown in Figure 8.1b. To stiffen and harden the 3D printed structure, we trigger the MICP process by transferring the structure to a mineralizing environment containing yest extract, urea, and $CaCl_2$, as shown in Figure 8.1c. The encapsulated *S. pasteurii* hydrolyze urea, leading to the formation of carbonate ions that react with the calcium ions (Ca^{2+}) dispersed in solution to precipitate $CaCO_3$ minerals in the vicinity of the bacteria, as schematically shown in Figure 8.1d. The resulting $CaCO_3$ minerals, that are formed within the 3D printed granu-
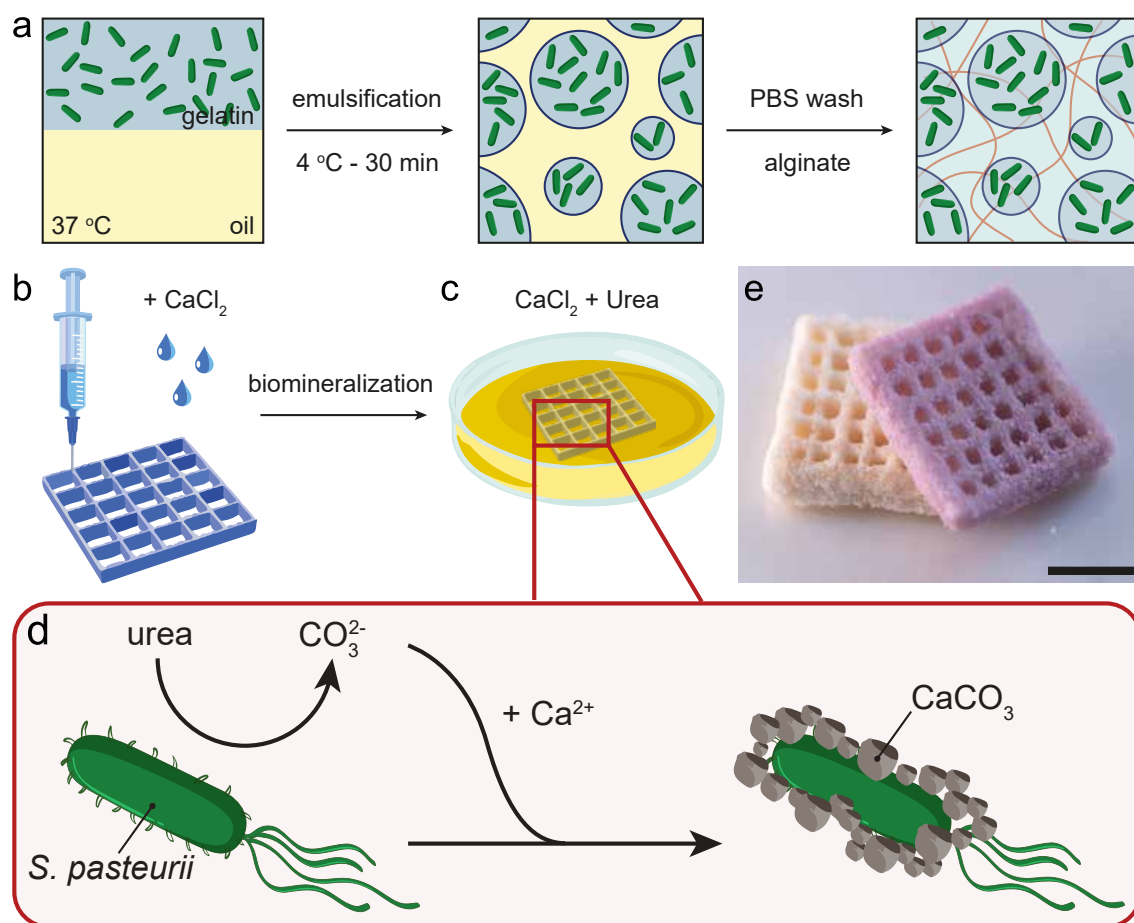
Figure 8.1: Fabrication of 3D printed biomineral composites. a, Schematic representation of the manufacturing process of the BactoInk. A gelatin solution containing bacteria is emulsified, the aqueous drops converted into microgels by lowering the temperature and the resulting microgels washed to remove the oil and surfactants. The bacteria-loaded microgels are mixed with a solution containing alginate prior to jamming. b, The BactoInk is 3D printed and the structure is stabilized by exposure to a 1 M CaCl$_2$ solution. c, Mineralization is triggered by immersing the stabilized BactoInk scaffold in a solution containing 0.5 M CaCl$_2$, 0.75 M urea, and 0.4 wt% yeast. d, Schematic representation of the MICP process mediated by *S. pasteurii*. e, Photograph of a 3D printed biomineral composite after 4 days of MICP. Scale bar is 10 mm.

lar hydrogel scaffold, transform this soft scaffold into a load-bearing biomineral composite, as illustrated on the photographs in Figure 8.1e.

8.4.2   Rheological Characterization of BactoInk

The rheological behavior of granular inks is independent of the material composition [130, 132]. To verify that the addition of bacteria to microgels does not significantly change the rheological properties of the granular ink, we perform oscillatory rheology on our samples and compare the results to gelatin-only microgels. As expected, both inks present a shear-thinning behavior with no significant difference in viscosity, as shown in

Figure 8.2a. Additionally, both materials display a relatively low yield point of around 1 kPa, as shown in Figure 8.2b, making them well suited for bioprinting. The moderately higher storage modulus (G') of the BactoInk is assigned to the presence of bacteria within the microgels that act as fillers, thereby stiffening them [127].

To ensure good printing resolution, the BactoInk should extrude into filaments in a continuous flow. To enable the transfer of the 3D printed construct into a mineralizing solution, the structure must be free-standing and support its own weight. To test if these prerequisites are met by our system, we investigate the influence of the concentration of gelatin within the microgels and that of alginate outside them on the printability and shape-retaining properties of our material using a filament hanging assay. Gelatin concentrations below 20 wt% yield microgels that are too soft to be sufficiently jammed such that the resulting ink drips, as shown in the photograph in Figure 8.2c, and summarized in Figure 8.2d. This behavior prevents printing of the ink. Microgels that are formulated from solutions containing gelatin concentrations exceeding 20 wt% display a proper jamming behavior. As a result, ink formulations made from these microgels can be 3D printed independent of the alginate concentrations, as exemplified on the photograph in Figure 8.2e for inks made with microgels composed of 25 wt% gelatin. However, if the alginate content in the solution surrounding the microparticles is below 3 wt%, the inter-particle adhesion is too weak even upon contact with a $CaCl_2$ solution, such that the printed structure is not self-sustaining. By contrast, at higher alginate concentrations, the 3D printed structure becomes self-sustaining as soon as it has been exposed to a $CaCl_2$ solution, as shown in Figure 8.3. We assign the good stability of the 3D printed substrate to the alginate that gels upon contact with Ca^{2+}, thereby firmly connecting adjacent microparticles. Based on these findings, we use the BactoInk composed of microgels made from solutions containing 25 wt% gelatin that are dispersed in an aqueous solution containing 5 wt% alginate for the following experiments.

8.4.3 Mineralization of 3D Printed BactoInk

The $CaCO_3$ precipitation yield is dependent on the relative concentration of urea and $CaCl_2$ in solution, as well as on the time of exposure to the mineralizing solution [183]. To test the evolution of the mineral content over time, we quantify this parameter using thermogravimetry analysis (TGA). To minimize the amount of energy needed to fabricate these materials, we incubate the soft substrates at room temperature. The degree of mineralization gradually increases within 4 days of incubation, as shown in Figure 8.4a. If samples are incubated in a solution containing 0.75 M urea and 0.5 M $CaCl_2$, they reach a mineral content of around 93 wt% after 4 days, as summarized in Figure 8.4a. To
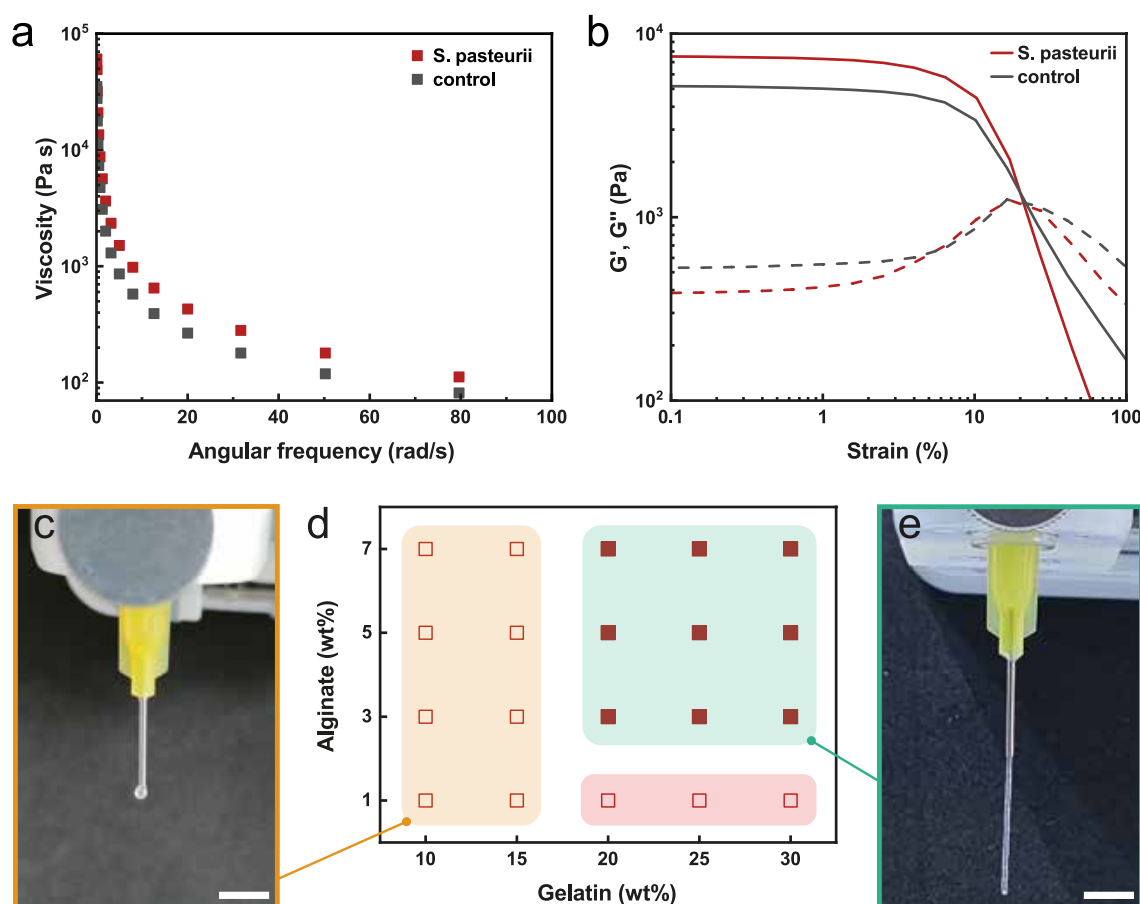
Figure 8.2: Rheology of BactoInk. a, Frequency dependent viscosity of jammed bacteria-loaded microgels (red) versus bare gelatin microgels (grey). Both inks display a shear-thinning behavior. b, Amplitude sweep of BactoInk (red) versus bare gelatin microgels (grey). Despite the moderate difference in G', both inks show a similar flow point. c, Photograph of BactoInk composed of jammed microparticles made from a solution containing 15 wt% gelatin dispersed in an aqueous solution containing 5 wt% alginate dripping from a nozzle. d, BactoInk printability window as a function of gelatin and alginate concentrations. e, Photograph of BactoInk made of jammed microparticles that have been fabricated from a solution containing 25 wt% gelatin dispersed in an aqueous solution containing 5 wt% alginate extruding in a stable filament from a nozzle. At gelatin concentrations below 20 wt%, the ink is too soft such that a proper jamming cannot be obtained and the material displays a dripping behavior, as exemplified in (c). At gelatin concentrations exceeding 20 wt%, all the tested formulations show a continuous filament extrusion such that they are suitable for 3D printing, as exemplified in (e). Alginate concentrations above 3 wt% are required to successfully stabilize the 3D printed structure upon exposure to $CaCl_2$ that forms a percolating alginate network which firmly interconnects the microparticles. Scale bars are 5 mm.
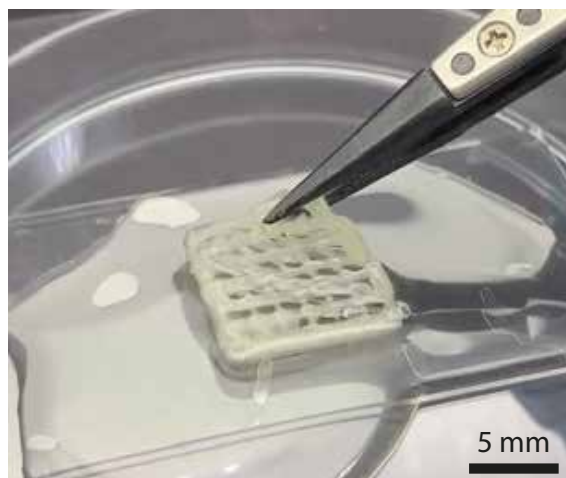
Figure 8.3: 3D printed and stabilized BactoInk granular scaffold. Photograph of a 3D printed BactoInk scaffold immersed in a CaCl$_2$ solution. The structure is free-standing and can be lifted from the gelling bath.

test if we can increase the mineral content even more, we assess the influence of the urea concentration on the degree of mineralization measured after 4 days of incubation. The degree of mineralization increases up to 20% if the urea concentration is increased from 0.05 M to 0.25 M, independent of the CaCl$_2$ concentration, as summarized in Figure 8.4b. By contrast, for urea concentrations $\geq$0.25 M, we do not observe any significant influence of the urea or CaCl$_2$ concentrations on the degree of mineralization, as summarized in Figure 8.4b. These results suggest that the mineralization process is limited by the MICP. We attribute this limitation to the non-ideal enzymatic activity of *S. pasteurii*. To ensure maximum yield of the precipitated CaCO$_3$, we choose a solution containing 0.75 M urea and 0.5 M CaCl$_2$.

To evaluate the effect of the incubation time on the overall CaCO$_3$ mineral content, we perform TGA on the biomineralized samples as a function of incubation days. Remarkably, bacteria produce up to 77 wt% of CaCO$_3$ within 24 h, and up to 93 wt% after 4 days of incubation, as shown in Figure 8.4a. This high mineral content is surprising as we start from a purely organic scaffold that contains approximately 30 wt% of polymers. Assuming that all the volume initially occupied by water is replaced by CaCO$_3$, we would expect a maximum mineral content of 86 wt%. The measured mineralization value is higher than the theoretically calculated upper limit. This result suggests that a fraction of the polymer initially contained within the scaffold is degraded or washed away during the mineralization. Indeed, some bacteria are known to metabolize small peptides and proteins, including gelatin, leading to the secretion of gelatinase [356]. To test whether *S. pasteurii* degrades and metabolizes the gelatin scaffold, we monitor the change in microgel structure and pH with time. To facilitate the visualization, we perform these tests on individually dispersed bacteria-loaded microgels. In the absence of urea, bacteria-loaded
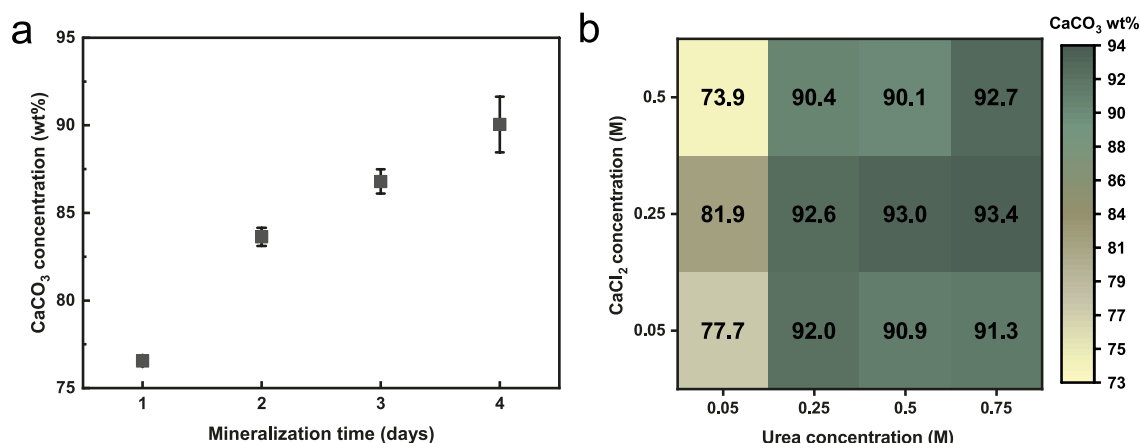
Figure 8.4: Mineralization. $CaCO_3$ content of biomineralized BactoInk determined with TGA as a function of a, mineralization time for samples incubated in an aqueous solution containing 0.5 M $CaCl_2$ and 0.75 M urea and b, different $CaCl_2$ and urea concentrations measured after 4 days of incubation at room temperature.

microgels are stable and do not degrade over time, as shown in Figure 8.5a. These results suggest that *S. pasteurii* do not possess the enzymatic capacity to hydrolyze and degrade gelatin. By contrast, in the presence of urea, gelatin microgels lose their integrity and bacteria are no longer encapsulated, as exemplified in the time-lapse optical micrographs in Figure 8.5b. We assign this observation to the increase in pH from 6.5 to 10 caused by the urea hydrolysis, as shown in Figure 8.5c. The zwitterionic nature of gelatin helices makes its structural integrity pH-dependent, leading to a partial disintegration at pH values exceeding 9 [357]. These results suggest that the gelatin microgels partially disintegrate during the mineralization of the scaffold, allowing the mineral content to increase beyond the maximum theoretical value. Importantly, the gelatin dissolution does not compromise the printing fidelity or resolution as this process happens only after the surfaces of the microgels have been mineralized, as shown in Figure 8.5d.

8.4.4 Structural Analysis of Mineralized BactoInk

A key parameter that determines the quality of a 3D printed construct is its shape fidelity. To assess if this parameter is impacted by the mineralization of the scaffold, that occurs after the 3D printing process has been completed, we compute the volume change of 3D printed parts upon drying as a function of the mineralization time, assuming a negligible volume change of fully mineralized materials upon their drying. As expected, the dried hydrogel scaffold loses more than 80% of its initial volume due to water evaporation, as shown in Figure 8.6a. This large change in volume severely compromises the shape fidelity. Moreover, the dried product becomes very brittle, making it unsuitable for any further operation. Remarkably, after only 24 h of mineralization, the volume loss is much smaller,
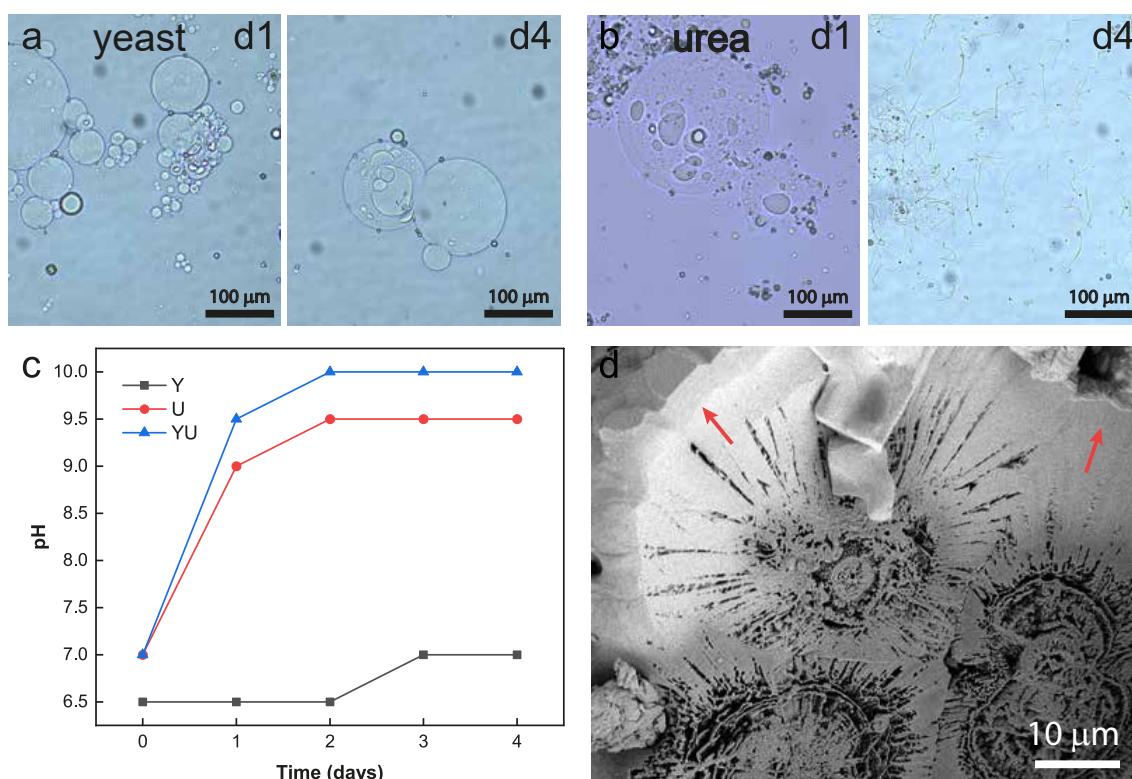
Figure 8.5: Microgel stability in various culturing media. a, Optical micrograph of bacteria-loaded microgels immersed in a solution containing 0.4 wt% yeast extract after 1 and 4 days of incubation. Microgels appear stable over time and bacteria are still contained in the network. b, Optical micrograph of bacteria-loaded microgels immersed in a solution containing 0.75 M urea after 1 and 4 days of incubation. After 4 days, bacteria are released in solution due to gelatin degradation. c, pH change as a function of time of incubation in an aqueous solution containing 0.4 wt% yeast (Y), 0.75 M urea (U), 0.4 wt% yeast and 0.75 M urea (YU). In the presence of urea, a steep increase in pH is measured after 1 day of incubation due to the hydrolysis of urea. d, SEM micrograph of bacteria-loaded microgels after 4 days of mineralization. Mineralization occurs predominantly at the interface between the microgel and the outer solution, as highlighted by the red arrows.

20%. This result suggests that within 24 h, minerals form an interconnected structure that prevents the 3D printed parts from collapsing. The change in volume decreases further with mineralization time until at day 4, we observe an increase in volume of 10%, suggesting the onset of an over-mineralization of the structure. To avoid a strong over-mineralization, which would compromise the shape fidelity, we stop the mineralization of our scaffolds after 4 days.

Our results indicate that within 24 h of incubation, the minerals form an interconnected network that gradually densifies within the next 72 h of incubation. To test this suggestion, we quantify the change in density of the composite over time. After 24 h of mineralization the composite density is as low as 0.7 g·cm^{-3}, as shown in Figure 8.6b. This result suggests that the mineral has already formed an interconnected network, despite the low degree of mineralization. This interconnected mineral network prevents the material from

collapsing upon drying, while maintaining the intrinsic high porosity of the initial hydrogel network, well in agreement with our previous results. The density gradually increases with incubation time, as shown in Figure 8.6b. This finding supports our TGA results that indicate that the degree of mineralization increases during the first four days of incubation while the amount of polymer contained in the composite decreases due to a pH-driven partial dissolution of the gelatin. Yet, even after 4 days of mineralization, the density reaches values around 0.9 g·cm^{-3}, which is far below the density of calcite of 2.71 g·cm^{-3} [358], suggesting that the generated composite is porous. Indeed, granular structures typically possess microporosity arising from the voids present between jammed microgels [130, 131]. To test if this is the case in our composite, we perform scanning electron microscopy (SEM) imaging on mineralized samples as a function of the mineralization time. All measured samples possess pores with diameters up to 300 µm compatible with the expected internal microporosity of granular materials, as shown in Figure 8.6c. To quantify the internal porosity of samples that have been mineralized for 4 days, we perform micro computed tomography (µCT) on them. Indeed, 2D slices and 3D reconstructions confirm a degree of porosity of 47 vol%, as shown in Figure 8.6d, Figure 8.6e and Movie M2. This porosity is below the value we calculate from the measured density of 67 vol%. We assign this difference to the spatial resolution of the µCT that is limited to 1 µm, which prevents us from detecting smaller pores. This comparison indicates that our composites possess a significant fraction of pores with at least one dimension below 1 µm.

8.4.5   Mechanical Characterization of Mineralized BactoInk

The mineralization of our organic scaffolds strongly increases their stiffness and hardness. The extent of the increase in stiffness and hardness depends on the mechanical properties of the CaCO$_3$ which are a function of its structure [359, 360]. To assess the structure of the CaCO$_3$ formed in our scaffolds, we perform X-ray diffraction (XRD) on our samples as a function of the mineralization time. Samples that have been mineralized for 24 h contain a mixture of vaterite and calcite, as shown in the XRD traces in Figure 8.9a. The coexistence of the two phases is confirmed by SEM where we see the sphere-like structure characteristic for vaterite and the cubes, characteristic for calcite, as shown in Figure 8.7a. As the incubation time increases, the intensity of the calcite peak grows at the expense of that of the vaterite peak. After four days of incubation, the intensity ratio of calcite to vaterite, measured through XRD, increases 8-fold, as summarized in Figure 8.9b.

The CaCO$_3$ polymorph that is formed through the MICP reaction depends on the metabolic activity of the bacteria [361]. Our XRD results suggest that the metabolic activity in the first 24 h is moderate and strongly increases thereafter. To test this suggestion, we quan-
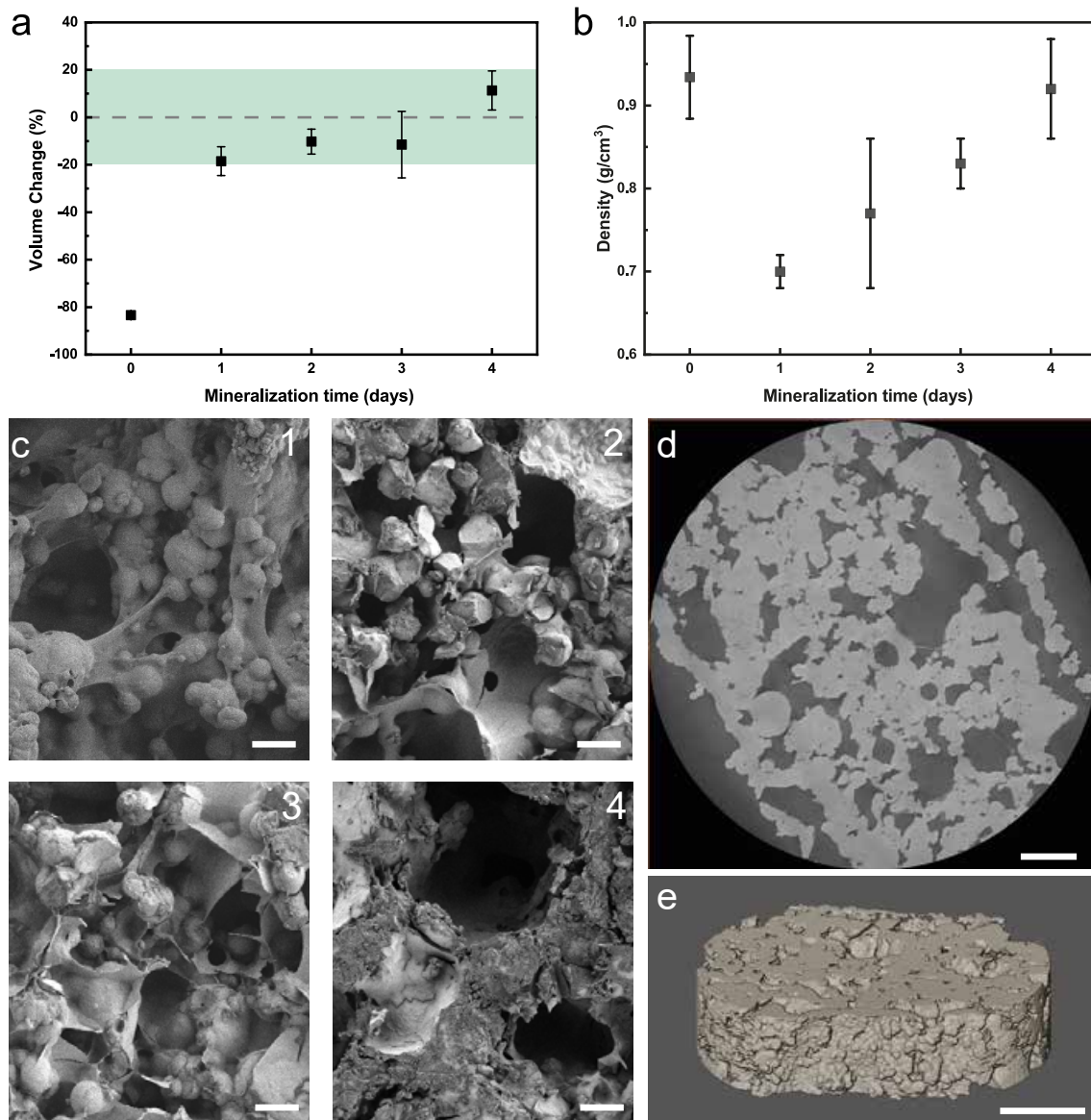
Figure 8.6: Biomineral composite structural analysis. a, Volume change of dried 3D printed biomineralized BactoInk as a function of time. At day 0, in the absence of biominerals, the structure collapses upon drying such that it loses 80% of its initial volume. The shrinkage upon drying strongly decreases with mineralization time. After 4 days of mineralization, an increase in volume is measured, indicating that the scaffold is over-mineralized. b, Density change as a function of mineralization time. In the absence of biominerals, the dried polymeric scaffold possesses a dense structure. After 24 h of mineralization, the density of the scaffold decreases, suggesting the presence of a large fraction of pores. As the mineralization progresses, a steady increase in density is observed. c, SEM micrographs of biomineralized scaffolds as a function of time. After 24 h of mineralization, biominerals and the polymer scaffold co-exist. As the mineralization progresses, the polymer content decreases. After 4 days of mineralization, the individual mineralized particles are fused together forming mineral bridges. Scale bars are 100 μm. d-e, (d) μCT scan and (e) 3D reconstruction of a biomineralized scaffold after 4 days of mineralization. The cross-section reveals a trabecular structure with a relative porosity of 47 vol%. Scale bar in (d) is 250 μm, and (e) is 500 μm.
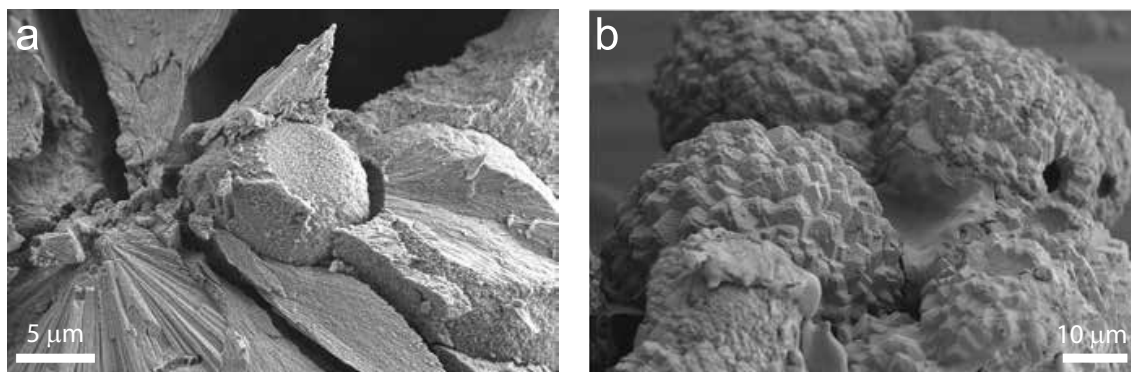
Figure 8.7: CaCO$_3$ polymorph evolution over time. a, SEM micrograph of a mineralized sample after 1 day of incubation. The image reveals sphere-like structures typical of vaterite crystals. b, SEM micrograph of a mineralized sample after 4 days of incubation. The image reveals cubic-like, structures characteristic of calcite crystals growing around spherical microgels.

tify the metabolic activity of our 3D printed bacteria, by measuring the bacterial growth within individually dispersed microgels through optical density measurements (OD600), as shown in Figure 8.8; the optical density is directly correlated to bacteria enzymatic activity [183, 194]. Indeed, within the first 24 h, bacteria display a relatively low activity, that increases over time. We assign the low bacteria activity within the first 24 h to the thawing and encapsulation process that might stresses the bacteria, limiting their full metabolic activity. This result is in excellent agreement with our XRD analysis: In the initial dormant state, the MICP favors the precipitation of metastable CaCO$_3$ crystals, such as vaterite, that require a moderately alkaline environment and less energy to be formed [361]. Upon full metabolic recovery and thanks to the increased alkalinity of the solution, the biomineralization reaction shifts towards the precipitation of calcite, as shown in Figure 8.7b. This change in CaCO$_3$ structure results in stronger biomineralized scaffolds capable of withstanding significant loads, as exemplified on the photograph in Figure 8.9c.

To quantify the impact of the MICP on the compressive strength of our material, we prepare cylindrical samples and test them under uniaxial compression. No significant change in stiffness is observed for samples after 24 h of mineralization compared to the unmineralized polymer, as shown in Figure 8.9d. This result indicates that after 24 h of mineralization, we form an interconnected mineral network that can withstand its own weight, yet, this network is fragile such that it becomes defective as soon as it is compressed. By contrast, after 4 days of mineralization, the mineral network is sufficiently robust such that a structure with a cross-section of 50 mm^2 can bear loads up to 175 N under compression. This behavior results in a compressive stiffness of the composite of 95 MPa, a value that is 3-fold higher than that of unmineralized counterparts, as shown in Figure 8.9d.
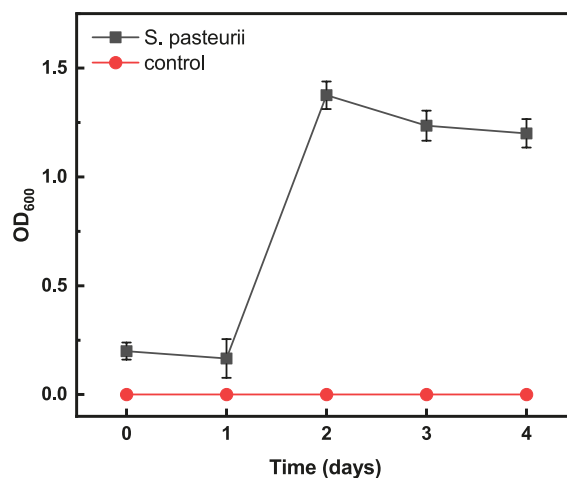
Figure 8.8: Bacteria growth. Optical density measurement for bacteria-loaded microgels incubated in 0.4 wt% yeast extract and 0.75 M urea. A steep increase in optical density is observed after 2 days of incubation confirming bacteria viability. The control refers to cultivating media alone in the absence of bacteria-loaded microgels.

The mechanical behavior of porous materials depends on their density [362]. To account for the variable porosities of our samples, we normalize the compressive moduli with the sample density. While the dried polymer has a density close to 1 g·cm^{-3}, the samples that have been mineralized for 24 h encompass a significant fraction of pores. Hence, the normalization of the compressive modulus with the porosity yields an increase in specific modulus of the sample after 24 h of mineralization with respect to the pure polymer counterpart, as shown in Figure 8.9e. Samples incubated for 2 - 3 days display a sudden drop in mechanical performance, despite their relatively low density, as shown in Figure 8.9e. This can be explained by the pH-dependent gelatin degradation which results in loose mineralized fragments that do not bear any load, yet, that contribute to the density of the composite. As a result, the overall specific stiffness of the structure is lowered. However, with the MICP continuing, more and more mineral is precipitated and load-bearing mineral bridges are formed while loose gelatin diffuses out of the material. As a result of this evolution of the composite, its specific modulus increases up to 90 MPa·g^{-1}·cm^3 after 4 days of mineralization.

To benchmark the MICP process with conventional composites created by mixing reactants in bulk, we premix our initial gel formulation with 75 wt% of inorganic $CaCO_3$ filler. As expected, premixed samples prepared in bulk are much softer than the composite that has been biomineralized *in situ* for 24 h, displaying a compressive stiffness 8 times lower than the mineralized sample, as shown in Figure 8.9f. We assign the large difference in compression moduli to the mineral bridges that form in biomineralized samples which result in an interconnected inorganic network. This interconnected inorganic network in-

creases the stiffness of the composite much more efficiently than individually dispersed fillers present in the bulk sample, as schematically summarized in Figure 8.9g and 8.9h. This result highlights the benefit of combining the granular microgel approach with the MICP process for the fabrication of load-bearing biomineral composites.

8.4.6 Applications of Engineered Living Biocomposites

To demonstrate the potential of our BactoInk to produce macroscopic load-bearing porous 3D composites in an energy efficient manner, we 3D print a sphinx that we subsequently mineralize. The combination of granular printing and MICP allows the fabrication of 3D printed structures with a high printing resolution and shape fidelity, as shown in Figure 8.10a. Additionally, the BactoInk injectability and harmless biomineralization offer a new potential solution for art restoration, as exemplified on a statue that contained a hole. This hole can be filled with the BactoInk and upon mineralization, the defect becomes much less severe, as shown in Figure 8.10b. To demonstrate the versatility of our approach, we cast the BactoInk into a mold with the shape of a coral. We first produce a negative mold using a commercial cast formulation and a coral master made of poly(lactic acid). Subsequently, we inject the BactoInk in the mold, stabilize the structure by immersing it in a $CaCl_2$ solution and transfer the scaffold in the mineralizing solution for 4 days. The final structure is dried resulting in a cm-sized free-standing coral, as shown in Figure 8.10c. These results demonstrate the potential of the BactoInk to restore or repair broken or partially degraded natural minerals.
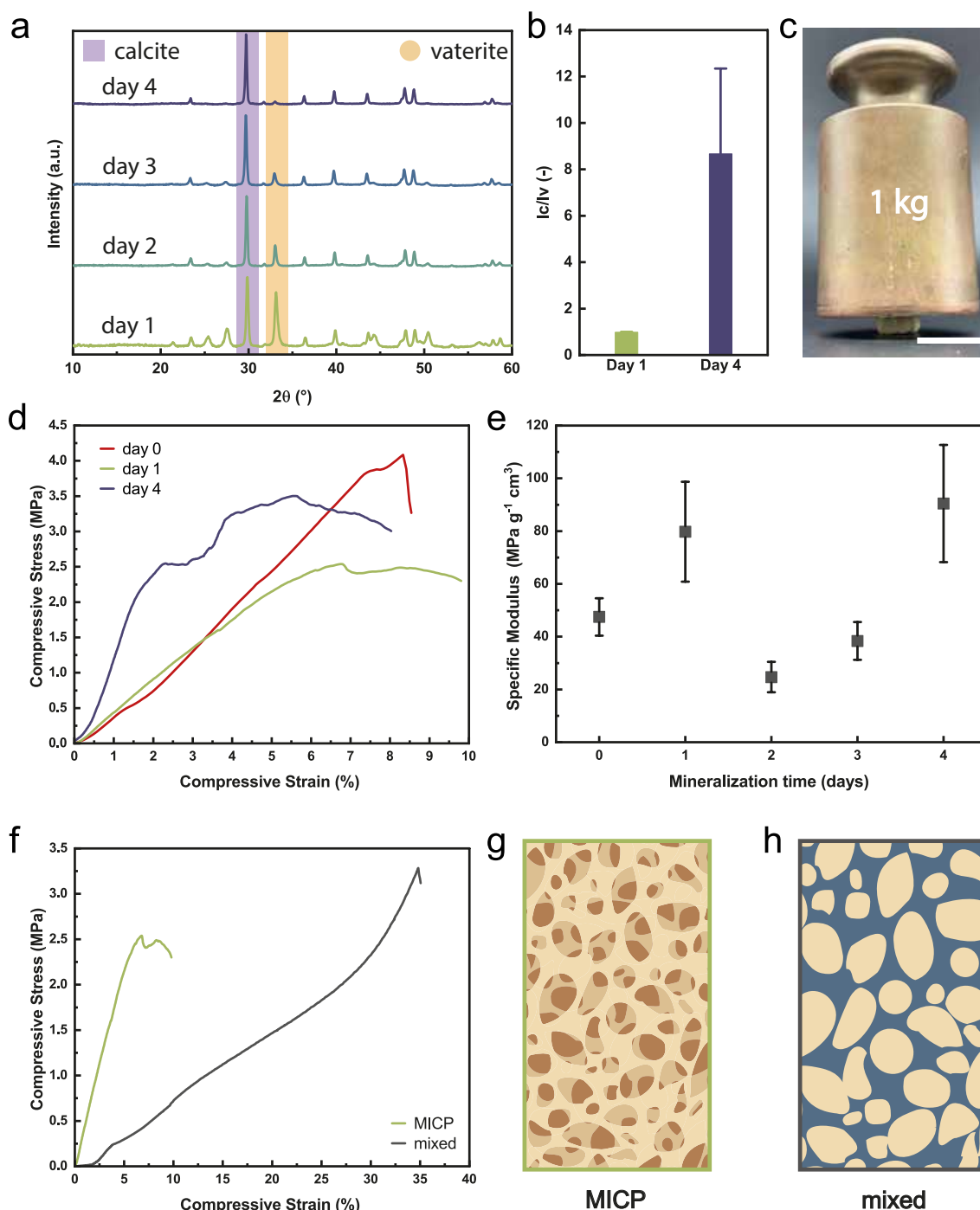
Figure 8.9: Phase evolution of $CaCO_3$ and mechanical analysis of biomineralized BactoInk. a, XRD scans of samples as a function of the mineralization time. Over time, the calcite peak, indicated in violet, increases with respect to the vaterite peak, indicated in orange. b, XRD peak intensity ratio of the peak at $29.7°$, characteristic of calcite versus that at $33°$, characteristic of vaterite. The intensity ratio increases 8-fold if samples are mineralized for 4 days compared to those mineralized for 1 day. c, Photograph of a biomineralized scaffold sustaining a 1 kg weight. Scale bar is 20 mm. d, Compression curves of samples as a function of the mineralization time. A 3-fold increase in stiffness is measured upon mineralization of samples for 4 days. e, Compressive modulus normalized by the sample density, called specific modulus, of biomineralized scaffolds as a function of the incubation time. An increase in stiffness with respect to the bare polymer is measured already after 24 h, suggesting the formation of an interconnected inorganic network within this time frame. Between day 1 and day 4, a strong decrease in specific modulus is observed. We assign this decrease to the pH-induced gelatin degradation that lowers the specific modulus of the polymer. After 4 days, the mineral content significantly increases, leading to a strong increase in modulus. f, Compression curves of MICP (green) versus pre-mixed (grey) composite after 24 h of biomineralization. Schematic representation of g, the trabecular structure formed by the MICP process and h, the filler-reinforced structure. The MICP process endows the biocomposite with higher mechanical stiffness compared to the bulk mixing with fillers.
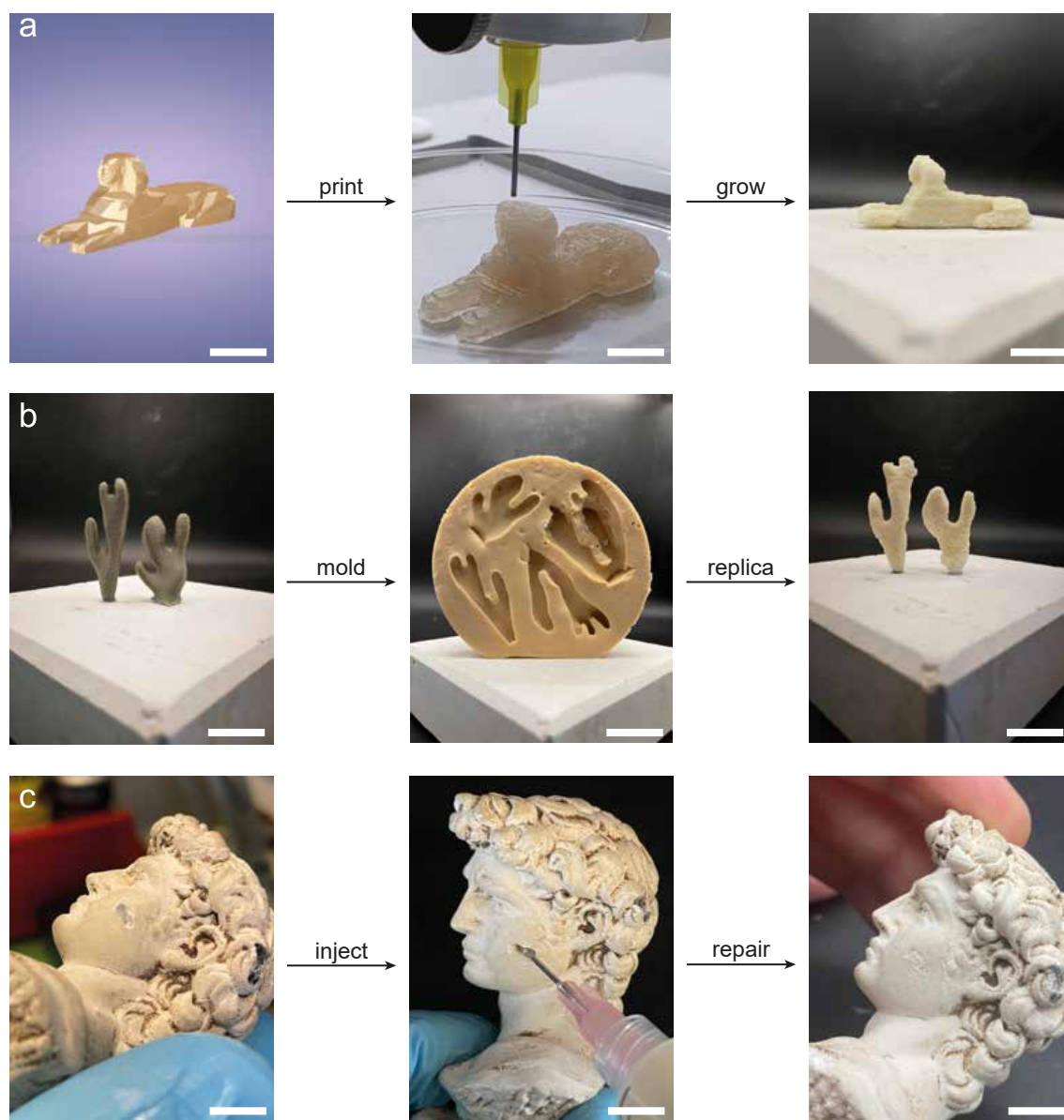
Figure 8.10: Proof of concept of BactoInk biomineral composites. a, 3D printing of BactoInk into a sphinx. The printed scaffold is biomineralized yielding a hard free-standing object. Scale bar is 20 mm. b, Application of BactoInk as a repairing paste for art restoration. The BactoInk is injected in a damaged statue and biomineralized to fill the cavity. Scale bar is 10 mm. c, Replica molding of corals. The BactoInk is casted into a negative mold to obtain a biomineralized coral that could be used for reef restoration. Scale bar is 20 mm.

8.5 Conclusion

We introduce 3D printable bacteria-loaded microgels that can be converted into macroscopic strong organic/inorganic composites comprising mineral contents up to 93 wt% through an energy-efficient MICP process. The synergistic combination of jammed microgels that enable 3D printing and the MICP produces a light weight inorganic porous trabecular structure that resembles that of many natural materials, such as trabecular bones. Importantly, the formulation exclusively contains nature-derived materials. Thanks to the formation of mineral bridges within the material, the obtained inorganic scaffolds are interconnected, such that the composites are able to bear pressures up to 3.5 MPa. The low energy impact of the BactoInk combined with its ability to be 3D printed open up new possibilities to restore defective mineral-based structures or to build synthetic mineral analogues that, thanks to the 3D printability of the ink, possess well-defined structures on the micrometer length scale and above. We envisage the versability of the processing of this ink combined with its low environmental impact and the excellent mechanical properties of the mineralized materials to open up new possibilities to fabricate lightweight load-bearing composites whose structure, composition, and hence mechanical properties resemble more closely those of natural counterparts than those of current synthetic composites.

CHAPTER 9

Conclusion

At the beginning of this thesis, I condensed the current state-of-the-art of manmade hydrogels for load-bearing applications, with a particular focus on the development of strong and tough hydrogel networks inspired by nature. I highlighted the main limitations of current solutions and their potential advancements. Based on these premises, I laid the foundations for my doctoral investigation and presented my scientific efforts towards the fabrication of synthetic hydrogels with controlled microstructure and superior mechanical properties, namely high stiffness and high toughness. Here, I recapitulate the main results accomplished and draw the conclusion that could set the basis for future research in the field.

In Chapter 4, I introduced a novel load-bearing granular hydrogel based on the combination of 3D printing of jammed microgel inks and mechanical reinforcement of double network hydrogels. This new material displays unique rheological and physicochemical properties given by the intrinsic heterogeneity of the granular precursor. Jammed microgel inks display shear-thinning, relatively low yield stress, and fast shear recovery, that render them a perfect candidate for injection and 3D extrusion printing. These microgels can be loaded with a second precursor solution that can be converted in a percolating hydrogel network that bridges the individual microgels together. As a result, the formation of a double network granular hydrogel enables the fabrication of 3D printed complex structures with superior mechanical performances.

In Chapter 5, I discussed the possibility to expand the application window of double network granular hydrogels by introducing a degradation mechanism in the structure, thus rendering the material recyclable. Furthermore, I proved the versatility of this approach for the fabrication of recyclable hard plastics based on a granular precursor. This technique could constitute a shift in paradigm for the fabrication of the next generation sustainable plastics.

In Chapters 6 and 7, I investigated the potential of metal-coordination for the selective reinforcement of bulk and double network granular hydrogels. These two sections demonstrated the versatility of metal-coordination, as well as its unique reinforcement effect for the fabrication of strong and tough double network granular hydrogels with local varying composition. Proof-of-concept of a scalable, high-throughput microgel production was also discussed in the attempt to convince the audience of the translational potential of granular materials.

In Chapter 8, I proposed a new approach for the future development of smart adaptive materials, based on the combination of a granular hydrogel with bacteria to fabricate the next generation of engineered living materials. The jammed microgel precursor allowed the fabrication of arbitrarily complex structures, while the bacteria converted the soft scaffold in a hard load-bearing biocomposite. The proposed solution demonstrated a degree of control unattainable by any synthetic process and showed the possibility to fabricate composite materials in a sustainable, resource-efficient way.

Overall, I demonstrated the almost limitless potential of microgel-based materials, as well as the emerging properties of double network granular hydrogels. The possibility to control size, shape, composition, and arrangement down to the individual microgel level renders granular hydrogels the best candidate to finally mimic nature's complex architectures. Furthermore, the easiness of implementation, scalability, and relatively low cost of microgel production set the premise for a direct translation to real-life industrial applications. Ultimately, the synergistic combination of granular hydrogels with conventional hydrogel reinforcement techniques proves the successful integration of well-known technologies with cutting-edge research, thus bringing the field of soft matter towards uncharted territories. Despite the extensive discussion made in this thesis and the level of maturity reached by the field, I still believe that a great gap of knowledge needs to be filled before considering our quest for nature-inspired soft materials concluded.

In the following chapter, I will provide an outlook on research topics I consider key for the future advancement of granular hydrogel research.

CHAPTER 10

Outlook

In this chapter, I present a series of unpublished ideas that could serve as foundation for the future development of advanced soft materials. I hope this section will provide the right momentum to the hydrogel field to extend the application potential of granular materials to different domains, including that of soft robotics and smart adaptive materials.

10.1 Microgels as Rheological Modifiers

The unique rheological behavior of jammed microgels has yet to demonstrate its full potential. While variations in microgel formulation have shown to have limited effect on printability [154], no research has been conducted on the use of microgels as rheological modifiers. Due to their collective rheological behavior, microgels can be assimilated to thickeners added to a solution to increase its relative viscosity. Potentially, microgels can be added to a hydrogel precursor solution to modify its rheological behavior, thus rendering it shear-thinning, and hence 3D printable. If proven to be effective, this synergistic combination would allow to further expand the toolbox of available hydrogel inks for additive manufacturing. Furthermore, the heterogeneous composition of the ink would enable the design of more complex materials with unique physicochemical properties. For example, two different populations of microorganisms could be separately encapsulated either in the microgels or in the continuous phase to enable their chemical interaction, while preventing any physical contact.

10.2 Porous Double Network Granular Hydrogels

Double network granular hydrogel superior mechanics come at the expense of the suppression of macroporosity [149]. Indeed, a second percolating network backfills all the

interparticle pores, thus forming a continuous matrix. Strategies to restore macroporosity in a granular scaffold would be beneficial for applications of double network granular hydrogels in tissue engineering, where a certain degree of porosity is needed to guarantee sufficient cell viability. Here, I propose two possible strategies to introduce micrometer-sized pores in a double network granular hydrogel: the sacrificial and the phase separation method. In the sacrificial method, the combination of two microgel populations is needed. The granular hydrogel is formed from one microgel population and the second population that acts as sacrificial particles that are degraded after the material has been assembled, leaving voids within the granular matrix. However, the biocompatibility of the scaffold might be compromised depending on the selected degradation process. In the phase separation method, two hydrophilic polymers known to phase separate are mixed. One of these polymers must be responsive, the other inert. The degree of phase separation, and hence the internal porosity, can be precisely controlled by changing several physicochemical parameters, including molecular weight, temperature, and ionic strength, such that granular hydrogels with controlled porosity can be fabricated.

10.3   Double Network Granular Elastomers

The intrinsic sensitivity to moisture content in hydrogels strongly hinders their use in more real-life applications, such as for example the design of soft actuators. While examples of hydrogel-based actuators have been reported in literature, their actuation mechanism is mainly based on diffusion of water or small molecules, thus severely limiting their actuation speed [363, 364]. A way to circumvent this shortcoming is to design elastomer-based actuators. However, conventional elastomer fabrication techniques rely on casting or molding, thus limiting their structural complexity. Double network elastomers have been shown to work under the same rationale as double network hydrogels [221], thus setting the premise for the production of double network granular elastomers. By doing so, the favorable rheological properties and printability of jammed granular precursors can be combined with the high mechanical performance and moisture insensitivity of elastomeric materials. As a result, soft actuators with complex structures and high environmental stability could be easily fabricated.

10.4   Multi-Functional Granular Hydrogels

Throughout the thesis, I discussed the intrinsic modularity of double network granular hydrogels and suggested potential applications [149, 255]. Despite the several examples

proposed, no thorough investigation has been conducted on how to harness their full potential. Modularity and heterogeneity are two of the main assets of granular hydrogels, yet they are the least discussed. In the future, research on the combination of microgels with complementary, counteracting, or orthogonal properties must become the focal point to increase the degree of complexity achievable with 3D printed granular materials. For example, pH- and T-responsive microgels can be mixed in the same granular material to endow the construct with orthogonal sensing properties. Alternatively, high swelling and low swelling microgels can be assembled together to enable shape morphing and autonomous locomotion. Ultimately, amphiphilic granular hydrogels can be formed if hydrophilic and hydrophobic microgels are mixed together, a feature extremely difficult, if not impossible, to obtain in bulk due to the immiscibility of the two phases. These combinations are just a few examples of potential heterogeneous architectures that could be implemented with a granular precursor. I foresee this particular research to hold the greatest potential for the fabrication of smart adaptive hydrogel composites and, in general, for the future development of soft matter research.

APPENDIX A

Abbreviations

$3D$	three dimensional
AA	acrylic acid
AM	acrylamide
$AMPS$	2-acrylamido-2-methylpropane sulfonic acid
APS	ammonium peroxydisulfate
KGA	α-ketoglutaric acid
d	diameter
D_2O	deuterium oxide
DAT	data file extension
DN	double network
$DNGH$	double network granular hydrogel
ECM	extracellular matrix
EWC	equilibrium water content
$CaCO_3$	calcium carbonate
$FeCl_3$	iron III chloride
$AlCl_3$	aluminium chloride
$CaCl_2$	calcium chloride
$ZnCl_2$	zinc chloride
$AgNO_3$	silver nitrate
γ	shear
G	stress relaxation modulus
G_i	initial stress relaxation modulus
G_0	plateau stress relaxation modulus
G'	viscoelastic storage modulus
G''	viscoelastic loss modulus

h	height
H	relaxation spectrum
H_2O	water
HCl	hydrogen chloride
I	scattering intensity
k_B	Boltzmann constant
$mol\%$	molar percentage
MBA	N,N′-methylene bisacrylamide
$NaCl$	sodium chloride
$NaOH$	sodium hydroxide
NMR	nuclear magnetic resonance
ξ	short correlation length
PAA	poly(acrylic acid)
PAM	poly(acrylamide)
$PAMPS$	poly(sodium 2-acrylamido-2-methyl-1-propanesulfonate)
PEG	poly(ethylene glycol)
PI	photoinitiator
$PNIPAM$	poly(N-isopropylacrylamide)
$PVCL$	poly(N-vinyl caprolactam)
PVA	poly(vinyl alcool)
τ	relaxation time
t	time
T	temperature
SEM	scanning electron microscopy
EDX	energy dispersive X-Ray analysis
UV	ultraviolet
V	volume
W_{ap}	as-prepared sample weight
W_d	dry sample weight
$wt\%$	weight percentage
XRD	X-ray diffraction
φ	volume fraction

APPENDIX B

Units

cm	centimeter
Da	dalton
g	gram
h	hour
J	joule
kDa	kilodalton
kg	kilogram
kPa	kilopascal
L	litter
µg	microgram
µL	microlitter
µm	micrometer
mg	milligram
min	minute
mL	milliliter
mm	millimeter
M	molar
MHz	megahertz
MPa	megapascal
mmol	millimollar
mW	milliwatt
N	newton
nm	nanometer
Pa	pascal
rad	radian

s	second
W	watt

Bibliography

[1] Po-Yu Chen, Joanna McKittrick, and Marc André Meyers. Biological materials: Functional adaptations and bioinspired designs. *Progress in Materials Science*, 57(8):1492–1704, November 2012.

[2] Georg E. Fantner, Tue Hassenkam, Johannes H. Kindt, James C. Weaver, Henrik Birkedal, Leonid Pechenik, Jacqueline A. Cutroni, Geraldo A. G. Cidade, Galen D. Stucky, Daniel E. Morse, and Paul K. Hansma. Sacrificial bonds and hidden length dissipate energy as mineralized fibrils separate during bone fracture. *Nature Materials*, 4(8):612–616, August 2005. Number: 8 Publisher: Nature Publishing Group.

[3] Misch Ce, Qu Z, and Bidez Mw. Mechanical properties of trabecular bone in the human mandible: implications for dental implant treatment planning and surgical placement. *Journal of oral and maxillofacial surgery : official journal of the American Association of Oral and Maxillofacial Surgeons*, 57(6), June 1999. Publisher: J Oral Maxillofac Surg.

[4] Natalie Reznikov, Matthew Bilton, Leonardo Lari, Molly M. Stevens, and Roland Kröger. Fractal-like Hierarchical Organization of Bone Begins at the Nanoscale. *Science*, 360(6388):eaao2189, May 2018.

[5] L. Rossetti, L. A. Kuntz, E. Kunold, J. Schock, K. W. Müller, H. Grabmayr, J. Stolberg-Stolberg, F. Pfeiffer, S. A. Sieber, R. Burgkart, and A. R. Bausch. The Microstructure and Micromechanics of the Tendon– Bone Insertion. *Nature Materials*, 16(6):664–670, June 2017. Publisher: Nature Publishing Group.

[6] Chaoji Chen, Yudi Kuang, Shuze Zhu, Ingo Burgert, Tobias Keplinger, Amy Gong, Teng Li, Lars Berglund, Stephen J. Eichhorn, and Liangbing Hu. Structure–property–function relationships of natural and engineered wood. *Nature Reviews Materials*, pages 1–25, May 2020. Publisher: Nature Publishing Group.

[7] Lars A. Berglund and Ingo Burgert. Bioinspired Wood Nanotechnology for Functional Materials. *Advanced Materials*, 30(19):1704285, 2018. _eprint: https://onlinelibrary.wiley.com/doi/pdf/10.1002/adma.201704285.

[8] Lorna J. Gibson. The hierarchical structure and mechanics of plant materials. *Journal of The Royal Society Interface*, 9(76):2749–2766, November 2012. Publisher: Royal Society.

[9] Haeshin Lee, Norbert F. Scherer, and Phillip B. Messersmith. Single-Molecule Mechanics of Mussel Adhesion. *Proceedings of the National Academy of Sciences*, 103(35):12999–13003, August 2006.

[10] Christopher E. Killian, Rebecca A. Metzler, Yutao Gong, Tyler H. Churchill, Ian C. Olson, Vasily Trubetskoy, Matthew B. Christensen, John H. Fournelle, Francesco De Carlo, Sidney Cohen, Julia Mahamid, Andreas Scholl, Anthony Young, Andrew Doran, Fred H. Wilt, Susan N. Coppersmith, and Pupa U. P. A. Gilbert. Self-Sharpening Mechanism of the Sea Urchin Tooth. *Advanced Functional Materials*, 21(4):682–690, 2011. _eprint: https://onlinelibrary.wiley.com/doi/pdf/10.1002/adfm.201001546.

[11] Jiseok Gim, Noah Schnitzer, Laura M. Otter, Yuchi Cui, Sébastien Motreuil, Frédéric Marin, Stephan E. Wolf, Dorrit E. Jacob, Amit Misra, and Robert Hovden. Nanoscale deformation mechanics reveal resilience in nacre of Pinna nobilis shell. *Nature Communications*, 10(1):4822, October 2019. Number: 1 Publisher: Nature Publishing Group.

[12] Madeleine Grossman, Dmitriy Pivovarov, Florian Bouville, Clemens Dransfeld, Kunal Masania, and André R. Studart. Hierarchical Toughening of Nacre-Like Composites. *Advanced Functional Materials*, 29(9):1806800, 2019.

[13] Jiyu Sun and Bharat Bhushan. Hierarchical structure and mechanical properties of nacre: a review. *RSC Advances*, 2(20):7617–7632, August 2012. Publisher: The Royal Society of Chemistry.

[14] Ulrike G.K. Wegst, Hao Bai, Eduardo Saiz, Antoni P. Tomsia, and Robert O. Ritchie. Bioinspired Structural Materials. *Nature Materials*, 14(1):23–36, 2015.

[15] Esther Amstad and Matthew J. Harrington. From Vesicles to Materials: Bioinspired Strategies for Fabricating Hierarchically Structured Soft Matter. *Philosophical Transactions of the Royal Society A: Mathematical, Physical and Engineering Sciences*, 379(2206):20200338, September 2021. Publisher: Royal Society.

[16] Florian Bouville, Eric Maire, Sylvain Meille, Bertrand Van de Moortèle, Adam J. Stevenson, and Sylvain Deville. Strong, tough and stiff bioinspired ceramics from brittle constituents. *Nature Materials*, 13(5):508–514, May 2014. Number: 5 Publisher: Nature Publishing Group.

[17] Fanfan Fu, Luoran Shang, Zhuoyue Chen, Yunru Yu, and Yuanjin Zhao. Bioinspired living structural color hydrogels. *Science Robotics*, 3(16):eaar8580, March 2018. Publisher: American Association for the Advancement of Science.

[18] Yifan Si, Zhichao Dong, and Lei Jiang. Bioinspired Designs of Superhydrophobic and Superhydrophilic Materials. *ACS Central Science*, 4(9):1102–1112, September 2018. Publisher: American Chemical Society.

[19] Wei Huang, David Restrepo, Jae-Young Jung, Frances Y. Su, Zengqian Liu, Robert O. Ritchie, Joanna McKittrick, Pablo Zavattieri, and David Kisailus. Multiscale Toughening Mechanisms in Biological Materials and Bioinspired Designs. *Advanced Materials*, 31(43):1901561, 2019. _eprint: https://onlinelibrary.wiley.com/doi/pdf/10.1002/adma.201901561.

[20] Robert O Ritchie. The Conflicts between Strength and Toughness. *Nature Publishing Group*, 10, 2011.

[21] Xuanhe Zhao, Xiaoyu Chen, Hyunwoo Yuk, Shaoting Lin, Xinyue Liu, and German Parada. Soft Materials by Design: Unconventional Polymer Networks Give Extreme Properties. *Chemical Reviews*, 121(8):4309–4372, April 2021. Publisher: American Chemical Society.

[22] Joanna Aizenberg and Peter Fratzl. Biological and Biomimetic Materials. *Advanced Materials*, 21(4):387–388, 2009. _eprint: https://onlinelibrary.wiley.com/doi/pdf/10.1002/adma.200803699.

[23] Peter Fratzl. Biomimetic materials research: what can we really learn from nature's structural materials? *Journal of the Royal Society Interface*, 4(15):637–642, August 2007.

[24] Peter Fratzl and Richard Weinkamer. Nature's hierarchical materials. *Progress in Materials Science*, 52(8):1263–1334, November 2007.

[25] Aleksander Cholewinski, Fut (Kuo) Yang, and Boxin Zhao. Algae– Mussel-Inspired Hydrogel Composite Glue for Underwater Bonding. *Materials Horizons*, 6(2):285–293, 2019.

[26] Sushila Maharjan, Jacqueline Alva, Cassandra Cámara, Andrés G. Rubio, David Hernández, Clément Delavaux, Erandy Correa, Mariana D. Romo, Diana Bonilla, Mille Luis Santiago, Wanlu Li, Feng Cheng, Guoliang Ying, and Yu Shrike Zhang. Symbiotic Photosynthetic Oxygenation within 3D-Bioprinted Vascularized Tissues. *Matter*, 4(1):217–240, January 2021. Publisher: Elsevier.

[27] Maria Feofilova, Silvan Schüepp, Roman Schmid, Florian Hacker, Hendrik T. Spanke, Nicolas Bain, Katharine E. Jensen, and Eric R. Dufresne. Geometrical frustration of phase-separated domains in Coscinodiscus diatom frustules. *Proceedings of the National Academy of Sciences*, 119(31):e2201014119, August 2022. Publisher: Proceedings of the National Academy of Sciences.

[28] Matthew J. Harrington, Franziska Jehle, and Tobias Priemel. Mussel Byssus Structure-Function and Fabrication as Inspiration for Biotechnological Production of Advanced Materials. *Biotechnology Journal*, 13(12):1800133, 2018.

[29] Hailong Fan, Jiahui Wang, and Jian Ping Gong. Barnacle Cement Proteins-Inspired Tough Hydrogels with Robust, Long-Lasting, and Repeatable Underwater Adhesion. *Advanced Functional Materials*, 31(11):2009334, 2021.

[30] Emmanouela Filippidi, Daniel G. DeMartini, Paula Malo de Molina, Eric W. Danner, Juntae Kim, Matthew E. Helgeson, J. Herbert Waite, and Megan T. Valentine. The Microscopic Network Structure of Mussel (Mytilus) Adhesive Plaques. *Journal of The Royal Society Interface*, 12(113):20150827–20150827, 2015.

[31] Andressa Jantzen da Silva Lucas, Eliézer Quadro Oreste, Helena Leão Gouveia Costa, Héctor Martín López, Carolina Dias Medeiros Saad, and Carlos Prentice. Extraction, physicochemical characterization, and morphological properties of chitin and chitosan from cuticles of edible insects. *Food Chemistry*, 343:128550, May 2021.

[32] Kun Yan Zhu, Hans Merzendorfer, Wenqing Zhang, Jianzhen Zhang, and Subbaratnam Muthukrishnan. Biosynthesis, Turnover, and Functions of Chitin in Insects. *Annual Review of Entomology*, 61(1):177–196, 2016. _eprint: https://doi.org/10.1146/annurev-ento-010715-023933.

[33] O. Wichterle and D. Lím. Hydrophilic Gels for Biological Use. *Nature*, 185(4706):117–118, January 1960. Number: 4706 Publisher: Nature Publishing Group.

[34] Gary W. Ashley, Jeff Henise, Ralph Reid, and Daniel V. Santi. Hydrogel Drug Delivery System with Predictable and Tunable Drug Release and Degradation Rates.

Proceedings of the National Academy of Sciences, 110(6):2318–2323, February 2013. Publisher: National Academy of Sciences Section: Biological Sciences.

[35] Todd R. Hoare and Daniel S. Kohane. Hydrogels in drug delivery: Progress and challenges. *Polymer*, 49(8):1993–2007, April 2008.

[36] Kalpana R. Kamath and Kinam Park. Biodegradable Hydrogels in Drug Delivery. *Advanced Drug Delivery Reviews*, 11(1):59–84, July 1993.

[37] Jianyu Li and David J. Mooney. Designing hydrogels for controlled drug delivery. *Nature Reviews Materials*, 1(12), December 2016.

[38] Thomas Billiet, Mieke Vandenhaute, Jorg Schelfhout, Sandra Van Vlierberghe, and Peter Dubruel. A Review of Trends and Limitations in Hydrogel-Rapid Prototyping for Tissue Engineering. *Biomaterials*, 33(26):6020–6041, September 2012.

[39] Natalie Boehnke, Cynthia Cam, Erhan Bat, Tatiana Segura, and Heather D. Maynard. Imine Hydrogels with Tunable Degradability for Tissue Engineering. *Biomacromolecules*, 16(7):2101–2108, July 2015. Publisher: American Chemical Society.

[40] Sayan Deb Dutta, Dinesh K. Patel, and Ki-Taek Lim. Functional cellulose-based hydrogels as extracellular matrices for tissue engineering. *Journal of Biological Engineering*, 13(1):55, June 2019.

[41] Richun Liu, Shichen Zhang, and Xiao Chen. Injectable Hydrogels for Tendon and Ligament Tissue Engineering. *Journal of Tissue Engineering and Regenerative Medicine*, 14(9):1333–1348, 2020.

[42] Taimoor H. Qazi and Jason A. Burdick. Granular hydrogels for endogenous tissue repair. *Biomaterials and Biosystems*, 1:100008, March 2021.

[43] Biji Balakrishnan, M. Mohanty, P. R. Umashankar, and A. Jayakrishnan. Evaluation of an in situ forming hydrogel wound dressing based on oxidized alginate and gelatin. *Biomaterials*, 26(32):6335–6342, November 2005.

[44] Qingchen Cao, Guofei Sun, Xing Wang, Fei Yang, Licheng Zhang, and Decheng Wu. Bioinspired Self-Degradable Hydrogels towards Wound Sealing. *Biomaterials Science*, 9(10):3645–3649, 2021. Publisher: Royal Society of Chemistry.

[45] Xiaodong Jing, Yanzhen Sun, Xiaoli Ma, and Hao Hu. Marine Polysaccharides: Green and Recyclable Resources as Wound Dressings. *Materials Chemistry Frontiers*, 5(15):5595–5616, July 2021. Publisher: The Royal Society of Chemistry.

[46] Donald R. Griffin, Westbrook M. Weaver, Philip O. Scumpia, Dino Di Carlo, and Tatiana Segura. Accelerated Wound Healing by Injectable Microporous Gel Scaffolds Assembled from Annealed Building Blocks. *Nature Materials*, 14(7):737–744, July 2015. Publisher: Nature Publishing Group.

[47] S. H. Aswathy, U. Narendrakumar, and I. Manjubala. Commercial hydrogels for biomedical applications. *Heliyon*, 6(4):e03719, April 2020.

[48] Enrica Caló and Vitaliy V Khutoryanskiy. Biomedical Applications of Hydrogels: A Review of Patents and Commercial Products. 2015.

[49] Stefan Zechel, Martin D. Hager, Tobias Priemel, and Matthew J. Harrington. Healing through Histidine: Bioinspired Pathways to Self-Healing Polymers via Imidazole–Metal Coordination. *Biomimetics*, 4(1):20, March 2019.

[50] Leslie Ng, Mark A. Elgar, and Devi Stuart-Fox. From Bioinspired to Bioinformed: Benefits of Greater Engagement From Biologists. *Frontiers in Ecology and Evolution*, 9, 2021.

[51] Ruobing Bai, Jiawei Yang, and Zhigang Suo. Fatigue of Hydrogels. *European Journal of Mechanics - A/Solids*, 74:337–370, March 2019.

[52] Mitsuhiro Shibayama, Xiang Li, and Takamasa Sakai. Precision polymer network science with tetra-PEG gels—a decade history and future. *Colloid and Polymer Science*, 297(1):1–12, January 2019.

[53] J. P. Gong, Y. Katsuyama, T. Kurokawa, and Y. Osada. Double-Network Hydrogels with Extremely High Mechanical Strength. *Advanced Materials*, 15(14):1155–1158, 2003.

[54] Tasuku Nakajima and Jian Ping Gong. Double-Network Hydrogels: Soft and Tough IPN. In Shiro Kobayashi and Klaus Müllen, editors, *Encyclopedia of Polymeric Nanomaterials*, pages 1–6. Springer, Berlin, Heidelberg, 2021.

[55] Jian Ping Gong. Why Are Double Network Hydrogels so Tough? *Soft Matter*, 6(12):2583–2590, June 2010.

[56] Md. Anamul Haque, Takayuki Kurokawa, and Jian Ping Gong. Super tough double network hydrogels and their application as biomaterials. *Polymer*, 53(9):1805–1822, April 2012.

[57] Jeong-Yun Sun, Xuanhe Zhao, Widusha R. K. Illeperuma, Ovijit Chaudhuri, Kyu Hwan Oh, David J. Mooney, Joost J. Vlassak, and Zhigang Suo. Highly Stretchable and Tough Hydrogels. *Nature*, 489(7414):133–136, September 2012. Publisher: Nature Publishing Group.

[58] Jianyu Li, Widusha R. K. Illeperuma, Zhigang Suo, and Joost J. Vlassak. Hybrid Hydrogels with Extremely High Stiffness and Toughness. *ACS Macro Letters*, 3(6):520–523, June 2014. Publisher: American Chemical Society.

[59] Xinxin Huang, Jingchao Li, Jing Luo, Qiang Gao, An Mao, and Jianzhang Li. Research progress on double-network hydrogels. *Materials Today Communications*, 29:102757, December 2021.

[60] Qiang Chen, Hong Chen, Lin Zhu, and Jie Zheng. Fundamentals of Double Network Hydrogels. *J. Mater. Chem. B*, 3, March 2015.

[61] Takayuki Nonoyama and Jian Ping Gong. Tough Double Network Hydrogel and Its Biomedical Applications. *Annual Review of Chemical and Biomolecular Engineering*, 12(1):null, 2021.

[62] Huiqiong Wu, Jun Zheng, Anna [U+2010] Lena Kjøniksen, Wei Wang, Yi Zhang, and Jianmin Ma. Metallogels: Availability, Applicability, and Advanceability. *Advanced Materials*, 31(12):1806204, March 2019.

[63] Niels Holten-Andersen, Aditya Jaishankar, Matthew J. Harrington, Dominic E. Fullenkamp, Genevieve DiMarco, Lihong He, Gareth H. McKinley, Phillip B. Messersmith, and Ka Yee C. Lee. Metal-coordination: using one of nature's tricks to control soft material mechanics. *Journal of Materials Chemistry B*, 2(17):2467–2472, April 2014.

[64] Eesha Khare, Niels Holten-Andersen, and Markus J. Buehler. Transition-Metal Coordinate Bonds for Bioinspired Macromolecules with Tunable Mechanical Properties. *Nature Reviews Materials*, pages 1–16, February 2021. Publisher: Nature Publishing Group.

[65] Ming Zhong, Yi-Tao Liu, Xiao-Ying Liu, Fu-Kuan Shi, Li-Qin Zhang, Mei-Fang Zhu, and Xu-Ming Xie. Dually cross-linked single network poly(acrylic acid) hydrogels with superior mechanical properties and water absorbency. *Soft Matter*, 12(24):5420–5428, 2016.

[66] Amanda Andersen, Marie Krogsgaard, and Henrik Birkedal. Mussel-Inspired Self-Healing Double-Cross-Linked Hydrogels by Controlled Combination of Metal Coordination and Covalent Cross-Linking. *Biomacromolecules*, 19(5):1402–1409, May 2018. Publisher: American Chemical Society.

[67] Dominic E. Fullenkamp, Lihong He, Devin G. Barrett, Wesley R. Burghardt, and Phillip B. Messersmith. Mussel-Inspired Histidine-Based Transient Network Metal Coordination Hydrogels. *Macromolecules*, 46(3):1167–1174, February 2013. Publisher: American Chemical Society.

[68] Si Yu Zheng, Hongyao Ding, Jin Qian, Jun Yin, Zi Liang Wu, Yihu Song, and Qiang Zheng. Metal-Coordination Complexes Mediated Physical Hydrogels with High Toughness, Stick–Slip Tearing Behavior, and Good Processability. *Macromolecules*, 49(24):9637–9646, December 2016. Publisher: American Chemical Society.

[69] Matteo Hirsch, Mathias Steinacher, Ran Zhao, and Esther Amstad. Load-bearing hydrogels ionically reinforced through competitive ligand exchanges. *Biomaterials Science*, August 2021. Publisher: The Royal Society of Chemistry.

[70] Quan Xu, Meng Xu, Chun-Yu Lin, Qiang Zhao, Rui Zhang, Xiaoxiao Dong, Yida Zhang, Shouceng Tian, Yu Tian, and Zhenhai Xia. Metal Coordination-Mediated Functional Grading and Self-Healing in Mussel Byssus Cuticle. *Advanced Science*, 6(23):1902043, December 2019.

[71] Progyateg Chakma and Dominik Konkolewicz. Dynamic Covalent Bonds in Polymeric Materials. *Angewandte Chemie International Edition*, 58(29):9682–9695, 2019. _eprint: https://onlinelibrary.wiley.com/doi/pdf/10.1002/anie.201813525.

[72] M. Mario Perera and Neil Ayres. Dynamic Covalent Bonds in Self-Healing, Shape Memory, and Controllable Stiffness Hydrogels. *Polymer Chemistry*, 11(8):1410–1423, February 2020. Publisher: The Royal Society of Chemistry.

[73] Yunjiao Che, Stefan Zschoche, Franziska Obst, Dietmar Appelhans, and Brigitte Voit. Double-Crosslinked Reversible Redox-Responsive Hydrogels Based on Disulfide– Thiol Interchange. *Journal of Polymer Science Part A: Polymer Chemistry*, 57(24):2590–2601, 2019.

[74] John A. Burns, James C. Butler, John Moran, and George M. Whitesides. Selective Reduction of Disulfides by Tris(2-Carboxyethyl)Phosphine. *The Journal of Organic Chemistry*, 56(8):2648–2650, April 1991. Publisher: American Chemical Society.

[75] Larissa Hammer, Nathan J. Van Zee, and Renaud Nicolaÿ. Dually Crosslinked Polymer Networks Incorporating Dynamic Covalent Bonds. *Polymers*, 13(3):396, January 2021. Publisher: Multidisciplinary Digital Publishing Institute.

[76] Liming Cao, Jianfeng Fan, Jiarong Huang, and Yukun Chen. A Robust and Stretchable Cross-Linked Rubber Network with Recyclable and Self-Healable Capabilities Based on Dynamic Covalent Bonds. *Journal of Materials Chemistry A*, 7(9):4922–4933, February 2019. Publisher: The Royal Society of Chemistry.

[77] Muhammad Rizwan, Alexander E. G. Baker, and Molly S. Shoichet. Designing Hydrogels for 3D Cell Culture Using Dynamic Covalent Crosslinking. *Advanced Healthcare Materials*, 10(12):2100234, 2021.

[78] Lijing Teng, Yunhua Chen, Yong-Guang Jia, and Li Ren. Supramolecular and Dynamic Covalent Hydrogel Scaffolds: From Gelation Chemistry to Enhanced Cell Retention and Cartilage Regeneration. *Journal of Materials Chemistry B*, 7(43):6705–6736, November 2019. Publisher: The Royal Society of Chemistry.

[79] Abu Bin Imran, Kenta Esaki, Hiroaki Gotoh, Takahiro Seki, Kohzo Ito, Yasuhiro Sakai, and Yukikazu Takeoka. Extremely Stretchable Thermosensitive Hydrogels by Introducing Slide-Ring Polyrotaxane Cross-Linkers and Ionic Groups into the Polymer Network. *Nature Communications*, 5(1):5124, October 2014. Publisher: Nature Publishing Group.

[80] Phillip R. A. Chivers and David K. Smith. Shaping and structuring supramolecular gels. *Nature Reviews Materials*, 4(7):463–478, July 2019.

[81] Jade A. McCune, Stefan Mommer, Christopher C. Parkins, and Oren A. Scherman. Design Principles for Aqueous Interactive Materials: Lessons from Small Molecules and Stimuli-Responsive Systems. *Advanced Materials*, n/a(n/a):1906890, 2020.

[82] Xiaoyu Chen, Chaoqun Dong, Kongchang Wei, Yifei Yao, Qian Feng, Kunyu Zhang, Fengxuan Han, Arthur Fuk-Tat Mak, Bin Li, and Liming Bian. Supramolecular Hydrogels Cross-Linked by Preassembled Host– Guest PEG Cross-Linkers Resist Excessive, Ultrafast, and Non-Resting Cyclic Compression. *NPG Asia Materials*, 10(8):788–799, August 2018. Publisher: Nature Publishing Group.

[83] Beverly Miller, Audrey Hansrisuk, Christopher B. Highley, and Steven R. Caliari. Guest–Host Supramolecular Assembly of Injectable Hydrogel Nanofibers for Cell Encapsulation. *ACS Biomaterials Science & Engineering*, 7(9):4164–4174, September 2021. Publisher: American Chemical Society.

[84] Adrienne E. Widener, Senthilkumar Duraivel, Thomas E. Angelini, and Edward A. Phelps. Injectable Microporous Annealed Particle Hydrogel Based on Guest–Host-Interlinked Polyethylene Glycol Maleimide Microgels. *Advanced NanoBiomed Research*, 2(10):2200030, 2022. _eprint: https://onlinelibrary.wiley.com/doi/pdf/10.1002/anbr.202200030.

[85] Eric A. Appel, Mark W. Tibbitt, Matthew J. Webber, Bradley A. Mattix, Omid Veiseh, and Robert Langer. Self-Assembled Hydrogels Utilizing Polymer– Nanoparticle Interactions. *Nature Communications*, 6(1):1–9, February 2015.

[86] Donglin Gan, Wensi Xing, Lili Jiang, Ju Fang, Cancan Zhao, Fuzeng Ren, Liming Fang, Kefeng Wang, and Xiong Lu. Plant-inspired adhesive and tough hydrogel based on Ag-Lignin nanoparticles-triggered dynamic redox catechol chemistry. *Nature Communications*, 10(1):1–10, April 2019.

[87] Sytze J. Buwalda, Pieter J. Dijkstra, and Jan Feijen. Poly(Ethylene Glycol)– Poly(L-Lactide) Star Block Copolymer Hydrogels Crosslinked by Metal– Ligand Coordination. *Journal of Polymer Science Part A: Polymer Chemistry*, 50(9):1783–1791, 2012.

[88] Robert Murphy, David P. Walsh, Charles A. Hamilton, Sally-Ann Cryan, Marc in het Panhuis, and Andreas Heise. Degradable 3D-Printed Hydrogels Based on Star-Shaped Copolypeptides. *Biomacromolecules*, 19(7):2691–2699, July 2018. Publisher: American Chemical Society.

[89] Sara Azevedo, Ana M.S. Costa, Amanda Andersen, Insung S. Choi, Henrik Birkedal, and João F. Mano. Bioinspired Ultratough Hydrogel with Fast Recovery, Self-Healing, Injectability and Cytocompatibility. *Advanced Materials*, 29(28):1–6, 2017.

[90] S.C. Scott C Grindy, Robert Learsch, Davoud Mozhdehi, Jing Cheng, D.G. Devin G Barrett, Zhibin Guan, P.B. Phillip B Messersmith, and Niels Holten-Andersen. Control of Hierarchical Polymer Mechanics with Bioinspired Metal-Coordination Dynamics. *Nature Materials*, 14(12):1210–1216, 2015.

[91] Kazutoshi Haraguchi and Huan-Jun Li. Mechanical Properties and Structure of Polymer−Clay Nanocomposite Gels with High Clay Content. *Macromolecules*, 39(5):1898–1905, March 2006.

[92] Lu Han, Xiong Lu, Kezhi Liu, Kefeng Wang, Liming Fang, Lu-Tao Weng, Hongping Zhang, Youhong Tang, Fuzeng Ren, Cancan Zhao, Guoxing Sun, Rui Liang,

and Zongjin Li. Mussel-Inspired Adhesive and Tough Hydrogel Based on Nanoclay Confined Dopamine Polymerization. *ACS nano*, 11(3):2561–2574, March 2017.

[93] Tao Yuan, Xinming Cui, Xiaokong Liu, Xinxin Qu, and Junqi Sun. Highly Tough, Stretchable, Self-Healing, and Recyclable Hydrogels Reinforced by in Situ-Formed Polyelectrolyte Complex Nanoparticles. *Macromolecules*, 52(8):3141–3149, April 2019. Publisher: American Chemical Society.

[94] Praveen Thoniyot, Mein Jin Tan, Anis Abdul Karim, David James Young, and Xian Jun Loh. Nanoparticle-Hydrogel Composites: Concept, Design, and Applications of These Promising, Multi-Functional Materials. *Advanced Science*, 2(1-2):1400010, February 2015.

[95] Naresh Kasoju, Nicholas Hawkins, Ognen Pop-Georgievski, Dana Kubies, and Fritz Vollrath. Silk Fibroin Gelation via Non-Solvent Induced Phase Separation. *Biomaterials Science*, 4(3):460–473, February 2016. Publisher: The Royal Society of Chemistry.

[96] Wenwei Lei, Shuanhu Qi, Qinfeng Rong, Jin Huang, Yichao Xu, Ruochen Fang, Kesong Liu, Lei Jiang, and Mingjie Liu. Diffusion–Freezing-Induced Microphase Separation for Constructing Large-Area Multiscale Structures on Hydrogel Surfaces. *Advanced Materials*, 31(32):1808217, 2019.

[97] Sanghak Cha, Hyun Gyu Lim, Martin F. Haase, Kathleen J. Stebe, Gyoo Yeol Jung, and Daeyeon Lee. Bicontinuous Interfacially Jammed Emulsion Gels (bijels) as Media for Enabling Enzymatic Reactive Separation of a Highly Water Insoluble Substrate. *Scientific Reports*, 9(1):6363, April 2019. Number: 1 Publisher: Nature Publishing Group.

[98] Jing Lyu, Mark D. Hammig, Lehao Liu, Lizhi Xu, Hang Chi, Ctirad Uher, Tiehu Li, and Nicholas A. Kotov. Stretchable Conductors by Kirigami Patterning of Aramid-Silver Nanocomposites with Zero Conductance Gradient. *Applied Physics Letters*, 111(16):161901, October 2017. Publisher: American Institute of Physics.

[99] Jeremy M. Lowen and J. Kent Leach. Functionally Graded Biomaterials for Use as Model Systems and Replacement Tissues. *Advanced Functional Materials*, 30(44):1909089, 2020.

[100] Stephen C. Cowin, editor. *Bone Mechanics Handbook*. CRC Press, Boca Raton, 2 edition, March 2013.

[101] Nancy S. Landínez-Parra, Diego A. Garzón-Alvarado, and Juan Carlos Vanegas-Acosta. Mechanical Behavior of Articular Cartilage. *Injury and Skeletal Biomechanics*, August 2012.

[102] Lauriane Alison, Stefano Menasce, Florian Bouville, Elena Tervoort, Iacopo Mattich, Alessandro Ofner, and André R. Studart. 3D Printing of Sacrificial Templates into Hierarchical Porous Materials. *Scientific Reports*, 9(1):409, January 2019.

[103] Levent Aydin, Serdar Kucuk, and Halime Kenar. A universal self-eroding sacrificial bioink that enables bioprinting at room temperature. *Polymers for Advanced Technologies*, March 2020.

[104] Ashley M. Compaan, Kyle Christensen, and Yong Huang. Inkjet Bioprinting of 3D Silk Fibroin Cellular Constructs Using Sacrificial Alginate. *ACS Biomaterials Science & Engineering*, 3(8):1519–1526, August 2017.

[105] Emily Asenath[U+2010]Smith, Hanying Li, Ellen C. Keene, Zhi Wei Seh, and Lara A. Estroff. Crystal Growth of Calcium Carbonate in Hydrogels as a Model of Biomineralization. *Advanced Functional Materials*, 22(14):2891–2914, 2012.

[106] Kazuki Fukao, Kazuki Tanaka, Ryuji Kiyama, Takayuki Nonoyama, and Jian Ping Gong. Hydrogels toughened by biominerals providing energy-dissipative sacrificial bonds. *Journal of Materials Chemistry B*, May 2020. Publisher: The Royal Society of Chemistry.

[107] Marko Milovanovic, Marvin T. Unruh, Volker Brandt, and Joerg C. Tiller. Forming Amorphous Calcium Carbonate within Hydrogels by Enzyme-induced Mineralization in the Presence of N-(phosphonomethyl)glycine. *Journal of Colloid and Interface Science*, June 2020.

[108] Sadiya Anjum, Pramod M Gurave, and Bhuvanesh Gupta. Calcium ion-induced self-healing pattern of chemically crosslinked poly(acrylic acid) hydrogels. *Polymer International*, 67(3):250–257, 2018. _eprint: https://onlinelibrary.wiley.com/doi/pdf/10.1002/pi.5517.

[109] Céline Samira Wyss, Peyman Karami, Pierre-Etienne Bourban, and Dominique P. Pioletti. Cyclic loading of a cellulose/hydrogel composite increases its fracture strength. *Extreme Mechanics Letters*, 24:66–74, October 2018.

[110] Peyman Karami, Céline Samira Wyss, Azadeh Khoushabi, Andreas Schmocker, Martin Broome, Christophe Moser, Pierre-Etienne Bourban, and Dominique P. Pioletti.

Composite Double-Network Hydrogels To Improve Adhesion on Biological Surfaces. *ACS Applied Materials & Interfaces*, 10(45):38692–38699, November 2018.

[111] Arti Vashist, Ajeet Kaushik, Anujit Ghosal, Jyoti Bala, Roozbeh Nikkhah-Moshaie, Waseem A. Wani, Pandiaraj Manickam, and Madhavan Nair. Nanocomposite Hydrogels: Advances in Nanofillers Used for Nanomedicine. *Gels*, 4(3):75, September 2018.

[112] Emily C. Davidson, Arda Kotikian, Shucong Li, Joanna Aizenberg, and Jennifer A. Lewis. 3D Printable and Reconfigurable Liquid Crystal Elastomers with Light-Induced Shape Memory via Dynamic Bond Exchange. *Advanced Materials*, 32(1):1905682, 2020.

[113] Shaoting Lin, Changyong Cao, Qiming Wang, Mark Gonzalez, John E. Dolbow, and Xuanhe Zhao. Design of Stiff, Tough and Stretchy Hydrogel Composites via Nanoscale Hybrid Crosslinking and Macroscale Fiber Reinforcement. *Soft Matter*, 10(38):7519–7527, September 2014.

[114] Koki Sano, Yasuhiro Ishida, and Takuzo Aida. Synthesis of Anisotropic Hydrogels and Their Applications. *Angewandte Chemie International Edition*, 57(10):2532–2543, 2018. _eprint: https://onlinelibrary.wiley.com/doi/pdf/10.1002/anie.201708196.

[115] Young Jung No, Solaiman Tarafder, Barbara Reischl, Yogambha Ramaswamy, Colin Dunstan, Oliver Friedrich, Chang Hun Lee, and Hala Zreiqat. High-Strength Fiber-Reinforced Composite Hydrogel Scaffolds as Biosynthetic Tendon Graft Material. *ACS Biomaterials Science & Engineering*, 6(4):1887–1898, April 2020. Publisher: American Chemical Society.

[116] Céline Samira Wyss, Peyman Karami, Adrien Demongeot, Pierre-Etienne Bourban, and Dominique P. Pioletti. Silk Granular Hydrogels Self-Reinforced with Regenerated Silk Fibroin Fibers. *Soft Matter*, 17(29):7038–7046, July 2021. Publisher: The Royal Society of Chemistry.

[117] K. Subramani. Chapter 11 - Fabrication of Hydrogel Micropatterns by Soft Photolithography. In Waqar Ahmed and Mark J. Jackson, editors, *Emerging Nanotechnologies for Manufacturing*, Micro and Nano Technologies, pages 261–276. William Andrew Publishing, Boston, January 2010.

[118] April M. Kloxin, Julie A. Benton, and Kristi S. Anseth. In Situ Elasticity Modulation with Dynamic Substrates to Direct Cell Phenotype. *Biomaterials*, 31(1):1–8, 2010.

[119] Roger Y. Tam, Laura J. Smith, and Molly S. Shoichet. Engineering Cellular Microenvironments with Photo- and Enzymatically Responsive Hydrogels: Toward Biomimetic 3D Cell Culture Models. *Accounts of Chemical Research*, 50(4):703–713, April 2017. Publisher: American Chemical Society.

[120] Martin P. de Beer, Harry L. van der Laan, Megan A. Cole, Riley J. Whelan, Mark A. Burns, and Timothy F. Scott. Rapid, continuous additive manufacturing by volumetric polymerization inhibition patterning. *Science Advances*, 5(1):eaau8723, January 2019. Publisher: American Association for the Advancement of Science Section: Research Article.

[121] Brett E. Kelly, Indrasen Bhattacharya, Hossein Heidari, Maxim Shusteff, Christopher M. Spadaccini, and Hayden K. Taylor. Volumetric additive manufacturing via tomographic reconstruction. *Science*, 363(6431):1075–1079, March 2019. Publisher: American Association for the Advancement of Science Section: Report.

[122] Jiajia Xue, Jingwei Xie, Wenying Liu, and Younan Xia. Electrospun Nanofibers: New Concepts, Materials, and Applications. *Accounts of Chemical Research*, 50(8):1976–1987, August 2017. Publisher: American Chemical Society.

[123] Xiang Wang, Zhaomiao Liu, and Yan Pang. Concentration gradient generation methods based on microfluidic systems. *RSC Advances*, 7(48):29966–29984, June 2017. Publisher: The Royal Society of Chemistry.

[124] Jason A Burdick, Ali Khademhosseini, and Robert Langer. Fabrication of Gradient Hydrogels Using a Microfluidics/Photopolymerization Process. *Langmuir*, 20(13):5153–5156, 2004.

[125] Michael Kessler, Hervé Elettro, Isabelle Heimgartner, Soujanya Madasu, Kenneth A. Brakke, François Gallaire, and Esther Amstad. Everything in Its Right Place: Controlling the Local Composition of Hydrogels Using Microfluidic Traps. *Lab on a Chip*, 2020. Publisher: Royal Society of Chemistry.

[126] Mihyun Lee, Riccardo Rizzo, František Surman, and Marcy Zenobi-Wong. Guiding Lights: Tissue Bioprinting Using Photoactivated Materials. *Chemical Reviews*, 120(19):10950–11027, October 2020. Publisher: American Chemical Society.

[127] Andrea Schwab, Riccardo Levato, Matteo D'Este, Susanna Piluso, David Eglin, and Jos Malda. Printability and Shape Fidelity of Bioinks in 3D Bioprinting. *Chemical Reviews*, 120(19):11028–11055, October 2020. Publisher: American Chemical Society.

[128] Yu Shrike Zhang, Ghazaleh Haghiashtiani, Tania Hübscher, Daniel J. Kelly, Jia Min Lee, Matthias Lutolf, Michael C. McAlpine, Wai Yee Yeong, Marcy Zenobi-Wong, and Jos Malda. 3D extrusion bioprinting. *Nature Reviews Methods Primers*, 1(1):1–20, November 2021. Number: 1 Publisher: Nature Publishing Group.

[129] Thomas Mezger. *The Rheology Handbook: For users of rotational and oscillatory rheometers*. European Coatings, August 2020. Google-Books-ID: Xxv5DwAAQBAJ.

[130] Lindsay Riley, Lucas Schirmer, and Tatiana Segura. Granular Hydrogels: Emergent Properties of Jammed Hydrogel Microparticles and Their Applications in Tissue Repair and Regeneration. *Current Opinion in Biotechnology*, 60:1–8, December 2019.

[131] Andrew C. Daly, Lindsay Riley, Tatiana Segura, and Jason A. Burdick. Hydrogel Microparticles for Biomedical Applications. *Nature Reviews Materials*, 5(1):20–43, January 2020. Publisher: Nature Publishing Group.

[132] Christopher B. Highley, Kwang Hoon Song, Andrew C. Daly, and Jason A. Burdick. Jammed Microgel Inks for 3D Printing Applications. *Advanced Science*, 6(1):1801076, January 2019.

[133] Thomas Heida, Jens W. Neubauer, Maximilian Seuss, Nicolas Hauck, Julian Thiele, and Andreas Fery. Mechanically Defined Microgels by Droplet Microfluidics. *Macromolecular Chemistry and Physics*, 218(2):1600418, 2017. _eprint: https://onlinelibrary.wiley.com/doi/pdf/10.1002/macp.201600418.

[134] Luis P. B. Guerzoni, Jonas C. Rose, David B. Gehlen, Alexander Jans, Tamàs Haraszti, Matthias Wessling, Alexander J. C. Kuehne, and Laura De Laporte. Cell Encapsulation in Soft, Anisometric Poly(Ethylene) Glycol Microgels Using a Novel Radical-Free Microfluidic System. *Small*, 15(20):1900692, May 2019.

[135] Shaohua Ma. Microfluidics tubing as a synthesizer for ordered microgel networks. *Soft Matter*, 15(19):3848–3853, 2019.

[136] Joseph Michael de Rutte, Jaekyung Koh, and Dino Di Carlo. Scalable High-Throughput Production of Modular Microgels for In Situ Assembly of Microporous Tissue Scaffolds. *Advanced Functional Materials*, 29(25):1900071, 2019.

[137] Elad Stolovicki, Roy Ziblat, and David A Weitz. Lab on a Chip Throughput Enhancement of Parallel Step Emulsifier Devices by Shear-Free and Efficient Nozzle Clearance †. 18:132–132, 2018.

[138] E. Amstad, M. Chemama, M. Eggersdorfer, L. R. Arriaga, M. P. Brenner, and D. A. Weitz. Robust Scalable High Throughput Production of Monodisperse Drops. *Lab on a Chip*, 16(21):4163–4172, 2016.

[139] Esther Amstad, Xiaoming Chen, Max Eggersdorfer, Noa Cohen, Thomas E Kodger, Carolyn L Ren, and David A Weitz. Parallelization of Microfluidic Flow-Focusing Devices. *Physical Review Letters E*, 95(043105):1–6, 2017.

[140] Huachuan Du, Alice Cont, Mathias Steinacher, and Esther Amstad. Fabrication of Hexagonal-Prismatic Granular Hydrogel Sheets. *Langmuir*, 34:3459–3466, 2018.

[141] Taimoor H. Qazi, Jingyu Wu, Victoria G. Muir, Shoshana Weintraub, Sarah E. Gullbrand, Daeyeon Lee, David Issadore, and Jason A. Burdick. Anisotropic Rod-Shaped Particles Influence Injectable Granular Hydrogel Properties and Cell Invasion. *Advanced Materials*, 34(12):2109194, 2022. _eprint: https://onlinelibrary.wiley.com/doi/pdf/10.1002/adma.202109194.

[142] Syeda M. Naqvi, Srujana Vedicherla, Jennifer Gansau, Tom McIntyre, Michelle Doherty, and Conor T. Buckley. Living Cell Factories - Electrosprayed Microcapsules and Microcarriers for Minimally Invasive Delivery. *Advanced Materials*, 28(27):5662–5671, 2016.

[143] Jennifer Gansau, Lara Kelly, and Conor Timothy Buckley. Influence of key processing parameters and seeding density effects of microencapsulated chondrocytes fabricated using electrohydrodynamic spraying. *Biofabrication*, 10(3):035011, June 2018. Publisher: IOP Publishing.

[144] Mathias Steinacher and Esther Amstad. Spray-Assisted Formation of Micrometer-Sized Emulsions. *ACS Applied Materials & Interfaces*, 14(11):13952–13961, March 2022. Publisher: American Chemical Society.

[145] Andrew Sinclair, Mary Beth O'Kelly, Tao Bai, Hsiang-Chieh Hung, Priyesh Jain, and Shaoyi Jiang. Self-Healing Zwitterionic Microgels as a Versatile Platform for Malleable Cell Constructs and Injectable Therapies. *Advanced Materials*, 30(39):1803087, 2018. _eprint: https://onlinelibrary.wiley.com/doi/pdf/10.1002/adma.201803087.

[146] Victoria G. Muir, Taimoor H. Qazi, Junwen Shan, Jürgen Groll, and Jason A. Burdick. Influence of Microgel Fabrication Technique on Granular Hydrogel Properties. *ACS Biomaterials Science & Engineering*, 7(9):4269–4281, September 2021. Publisher: American Chemical Society.

[147] Benjamin Kessel, Mihyun Lee, Angela Bonato, Yann Tinguely, Enrico Tosoratti, and Marcy Zenobi-Wong. 3D Bioprinting of Macroporous Materials Based on Entangled Hydrogel Microstrands. *Advanced Science*, 7(18):2001419, 2020.

[148] Hyunwoo Yuk, Jingjing Wu, Tiffany L. Sarrafian, Xinyu Mao, Claudia E. Varela, Ellen T. Roche, Leigh G. Griffiths, Christoph S. Nabzdyk, and Xuanhe Zhao. Rapid and coagulation-independent haemostatic sealing by a paste inspired by barnacle glue. *Nature Biomedical Engineering*, pages 1–12, August 2021. Bandiera_abtest: a Cg_type: Nature Research Journals Primary_atype: Research Publisher: Nature Publishing Group Subject_term: Bioinspired materials;Biomedical engineering;Mechanical engineering Subject_term_id: bioinspired-materials;biomedical-engineering;mechanical-engineering.

[149] Matteo Hirsch, Alvaro Charlet, and Esther Amstad. 3D Printing of Strong and Tough Double Network Granular Hydrogels. *Advanced Functional Materials*, 31(5):2005929, January 2021.

[150] M. van Hecke. Jamming of soft particles: geometry, mechanics, scaling and isostaticity. *Journal of Physics: Condensed Matter*, 22(3):033101, December 2009. Publisher: IOP Publishing.

[151] Trystan Domenech and Patrick S. Doyle. High Loading Capacity Nanoencapsulation and Release of Hydrophobic Drug Nanocrystals from Microgel Particles. *Chemistry of Materials*, 32(1):498–509, January 2020. Publisher: American Chemical Society.

[152] Jun Fang, Jaekyung Koh, Qizhi Fang, Huiliang Qiu, Maani M. Archang, Mohammad Mahdi Hasani-Sadrabadi, Hiromi Miwa, Xintong Zhong, Richard Sievers, Dong-Wei Gao, Randall Lee, Dino Di Carlo, and Song Li. Injectable Drug-Releasing Microporous Annealed Particle Scaffolds for Treating Myocardial Infarction. *Advanced Functional Materials*, 30(43):2004307, 2020.

[153] Vivian Rachel Feig, Sruthi Santhanam, Kelly Wu McConnell, Kathy Liu, Matine Azadian, Lucia Giulia Brunel, Zhuojun Huang, Helen Tran, Paul M. George, and Zhenan Bao. Conducting Polymer-Based Granular Hydrogels for Injectable 3D Cell Scaffolds. *Advanced Materials Technologies*, 6(6):2100162, 2021.

[154] Joshua E. Mealy, Jennifer J. Chung, Heon-Ho Jeong, David Issadore, Daeyeon Lee, Pavan Atluri, and Jason A. Burdick. Injectable Granular Hydrogels with Multifunctional Properties for Biomedical Applications. *Advanced Materials*, 30(20):1705912, 2018.

[155] Jian Hu, Kenta Hiwatashi, Takayuki Kurokawa, Song Miao Liang, Zi Liang Wu, and Jian Ping Gong. Microgel-Reinforced Hydrogel Films with High Mechanical Strength and Their Visible Mesoscale Fracture Structure. *Macromolecules*, 44(19):7775–7781, October 2011.

[156] Alexander S. Caldwell, Gavin T. Campbell, Kelly M. T. Shekiro, and Kristi S. Anseth. Clickable Microgel Scaffolds as Platforms for 3D Cell Encapsulation. *Advanced Healthcare Materials*, 6(15):1700254, 2017.

[157] Oju Jeon, Yu Bin Lee, Thomas J. Hinton, Adam W. Feinberg, and Eben Alsberg. Cryopreserved Cell-Laden Alginate Microgel Bioink for 3D Bioprinting of Living Tissues. *Materials today. Chemistry*, 2019.

[158] Christopher S. O'Bryan, Tapomoy Bhattacharjee, Samantha L. Marshall, W. Gregory Sawyer, and Thomas E. Angelini. Commercially available microgels for 3D bioprinting. *Bioprinting*, 11:e00037, September 2018.

[159] Alexis J. Seymour, Sungchul Shin, and Sarah C. Heilshorn. 3D Printing of Microgel Scaffolds with Tunable Void Fraction to Promote Cell Infiltration. *Advanced Healthcare Materials*, 10(18):2100644, 2021. _eprint: https://onlinelibrary.wiley.com/doi/pdf/10.1002/adhm.202100644.

[160] Christopher S. O'Bryan, Christopher P. Kabb, Brent S. Sumerlin, and Thomas E. Angelini. Jammed Polyelectrolyte Microgels for 3D Cell Culture Applications: Rheological Behavior with Added Salts. *ACS Applied Bio Materials*, 2(4):1509–1517, April 2019. Publisher: American Chemical Society.

[161] Tapomoy Bhattacharjee, Steven M. Zehnder, Kyle G. Rowe, Suhani Jain, Ryan M. Nixon, W. Gregory Sawyer, and Thomas E. Angelini. Writing in the Granular Gel Medium. *Science Advances*, 1(8):e1500655, September 2015. Publisher: American Association for the Advancement of Science Section: Research Article.

[162] Kyle J. LeBlanc, Sean R. Niemi, Alexander I. Bennett, Kathryn L. Harris, Kyle D. Schulze, W. Gregory Sawyer, Curtis Taylor, and Thomas E. Angelini. Stability of High Speed 3D Printing in Liquid-Like Solids. *ACS Biomaterials Science & Engineering*, 2(10):1796–1799, October 2016. Publisher: American Chemical Society.

[163] Houman Savoji, Locke Davenport Huyer, Mohammad Hossein Mohammadi, Benjamin Fook Lun Lai, Naimeh Rafatian, Dawn Bannerman, Mohammad Shoaib, Erin R. Bobicki, Arun Ramachandran, and Milica Radisic. 3D Printing of Vascular Tubes Using Bioelastomer Prepolymers by Freeform Reversible Embedding.

ACS Biomaterials Science & Engineering, 6(3):1333–1343, March 2020. Publisher: American Chemical Society.

[164] Ashley M. Compaan, Kaidong Song, Wenxuan Chai, and Yong Huang. Cross-Linkable Microgel Composite Matrix Bath for Embedded Bioprinting of Perfusable Tissue Constructs and Sculpting of Solid Objects. *ACS Applied Materials & Interfaces*, 12(7):7855–7868, February 2020. Publisher: American Chemical Society.

[165] Taimoor H. Qazi and Jason A. Burdick. Granular Hydrogels for Endogenous Tissue Repair. *Biomaterials and Biosystems*, 1:100008, March 2021.

[166] Shangjing Xin, David Chimene, Jay E. Garza, Akhilesh K. Gaharwar, and Daniel L. Alge. Clickable PEG Hydrogel Microspheres as Building Blocks for 3D Bioprinting. *Biomaterials Science*, 7(3):1179–1187, February 2019. Publisher: The Royal Society of Chemistry.

[167] Kaidong Song, Ashley M. Compaan, Wenxuan Chai, and Yong Huang. Injectable Gelatin Microgel-Based Composite Ink for 3D Bioprinting in Air. *ACS Applied Materials & Interfaces*, 12(20):22453–22466, May 2020. Publisher: American Chemical Society.

[168] David Chimene, Roland Kaunas, and Akhilesh K. Gaharwar. Hydrogel Bioink Reinforcement for Additive Manufacturing: A Focused Review of Emerging Strategies. *Advanced Materials*, 32(1):1902026, 2020.

[169] Wei Cheng, Jing Zhang, Ji Liu, and Ziyi Yu. Granular hydrogels for 3D bioprinting applications. *VIEW*, 1(3):20200060, 2020. _eprint: https://onlinelibrary.wiley.com/doi/pdf/10.1002/VIW.20200060.

[170] Joseph Michael de Rutte, Jaekyung Koh, and Dino Di Carlo. Scalable High[U+2010]Throughput Production of Modular Microgels for In Situ Assembly of Microporous Tissue Scaffolds. *Advanced Functional Materials*, page 1900071, March 2019.

[171] Zaman Ataie, Sina Kheirabadi, Jenna Wanjing Zhang, Alexander Kedzierski, Carter Petrosky, Rhea Jiang, Christian Vollberg, and Amir Sheikhi. Nanoengineered Granular Hydrogel Bioinks with Preserved Interconnected Microporosity for Extrusion Bioprinting. *Small*, 18(37):2202390, 2022. _eprint: https://onlinelibrary.wiley.com/doi/pdf/10.1002/smll.202202390.

[172] Alvaro Charlet, Francesca Bono, and Esther Amstad. Mechanical reinforcement of granular hydrogels. *Chemical Science*, 13(11):3082–3093, 2022. Publisher: Royal Society of Chemistry.

[173] Xinyue Liu, Maria Eugenia Inda, Yong Lai, Timothy K. Lu, and Xuanhe Zhao. Engineered Living Hydrogels. *Advanced Materials*, 34(26):2201326, 2022. _eprint: https://onlinelibrary.wiley.com/doi/pdf/10.1002/adma.202201326.

[174] Wil V Srubar Iii. Engineered Living Materials: Taxonomies and Emerging Trends. *Trends in Biotechnology*, page 10.

[175] Peter Q. Nguyen, Noémie-Manuelle Dorval Courchesne, Anna Duraj-Thatte, Pichet Praveschotinunt, and Neel S. Joshi. Engineered Living Materials: Prospects and Challenges for Using Biological Systems to Direct the Assembly of Smart Materials. *Advanced Materials*, 30(19):1704847, 2018. _eprint: https://onlinelibrary.wiley.com/doi/pdf/10.1002/adma.201704847.

[176] Aleixandre Rodrigo-Navarro, Shrikrishnan Sankaran, Matthew J. Dalby, Aránzazu del Campo, and Manuel Salmeron-Sanchez. Engineered living biomaterials. *Nature Reviews Materials*, 6(12):1175–1190, December 2021. Number: 12 Publisher: Nature Publishing Group.

[177] Steven S. Branda, Åshild Vik, Lisa Friedman, and Roberto Kolter. Biofilms: the matrix revisited. *Trends in Microbiology*, 13(1):20–26, January 2005.

[178] Y.-C. Hsieh, H. Yano, M. Nogi, and S. J. Eichhorn. An estimation of the Young's modulus of bacterial cellulose filaments. *Cellulose*, 15(4):507–513, August 2008.

[179] A. Nakayama, A. Kakugo, J. P. Gong, Y. Osada, M. Takai, T. Erata, and S. Kawano. High Mechanical Strength Double-Network Hydrogel with Bacterial Cellulose. *Advanced Functional Materials*, 14(11):1124–1128, 2004.

[180] Ruchira Mitra, Tong Xu, Hua Xiang, and Jing Han. Current developments on polyhydroxyalkanoates synthesis by using halophiles as a promising cell factory. *Microbial Cell Factories*, 19(1):86, April 2020.

[181] Andrew Currin, Neil Swainston, Philip J. Day, and Douglas B. Kell. Synthetic biology for the directed evolution of protein biocatalysts: navigating sequence space intelligently. *Chemical Society Reviews*, 44(5):1172–1239, February 2015. Publisher: The Royal Society of Chemistry.

[182] Tuomas P. J. Knowles and Markus J. Buehler. Nanomechanics of functional and pathological amyloid materials. *Nature Nanotechnology*, 6(8):469–479, August 2011. Number: 8 Publisher: Nature Publishing Group.

[183] Alexandra Clarà Saracho, Lorenzo Lucherini, Matteo Hirsch, Hannes M. Peter, Dimitrios Terzis, Esther Amstad, and Lyesse Laloui. Controlling the calcium carbonate microstructure of engineered living building materials. *Journal of Materials Chemistry A*, 9(43):24438–24451, 2021. Publisher: Royal Society of Chemistry.

[184] Dimitrios Terzis and Lyesse Laloui. 3-D micro-architecture and mechanical response of soil cemented via microbial-induced calcite precipitation. *Scientific Reports*, 8(1):1416, January 2018. Number: 1 Publisher: Nature Publishing Group.

[185] Zhuojun Dai, Xiaoyu Yang, Feilun Wu, Lihua Wang, Kun Xiang, Pengcheng Li, Qingqing Lv, Jinhui Tang, Anders Dohlman, Lei Dai, Xiling Shen, and Lingchong You. Living fabrication of functional semi-interpenetrating polymeric materials. *Nature Communications*, 12(1):3422, June 2021. Number: 1 Publisher: Nature Publishing Group.

[186] Alice Cont, Tamara Rossy, Zainebe Al-Mayyah, and Alexandre Persat. Biofilms deform soft surfaces and disrupt epithelia. *eLife*, 9:e56533, October 2020. Publisher: eLife Sciences Publications, Ltd.

[187] Chenyi Fei, Sheng Mao, Jing Yan, Ricard Alert, Howard A. Stone, Bonnie L. Bassler, Ned S. Wingreen, and Andrej Košmrlj. Nonuniform growth and surface friction determine bacterial biofilm morphology on soft substrates. *Proceedings of the National Academy of Sciences*, 117(14):7622–7632, April 2020. Publisher: Proceedings of the National Academy of Sciences.

[188] Sangrila Sadhu, Pradipta Saha, Sukanta K. Sen, Shanmugam Mayilraj, and Tushar Kanti Maiti. Production, purification and characterization of a novel thermotolerant endoglucanase (CMCase) from Bacillus strain isolated from cow dung. *SpringerPlus*, 2(1):10, January 2013.

[189] Shosuke Yoshida, Kazumi Hiraga, Toshihiko Takehana, Ikuo Taniguchi, Hironao Yamaji, Yasuhito Maeda, Kiyotsuna Toyohara, Kenji Miyamoto, Yoshiharu Kimura, and Kohei Oda. A bacterium that degrades and assimilates poly(ethylene terephthalate). *Science*, 351(6278):1196–1199, March 2016. Publisher: American Association for the Advancement of Science.

[190] Tzu-Chieh Tang, Bolin An, Yuanyuan Huang, Sangita Vasikaran, Yanyi Wang, Xi-aoyu Jiang, Timothy K. Lu, and Chao Zhong. Materials design by synthetic biology. *Nature Reviews Materials*, 6(4):332–350, April 2021. Number: 4 Publisher: Nature Publishing Group.

[191] Allen P. Liu, Eric A. Appel, Paul D. Ashby, Brendon M. Baker, Elisa Franco, Luo Gu, Karmella Haynes, Neel S. Joshi, April M. Kloxin, Paul H. J. Kouwer, Jeetain Mittal, Leonardo Morsut, Vincent Noireaux, Sapun Parekh, Rebecca Schulman, Sindy K. Y. Tang, Megan T. Valentine, Sebastián L. Vega, Wilfried Weber, Nicholas Stephanopoulos, and Ovijit Chaudhuri. The living interface between synthetic biology and biomaterial design. *Nature Materials*, 21(4):390–397, April 2022. Number: 4 Publisher: Nature Publishing Group.

[192] Matthew L. Bedell, Adam M. Navara, Yingying Du, Shengmin Zhang, and Antonios G. Mikos. Polymeric Systems for Bioprinting. *Chemical Reviews*, 120(19):10744–10792, October 2020. Publisher: American Chemical Society.

[193] Benjamin A. E. Lehner, Dominik T. Schmieden, and Anne S. Meyer. A Straightfor-ward Approach for 3D Bacterial Printing. *ACS Synthetic Biology*, 6(7):1124–1130, July 2017. Publisher: American Chemical Society.

[194] Manuel Schaffner, Patrick A. Rühs, Fergal Coulter, Samuel Kilcher, and André R. Studart. 3D Printing of Bacteria into Functional Complex Materials. *Science Advances*, 3(12):eaao6804, December 2017. Publisher: American Association for the Advancement of Science Section: Research Article.

[195] Xinyue Liu, Hyunwoo Yuk, Shaoting Lin, German Alberto Parada, Tzu-Chieh Tang, Eléonore Tham, Cesar de la Fuente-Nunez, Timothy K. Lu, and Xuanhe Zhao. 3D Printing of Living Responsive Materi-als and Devices. *Advanced Materials*, 30(4):1704821, 2018. _eprint: https://onlinelibrary.wiley.com/doi/pdf/10.1002/adma.201704821.

[196] Anna M. Duraj-Thatte, Avinash Manjula-Basavanna, Jarod Rutledge, Jing Xia, Shabir Hassan, Arjirios Sourlis, Andrés G. Rubio, Ami Lesha, Michael Zenkl, Anton Kan, David A. Weitz, Yu Shrike Zhang, and Neel S. Joshi. Programmable microbial ink for 3D printing of living materials produced from genetically engineered protein nanofibers. *Nature Communications*, 12(1):6600, November 2021. Number: 1 Pub-lisher: Nature Publishing Group.

[197] Srikkanth Balasubramanian, Marie-Eve Aubin-Tam, and Anne S. Meyer. 3D Printing for the Fabrication of Biofilm-Based Functional Living Materials. *ACS Synthetic Biology*, 8(7):1564–1567, July 2019. Publisher: American Chemical Society.

[198] Jiaofang Huang, Suying Liu, Chen Zhang, Xinyu Wang, Jiahua Pu, Fang Ba, Shuai Xue, Haifeng Ye, Tianxin Zhao, Ke Li, Yanyi Wang, Jicong Zhang, Lihua Wang, Chunhai Fan, Timothy K. Lu, and Chao Zhong. Programmable and printable Bacillus subtilis biofilms as engineered living materials. *Nature Chemical Biology*, 15(1):34–41, January 2019. Number: 1 Publisher: Nature Publishing Group.

[199] Scott C Grindy, Martin Lenz, and Niels Holten-Andersen. Engineering Elasticity and Relaxation Time in Metal-Coordinate Cross-Linked Hydrogels. *Macromolecules*, 49:8306–8312, 2016.

[200] Eric A. Appel, Jesús del Barrio, Xian Jun Loh, and Oren A. Scherman. Supramolecular Polymeric Hydrogels. *Chemical Society Reviews*, 41(18):6195–6214, August 2012.

[201] Qiaochu Li, Devin G Barrett, Phillip B Messersmith, and Niels Holten-Andersen. Controlling Hydrogel Mechanics via Bio-Inspired Polymer–Nanoparticle Bond Dynamics. *ACS Nano*, 10(1):1317–1324, 2016.

[202] Lu Han, Xiong Lu, Menghao Wang, Donglin Gan, Weili Deng, Kefeng Wang, Liming Fang, Kezhi Liu, Chun Wai Chan, Youhong Tang, Lu-Tao Weng, and Huipin Yuan. A Mussel-Inspired Conductive, Self-Adhesive, and Self-Healable Tough Hydrogel as Cell Stimulators and Implantable Bioelectronics. *Small*, 13(2):1601916, 2017.

[203] Zhen Tao, Hailong Fan, Junchao Huang, Taolin Sun, Takayuki Kurokawa, and Jian Ping Gong. Fabrication of Tough Hydrogel Composites from Photoresponsive Polymers to Show Double-Network Effect. *ACS Applied Materials & Interfaces*, 11(40):37139–37146, October 2019. Publisher: American Chemical Society.

[204] Takayuki Nonoyama, Susumu Wada, Ryuji Kiyama, Nobuto Kitamura, Md Tariful Islam Mredha, Xi Zhang, Takayuki Kurokawa, Tasuku Nakajima, Yasuaki Takagi, Kazunori Yasuda, and Jian Ping Gong. Double-Network Hydrogels Strongly Bondable to Bones by Spontaneous Osteogenesis Penetration. *Advanced Materials*, 28(31):6740–6745, 2016.

[205] Jian Ping Gong. Materials Both Tough and Soft. *Science*, 344(6180):161–162, April 2014. Publisher: American Association for the Advancement of Science Section: Perspective.

[206] Zhengzhi Wang. Spatial and Temporal Tunability of Magnetically-Actuated Gradient Nanocomposites. *Soft Matter*, 15(15):3133–3148, April 2019. Publisher: The Royal Society of Chemistry.

[207] William M. Gramlich, Iris L. Kim, and Jason A. Burdick. Synthesis and Orthogonal Photopatterning of Hyaluronic Acid Hydrogels with Thiol-Norbornene Chemistry. *Biomaterials*, 34(38):9803–9811, December 2013.

[208] Hyemin Lee, Jun-Hyun Kim, Gaoxiang Wu, Hae-Min Lee, Jaekyoung Kim, Dokyeong Kwon, Shu Yang, Chang-Koo Kim, and Hyunsik Yoon. Clustering and Self-Recovery of Slanted Hydrogel Micropillars. *Advanced Materials Interfaces*, 5(24):1801142, 2018.

[209] Tobias Priemel, Elena Degtyar, Mason N. Dean, and Matthew J. Harrington. Rapid self-assembly of complex biomolecular architectures during mussel byssus biofabrication. *Nature Communications*, 8(1), April 2017.

[210] Florence G. Downs, David J. Lunn, Michael J. Booth, Joshua B. Sauer, William J. Ramsay, R. George Klemperer, Craig J. Hawker, and Hagan Bayley. Multi-responsive hydrogel structures from patterned droplet networks. *Nature Chemistry*, 12(4):363–371, April 2020. Number: 4 Publisher: Nature Publishing Group.

[211] Amir Sheikhi, Joseph de Rutte, Reihaneh Haghniaz, Outman Akouissi, Alireza Sohrabi, Dino Di Carlo, and Ali Khademhosseini. Microfluidic-enabled bottom-up hydrogels from annealable naturally-derived protein microbeads. *Biomaterials*, 192:560–568, February 2019.

[212] Mikyung Shin, Kwang Hoon Song, Justin C. Burrell, D. Kacy Cullen, and Jason A. Burdick. Injectable and Conductive Granular Hydrogels for 3D Printing and Electroactive Tissue Support. *Advanced Science*, 6(20):1901229, 2019.

[213] Amir Sheikhi, Joseph de Rutte, Reihaneh Haghniaz, Outman Akouissi, Alireza Sohrabi, Dino Di Carlo, and Ali Khademhosseini. Modular Microporous Hydrogels Formed from Microgel Beads with Orthogonal Thermo-Chemical Responsivity: Microfluidic Fabrication and Characterization. *MethodsX*, 6:1747–1752, January 2019.

[214] Junji Saito, Hidemitsu Furukawa, Takayuki Kurokawa, Rikimaru Kuwabara, Shinya Kuroda, Jian Hu, Yoshimi Tanaka, Jian Ping Gong, Nobuto Kitamura, and

Kazunori Yasuda. Robust bonding and one-step facile synthesis of tough hydrogels with desirable shape by virtue of the double network structure. *Polym. Chem.*, 2(3):575–580, 2011.

[215] Riku Takahashi, Kouichi Shimano, Haruka Okazaki, Takayuki Kurokawa, Tasuku Nakajima, Takayuki Nonoyama, Daniel R. King, and Jian Ping Gong. Tough Particle-Based Double Network Hydrogels for Functional Solid Surface Coatings. *Advanced Materials Interfaces*, 5(23):1801018, 2018.

[216] David Chimene, Charles W. Peak, James L. Gentry, James K. Carrow, Lauren M. Cross, Eli Mondragon, Guinea B. Cardoso, Roland Kaunas, and Akhilesh K. Gaharwar. Nanoengineered Ionic–Covalent Entanglement (NICE) Bioinks for 3D Bioprinting. *ACS Applied Materials & Interfaces*, 10(12):9957–9968, March 2018. Publisher: American Chemical Society.

[217] David Chimene, Logan Miller, Lauren M. Cross, Manish K. Jaiswal, Irtisha Singh, and Akhilesh K. Gaharwar. Nanoengineered Osteoinductive Bioink for 3D Bioprinting Bone Tissue. *ACS Applied Materials & Interfaces*, 12(14):15976–15988, April 2020. Publisher: American Chemical Society.

[218] Paul Menut, Sebastian Seiffert, Joris Sprakel, and David A. Weitz. Does Size Matter? Elasticity of Compressed Suspensions of Colloidal- and Granular-Scale Microgels. *Soft Matter*, 8(1):156–164, December 2011. Publisher: The Royal Society of Chemistry.

[219] Jian Hu, Takayuki Kurokawa, Kenta Hiwatashi, Tasuku Nakajima, Zi Liang Wu, Song Miao Liang, and Jian Ping Gong. Structure Optimization and Mechanical Model for Microgel-Reinforced Hydrogels with High Strength and Toughness. *Macromolecules*, 45(12):5218–5228, June 2012. Publisher: American Chemical Society.

[220] Carlos F. Guimarães, Luca Gasperini, Alexandra P. Marques, and Rui L. Reis. The Stiffness of Living Tissues and Its Implications for Tissue Engineering. *Nature Reviews Materials*, 5(5):351–370, May 2020. Publisher: Nature Publishing Group.

[221] Etienne Ducrot, Yulan Chen, Markus Bulters, Rint P. Sijbesma, and Costantino Creton. Toughening Elastomers with Sacrificial Bonds and Watching Them Break. *Science*, 344(6180):186–189, April 2014. Publisher: American Association for the Advancement of Science Section: Report.

[222] Shouling Ding, Bin Zou, Peng Wang, and Hongjian Ding. Effects of Nozzle Temperature and Building Orientation on Mechanical Properties and Microstructure of PEEK and PEI Printed by 3D-FDM. *Polymer Testing*, 78:105948, September 2019.

[223] Mei Liu, Xin Zeng, Chao Ma, Huan Yi, Zeeshan Ali, Xianbo Mou, Song Li, Yan Deng, and Nongyue He. Injectable Hydrogels for Cartilage and Bone Tissue Engineering. *Bone Research*, 5(1):1–20, May 2017. Publisher: Nature Publishing Group.

[224] Guo-Liang Ying, Nan Jiang, Sushila Maharjan, Yi-Xia Yin, Rong-Rong Chai, Xia Cao, Jing-Zhou Yang, Amir K. Miri, Shabir Hassan, and Yu Shrike Zhang. Aqueous Two-Phase Emulsion Bioink-Enabled 3D Bioprinting of Porous Hydrogels. *Advanced Materials*, 30(50):1805460, 2018.

[225] Zhe Chen, Donghao Zhao, Binhong Liu, Guodong Nian, Xiaokeng Li, Jun Yin, Shaoxing Qu, and Wei Yang. 3D Printing of Multifunctional Hydrogels. *Advanced Functional Materials*, 29(20):1900971, 2019.

[226] Wangqu Liu, Ozan Erol, and David H. Gracias. 3D Printing of an In Situ Grown MOF Hydrogel with Tunable Mechanical Properties. *ACS Applied Materials & Interfaces*, 12(29):33267–33275, July 2020. Publisher: American Chemical Society.

[227] Yin Cheng, Kwok Hoe Chan, Xiao-Qiao Wang, Tianpeng Ding, Tongtao Li, Xin Lu, and Ghim Wei Ho. Direct-Ink-Write 3D Printing of Hydrogels into Biomimetic Soft Robots. *ACS Nano*, 13(11):13176–13184, November 2019. Publisher: American Chemical Society.

[228] Feichen Yang, Vaibhav Tadepalli, and Benjamin J. Wiley. 3D Printing of a Double Network Hydrogel with a Compression Strength and Elastic Modulus Greater than Those of Cartilage. *ACS Biomaterials Science & Engineering*, 3(5):863–869, May 2017. Publisher: American Chemical Society.

[229] L. A. Hockaday, K. H. Kang, N. W. Colangelo, P. Y. C. Cheung, B. Duan, E. Malone, J. Wu, L. N. Girardi, L. J. Bonassar, H. Lipson, C. C. Chu, and J. T. Butcher. Rapid 3D Printing of Anatomically Accurate and Mechanically Heterogeneous Aortic Valve Hydrogel Scaffolds. *Biofabrication*, 4(3):035005, August 2012. Publisher: IOP Publishing.

[230] Junhua Wei, Jilong Wang, Siheng Su, Shiren Wang, Jingjing Qiu, Zhenhuan Zhang, Gordon Christopher, Fuda Ning, and Weilong Cong. 3D Printing of an Extremely Tough Hydrogel. *RSC Advances*, 5(99):81324–81329, September 2015. Publisher: The Royal Society of Chemistry.

[231] Sungmin Hong, Dalton Sycks, Hon Fai Chan, Shaoting Lin, Gabriel P. Lopez, Farshid Guilak, Kam W. Leong, and Xuanhe Zhao. 3D Printing of Highly Stretchable and Tough Hydrogels into Complex, Cellularized Structures. *Advanced Materials*, 27(27):4035–4040, July 2015.

[232] Elia A. Guzzi, Giovanni Bovone, and Mark W. Tibbitt. Universal Nanocarrier Ink Platform for Biomaterials Additive Manufacturing. *Small*, 15(51):1905421, 2019.

[233] Biao Zhang, Shiya Li, Hardik Hingorani, Ahmad Serjouei, Liraz Larush, Amol A. Pawar, Wei Huang Goh, Amir Hosein Sakhaei, Michinao Hashimoto, Kavin Kowsari, Shlomo Magdassi, and Qi Ge. Highly Stretchable Hydrogels for UV Curing Based High-Resolution Multimaterial 3D Printing. *Journal of Materials Chemistry B*, 6(20):3246–3253, May 2018. Publisher: The Royal Society of Chemistry.

[234] A. Sydney Gladman, Elisabetta A. Matsumoto, Ralph G. Nuzzo, L. Mahadevan, and Jennifer A. Lewis. Biomimetic 4D Printing. *Nature Materials*, 15(4):413–418, April 2016. Publisher: Nature Publishing Group.

[235] Ozan Erol, Aishwarya Pantula, Wangqu Liu, and David H. Gracias. Transformer Hydrogels: A Review. *Advanced Materials Technologies*, 4(4):1900043, April 2019.

[236] Yoonho Kim, Hyunwoo Yuk, Ruike Zhao, Shawn A. Chester, and Xuanhe Zhao. Printing Ferromagnetic Domains for Untethered Fast-Transforming Soft Materials. *Nature*, 558(7709):274–279, June 2018. Publisher: Nature Publishing Group.

[237] Lili Jia, Steve Evans, and Sander van der Linden. Motivating Actions to Mitigate Plastic Pollution. *Nature Communications*, 10(1):4582, October 2019. Publisher: Nature Publishing Group.

[238] Matthew MacLeod, Hans Peter H. Arp, Mine B. Tekman, and Annika Jahnke. The Global Threat from Plastic Pollution. *Science*, 373(6550):61–65, July 2021. Publisher: American Association for the Advancement of Science.

[239] Zoé O. G. Schyns and Michael P. Shaver. Mechanical Recycling of Packaging Plastics: A Review. *Macromolecular Rapid Communications*, 42(3):2000415, 2021.

[240] AliReza Rahimi and Jeannette M. García. Chemical Recycling of Waste Plastics for New Materials Production. *Nature Reviews Chemistry*, 1(6):1–11, June 2017. Publisher: Nature Publishing Group.

[241] Simone Giaveri, Adeline M. Schmitt, Laura Roset Julià, Anna Murello, Laure Menin, Daniel Ortiz, Luc Patiny, Sreenath Bolisetty, Raffaele Mezzenga, Sebastian J.

Maerkl, and Francesco Stellacci. Nature-Inspired Circular-Economy Recycling (NaCRe) for Proteins: Proof of Concept, September 2020. Pages: 2020.09.23.309799 Section: New Results.

[242] Weina Liu, Simone Giaveri, Daniel Ortiz, and Francesco Stellacci. DNA as a Recyclable Natural Polymer, September 2021. Pages: 2021.08.31.458327 Section: New Results.

[243] Alan M. Wemyss, Chris Bowen, Cédric Plesse, Cédric Vancaeyzeele, Giao T. M. Nguyen, Frédéric Vidal, and Chaoying Wan. Dynamic Crosslinked Rubbers for a Green Future: A Material Perspective. *Materials Science and Engineering: R: Reports*, 141:100561, July 2020.

[244] Lucie Imbernon and Sophie Norvez. From Landfilling to Vitrimer Chemistry in Rubber Life Cycle. *European Polymer Journal*, 82:347–376, September 2016.

[245] Yi Li, Hong Yu Yang, and Doo Sung Lee. Advances in Biodegradable and Injectable Hydrogels for Biomedical Applications. *Journal of Controlled Release*, 330:151–160, February 2021.

[246] Hang Yang, Chenghai Li, Jingda Tang, and Zhigang Suo. Strong and Degradable Adhesion of Hydrogels. *ACS Applied Bio Materials*, 2(5):1781–1786, May 2019. Publisher: American Chemical Society.

[247] Benjamin R. Freedman, Oktay Uzun, Nadja M. Maldonado Luna, Anna Rock, Charles Clifford, Emily Stoler, Gabrielle Östlund Sholars, Christopher Johnson, and David J. Mooney. Degradable and Removable Tough Adhesive Hydrogels. *Advanced Materials*, 33(17):2008553, 2021.

[248] Yang Gao, Kangling Wu, and Zhigang Suo. Photodetachable Adhesion. *Advanced Materials*, 31(6):1806948, 2019.

[249] Hyunwoo Yuk, Claudia E. Varela, Christoph S. Nabzdyk, Xinyu Mao, Robert F. Padera, Ellen T. Roche, and Xuanhe Zhao. Dry double-sided tape for adhesion of wet tissues and devices. *Nature*, October 2019.

[250] Mélanie Despeisse and Simon Ford. The Role of Additive Manufacturing in Improving Resource Efficiency and Sustainability. In Shigeki Umeda, Masaru Nakano, Hajime Mizuyama, Hironori Hibino, Dimitris Kiritsis, and Gregor von Cieminski, editors, *Advances in Production Management Systems: Innovative Production Management Towards Sustainable Growth*, IFIP Advances in Information and Communication Technology, pages 129–136, Cham, 2015. Springer International Publishing.

[251] Malte Gebler, Anton J. M. Schoot Uiterkamp, and Cindy Visser. A Global Sustainability Perspective on 3D Printing Technologies. *Energy Policy*, 74:158–167, November 2014.

[252] Margaret E. Prendergast and Jason A. Burdick. Recent Advances in Enabling Technologies in 3D Printing for Precision Medicine. *Advanced Materials*, 32(13):1902516, 2020.

[253] Wei Sun, Binil Starly, Andrew C. Daly, Jason A. Burdick, Jürgen Groll, Gregor Skeldon, Wenmiao Shu, Yasuyuki Sakai, Marie Shinohara, Masaki Nishikawa, Jinah Jang, Dong-Woo Cho, Minghao Nie, Shoji Takeuchi, Serge Ostrovidov, Ali Khademhosseini, Roger D. Kamm, Vladimir Mironov, Lorenzo Moroni, and Ibrahim T. Ozbolat. The Bioprinting Roadmap. *Biofabrication*, 12(2):022002, February 2020. Publisher: IOP Publishing.

[254] Elia A. Guzzi and Mark W. Tibbitt. Additive Manufacturing of Precision Biomaterials. *Advanced Materials*, 32(13):1901994, 2020.

[255] Alvaro Charlet, Matteo Hirsch, Sanjay Schreiber, and Esther Amstad. Recycling of Load-Bearing 3D Printable Double Network Granular Hydrogels. *Small*, 18(12):2107128, 2022. _eprint: https://onlinelibrary.wiley.com/doi/pdf/10.1002/smll.202107128.

[256] Florian Hartmann, Melanie Baumgartner, and Martin Kaltenbrunner. Becoming Sustainable, The New Frontier in Soft Robotics. *Advanced Materials*, 33(19):2004413, 2021.

[257] Paul Bazylewski, Ranjith Divigalpitiya, and Giovanni Fanchini. In Situ Raman Spectroscopy Distinguishes between Reversible and Irreversible Thiol Modifications in ʟ -Cysteine. *RSC Advances*, 7(5):2964–2970, 2017.

[258] Rosaria Ciriminna and Mario Pagliaro. Biodegradable and Compostable Plastics: A Critical Perspective on the Dawn of Their Global Adoption. *ChemistryOpen*, 9(1):8–13, 2020.

[259] Jian Hu, Takayuki Kurokawa, Tasuku Nakajima, Zi Liang Wu, Song Miao Liang, and Jian Ping Gong. Fracture Process of Microgel-Reinforced Hydrogels under Uniaxial Tension. *Macromolecules*, 47(11):3587–3594, June 2014.

[260] Jian Hu, Takayuki Kurokawa, Tasuku Nakajima, Tao Lin Sun, Tiffany Suekama, Zi Liang Wu, Song Miao Liang, and Jian Ping Gong. High Fracture Efficiency

and Stress Concentration Phenomenon for Microgel-Reinforced Hydrogels Based on Double-Network Principle. *Macromolecules*, 45(23):9445–9451, December 2012. Publisher: American Chemical Society.

[261] Jinhua Li, Chengtie Wu, Paul K. Chu, and Michael Gelinsky. 3D Printing of Hydrogels: Rational Design Strategies and Emerging Biomedical Applications. *Materials Science and Engineering: R: Reports*, 140:100543, April 2020.

[262] Takayuki Nonoyama, Yong Woo Lee, Kumi Ota, Keigo Fujioka, Wei Hong, and Jian Ping Gong. Instant Thermal Switching from Soft Hydrogel to Rigid Plastics Inspired by Thermophile Proteins. *Advanced Materials*, 32(4):1905878, January 2020.

[263] Mike Ashby. Hybrid Materials to Expand the Boundaries of Material-Property Space. *Journal of the American Ceramic Society*, 94(s1):s3–s14, 2011.

[264] Akbar Ali and Shakeel Ahmed. Recent Advances in Edible Polymer Based Hydrogels as a Sustainable Alternative to Conventional Polymers. *Journal of Agricultural and Food Chemistry*, 66(27):6940–6967, July 2018.

[265] Marcos R. Guilherme, Fauze A. Aouada, André R. Fajardo, Alessandro F. Martins, Alexandre T. Paulino, Magali F. T. Davi, Adley F. Rubira, and Edvani C. Muniz. Superabsorbent hydrogels based on polysaccharides for application in agriculture as soil conditioner and nutrient carrier: A review. *European Polymer Journal*, 72:365–385, November 2015.

[266] Hao Xu, Fu-Kuan Shi, Xiao-Ying Liu, Ming Zhong, and Xu-Ming Xie. How can multi-bond network hydrogels dissipate energy more effectively: an investigation on the relationship between network structure and properties. *Soft Matter*, 16(18):4407–4413, 2020.

[267] Lizhi Xu, Xueli Zhao, Chuanlai Xu, and Nicholas A. Kotov. Water-Rich Biomimetic Composites with Abiotic Self-Organizing Nanofiber Network. *Advanced Materials*, 30(1):1703343, 2018.

[268] Yuanxin Deng, Qi Zhang, Ben L. Feringa, He Tian, and Da-Hui Qu. Toughening a Self-Healable Supramolecular Polymer by Ionic Cluster-Enhanced Iron-Carboxylate Complexes. *Angewandte Chemie*, 132(13):5316–5321, 2020. _eprint: https://onlinelibrary.wiley.com/doi/pdf/10.1002/ange.201913893.

[269] Peng Lin, Shuanhong Ma, Xiaolong Wang, and Feng Zhou. Molecularly Engineered Dual-Crosslinked Hydrogel with Ultrahigh Mechanical Strength, Toughness, and Good Self-Recovery. *Advanced Materials*, 27(12):2054–2059, 2015.

[270] Can Hui Yang, Mei Xiang Wang, Hussain Haider, Jian Hai Yang, Jeong-Yun Sun, Yong Mei Chen, Jinxiong Zhou, and Zhigang Suo. Strengthening Alginate/Polyacrylamide Hydrogels Using Various Multivalent Cations. *ACS Applied Materials & Interfaces*, 5(21):10418–10422, November 2013.

[271] Xiaohu Zhou, Chun Li, Lifei Zhu, and Xuechang Zhou. Engineering hydrogels by soaking: from mechanical strengthening to environmental adaptation. *Chemical Communications*, 56(89):13731–13747, November 2020. Publisher: The Royal Society of Chemistry.

[272] Chenglong Dong, Hailong Fan, Feng Tang, Xiaobin Gao, Kai Feng, Jiahui Wang, and Zhaoxia Jin. Mussel byssus cuticle-inspired ultrastiff and stretchable triple-crosslinked hydrogels. *Journal of Materials Chemistry B*, 9(2):373–380, January 2021. Publisher: The Royal Society of Chemistry.

[273] Xiao-Ying Liu, Hao Xu, Li-Qin Zhang, Ming Zhong, and Xu-Ming Xie. Homogeneous and Real Super Tough Multi-Bond Network Hydrogels Created through a Controllable Metal Ion Permeation Strategy. *ACS Applied Materials & Interfaces*, 11(45):42856–42864, November 2019. Publisher: American Chemical Society.

[274] Gaolai Du, Fengxiang Wu, Yang Cong, Lei Nie, Shuhui Liu, Guorong Gao, and Jun Fu. Versatile controlled ion release for synthesis of recoverable hybrid hydrogels with high stretchability and notch-insensitivity. *Chemical Communications*, 51(85):15534–15537, 2015. Publisher: Royal Society of Chemistry.

[275] Tobias Priemel, Elena Degtyar, Mason N Dean, and Matthew J Harrington. ARTICLE Rapid Self-Assembly of Complex Biomolecular Architectures during Mussel Byssus Biofabrication. *Nature Communications*, 8, 2017.

[276] B. Y. Santosh Kumar, Arun M. Isloor, G. C. Mohan Kumar, Inamuddin, and Abdullah M. Asiri. Nanohydroxyapatite Reinforced Chitosan Composite Hydrogel with Tunable Mechanical and Biological Properties for Cartilage Regeneration. *Scientific Reports*, 9(1):1–13, November 2019.

[277] Lan Li, Fei Yu, Liming Zheng, Rongliang Wang, Wenqiang Yan, Zixu Wang, Jia Xu, Jianxiang Wu, Dongquan Shi, Liya Zhu, Xingsong Wang, and Qing Jiang. Natu-

ral hydrogels for cartilage regeneration: Modification, preparation and application. *Journal of Orthopaedic Translation*, 17:26–41, April 2019.

[278] Shaoting Lin, Ji Liu, Xinyue Liu, and Xuanhe Zhao. Muscle-like fatigue-resistant hydrogels by mechanical training. *Proceedings of the National Academy of Sciences*, 116(21):10244–10249, May 2019. Publisher: National Academy of Sciences Section: Physical Sciences.

[279] Takahiro Matsuda, Runa Kawakami, Ryo Namba, Tasuku Nakajima, and Jian Ping Gong. Mechanoresponsive self-growing hydrogels inspired by muscle training. *Science*, 363(6426):504–508, February 2019.

[280] Canhui Yang and Zhigang Suo. Hydrogel Ionotronics. *Nature Reviews Materials*, 3(6):125–142, June 2018. Publisher: Nature Publishing Group.

[281] Lian-Hua Fu, Chao Qi, Ming-Guo Ma, and Pengbo Wan. Multifunctional cellulose-based hydrogels for biomedical applications. *Journal of Materials Chemistry B*, 7(10):1541–1562, March 2019. Publisher: The Royal Society of Chemistry.

[282] Xiaoye Gao, Yue Cao, Xiangfu Song, Zhe Zhang, Xiuli Zhuang, Chaoliang He, and Xuesi Chen. Biodegradable, pH-Responsive Carboxymethyl Cellulose/Poly(Acrylic Acid) Hydrogels for Oral Insulin Delivery. *Macromolecular Bioscience*, 14(4):565–575, 2014.

[283] Diana E. Ciolacu and Dana M. Suflet. 11 - Cellulose-Based Hydrogels for Medical/Pharmaceutical Applications. In Valentin Popa and Irina Volf, editors, *Biomass as Renewable Raw Material to Obtain Bioproducts of High-Tech Value*, pages 401–439. Elsevier, January 2018.

[284] Hongliang Kang, Ruigang Liu, and Yong Huang. Cellulose-Based Gels. *Macromolecular Chemistry and Physics*, 217(12):1322–1334, 2016.

[285] J. Glasing, J. Bouchard, P. G. Jessop, P. Champagne, and M. F. Cunningham. Grafting well-defined CO 2 -responsive polymers to cellulose nanocrystals via nitroxide-mediated polymerisation: effect of graft density and molecular weight on dispersion behaviour. *Polymer Chemistry*, 8(38):6000–6012, 2017. Publisher: Royal Society of Chemistry.

[286] Wei Chen, Yunhao Bu, Delin Li, Chuanjie Liu, Guangxue Chen, Xiaofang Wan, and Nan Li. High-Strength, Tough, and Self-Healing Hydrogel Based on Carboxymethyl Cellulose. *Cellulose*, 27(2):853–865, January 2020.

[287] Yongzhi Liang, Jinqiao Xue, Binyang Du, and Jingjing Nie. Ultrastiff, Tough, and Healable Ionic–Hydrogen Bond Cross-Linked Hydrogels and Their Uses as Building Blocks To Construct Complex Hydrogel Structures. *ACS Applied Materials & Interfaces*, 11(5):5441–5454, February 2019.

[288] Imtiaz Hussain, Sayed Mir Sayed, Shunli Liu, Fang Yao, Olayinka Oderinde, and Guodong Fu. Hydroxyethyl cellulose-based self-healing hydrogels with enhanced mechanical properties via metal-ligand bond interactions. *European Polymer Journal*, 100:219–227, March 2018.

[289] L. I. Abramov, Ye. N. Zilberman, and V. I. Ivanova. Effect of copper and iron salts on the radical polymerization of acrylamide in water. *Polymer Science U.S.S.R.*, 31(7):1573–1578, January 1989.

[290] Barry Halliwell and John M. C. Gutteridge. Iron and free radical reactions: two aspects of antioxidant protection. *Trends in Biochemical Sciences*, 11(9):372–375, September 1986.

[291] Xuefeng Li, Hui Wang, Dapeng Li, Shijun Long, Gaowen Zhang, and ZiLiang Wu. Dual Ionically Cross-linked Double-Network Hydrogels with High Strength, Toughness, Swelling Resistance, and Improved 3D Printing Processability. *ACS Applied Materials & Interfaces*, 10(37):31198–31207, September 2018. Publisher: American Chemical Society.

[292] Xuefeng Yang, Guoqiang Liu, Liao Peng, Jinhua Guo, Lei Tao, Jinying Yuan, Chunyu Chang, Yen Wei, and Lina Zhang. Highly Efficient Self-Healable and Dual Responsive Cellulose-Based Hydrogels for Controlled Release and 3D Cell Culture. *Advanced Functional Materials*, 27(40):1703174, 2017. _eprint: https://onlinelibrary.wiley.com/doi/pdf/10.1002/adfm.201703174.

[293] Rebecca E. Webber, Costantino Creton, Hugh R. Brown, and Jian Ping Gong. Large Strain Hysteresis and Mullins Effect of Tough Double-Network Hydrogels. *Macromolecules*, 40(8):2919–2927, April 2007.

[294] Tasuku Nakajima, Yuhei Ozaki, Ryo Namba, Kumi Ota, Yuki Maida, Takahiro Matsuda, Takayuki Kurokawa, and Jian Ping Gong. Tough Double-Network Gels and Elastomers from the Nonprestretched First Network. *ACS Macro Letters*, 8(11):1407–1412, November 2019. Publisher: American Chemical Society.

[295] Jess M. Clough, Costantino Creton, Stephen L. Craig, and Rint P. Sijbesma. Covalent Bond Scission in the Mullins Effect of a Filled Elastomer: Real-Time Visualiza-

tion with Mechanoluminescence. *Advanced Functional Materials*, 26(48):9063–9074, 2016. _eprint: https://onlinelibrary.wiley.com/doi/pdf/10.1002/adfm.201602490.

[296] David C. Bassett, Armend G. Håti, Thor B. Melø, Bjørn T. Stokke, and Pawel Sikorski. Competitive Ligand Exchange of Crosslinking Ions for Ionotropic Hydrogel Formation. *Journal of Materials Chemistry B*, 4(37):6175–6182, 2016.

[297] Kyoko Yamamoto, Yoshiaki Yuguchi, Bjørn Torger Stokke, Pawel Sikorski, and David C. Bassett. Local Structure of Ca2+ Alginate Hydrogels Gelled via Competitive Ligand Exchange and Measured by Small Angle X-Ray Scattering. *Gels*, 5(1):3, January 2019.

[298] Arthur E. Martell, Robert D. Hancock, Robert M. Smith, and Ramunas J. Motekaitis. Coordination of Al(III) in the environment and in biological systems. *Coordination Chemistry Reviews*, 149:311–328, May 1996.

[299] Yufeng Lei, Weiyan Huang, Qiuping Huang, and Anqiang Zhang. A novel polysiloxane elastomer based on reversible aluminum-carboxylate coordination. *New Journal of Chemistry*, 43(1):261–268, December 2018. Publisher: The Royal Society of Chemistry.

[300] Clemens N. Z. Schmitt, Yael Politi, Antje Reinecke, and Matthew J. Harrington. Role of Sacrificial Protein–Metal Bond Exchange in Mussel Byssal Thread Self-Healing. *Biomacromolecules*, 16(9):2852–2861, September 2015.

[301] Matthew J Harrington, Admir Masic, and Niels Holten-andersen. Iron-Clad Fibers : A Metal-Based. *Science*, 328(April):216–220, 2010.

[302] M. Krogsgaard, A. Andersen, and H. Birkedal. Gels and Threads: Mussel-Inspired One-Pot Route to Advanced Responsive Materials. *Chemical Communications (Cambridge, England)*, 50(87):13278–13281, November 2014.

[303] Xuanhe Zhao. Multi-scale multi-mechanism design of tough hydrogels: building dissipation into stretchy networks. *Soft Matter*, 10(5):672–687, January 2014.

[304] Chuang Li, Matthew J. Rowland, Yu Shao, Tianyang Cao, Chun Chen, Haoyang Jia, Xu Zhou, Zhongqiang Yang, Oren A. Scherman, and Dongsheng Liu. Responsive Double Network Hydrogels of Interpenetrating DNA and CB[8] Host–Guest Supramolecular Systems. *Advanced Materials*, 27(21):3298–3304, 2015.

[305] Jiahong Jin, Lili Cai, Yong-Guang Jia, Sa Liu, Yunhua Chen, and Li Ren. Progress in Self-Healing Hydrogels Assembled by Host– Guest Interactions: Preparation and

Biomedical Applications. *Journal of Materials Chemistry B*, 7(10):1637–1651, March 2019. Publisher: The Royal Society of Chemistry.

[306] Jing Chen, Ran An, Linglin Han, Xiangdong Wang, Yulin Zhang, Lingying Shi, and Rong Ran. Tough Hydrophobic Association Hydrogels with Self-Healing and Reforming Capabilities Achieved by Polymeric Core-Shell Nanoparticles. *Materials Science and Engineering: C*, 99:460–467, June 2019.

[307] Alvaro Charlet, Viviane Lutz-Bueno, Raffaele Mezzenga, and Esther Amstad. Shape Retaining Self-Healing Metal-Coordinated Hydrogels. *Nanoscale*, 13(7):4073–4084, 2021.

[308] Ning Zheng, Yang Xu, Qian Zhao, and Tao Xie. Dynamic Covalent Polymer Networks: A Molecular Platform for Designing Functions beyond Chemical Recycling and Self-Healing. *Chemical Reviews*, 121(3):1716–1745, February 2021. Publisher: American Chemical Society.

[309] Franziska Jehle, Peter Fratzl, and Matthew J. Harrington. Metal-Tunable Self-Assembly of Hierarchical Structure in Mussel-Inspired Peptide Films. *ACS Nano*, 12(3):2160–2168, March 2018.

[310] Huaping Tan, Chao Xiao, Jinchen Sun, Dangsheng Xiong, and Xiaohong Hu. Biological Self-Assembly of Injectable Hydrogel as Cell Scaffold via Specific Nucleobase Pairing. *Chemical Communications*, 48(83):10289–10291, September 2012. Publisher: The Royal Society of Chemistry.

[311] Rebecca Blell, Xiaofeng Lin, Tom Lindström, Mikael Ankerfors, Matthias Pauly, Olivier Felix, and Gero Decher. Generating in-Plane Orientational Order in Multilayer Films Prepared by Spray-Assisted Layer-by-Layer Assembly. *ACS Nano*, 11(1):84–94, January 2017. Publisher: American Chemical Society.

[312] Wenxing Li, Peng Zhao, Chao Lin, Xuejun Wen, Eleni Katsanevakis, Decher Gero, Olivier Félix, and Yuehua Liu. Natural Polyelectrolyte Self-Assembled Multilayers Based on Collagen and Alginate: Stability and Cytocompatibility. *Biomacromolecules*, 14(8):2647–2656, August 2013. Publisher: American Chemical Society.

[313] Giuseppe Di Vitantonio, Tiancheng Wang, Martin F. Haase, Kathleen J. Stebe, and Daeyeon Lee. Robust Bijels for Reactive Separation via Silica-Reinforced Nanoparticle Layers. *ACS Nano*, 13(1):26–31, January 2019. Publisher: American Chemical Society.

[314] Weitao Jia, P. Selcan Gungor-Ozkerim, Yu Shrike Zhang, Kan Yue, Kai Zhu, Wanjun Liu, Qingment Pi, Batzaya Byambaa, Mehmet Remzi Dokmeci, Su Ryon Shin, and Ali Khademhosseini. Direct 3D Bioprinting of Perfusable Vascular Constructs Using a Blend Bioink. *Biomaterials*, 106:58–68, November 2016.

[315] Guoliang Ying, Nan Jiang, Carolina Parra-Cantu, Guosheng Tang, Jingyi Zhang, Hongjun Wang, Shixuan Chen, Ning-Ping Huang, Jingwei Xie, and Yu Shrike Zhang. Bioprinted Injectable Hierarchically Porous Gelatin Methacryloyl Hydrogel Constructs with Shape-Memory Properties. *Advanced Functional Materials*, 30(46):2003740, 2020.

[316] Riccardo Levato, Tomasz Jungst, Ruben G. Scheuring, Torsten Blunk, Juergen Groll, and Jos Malda. From Shape to Function: The Next Step in Bioprinting. *Advanced Materials*, 32(12):1906423, 2020. _eprint: https://onlinelibrary.wiley.com/doi/pdf/10.1002/adma.201906423.

[317] Khoon S Lim, Riccardo Levato, Pedro F Costa, Miguel D Castilho, Cesar R Alcala-Orozco, Kim M A van Dorenmalen, Ferry P W Melchels, Debby Gawlitta, Gary J Hooper, Jos Malda, and Tim B F Woodfield. Bio-resin for high resolution lithography-based biofabrication of complex cell-laden constructs. *Biofabrication*, 10(3):034101, May 2018.

[318] Andrew C. Daly, Matthew D. Davidson, and Jason A. Burdick. 3D bioprinting of high cell-density heterogeneous tissue models through spheroid fusion within self-healing hydrogels. *Nature Communications*, 12(1):753, February 2021. Number: 1 Publisher: Nature Publishing Group.

[319] Jing Fan, Shin Hyun Kim, Zi Chen, Shaobing Zhou, Esther Amstad, Tina Lin, and David A. Weitz. Creation of Faceted Polyhedral Microgels from Compressed Emulsions. *Small*, 13(31):1–7, 2017.

[320] Vittoria Chimisso, Simona Conti, Phally Kong, Csaba Fodor, and Wolfgang P. Meier. Metal cation responsive anionic microgels: behaviour towards biologically relevant divalent and trivalent ions. *Soft Matter*, 17(3):715–723, 2021.

[321] Dowon Moon, Min-Gyu Lee, Jeong-Yun Sun, Kwang Hoon Song, and Junsang Doh. Jammed Microgel-Based Inks for 3D Printing of Complex Structures Transformable via pH/Temperature Variations. *Macromolecular Rapid Communications*, n/a(n/a):2200271. _eprint: https://onlinelibrary.wiley.com/doi/pdf/10.1002/marc.202200271.

[322] Weichang Li, Xiaobo Liu, Zhishuang Deng, Yutong Chen, Qianqian Yu, Wen Tang, Tao Lin Sun, Yu Shrike Zhang, and Kan Yue. Tough Bonding, On-Demand Debonding, and Facile Rebonding between Hydrogels and Diverse Metal Surfaces. *Advanced Materials*, 31(48):1904732, November 2019.

[323] Ji Lin, Si Yu Zheng, Rui Xiao, Jun Yin, Zi Liang Wu, Qiang Zheng, and Jin Qian. Constitutive Behaviors of Tough Physical Hydrogels with Dynamic Metal-Coordinated Bonds. *Journal of the Mechanics and Physics of Solids*, 139:103935, June 2020.

[324] Lisa M. Fuhrer, Shengtong Sun, Volodymyr Boyko, Matthias Kellermeier, and Helmut Cölfen. Tuning the Properties of Hydrogels Made from Poly(Acrylic Acid) and Calcium Salts. *Physical Chemistry Chemical Physics*, 22(33):18631–18638, 2020.

[325] Michaela Eder, Shahrouz Amini, and Peter Fratzl. Biological composites—complex structures for functional diversity. *Science*, 362(6414):543–547, November 2018. Publisher: American Association for the Advancement of Science.

[326] James C. Weaver, Garrett W. Milliron, Ali Miserez, Kenneth Evans-Lutterodt, Steven Herrera, Isaias Gallana, William J. Mershon, Brook Swanson, Pablo Zavattieri, Elaine DiMasi, and David Kisailus. The Stomatopod Dactyl Club: A Formidable Damage-Tolerant Biological Hammer. *Science*, 336(6086):1275–1280, June 2012. Publisher: American Association for the Advancement of Science.

[327] Huachuan Du, Ullrich Steiner, and Esther Amstad. Nacre-inspired Hard and Tough Materials. *CHIMIA*, 73(1-2):29–29, February 2019. Number: 1-2.

[328] Horacio D. Espinosa, Allison L. Juster, Felix J. Latourte, Owen Y. Loh, David Gregoire, and Pablo D. Zavattieri. Tablet-level origin of toughening in abalone shells and translation to synthetic composite materials. *Nature Communications*, 2(1):173, February 2011. Number: 1 Publisher: Nature Publishing Group.

[329] Rachid Hsissou, Rajaa Seghiri, Zakaria Benzekri, Miloudi Hilali, Mohamed Rafik, and Ahmed Elharfi. Polymer composite materials: A comprehensive review. *Composite Structures*, 262:113640, April 2021.

[330] Munonyedi Kelvin Egbo. A fundamental review on composite materials and some of their applications in biomedical engineering. *Journal of King Saud University - Engineering Sciences*, 33(8):557–568, December 2021.

[331] George Mayer. Rigid Biological Systems as Models for Synthetic Composites. *Science*, 310(5751):1144–1147, November 2005. Publisher: American Association for the Advancement of Science.

[332] Xiaofu Dai, Jianquan Wang, Fei Teng, Ziqiang Shao, and Xiaonan Huang. Zr(IV)-Crosslinked Polyacrylamide/Polyanionic Cellulose Composite Hydrogels with High Strength and Unique Acid Resistance. *Journal of Polymer Science Part B: Polymer Physics*, 57(15):981–991, 2019.

[333] Tommaso Magrini, Florian Bouville, Alessandro Lauria, Hortense Le Ferrand, Tobias P. Niebel, and André R. Studart. Transparent and tough bulk composites inspired by nacre. *Nature Communications*, 10(1):2794, June 2019. Number: 1 Publisher: Nature Publishing Group.

[334] Xianpeng Yang, Subir K. Biswas, Hiroyuki Yano, and Kentaro Abe. Fabrication of ultrastiff and strong hydrogels by in situ polymerization in layered cellulose nanofibers. *Cellulose*, November 2019.

[335] Wei Cui, Yiwan Huang, Liang Chen, Yong Zheng, Yoshiyuki Saruwatari, Chung-Yuen Hui, Takayuki Kurokawa, Daniel R. King, and Jian Ping Gong. Tiny yet tough: Maximizing the toughness of fiber-reinforced soft composites in the absence of a fiber-fracture mechanism. *Matter*, 4(11):3646–3661, November 2021.

[336] Nicolas Rauner, Monika Meuris, Mirjana Zoric, and Joerg C Tiller. Enzymatic Mineralization Generates Ultrastiff and Tough Hydrogels with Tunable Mechanics. 2017.

[337] Guangda Chen, Xiangyu Liang, Pei Zhang, Shaoting Lin, Chengcheng Cai, Ziyi Yu, and Ji Liu. Bioinspired 3D Printing of Functional Materials by Harnessing Enzyme-Induced Biomineralization. *Advanced Functional Materials*, n/a(n/a):2113262. _eprint: https://onlinelibrary.wiley.com/doi/pdf/10.1002/adfm.202113262.

[338] Yipin Qi, Zheng Cheng, Zhou Ye, Hongli Zhu, and Conrado Aparicio. Bioinspired Mineralization with Hydroxyapatite and Hierarchical Naturally Aligned Nanofibrillar Cellulose. *ACS Applied Materials & Interfaces*, 11(31):27598–27604, August 2019.

[339] Huachuan Du, Tianyu Yuan, Ran Zhao, Matteo Hirsch, Michael Kessler, and Esther Amstad. Reinforcing hydrogels with in situ formed amorphous CaCO 3. *Biomaterials Science*, 2022. Publisher: Royal Society of Chemistry.

[340] Dimitri Kokkinis, Manuel Schaffner, and André R. Studart. Multimaterial Magnetically Assisted 3D Printing of Composite Materials. *Nature Communications*, 6:8643, October 2015.

[341] Yeqiao Meng, Jinlong Cao, Yue Chen, Yaru Yu, and Lin Ye. 3D Printing of a Poly(Vinyl Alcohol)-Based Nano-Composite Hydrogel as an Artificial Cartilage Replacement and the Improvement Mechanism of Printing Accuracy. *Journal of Materials Chemistry B*, 8(4):677–690, January 2020. Publisher: The Royal Society of Chemistry.

[342] Amar K. Mohanty, Singaravelu Vivekanandhan, Jean-Mathieu Pin, and Manjusri Misra. Composites from renewable and sustainable resources: Challenges and innovations. *Science*, 362(6414):536–542, November 2018. Publisher: American Association for the Advancement of Science.

[343] Alexandra Clarà Saracho, Stuart K. Haigh, and M. Ehsan Jorat. Flume study on the effects of microbial induced calcium carbonate precipitation (MICP) on the erosional behaviour of fine sand. *Géotechnique*, 71(12):1135–1149, December 2021. Publisher: ICE Publishing.

[344] Henk M. Jonkers, Arjan Thijssen, Gerard Muyzer, Oguzhan Copuroglu, and Erik Schlangen. Application of bacteria as self-healing agent for the development of sustainable concrete. *Ecological Engineering*, 36(2):230–235, February 2010.

[345] Souradeep Gupta, Harn Wei Kua, and Sze Dai Pang. Healing cement mortar by immobilization of bacteria in biochar: An integrated approach of self-healing and carbon sequestration. *Cement and Concrete Composites*, 86:238–254, February 2018.

[346] Jason T. DeJong, Brina M. Mortensen, Brian C. Martinez, and Douglas C. Nelson. Bio-mediated soil improvement. *Ecological Engineering*, 36(2):197–210, February 2010.

[347] Erick Ortega-Villamagua, Marco Gudiño-Gomezjurado, and Alex Palma-Cando. Microbiologically Induced Carbonate Precipitation in the Restoration and Conservation of Cultural Heritage Materials. *Molecules*, 25(23):5499, January 2020. Number: 23 Publisher: Multidisciplinary Digital Publishing Institute.

[348] Toshiro Hata, Alexandra Clarà Saracho, Stuart K. Haigh, Jun Yoneda, and Koji Yamamoto. Microbial-induced carbonate precipitation applicability with the methane hydrate-bearing layer microbe. *Journal of Natural Gas Science and Engineering*, 81:103490, September 2020.

[349] Sookie S. Bang, Johnna K. Galinat, and V. Ramakrishnan. Calcite precipitation induced by polyurethane-immobilized Bacillus pasteurii. *Enzyme and Microbial Technology*, 28(4):404–409, March 2001.

[350] Daniel Wangpraseurt, Yazhi Sun, Shangting You, Sing-Teng Chua, Samantha K. Noel, Helena F. Willard, David B. Berry, Alexander M. Clifford, Sydney Plummer, Yi Xiang, Henry H. Hwang, Jaap Kaandorp, Julia M. Diaz, Todd C. La Jeunesse, Mathieu Pernice, Silvia Vignolini, Martin Tresguerres, and Shaochen Chen. Bioprinted Living Coral Microenvironments Mimicking Coral-Algal Symbiosis. *Advanced Functional Materials*, n/a(n/a):2202273. _eprint: https://onlinelibrary.wiley.com/doi/pdf/10.1002/adfm.202202273.

[351] An Xin, Yipin Su, Shengwei Feng, Minliang Yan, Kunhao Yu, Zhangzhengrong Feng, Kyung Hoon Lee, Lizhi Sun, and Qiming Wang. Growing Living Composites with Ordered Microstructures and Exceptional Mechanical Properties. *Advanced Materials*, 33(13):2006946, 2021. _eprint: https://onlinelibrary.wiley.com/doi/pdf/10.1002/adma.202006946.

[352] Lutz-Christian Gerhardt and Aldo R. Boccaccini. Bioactive Glass and Glass-Ceramic Scaffolds for Bone Tissue Engineering. *Materials*, 3(7):3867–3910, July 2010. Number: 7 Publisher: Molecular Diversity Preservation International.

[353] Wissam Ghach, Mathieu Etienne, Patrick Billard, Frédéric P. A. Jorand, and Alain Walcarius. Electrochemically assisted bacteria encapsulation in thin hybrid sol–gel films. *Journal of Materials Chemistry B*, 1(7):1052–1059, January 2013. Publisher: The Royal Society of Chemistry.

[354] Mathias Steinacher, Alice Cont, Huachuan Du, Alexandre Persat, and Esther Amstad. Monodisperse Selectively Permeable Hydrogel Capsules Made from Single Emulsion Drops. *ACS Applied Materials & Interfaces*, 13(13):15601–15609, April 2021. Publisher: American Chemical Society.

[355] Wanjun Liu, Marcel A. Heinrich, Yixiao Zhou, Ali Akpek, Ning Hu, Xiao Liu, Xiaofei Guan, Zhe Zhong, Xiangyu Jin, Ali Khademhosseini, and Yu Shrike Zhang. Extrusion Bioprinting of Shear-Thinning Gelatin Methacryloyl Bioinks. *Advanced Healthcare Materials*, 6(12):1601451, 2017. _eprint: https://onlinelibrary.wiley.com/doi/pdf/10.1002/adhm.201601451.

[356] Eshetu Mekonnen, Ameha Kebede, Asefa Nigussie, Gessese Kebede, and Mesfin Tafesse. Isolation and Characterization of Urease-Producing Soil Bacteria. *International Journal of Microbiology*, 2021:e8888641, July 2021. Publisher: Hindawi.

[357] Michela Gioffrè, Paola Torricelli, Silvia Panzavolta, Katia Rubini, and Adriana Bigi. Role of pH on stability and mechanical properties of gelatin films. *Journal of Bioactive and Compatible Polymers*, 27(1):67–77, January 2012. Publisher: SAGE Publications Ltd STM.

[358] O. K. DeFoe and Arthur H. Compton. The Density of Rock Salt and Calcite. *Physical Review*, 25(5):618–620, May 1925. Publisher: American Physical Society.

[359] Radek Ševčík, Petr Šašek, and Alberto Viani. Physical and nanomechanical properties of the synthetic anhydrous crystalline CaCO3 polymorphs: vaterite, aragonite and calcite. *Journal of Materials Science*, 53(6):4022–4033, March 2018.

[360] Navdeep Kaur Dhami, Abhijit Mukherjee, and M. Sudhakara Reddy. Micrographical, minerological and nano-mechanical characterisation of microbial carbonates from urease and carbonic anhydrase producing bacteria. *Ecological Engineering*, 94:443–454, September 2016.

[361] Alexandra Clarà Saracho, Stuart K. Haigh, Toshiro Hata, Kenichi Soga, Stefan Farsang, Simon A. T. Redfern, and Ewa Marek. Characterisation of CaCO3 phases during strain-specific ureolytic precipitation. *Scientific Reports*, 10(1):10168, June 2020. Number: 1 Publisher: Nature Publishing Group.

[362] Olivier Coussy. *Mechanics and Physics of Porous Solids.* John Wiley & Sons, June 2011.

[363] Hyunwoo Yuk, Shaoting Lin, Chu Ma, Mahdi Takaffoli, Nicolas X. Fang, and Xuanhe Zhao. Hydraulic Hydrogel Actuators and Robots Optically and Sonically Camouflaged in Water. *Nature Communications*, 8(1):14230, February 2017. Publisher: Nature Publishing Group.

[364] Melanie Baumgartner, Florian Hartmann, Michael Drack, David Preninger, Daniela Wirthl, Robert Gerstmayr, Lukas Lehner, Guoyong Mao, Roland Pruckner, Stepan Demchyshyn, Lisa Reiter, Moritz Strobel, Thomas Stockinger, David Schiller, Susanne Kimeswenger, Florian Greibich, Gerda Buchberger, Elke Bradt, Sabine Hild, Siegfried Bauer, and Martin Kaltenbrunner. Resilient yet Entirely Degradable Gelatin-Based Biogels for Soft Robots and Electronics. *Nature Materials*, 19(10):1102–1109, October 2020. Publisher: Nature Publishing Group.

MATTEO HIRSCH | RESUME

❱ **Status:** PhD Student in Materials Science at École Polytechnique Fédérale de Lausanne

❱ **Keywords:** Soft Matter, Hydrogels, Additive Manufacturing, Sustainable Materials

❱ **Contacts:** matteo.hirsch@epfl.ch - matteo.hirsch@gmail.com - +41 77 816 33 71

❱ **Languages:** Italian (MT) - English (C1) - French (B2) - Spanish (B1)

❱❱❱ Summary

PhD student in Materials Science with experience in Soft Matter and Additive Manufacturing. Currently working on a novel class of 3D printed hydrogels with strong mechanics and local varying composition. Particularly interested in the translational potential of scientific research.

❱❱❱ Experience

Nov 2018 - now   **Doctoral Researcher (EPFL)**   Lausanne (CH)

❱ Fabrication of mechanically strong and tough hydrogels
❱ 3D printing of granular materials
❱ Synthesis and modification of biopolymers

March - October 2018   **Visiting Graduate Research Fellow (Houston Methodist)**   Houston, TX (USA)

❱ Realiziation of a theranostic platform for Lewis Lung Carcinoma (LLC) tumor model
❱ Development of a Gold-coated Super-Paramagnetic Iron Oxide Nanoparticle (SPION@Au), for radio-sensitization and magnetic resonance imaging (MRI) contrast enhancement
❱ Combined radio-immunotherapy for cancer treatment: stimulation of abscopal effect and adaptive immunity

June - August 2017   **Summer Internship (Ludwig Maximilians Universität)**   München (GE)

❱ Synthesis of liposome-coated Metal-Organic Framework nanoparticles (MOF@DOPC NPs) for drug delivery applications
❱ Calcein-loaded MOF@DOPC NPs *in vitro* delivery and release in HeLa and HEK-293 cells. Colocalization assessment of MOF and DOPC through Spinning-Disk Fluorescence Microscopy. Tentative of siRNA delivery with MOF@DOPC nanoparticles

March - June 2016   **Visiting Undergraduate Research Fellow (Chilab)**   Torino (IT)

❱ Design and fabrication of Organic ElectroChemical Transistors with standard lithographic techniques
❱ Optimization of lithographic techniques for organic materials; deposition and patterning of PEDOT:PSS layers

Sept 2014 - Jun 2016   **Student Assistant (Politecnico di Torino)**   Torino (IT)

❱ Assisted in practical laboratories of Technical Drawing and Computer Aided Design (SolidWorks, Rhino)
❱ Assisted in Signal Analysis exercise sessions

❱❱❱ Education

Nov 2018 - now   **PhD Candidate in Materials Science**   EPFL

❱ **Doctoral Title**: From Bioinspired to Bioinformed Design of Load-Bearing Soft Materials
❱ **Teaching Assistant Duties**: Exam Proctoring, Mise A Niveau (MAN), and Soft Matter
❱ **Student Mentoring**: Semester project, and Master's Thesis supervision

Matteo Hirsch · 27 February 1994 · Florence, Italy

| Sept 2016 - Dec 2018 | **Master's Degree in Nanotechnologies for ICTs** | PoliTO, INPG, EPFL |

> ❯ International program held by Politecnico di Torino, Institut Polytechnique de Grenoble and École polytechnique fédérale de Lausanne
> ❯ **Core Subjects**: Solid State Physics, Analog and Digital Electronics, Microfabrication, Optical Detectors
> ❯ **Additional Elective Courses**: Stem Cell Biology, Bioinspired Approaches to Engineering
> ❯ **Master Thesis**: Radio-immunotherapy for Lewis Lung Carcinoma (LLC) treatment

| Sept 2013 - Jun 2016 | **Bachelor's Degree in Biomedical Engineering** | PoliTO |

> ❯ **Core Subjects**: Biomechanics, Implantable Medical Devices, Tools for Medical Diagnostics
> ❯ **General Subjects**: Maths, Geometry, General Physics, Chemistry, Circuits and Electronics
> ❯ **Bachelor Thesis**: Design and characterization of an Organic ElectroChemical Transistor (OECT)

❯❯❯ Relevant Courses and Certificates

| 2022/03 | **AgilePM® Foundation** |

> ❯ Dynamic Systems Development Method - Agile Project Management
> ❯ QRP International

| 2021/11 | **Bench2Biz Start-up Training** |

> ❯ Business Identification and Feasibility Assessment
> ❯ National Centers of Competences in Research (NCCR)

| 2021/03 | **Innosuisse Start-up Training** |

> ❯ Business Creation for Engineering Startups
> ❯ Venture Lab

| 2020/10 | **Educate to Innovate** |

> ❯ Drug and Device Product Development and Regulation in Europe and the United States
> ❯ San Diego State University

❯❯❯ List of Selected Peer Reviewed Publications

| 2022/? | **Advanced Materials - under revision** |

> ❯ 3D Printing of Bacteria-loaded Microgels into Structural Living Materials
> ❯ **M. Hirsch***, L. Lucherini, R. Zhao, S. Ait Said, A. Clarà Saracho, E. Amstad

| 2022/01 | **Small** |

> ❯ Recycling of Load-Bearing 3D Printable Double Network Granular Hydrogels
> ❯ A. Charlet*, **M. Hirsch***, S. Schreiber, E. Amstad

| 2021/10 | **Journal of Materials Chemistry A** |

> ❯ Controlling the calcium carbonate microstructure of engineered living building materials
> ❯ A. Clarà Saracho, L. Lucherini, **M. Hirsch**, H. M. Peter, D. Terzis, E. Amstad, L. Laloui

| 2021/08 | **Biomaterials Science** |

> ❯ Load-bearing hydrogels ionically reinforced through competitive ligand exchanges
> ❯ **M. Hirsch**, M. Steinacher, R. Zhao, E. Amstad

2020/10	**Advanced Functional Materials**

❱ 3D Printing of Strong and Tough Double Network Granular Hydrogels

❱ **M. Hirsch***, A. Charlet*, E. Amstad

2020/09	**Nanomaterials**

❱ Gold Nanoparticles Radio-Sensitize and Reduce Cell Survival in Lewis Lung Carcinoma

❱ A. Pandey, V. Vighetto, N. Di Marzio, F. Ferraro, **M. Hirsch**, N. Ferrante, S. Mitra, A. Grattoni, C. S. Filgueira

2020/07	**IEEE 20th International Conference on Nanotechnology**

❱ Intratumoral Gold Nanoparticle-Enhanced CT Imaging: An in Vivo Investigation of Biodistribution and Retention

❱ R. Terracciano, M. L. Sprouse, D. K. Wang, S. Ricchetti, **M. Hirsch**, N. Ferrante, E. B. Butler, D. Demarchi, A. Grattoni, C. S. Filgueira

2019/11	**Advanced Drug Delivery Reviews**

❱ Technologies for intrapericardial delivery of therapeutics and cells

❱ C. S. Filgueira, S. R. Igo, D. K. Wang, **M. Hirsch**, D. G. Schulz, B. A. Bruckner, A. Grattoni

❱❱❱ Awards

2022/02	**Oral Presentation - Best Doctoral Student Talk**

❱ **3D Printing of Recyclable Double Network Granular Hydrogels**. **M. Hirsch**, E. Amstad

❱ EDMX Research Day 2022. Lausanne, Switzerland

2020/02	**Poster Presentation - Best Poster Award**

❱ **Bioinspired Dually-Crosslinked Hydrogels. M. Hirsch**, E. Amstad

❱ Swiss Soft Days 2020. Basel, Switzerland

2018/08	**Poster Presentation - Basic Science Award**

❱ **Radio-Immunotherapy of Lewis Lung Carcinoma in a Murine Model**. **M. Hirsch**, *et al.*

❱ 6th Annual Houston Methodist Cancer Symposium, HMRI. Houston, TX, USA

❱❱❱ Contact References

❱ **Prof. Esther Amstad** esther.amstad@epfl.ch

❱ **Prof. Valentina Cauda** valentina.cauda@polito.it

❱ **Prof. Alessandro Grattoni** agrattoni@houstonmethodist.org

❱ **Prof. Carly Filgueira** csfilgueira@houstonmethodist.org